POSITRON ANNIHILATION IN THE MILKY WAY:
Searching for the source of Galactic antimatter

Fiona H. Panther

A thesis submitted for the degree of
Doctor of Philosophy
The Australian National University

October 2019

Declaration of Contribution to Published Work

This thesis is submitted as a Thesis by Compilation in accordance with https://policies.anu.edu.au/ppl/document/ANUP_003405

I declare that the research presented in this Thesis represents original work that I carried out during my candidature at the Australian National University, except for contributions to multi-author papers incorporated in the Thesis where my contributions are specified in this Statement of Contribution.

Refereed Journal Articles

1. **Panther, F. H.**, "Positron Transport and Annihilation in the Galactic Bulge", published in *Galaxies* 2018, 6(2), 39, DOI 10.3390/galaxies6020039
   Section(s): Chapter Four
   Contributions: Manuscript preparation - 100%

2. **Panther, F. H.**, Seitenzahl, I. S., Crocker, R. M., Machacek, J. R., Murtagh, D. J., Siegert, T., Diehl, R., "The effect of positron-alkali metal atom interactions in the diffuse interstellar medium", published in *Physical Review D* 2018, 98, 023015, DOI 10.1103/PhysRevD.98.024015.
   Section(s): Chapter Five
   Contributions: Simulations - 100%, Manuscript preparation - 95%

3. **Panther, F. H.**, Crocker, R. M., Birnboim, Y., Seitenzahl, I. R., Ruiter, A. J., "Positron annihilation in the nuclear outflows of the Milky Way", published in *Monthly Notices of the Royal Astronomical Society: Letters*, 2018, Vol. 474, Issue 1, DOI 10.1093/mnrasl/slx183.
   Section(s): Chapter Six
   Contributions: Simulations - 90%, Manuscript preparation - 95%

4. **Panther, F. H.**, Ruiter, A. J., Seitenzahl, I. R., Crocker, R. M., Lidman, C., Wang, X. E., Tucker, B. E., Groves, B., "Age and metallicity of stellar populations hosting SN1991bg-like supernovae", Published in in *Publications of the Astronomical Society of Australia*, 2019, Volume 36, id. e031, DOI 10.1017/pasa.2019.24
   Section(s): Chapter Seven
   Contributions: Observations - 95%, Manuscript preparation - 95%

The proportional contributions of the author have been truthfully stated, and permission from each author has been sought to include the published material in this thesis.

Fiona H. Panther
13 October 2019

In loving memory of Hilda Mackenley and Nigel Panther.
Time passes, love endures.

Acknowledgements

He aha te mea nui o te ao. He tangata, he tangata, he tangata
What is the most important thing in the world? It is people, it is people, it is people.

My time at the Research School of Astronomy and Astrophysics has been a truly wonderful experience. I have been lucky to be surrounded by an incredible community of researchers and professional staff who have supported me over the past three years. I acknowledge the traditional owners of the land on which Mt Stromlo Observatory stands, the Ngunnawal people, and the land on which the ANU 2.3m telescope stands, the Gamilaraay people, and pay my respects to the elders past and present.

A PhD thesis cannot exist without PhD supervisors. I have had the immense privilege of working under the guidance of a group of incredible scientists. I wish to thank my thesis panel members: Ivo Seitenzahl, Ashley Ruiter, Chris Lidman and Anais Möller for all their support, guidance, and advice over the years. Your patience and willingness to generously offer your time to help me learn a wide variety of new skills and master new topics has been appreciated immeasurably, and I look forward to working together more in years to come.

In particular, without the support of Roland Crocker, none of this work would have been possible. Over the past four years, Roland has been a role model, a mentor, an advisor, my greatest supporter, but most of all, my friend. He deserves as much credit as I, if not more, for the work presented in this thesis. This project was borne out of his creativity and passion for high energy astrophysics. I cannot imagine a better PhD supervisor.

A hearty thanks also goes to Mark Krumholz, who has been my mentor and guide through the tricky process of navigating the beginnings of my scientific career. Without his encouragement, I likely would not have dared to pursue my PhD and future career with the ambition and determination that I have.

It is one thing to stand on the shoulders of giants, but quite another to be invited to stand along side them, learn from them, and receive their guidance. I have been exceedingly lucky to be welcomed into the gamma-ray astronomy community with such open arms. To all those involved in the *INTEGRAL* mission, and particularly to Roland Diehl, I extend my thanks.

I have also been exceedingly fortunate to meet an incredible collaborator in Thomas Siegert. I have greatly appreciated his help, guidance, and friendship. I look forward to many more years of exciting future scientific collaborations.

To all my friends at Mt Stromlo, thank you for your support during the ups, downs, and multiple visits to the proverbial 'Valley of Shit' as well as the coffee machine. Henry, Elly, Rajika, Adam R, Chris, Alec, Ryan, Adam T, Phil, Jamie, Tim, Ayan, Lara, Steph, Alex, Jens, and Matt - you are the people who have made it easy to call Mt Stromlo my home.

I also wish to thank the many others with whom I've had the joy of sharing interesting conversations about science, who have given me invaluable advice and insights, and many more things besides: Yuval Birnboim, Brent Groves, Rob Sharp, Josh Machacek, Daniel Murtagh, Eugene Churazov, Brian Schmidt, Elaine Sadler, Lister Staveley-Smith, Felix Aharonian, Stuart Sim, Fritz Röpke, Rüdiger Pakmor, Richard Bartels, Brad Tucker, Warrick Lawson, Ralph Sutherland, and the late Mike Dopita. I also wish to thank those who generously devoted their time to proofreading my thesis: Erin Ryan, Ben Pope, Eloise Birchall, Rebecca Blackwell and Katie Grasha.

Getting involved in outreach activities at RSAA has given me a welcome break from my PhD studies, and continually reminded me of the wonders of the Universe that first drew me to astronomy. A special thanks to the outreach team at Mt Stromlo for the wonderful memories of outreach evenings, pizza, and epic visitor center renovations.

I would also like to acknowledge the many sources of funding that have made this research possible. The Australian Government and the Research School of Astronomy and Astrophysics at the Australian National University, who provided my PhD stipend for the past three and a half years, and the DAAD and CAASTRO who have generously awarded funds for me to travel. In particular, I acknowledge the Joan Duffield bequest, the John Shaw foundation, and the award of the Alex Rogers travelling scholarship, for providing me with incredible opportunities to extend my research and learning over the years.

I am often asked who my 'science role models' are. Without a doubt, it is my parents, Robert and Denise. From the very beginning, you have inspired my curiosity in the world around me, answering my questions and ultimately giving me the freedom and the skills to find the answers for myself. Your love and support inspires me every day. I love you both with all my heart, and I am lucky to have such supportive and caring parents as you.

Finally, to David Gozzard, who has supported me with such unconditional love. I am so blessed to have you by my side in this adventure, and without your help I may not have come through the last few weeks with most of my sanity intact. Meeting you is undoubtedly one of the best things to come out of my PhD journey. You never cease to amaze and inspire me every day. Thank you.

Having entirely run out of superlatives, in the immortal words of Douglas Adams, '*I may not have gone where I intended to go, but I think I have ended up where I needed to be*'. There is no group of people other than the aforementioned I would rather have met along the way.

Abstract

For more than 50 years, the rate and distribution of positron (anti-electron) annihilation in the Milky Way has puzzled astronomers. Positrons with low ($\sim$ MeV) initial energies are likely to be predominantly produced by $\beta+$ unstable radioactive isotopes. However, the observed rate of positron annihilation in the interstellar medium of the Milky Way exceeds the predicted rate of positron production by 'conventional sources' such as core-collapse and Type Ia supernovae. Moreover, the observed distribution of positron annihilation in the Milky Way appears to trace the older stellar populations of the Galaxy (the Galactic bulge and a thick, truncated disk), while massive stars, core-collapse supernovae, and Type Ia supernovae – all important sites for synthesis of radioactive material and potential positron sources – largely occur in the thin disk of the Galaxy. In this thesis, I will constrain scenarios for positron injection and transport in the interstellar medium and energetic outflows of the Milky Way. I will also show that positron annihilation on alkali metal atoms constrains the annihilation timescale of the positrons we observe annihilating today to be $\sim 1\,\mathrm{Myr}$. Finally, I will show that the delay time distribution of SN1991bg-like supernovae, a highly plausible source of $\sim 90\%$ of Galactic positrons, is consistent with that required to explain the total Galactic positron annihilation line.

Contents

List of Figures

List of Tables

Chapter 1

Introduction

> The story so far:
> In the beginning the Universe was created.
> This has made a lot of people very angry and been widely regarded as a bad move.
>
> Douglas Adams

The discovery of antimatter - both theoretically by Paul Dirac (Dirac, 1931) and experimentally by Carl Anderson (Anderson, 1932) - laid the basis for what we know today as the Standard Model of Particle Physics. This theory describes how all particles and forces (with the exception of gravity) relate to and interact with one another. 'Antimatter' describes particles that are 'mirror images' of the matter which makes up the familiar world around us. Each particle has an antimatter counterpart with equal mass but opposite charge and quantum numbers.

Today, astronomers believe that all visible matter in our Universe - gas, stars and galaxies - is made up of ordinary matter, not antimatter (see Canetti et al., 2012, for an overview). However, this cannot be conclusively proven, as antimatter particles have the same quantum electrodynamical properties as ordinary matter. It will take many years of careful experiment to determine if, for example, the emission spectrum of anti-hydrogen differs from that of hydrogen (Ahmadi et al., 2017).

There are a number of theoretical explanations for the 'baryon asymmetry', the name given to the fact that the universe is dominated by matter, not equal parts matter and antimatter. Violation of charge-parity symmetry is one explanation for the overabundance of matter compared to antimatter (Sakharov, 1991). Another explanation is that gravitational interactions of antiparticles are not as we would expect from general relativity (Chardin and Manfredi, 2018).

It is clear that there is much we do not understand about antimatter. While we do not apparently observe antimatter left over from the moments after the Big Bang, the Milky Way contains its own antimatter mystery. For almost 50 years, scientists have observed the annihilation of antimatter positrons from the Milky Way. However, a consensus on an origin of these positrons that can explain the distribution of the annihilation radiation has not been reached.

In this thesis, I will explore the potential origins of this antimatter in the Milky Way. To understand the distribution or morphology of the annihilation radiation, we must not only consider the origin of positrons, but also their propagation and annihilation. Each of these topics is intimately connected. I will show that the majority of the positrons we observe annihilating today must have been produced close to their sources within the Milky Way, in the past one million years. I will also show that a peculiar type of sub-luminous thermonuclear supernova could be responsible for the origin of a large fraction of the Milky Way's positrons, and can be a natural explanation for the observed distribution of the annihilation radiation.

Chapter 2

A brief history of positron annihilation in the Milky Way

> We demand rigidly defined areas of doubt and uncertainty!
>
> Douglas Adams

2.1 Theoretical description of the positron

The discovery of antimatter by Dirac (1931) was unique when compared to the discovery of all other elementary particles up to that point. The discovery first of the electron (Thomson, 1897), then the proton (Rutherford, 1911), were experimental curiosities that later gained a mathematical interpretation. Antimatter, on the other hand, was described mathematically before its experimental discovery.

Paul Dirac formulated the relativistic wave equation to describe the motion of an electron. The existing relativistic wave equation, the Klein-Gordon equation, can be obtained from the relativistic energy equation in the same way as the Schrödinger equation can be obtained from the Newtonian equation for kinetic energy: The Schrödinger equation for a free, non-relativistic particle (electron) with wavefunction ψ,

$$i\hbar \frac{\partial \psi}{\partial t} = \frac{-\hbar^2}{2m} \nabla^2 \psi \tag{2.1}$$

is obtained from the Newtonian equation for kinetic energy

$$E = \frac{1}{2} m v^2 = \frac{p^2}{2m} \tag{2.2}$$

where m is the mass of the electron and p is the momentum, with the identification

$$E \to i\hbar \frac{\partial}{\partial t}, \quad p \to -i\hbar \nabla. \tag{2.3}$$

The same identities are used instead in the relativistic energy equation,

$$E^2 = m^2c^4 + c^2\mathbf{p^2}, \tag{2.4}$$

to yield the Klein-Gordon equation for a relativistic particle with relativistic wavefunction ϕ,

$$(i\hbar\frac{\partial}{\partial t})^2\phi = (i\hbar\nabla)^2c^2\phi + m^2c^4\phi, \tag{2.5}$$

or

$$(\Box - \mu^2)\phi = 0, \tag{2.6}$$

where

$$\Box = \partial_\mu\partial^\mu = \nabla^2 - \frac{1}{c^2}\frac{\partial^2}{\partial t^2}, \tag{2.7}$$

and $\mu = mc/\hbar$ and m is the mass of the particle being described.The interpretation of the Klein-Gordon equation poses a number of problems. In the case of the Schrödinger equation, it is possible to define the probability density,

$$\rho = \psi^*\psi, \tag{2.8}$$

and the probability current,

$$\mathbf{j} = -\frac{i\hbar}{2m}(\phi^*\nabla\phi - \phi\nabla\phi^*). \tag{2.9}$$

However, for the Klein-Gordon equation, choosing

$$\rho = \phi^*\phi, \tag{2.10}$$

as total probability will not be conserved and moreover, the Lorentz transformation properties that are required by relativity are incorrect.

While it is possible to define ρ in such a way that probability is conserved, the Klein-Gordon equation still suffers from a number of deficiencies, namely that it does not place time and space on an equal footing as is required by relativity. Of a greater concern to Dirac was the negative energy solutions to the equation. Thus, it is possible to have solutions to the equation which have a negative probability. It was clear to Dirac that the Klein-Gordon equation was quite inadequate as a wave equation to describe the relativistic electron.

Dirac recognized that while all relativistic particles must obey the Klein-Gordon equation in order to obey the correct relativistic energy-momentum relations, many of the issues with the equation came from it being second order in time. Dirac's solution was 'simply' to factor the equation, making it first order in both time and space, using a set of hypercomplex numbers we today refer to as the Dirac matricies. These hypercomplex numbers, γ^μ, obey a set of anticommutation relations,

$$\gamma^\mu\gamma^\nu + \gamma^\nu\gamma^\mu = -2g^{\mu\nu}, \quad \mu,\nu \in \{0,3\} \tag{2.11}$$

They are often represented as a set of 4x4 complex matricies. The Klein-Gordon equation,

$$(\partial_\mu \partial^\mu - \mu^2)\phi = 0, \tag{2.12}$$

can then be factorised to give

$$(\gamma^\nu \partial_\nu - i\mu)(\gamma^\mu \partial_\mu + i\mu)\psi = 0. \tag{2.13}$$

In the 4x4 representation of the Dirac matricies, the wavefunction solution ψ to the Dirac equation is referred to as a Dirac spinor. This equation simpifies using the above anticommutation relations to give the Dirac equation,

$$(\gamma^\nu \partial_\nu - i\mu)\psi = 0. \tag{2.14}$$

Any wavefunction that satisfies the Dirac equation also satisfies the Klein-Gordon equation, and hence the relativistic equations of motion.

While Dirac solved a number of the apparent problems with the Klein-Gordon equation, he found that it was still possible for negative energy solutions to this equation to exist. Dirac's solution to the problem of negative energy was to assume that all (or nearly all) the negative energy states are occupied, one electron to each state. The exclusion principle then prevents any more electrons entering this 'sea' of negative energy states. An unoccupied negative energy state (a hole) now appears as something with positive energy, since it may apparently be filled by adding an electron with negative energy. In his 1931 paper on 'Quantized Singularities in the Electric Field' (Dirac, 1931), Dirac coins the term anti-electron to describe these holes, emphasising that the particle he has described must have the same mass as the electron: 'A hole, if there were one, would be a new kind of particle, unknown to experimental physics, having the same mass and opposite charge to an electron. We may call such a particle an anti-electron'.

One of the defining features of antimatter particles is how they interact with their ordinary matter counterparts. This process is called annihilation, and only takes place between matter and antimatter particles. In layman's terms, the total mass of the matter and antimatter particle is converted into energy, which is released in the form of at least two gamma-ray photons if the interaction of the two particles is via a virtual photon. Thus, the annihilation of a positron-electron pair produces two gamma-rays, each with an energy of 511 keV. This means that the detection of a gamma-ray line with a centroid energy of 511 keV unambiguously indicates the annihilation of positrons.

2.2 Experimental discovery of positrons

Dirac did not expect this anti-electron ever to be discovered experimentally. He described it as being too short-lived to ever be found in nature unless it was created in the laboratory in a high vacuum: 'We should not expect to find any of them in nature, on account of their rapid rate of recombination with electrons, but if they could be produced experimentally in high vacuum they would be quite stable and amenable to observation.'

It was only a year later that American experimental physicist Carl Anderson independently identified a particle he referred to as the 'positron' in his 1932 paper 'The Positive

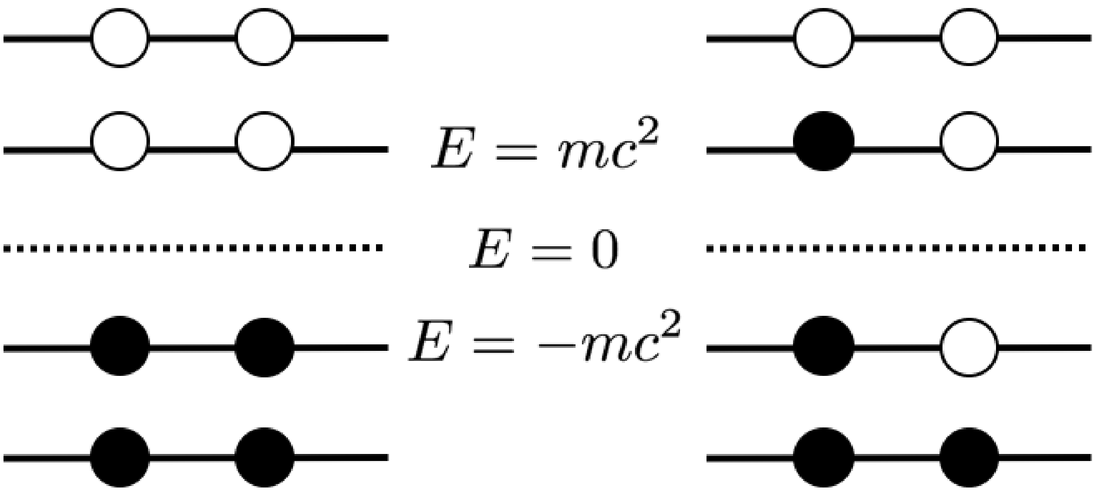

Figure 2.1: Schematic showing the 'Dirac Sea', Dirac's original conceptualization to understand the negative energy solution to the relativistic wave equation. On the left, all negative energy states are filled. On the right, a hole appears. The positive-energy electron can jump across the classically-forbidden region of energy states between $-mc^2 < E < mc^2$ to a negative energy, and thus fill the hole.

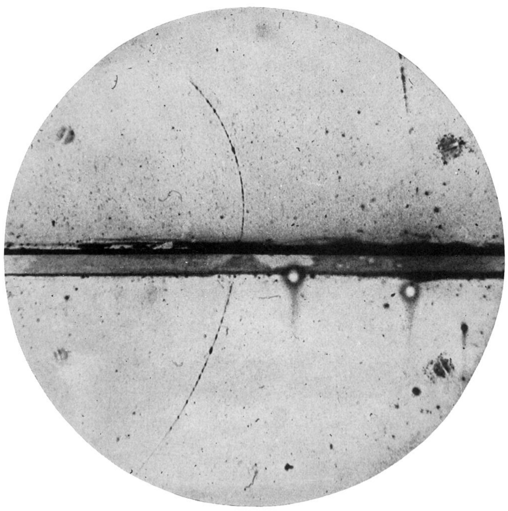

Figure 2.2: Detection of a positron in cloud chamber photographs from Anderson (1932). Anderson noted that the path of this particle was ten times greater in length than the path that would be expected from a proton of the same curvature.

Electron' (Anderson, 1932). Anderson describes the observation of tracks in cloud chamber photographs that were indicative of a positive particle that had a mass far smaller than that of the proton (Figure 2.2). While Anderson's paper was in preparation, his observations were confirmed by Blackett and Occhialini (1933), who connected their experimental observation of a particle with equal mass but opposite charge to the electron with Dirac's theoretical 'anti-electron'. Anderson received the Nobel Prize for his discovery.

2.3 Positronium

While the antimatter nature of positrons makes them unstable (they will annihilate on interaction with electrons), it is possible for them to form short-lived bound states. The simplest bound state in which a positron can exist is known as positronium, composed of a single positron and electron. The existence of positronium was theorized in the 1930s, not long after the discovery of the positron, by Mohorovičić (1934). However it was not observed in the laboratory until much later, and the discovery of positronium was announced by Deutsch (1951), who had performed the experimental work which led to its discovery at MIT. Positronium is the lightest electromagnetically-bound state of matter, with a reduced mass $\mu_{\mathrm{Ps}} = 0.5m_e$,half the reduced mass of the hydrogen atom ($\mu_H \sim 0.99m_e$). Thus, the binding energy of positronium is half that of the hydrogen atom ($E_B = 6.8\,\mathrm{eV}$).

As a hydrogen-like atom, positronium exhibits the same excitation, absorption, and emission transitions as hydrogen, however the wavelength of emitted or absorbed radiation for a given transition will be twice that of the same transition in the hydrogen atom. Thus, $n = 3$ to $n = 2$ Balmer-α transition in positronium results in emission at a wavelength of $1.31\,\mu$m, in the infra-red region of the spectrum (Ellis and Bland-Hawthorn, 2018). Next-generation IR spectrographs equipped with OH supression technology have the possibility of enabling the detection of positronium excitation and recombination lines (Ellis et al., 2018).

Like the hydrogen atom, positronium can exist in two spin states. In one, the spins of the electron and positron are parallel, a state referred to as ortho-positronium. The other in which the spin of the electon and positron are antiparallel, and this spin configuration is known as para-positronium. Positronium is inherently unstable and annihilates after only a fraction of a second. The lifetimes of parallel and antiparallel positronium differ significantly ($\tau_{\mathrm{pPs}} = 1.2 \times 10^{-10}\,\mathrm{s}$ for para-positronium, and $1.4 \times 10^{-7}\,\mathrm{s}$ for ortho-positronium). From the spin degeneracy, para-positronium will be formed $1/4$ of the time, and ortho-positronium will be formed $3/4$ of the time.

The different spin angular momenta of the two forms of positronium also mean that their annihilation produces different numbers of gamma-rays. Para-positronium annihilates to emit two gamma-rays while ortho-positronium annihilates to emit an odd number of gamma-ray photons, with a minimium of three. These emission processes result in the formation of a low energy ortho-positronium continuum (Ore and Powell, 1949) superimposed upon an emission line at 511 keV from the annihilation of para-positronium. The details of the spectrum are discussed further in Section 3.1.3.

Ortho-positronium can be 'quenched', or broken up into its constituent positron and electron, via collisional interactions when the density is sufficiently high (Murphy et al., 2005). These interactions occur in environments such as in the deep layers of the solar atmosphere. Quenching of ortho-positronium occurs at a higher rate than the quenching of para-positronium, as the lifetime of para-positronium is 1000 times shorter than that of ortho-positronium. Thus, the densities required for quenching to become significant are 1000 times greater in the case of para-positronium quenching. Consequently, quenching is typically only relevant for ortho-positronium in most astrophysical environments.

Quenching is caused by either ionization or by spin flip of positronium. Quenching typically becomes significant at densities $n > 10^{15}\,\mathrm{cm}^{-3}$ (however recent calculations of quenching cross-sections suggest they may be much larger than previously thought, and the densities at which quenching becomes important may be substantially lower) at temperatures of $\sim 10^4\,\mathrm{K}$ (Murphy et al., 2005). These conditions are typical of the solar chromosphere. In such environments, one must consider the quenching rate as it will affect the determination of the positronium fraction from the relative strengths of the ortho-positronium continnum flux and the 511 keV line flux (see Section 3.1).

2.4 Gamma-ray astronomy

Positron annihilation in the Milky Way is inferred from the detection of gamma-rays. Gamma-ray photons are detected at energies between $\sim$ 100 keV to PeV energies, and the fluxes of gamma-rays cover several decades of flux (De Angelis and Mallamaci, 2018). This great dynamic range has required the development of a number of different detection techniques and sophisticated statistical analysis tools.

Gamma-rays may be produced during continuous processes, such as the acceleration and energy losses of high energy particles as they interact with material, or through discrete processes such as radioactive decay or, in the case of positrons, annihilation. These processes produce different characteristic continuum emission or line emission that may be observed using instruments designed to detect and measure gamma-rays at MeV energies. Ultimately, this reflects the power-law distribution of the non-thermal cosmic ray populations that produce the radiation.

2.4.1 Gamma-ray continuum

A number of different physical processes result in gamma-ray continuum emission. These processes can be broadly separated into leptonic processs (involving electrons and positrons) or hadronic processes (involving protons or heavier ions). These processes result in background emission with a power-law spectrum when observed by MeV telescopes.

Leptonic emission occurs when electrons (or positrons) interact with the magnetic field or with photon fields. Interactions with the magnetic field, where a relativistic electron gyrates around the magnetic field line, produces synchrotron emission. The synchrotron emission itself may be in the form of photons with energies that correspond to, at most, the x-ray regime for typical maximal energies of cosmic ray electrons and typical ISM magnetic field amplitudes. These photons become part of the ambient photon field in the region in which the leptons are propagating.

Leptons will also interact with the ambient photon field via the inverse Compton process. Electrons scatter low energy photons, and the photon becomes up-scattered while the energy of the electron is down-scattered. However, in regions where both inverse Compton scattering and synchrotron processes take place it is possible for the population of relativistic electrons to be accelerated. Highly relativistic leptons accelerated in strong magnetic fields emit x-ray photons which subsequently undergo Compton scattering with the lepton that produced them, which can boost the photon energy into gamma-ray energies. This process is called Synchrotron Self-Compton (SSC) scattering. The continuum emission from this process typically peaks at GeV $-$ TeV energies.

Hadronic emission originates from the collisions of relativistic protons and atoms and nuclei in the interstellar or intergalactic medium. This creates what is known as a hadronic cascade, where a shower of pions is created. Neutral pions can decay into a pair of gamma-rays.

Hadronic gamma-ray emission can also originate from photohadronic interactions, with photons produced by the synchrotron radiation or from bremsstrahlung of accelerated electrons. Photohadronic interactions occur in regions where the target photon density is much higher than the matter density. Photohadronic reactions result in the production of cosmic ray pions, and the resulting spectral energy distribution of gamma-rays has a characteristic feature known as the 'pion bump' at $E_\gamma \sim m_\pi/2 \sim 70\,\mathrm{MeV}$, considered a signature of hadronic interactions.

2.4.2 Gamma-ray lines

Discrete processes such as positron annihilation and nuclear decay produce gamma-ray lines observable with MeV telescopes. The first and most intense gamma-ray line to be detected from beyond the solar system was the positron annihilation line (Johnson et al., 1972), and subsequently many other gamma-ray lines have been detected, all of which originate from the de-excitation or decay of nuclei.

Gamma-ray lines in the Milky Way include the emission lines from the radioactive decay of ^{26}Al decay, which traces regions containing massive stars and radioactive decay of ^{44}Ti, which is observed in core-collapse supernova remnant Casseopoeia A (Iyudin et al., 1994; Siegert et al., 2015; Grefenstette et al., 2016). These gamma-ray lines are the most compelling direct evidence of ongoing nucleosynthesis and chemical enrichment in the Milky Way (Diehl et al., 2017). Beyond the Milky Way, gamma-ray lines have been observed in a thermonuclear supernova, SN2014J, originating from the decay of nuclei such as ^{56}Ni and ^{56}Co, and the annihilation of positrons produced in this decay chain (Churazov et al., 2014; Diehl et al., 2014; Churazov et al., 2015). Decay lines of ^{44}Ti (Boggs et al., 2015) and ^{57}Co (Kurfess et al., 1992) have also been detected in the remnant of SN1987A in the LMC .

2.5 It came from outer space: positrons in the Milky Way

Initially all detected positrons were of terrestrial origin. Even those detected in the cloud chambers by Anderson (1932) and Blackett and Occhialini (1933) were created by the collision of cosmic rays with the atmosphere. Another terrestrial source of positrons is in radioactive decay of β^+ unstable radionuclides was identified by Joliot and Curie (1934).

The first positrons from beyond the Earth were discovered by De Shong et al. (1964), in an experiment that saw a spark chamber loaded onto a high-altitude balloon to detect charged particles in cosmic rays. Ginzburg (1956) had suggested that positrons should be produced by cosmic ray interactions in the interstellar medium, where $p - p$ interactions produce charged pions which subsequently decay to produce positrons was secondary cosmic rays.

2.5.1 Balloon-borne observatories

De Shong et al. (1964) detected the cosmic ray positrons themselves. In contrast, the detection of the 511 keV line indicates the presence of positrons via indirect evidence through annihilation. The atmosphere is opaque to the gamma-rays emitted by the annihilation of positrons, thus instruments must be flown above the atmosphere to observe them.

In the early days of gamma-ray astronomy, instruments mounted on stratospheric weather balloons were used to reach above the majority of the atmosphere. There are a number of downsides of balloon-borne instruments, however. These include that it is impossible to obtain detailed directional information as it is extremely hard to stabilize the instrument aboard the balloon and define its pointing. Furthermore, the size of the detectors is limited by the balloon, and early detectors had small fields of view due to the small sizes of the payloads.

Early reports of a 511 keV line were made in Peterson (1963) and Chupp et al. (1967), however the line was then attributed primarily to the decay of radioactive material produced in nuclear weapons tests. In Haymes et al. (1969), the first limit was placed on the 511 keV emission from the Galaxy in a series of balloon flights in the US and Australia. The centroid of the observed gamma-ray line attributed to positrons to calculate this limit appeared to be closer to 490 keV, and it was suggested that this line could be attributed to the decay of ^{108}Ru atoms from atomic bomb debris, or the decay of ^{7}Be produced by cosmic ray interactions in the atmosphere (e.g. Chupp et al., 1967). As the 511 keV line is expected to be contaminated by this proposed unresolved gamma-ray line, it was concluded that the true 511 keV flux is much smaller than their limit of 0.45 ± 0.09 photons cm^{-2} s^{-1} (Haymes et al., 1969).

The first confirmed detection of a gamma-ray line beyond the solar system occured in the late 1960s and was first reported by Johnson et al. (1972). A balloon flown from Paraná, Argentina, in 1970, carrying a sodium-iodide scintillator, had observed a distinctive spectral excess with the line center observed at $\sim 473 \pm 30$ keV with a flux of 1.8×10^{-3} photons cm^{-2} s^{-1}. This was the detection of the first gamma-ray line originating beyond the solar system, and the most intense (Figure 2.3). Once again, while the possibility of the line resulting from positron annihilation was suggested, the offset of the line led to the concern that the line was due to an hitherto unknown nuclear de-excitation. A second balloon flight by the same team confirmed the feature, as well as the offset of the line.

In Leventhal (1973), it was pointed out that the majority of positron annihilation in the ISM should be expected to occur via the formation of positronium. Thus, the observation of the spectrum of positronium annihilation (which produces both a 511 keV line and a low-energy ortho-positronium continuum) with a detector with comparatively poor spectral resolution should result in the observation of a gamma-ray line with a substantial offset from 511 keV.

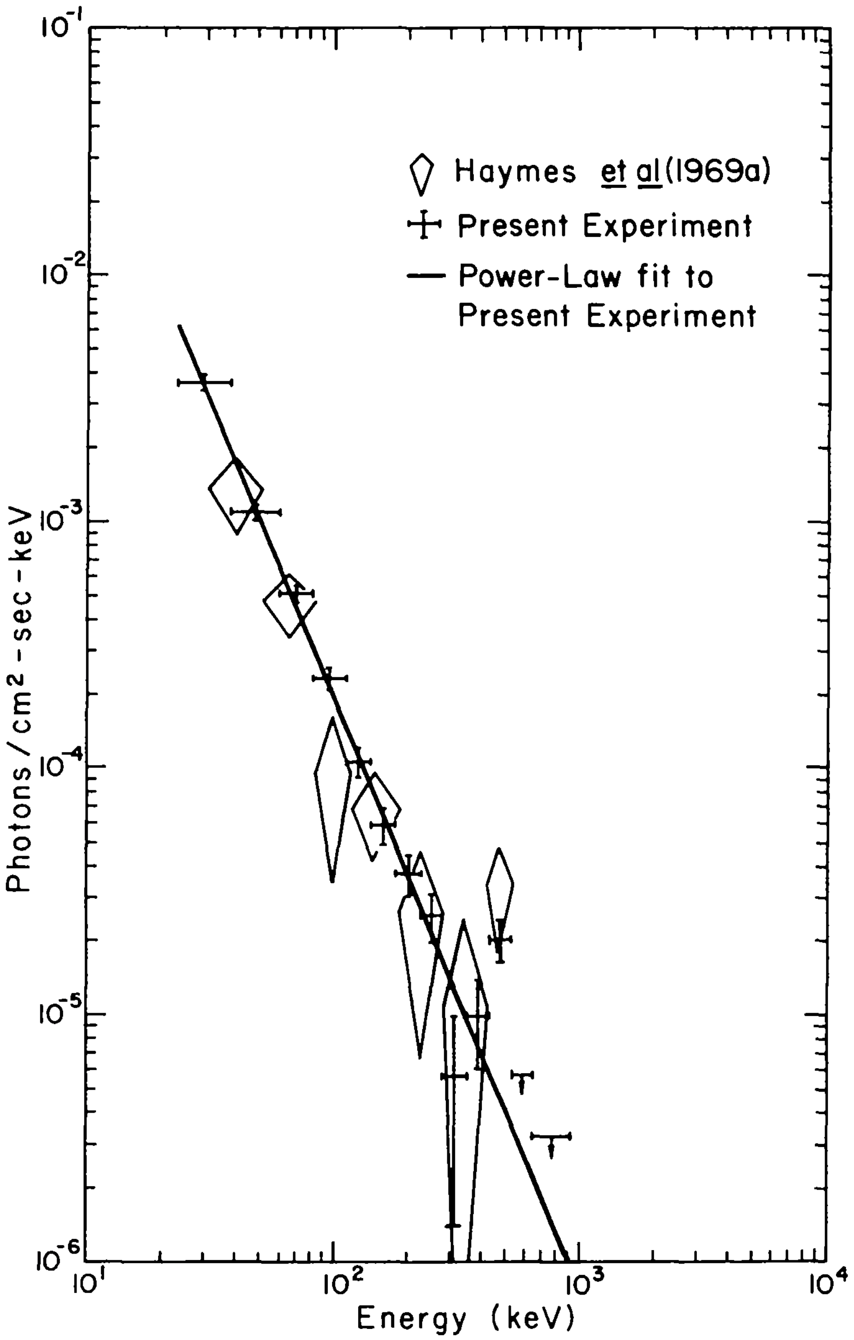

Figure 2.3: Spectrum of soft gamma-rays from the Milky Way Galaxy as measured by the balloon-borne spectrographs of Haymes et al. (1969) (open diamonds) and Johnson et al. (1972) (points with error bars). The broad emission line at $\sim$ 490 keV is clearly visible in both sets of measurements. A power law is fitted to describe the gamma-ray continuum emission from the Galaxy. From Johnson et al. (1972).

The challenges of building an improved gamma-ray detector meant it took several years before this suggestion could be tested. In 1978, a balloon-borne germanium spectrometer with a greatly improved spectral resolution was launched from Alice Springs in Australia, and successfully measured both the continuum and line associated with the positron annihilation in the Galaxy (Leventhal et al., 1978). Their line flux of 1.22×10^{-3} photons $\mathrm{cm}^{-2}\,\mathrm{s}^{-1}$ was lower than that measured by Johnson et al. (1972). This lower flux can be attributed to the superposition of the continuum and line emission in the Johnson et al. (1972) measurements.

During the late 1970s and 1980s, a number of teams began to utilize different balloon borne instruments to study the positron annihilation line from the Galaxy. During these years, measurements of the line flux varied considerably from instrument to instrument (Haymes et al., 1975; Leventhal et al., 1980; Albernhe et al., 1981; Gardner et al., 1982). The origin of this variability was discussed in Albernhe et al. (1981), who pointed out the connection between measurements of increased flux, and greater detector area. This implies that the 511 keV emission was extended, rather than point-like. However, as the balloons had poor pointing control, it was impossible to confirm the extended nature of the positron annihilation line and map its extent in the Milky Way. Thus, the steady-state nature of the positron annihilation flux could not be confirmed.

2.5.2 Satellite observations

While balloon-borne missions remain to this day the best way of testing the performance of gamma-ray detectors for celestial observations (Kierans et al., 2017), the practicality of such experiments became limited by the size of the payloads it was possible to launch around the early 1980s. Instruments with greater collecting areas were desired, and moreover, the pointing of a space-based instrument can be controlled, making them superior to the cheaper, balloon-borne alternative.

2.5.2.1 The false promise of variability

The first satellite to observe the positron annihilation line in the Milky Way was the *HEAO-3* satellite (positron annihilation in the Solar atmosphere was observed a few years earlier using a NaI scintillator aboard the *OSO-7* Satellite, (Chupp et al., 1975)). In Riegler et al. (1981), results from the satellite seemed to confirm the variability of the 511 keV line that had been observed with the balloon detectors. These observations suggested that the positron annihilation was associated with a compact region close to the center of the Milky Way, and found a factor of three decline in the 511 kev line flux between 1979 and 1980. The apparent variability led to interpretations that implicated the Galactic Center as the source of the positron annihilation line (Lingenfelter et al., 1981).

However, contemporary observations with other satellite experiments, including long term monitoring of the Galactic Center by the *Solar Maximum Mission* (*SMM*) between 1980 and 1987 failed to confirm this apparent variability. *SMM* had been designed to observe positron annihilation in solar flares, but did not observe any variability in the 511 keV line flux from the Galaxy. *SMM* constrained the variability of the 511 keV line to less than 30%, far less than the 300% claimed by *HEAO-3* (Share et al., 1988, 1990). The disagreement in the results can be understood by taking into account SMM's large field of view compared to *HEAO-3* and the balloon-borne missions, and that the positron annihilation was extended along the Galactic plane. An alternative explanation invokes a variable source close to the Galactic Center (Lingenfelter and Ramaty, 1989), which can account for the variability observed by *HEAO-3*, and a steady-state annihilation emission which is extended into the Galactic bulge and along the Galactic plane.

Enthusiasm for a highly time variable Galactic Center source was rejuvenated in the early 1990s after observations from the French SIGMA telescope. The SIGMA telescope design is an early predecessor of the exisitng SPI/*INTEGRAL* instrument, and was launched on the Russian *GRANAT* satellite (Bouchet et al., 2001). SIGMA was the first imaging gamma-ray instrument, with an angular resolution of $\sim 15\,\text{arcmin}$. In 1991, SIGMA observed an unusual spectrum from the x-ray source 1E1740.7-2942 (Bouchet et al., 1991; Sunyaev et al., 1991). This outburst lasted less than 24 hours, and could be interpreted as a very broad and red-shifted positron annihilation line superimposed on the hard x-ray spectrum of the black hole (Mirabel et al., 1991). Close to the Galactic Center, it was possible that 1E1740.7-2942 was the source of the variability observed during the era of the balloon-borne missions.

Despite the excitement around the SIGMA observation of a transient positron annihilation source, simultaneous observations with instruments aboard the NASA Compton gamma-ray Observatory (*CGRO*) with the Oriented Scintillation Spectrometer Experiment (OSSE) and BATSE instruments did not show any such outburst from the x-ray source (Jung et al., 1995; Smith et al., 1996), nor other x-ray sources which exhibited apparent variability in SIGMA observations ("Nova Muscae" (Goldwurm et al., 1992; Sunyaev et al., 1992) and the Crab nebula (Gilfanov et al., 1994).

No transient events from any part of the sky were discovered in all of the *SMM* data (Harris et al., 1994), and a subsequent reanalysis of the *HEAO-3* data revealed that the decrease in flux described by Riegler et al. (1981) was not as statistically significant as it appeared at the time (Mahoney et al., 1994). Recent analysis has shown that the apparent variabilty was likely due to the varying methods of deconvolving the data, as well as the variable fields of view of the telescope (Milne et al., 2001a). It is now well understood that a thorough understanding of the detector instrument and its background is vital to the accurate determination of the characteristics of positron annihilation (Diehl et al., 2017).

2.5.2.2 A picture emerges

A key aspect of finding the source of the positron annihilation signal is to understand the spatial distribution of the annihilating positrons. While the French SIGMA telescope had the capabilities of imaging gamma-rays, its angular resolution was extremely poor. Even at present, producing high resolution images of soft gamma-ray emission is fraught with difficulty, owing particularly to the fact that gamma-rays cannot be focused (see Section 2.6.1). Nonetheless, a few techniques exist to allow careful image reconstructions of gamma-ray emission to be made.

By the early 1990s, it had been established that the positron annihilation radiation was diffuse and extended to at least 25° longitude, however the morphology itself was poorly constrained (Leventhal et al., 1989). The launch of the OSSE collimated spectrograph on board *CGRO* revolutionised positron astrophysics.

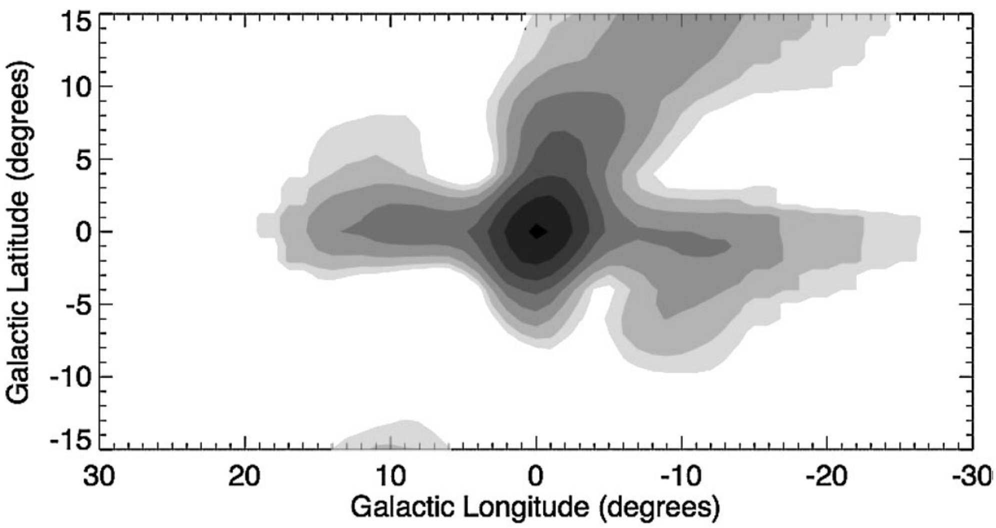

Figure 2.4: OSSE/*CGRO* map of the distribution of the 511 keV line emission from the Galaxy. The emission is centrally concentrated, and the feature stretching to high latitudes was dubbed the 'Positive Latitude Extension' and was later shown to be an artefact of the deconvolution method chosen to analyse the data. From Purcell et al. (1997)

The OSSE data excluded once and for all a single point source of 511 keV radiation (Purcell et al., 1994). There were two dominant components to the emission: The Galactic bulge was revealed to glow brightly with positron annihilation radiation, and emission stretched along the Galactic plane. Moreover, there was a tantalizing hint of a curious third component that stretched out of the Galactic Centre far to Galactic North, but this 'positive latitude enhancement' (PLE) was only weakly constrained by the data (Purcell et al., 1997).

The PLE spawned a number of works which postulated that past accretion activity associated with the central black hole may have produced a 'positron fountain' stretching several kiloparsecs above the Galactic Center (Dermer and Skibo, 1997). In hindsight, the PLE seems tantalizingly like a foreshadowing of the discovery of the Fermi Bubbles, a phenomenon similar in structure to the PLE but observed at much higher energies. However, unlike the Fermi Bubbles, the PLE turned out to be positron astrophysics's own 'white whale'.

Despite the great advances in imaging the distribution of the positron annihilation radiation with OSSE, the origin of Galactic positrons still remained unknown as the data did not constrain the morphology sufficiently to clarify what the underlying source population may be (Milne et al., 2001b,a). The observations remained puzzling: unlike at any other wavelength, the Galactic bulge dominates the emission. This became even more puzzling as the majority of proposed positron sources, including nucleosynthetic positron sources, were confined to the Galactic disk.

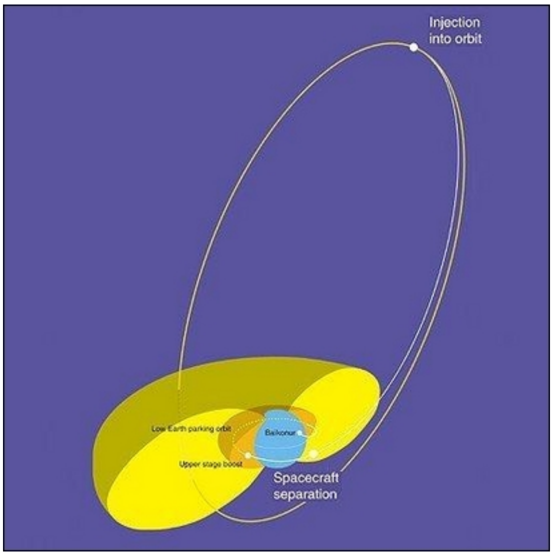

Figure 2.5: Schematic showing *INTEGRAL*'s launch and injection into its current highly eccentric orbit, designed to maximise the time the spacecraft spends outside of the van Allen belts. Image credit: ESA

2.6 Current constraints on positron annihilation in the Milky Way

2.6.1 SPI/INTEGRAL

The *International gamma-ray Laboratory* (*INTEGRAL*) was launched by ESA on board a proton rocket in 2002, and continues the mission of NASA's *Compton gamma-ray Observatory* (*CGRO*) to study the high energy universe (Winkler et al., 2003). *INTEGRAL* carries several instruments, but it is the Spectrometer on-board *INTEGRAL* (SPI) which has enabled revolutionary new measurements of the spectrum and morphology of the positron annihilation line (Vedrenne et al., 2003). The spacecraft has a highly eccentric (Figure 2.5), highly inclined orbit, which carries it far from the Van Allen belts for around two thirds of its orbit. This maximises the time the spacecraft is subjected to low levels of cosmic ray bombardment which affect its detectors.

INTEGRAL was intially designed to have only a three year life. However, the great success of the instrument across many fields of astrophysics have led to a number of mission extensions on a biannual basis. The telescope is expected to remain operational until at least the end of 2019 and in principle can operate until it deorbits in 2029, however degradation of the solar panels may become an issue toward the mid-2020s.

INTEGRAL carries four co-aligned instruments (Figure 2.6): IBIS, a high-resolution soft gamma-ray imager (which has excellent angular resolution at low energies, but poor spectral resolution, (Ubertini et al., 2003)), a soft x-ray monitor (JEM-X, which consists of two identical detectors mounted on the side of the telescope, (Lund et al., 2003)), the Optical Monitoring Camera (Mas-Hesse et al., 1998), and the SPI instrument, a gamma-ray imaging spectrometer with excellent spectral resolution (Vedrenne et al., 2003). This makes *INTEGRAL* an excellent

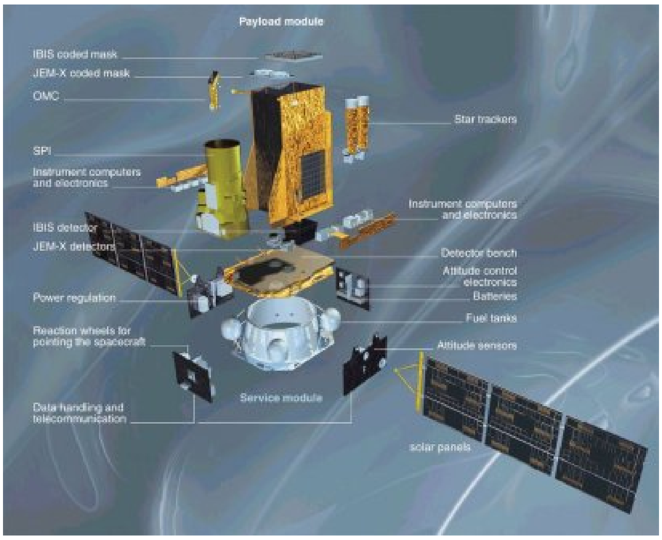

Figure 2.6: INTEGRAL satellite, showing the relative position of the four astronomical instruments. Image credit: ESA

facility for multiwavelength studies of the high energy universe. SPI in particular is used for studies of positron annihilation due to its high spectral resolution.

SPI consists of a camera composed of 19 Germanium scintillator crystals, creating a high spectral resolution detector (FWHM$\sim$ 2 keV). The detector crystals are arranged in a hexagonal lattice together with photomultiplier tubes beneath to provide the largest possible collecting area for incoming gamma-ray photons. The detectors must be re-annealed twice each year as the spectral resolution of the instrument degrades over time due to cosmic ray bombardment. During the re-annealing cycle, the crystals are heated and then gradually cooled. When operating, the detector is cooled to around 85 K, greatly reducing thermal noise (Vedrenne et al., 2003).

The detector array itself cannot function as an imaging telescope. For this reason, the detector plane sits around 2 m below a 'coded mask'. The coded mask is made of 127 hexagonal units, half of which are opaque to gamma-rays, and half of which allow gamma-rays to pass through (Vedrenne et al., 2003).

When gamma-rays pass through the coded mask, the produce a shadowgram on the detector plane (Figure 2.7). The coded mask is composed of a series of units which are either transparent or opaque to gamma-rays. Depending on the incoming direction of the gamma-ray, the shadowgram takes on a different appearance in the detector plane, enabling the reconstruction of directional information. Consequently, SPI can be used like a gamma-ray integral field unit, obtaining spectral information for each spatial element in the images it reconstructs.

Objects in Earth's orbit are subject to bombardment by cosmic rays which are produced both inside and beyond the heliosphere. SPI is surrounded by a series of anti-coincidence shields (ACS) to identify events which originate from interactions of cosmic rays with the body of the spacecraft. These systems reduce the photon and particle background within the

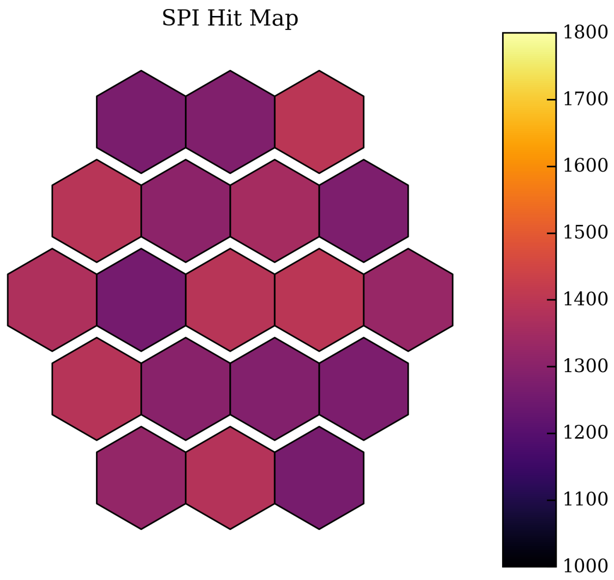

Figure 2.7: SPI's detector pattern. The colorbar indicates the number of counts registered by each detector during one 2-hour pointing at the Crab pulsar, used as a calibrator.

telescope. There are several ACS systems: one above the detector plane, one below, and one which surrounds the detector. Events detected by the main camera which coincide with hits on the ACS are 'vetoed'.

Cosmic rays may react with the nuclei in the body of the spacecraft. These interactions can create slow neutrons via spallation. If these neutrons are captured by nuclei inside the spacecraft, they may form radioactive isotopes. These new radioactive nuclei may decay on timescales of less than a nanosecond, to over many decades. These prompt and delayed gamma-ray emissions of newly created radioisotopes inside the body of the spacecraft account for the high instrumental background of SPI. This instrumental background accounts for 99% or more of the measured data in a single observation depending on the energy channel being used (Diehl et al., 2017).

In the early years of the SPI mission, simulations were used to understand this background, however modern background models are based on 15 years of housekeeping data. This new background model, presented in Diehl et al. (2017), will enable much more sophisticated analysis.

The high levels of background noise also led to complications in the analysis. It is not possible to simply subtract the background from the data. Instead, the background and signal must be fitted simultaneously. This process is particularly complicated for the diffuse emission of the positron annihilation line. The analysis methods do not allow for a true count-map of emission from the sky to be formed, and instead, analysis typically presents best-fit models to approximate the true emission (e.g. Siegert et al. (2016b)). However, any best-fit model is simply one of a family of models which may best describe the data. Thus, it is important not to over-interpret either the apparent smoothness or any small-scale features that are presented in the emission models.

2.6.2 Morphology

The first observations of positron annihilation made by SPI were based on one year of SPI data and presented in Knödlseder et al. (2005); Weidenspointner et al. (2006). Both the 511 keV line and the ortho-positronium continuum were mapped using Richardson-Lucy deconvolution of the SPI data. The best fit models presented by Knödlseder et al. (2005) and Weidenspointner et al. (2006) (Figure 2.8) are consistent with one another; this suggests that the positronium fraction does not vary over the sky. This inference is an important datum to understand the annihilation sites of the positrons, as if the positronium fraction varies across the sky, the annihilation sites may also vary. However, this does not seem to be the case.

Like the OSSE maps, the bulge region dominates the morphology of the SPI maps. In constrast to the OSSE data, however, there was no apparent disk component observed after the first year, with only a marginal significance of the disk signal and a very high bulge/disk ratio. This high bulge/disk flux ratio spawned a number of proposals of exotic sources of positrons, including dark matter. However, as pointed out in Prantzos (2006), a low-surface brightness disk could not yet be ruled out by the data.

A subsequent analysis of five years of SPI data began to reveal new information (Weidenspointner et al., 2008a). The improved exposure meant that low surface brightness features which had been visible in the OSSE data, such as the Galactic disk, began to be revealed (Fig-

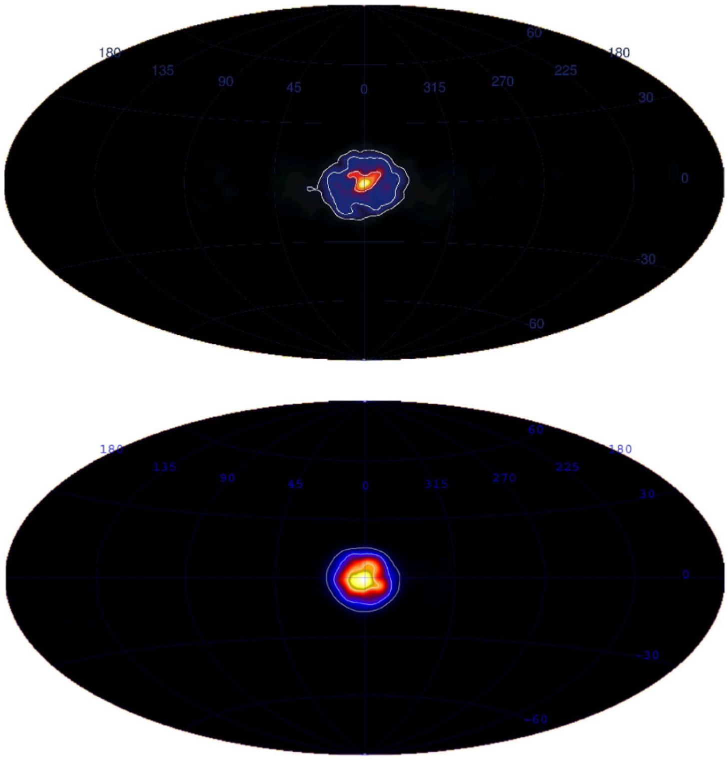

Figure 2.8: Positron annihilation radiation distribution from 3 yrs of SPI data from Knödlseder et al. (2005) (top) and Weidenspointner et al. (2006) (bottom). The bulge glows brightly with positron annihilation.

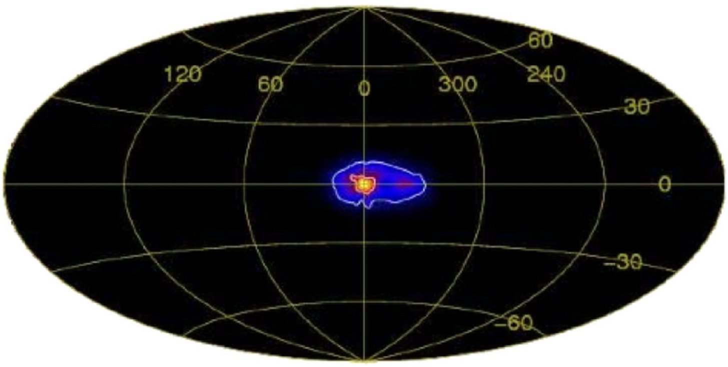

Figure 2.9: Positron annihilation radiation distribution from 5 yrs of SPI data from Weidenspointner et al. (2008a). The bulge glows brightly with positron annihilation, and the disk component is visible.

ure 2.9). While the emission must be described by an idealized parametric model, it became clear that the best fit to the observed emission involved a two-component bulge model: a narrow and broad two-dimensional Gaussian (in Galactic coordinate space) to describe the bulge, and a thick, narrow disk component with a vertical extent of ~ 7 degrees.

An alternative model was also proposed which fits the data almost equally well: an extended halo combined with a thinner disk with a thinner disk (4 degrees, Weidenspointner et al., 2008b). More SPI data began to reveal an apparent asymmetry in the disk emission in one analysis (Weidenspointner et al., 2008a), however a separate analysis did not find any evidence of this apparent asymmetry, however could not exclude it (Bouchet et al., 2008, 2010). Regardless of the chosen morpological model, two things were clear: the emission is dominated by the Galactic bulge, and the bulge/disk flux ratio was still high.

In Siegert et al. (2016b), 11 years of *INTEGRAL* data are analysed. Confirming earlier results (Knödlseder et al., 2003, 2005; Weidenspointner et al., 2008a), the central regions of the Galaxy show the highest intensity 511 keV line, and extended emission along the Galactic disk is observed now with a high significance (12σ), however this emission has a very low surface brightness in comparison to the Galactic bulge. These observations confirm that the observed morphology of the 511 keV line is unlike emission at any other wavelength. This is particularly apparent when comparing the disk 511 keV line intensity to the diffuse gamma-ray continuum emission from the Galactic disk (Bouchet et al., 2011), which is clearly detected.

The disk of the Galaxy is represented in the Siegert et al. (2016b) best fit model by a two-dimensional Gaussian first described in Skinner et al. (2015). The disk has a a longitude extent of 60^{+10}_{-5} degrees and a latitude extent of $10.5^{+2.5}_{-1.5}$ degrees. The disk model is somewhat sensitive to the modelling of the central Galaxy, however the flux from the disk region is only weakly dependent on the size of the disk.

The best fitting model for the Galactic bulge emission is two two-dimensional Gaussians, with the 'narrow bulge' (NB) component centered at $(l, b) = (-1.25^\circ, -0.25^\circ)$ with Gaussian widths of $(\sigma_l, \sigma_b) = (2.5^\circ, 2.5^\circ)$, and the 'broad bulge' (BB) component is centered at

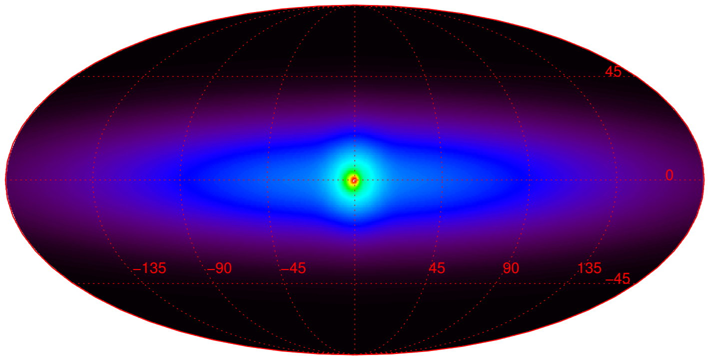

Figure 2.10: Positron annihilation radiation distribution from 11 yrs of SPI data from Siegert et al. (2016b). The bulge glows brightly with positron annihilation. The extended disk component, which has a large scale height in the best fit model, is clearly visible.

$(l, b) = (0^\circ, 0^\circ)$, extending to $(\sigma_l, \sigma_b) = (8.7^\circ, 8.7^\circ)$, based on Skinner et al. (2015).

Finally, an additional emission component is found coincident with the Galactic Center. This Galactic Center source (GCS) was first described in Skinner et al. (2015) and was found to be distinct from the central cusp of the Galactic bulge component. In the spatial model of Siegert et al. (2016b), the GCS is detected as a distinct component with 5σ significance. Due to the instrumental spatial resolution of SPI/*INTEGRAL*, it is not possible to distinguish whether the GCS is pointlike, or extended by $\sim 2^\circ$. The source is not variable on timescales > 30 days. The properties of the best fir morphology model are described in Table 2.1.

2.6.3 Spectra

The morphology of the observed positron annihilation in the Milky Way tells only part of the complex story we must understand in order to find the source of Galactic positrons. Understanding the spectrum is equally important. As previously mentioned, the spectrum of positron annihilation encodes a large amount of information about positron annihilation sites and can also encode some information about the origin of the positrons.

The gamma-ray spectrum of each component of the morphological models can be used to infer the annihilation conditions of the positrons. The positron annihilation spectrum is typically described by four parameters (e.g. Siegert et al. (2016b)): the 511 keV line intensity (I_{511}), the width of the line characterised as kinematic broadening (Γ), and the centroid shift (which can be interpreted as Doppler-shift from bulk motion ($\Delta E_0 = E_{\text{peak}} - 511\,\text{keV}$)), and the ortho-positronium continuum intensity (I_{oPs}). These measurements can be used to infer the fraction of positrons annihilating via positronium formation, f_{Ps}. If a fraction f_{Ps} of the positrons annihilates via positronium formation, ortho-positronium continuum will have an integrated intensity of

$$I_{\text{oPs}} \propto \frac{3}{4} 3 f_{\text{Ps}}, \tag{2.15}$$

where the 3/4 factor originates from the spin degeneracy of positronium meaning ortho-positronium is formed 3/4 of the time, and the additional factor of 3 from the fact three photons contribute to the observed intensity. The remaining fraction, $1 - f_{\rm Ps}$ will annihilate directly to two photons. These photons, combined with the annihilation via para-positronium give a narrow line intensity of

$$I_{511} \propto 2(1 - f_{\rm Ps}) + \frac{1}{2} f_{\rm Ps} \tag{2.16}$$

Thus by measuring the relative intensities $I_{\rm oPs}$ and I_{511}, the positronium fraction $f_{\rm Ps}$ can be determined using the equation

$$f_{\rm Ps} = \frac{8 I_{\rm oPs}/I_{511}}{9 + 6 I_{\rm oPs}/I_{511}} \tag{2.17}$$

The parameters that describe the annihilation spectrum can be compared to simulations of positron annihilation in different ISM conditions. This allows one to determine information about the annihilation conditions of the positrons. In particular, the inferred temperature and ionization fraction of the ISM at the positron annihilation sites provide information about where positrons annihilate (Churazov et al., 2005; Guessoum et al., 2005; Jean et al., 2006).

This analysis, like the analysis of the morphology, is somewhat dependent on the annihilation simulations and models used. The first detailed analysis of the positron annihilation spectrum with INTEGRAL data was performed by Churazov et al. (2005) and Jean et al. (2006). In those works it was found that the spectrum could be explained by positrons annihilating in a single phase of the warm, partially ionized phase (50 per cent warm ionized medium, 50 per cent warm neutral medium).

It was also found that the spectrum could be fit equally well by positrons annihilating in a multiphase ISM (Churazov et al., 2005). However, there is a strong constraint on the fraction of positrons annihilating in either the hot ionized phase, or cold molecular phase, based on the linewidth of the 511 keV line (see Table 3.1). No more than 10 per cent of positrons can annihilate in either the hot ionized medium or cold molecular medium - if they do so, the linewidth of the 511 keV line will be too broad to explain the observations. This observation is consistent with the scale height of the signal, as most of the molecular gas in the galaxy is confined to the thin disk of the galaxy.

The positron annihilation spectrum only encodes information about the positron annihilation sites. In Churazov et al. (2011), the impact of the radiative cooling of the ISM on the annihilation spectrum was investigated. In that work, the annihilation spectrum from the 6 years of *INTEGRAL* observations was analysed to determine the ISM conditions where and when the positrons would annihilate. It was found that the annihilation spectrum observed by *INTEGRAL* could be well described by the annihilation of positrons that originate in the hot, ionized phase of the ISM (with $T_{\rm init} \sim 3 \times 10^4 - 2 \times 10^6$ K).

In this scenario, plasma with initial temperatures in this range is able to radiatively cool to $\sim 10^4$ K before the positrons lose their initial kinetic energy and slow down to ~ 100 eV and annihilate. This results in an annihilation spectrum indistinguishable from that of positrons annihilating in the warm, partially ionized medium described in Churazov et al. (2011) and

Jean et al. (2006). The possibility that adiabatic cooling of the ISM may have a similar impact was noted by Churazov et al. (2011). In Chapter 6, I explore in detail how bulk motion and cooling of the ISM may transport positrons in the Milky Way and result in the observed annihilation spectrum.

The most recent observations of the positron annihilation spectrum suggest that the annihilation conditions of the positrons are relatively uniform across the Galaxy (Siegert et al., 2016b). The parameters describing the spectra from the Galactic disk, bulge and Galactic Center source are consistent with one another within errors (see Table 2.2). Further decomposition of the disk into regions of positive and negative longitude also indicate that the annihilation conditions within the disk do not significantly vary. The consistency of the annihilation signal strengthens the case for a single class of positron source, which produces positrons close to the warm, partially ionized phase of the ISM where the positrons are thought to annihilate.

Table 2.1: Spatial components of the 511 keV emission model in Galactic coordinates from Siegert et al. (2016b). A Longitude/Latitude FWHM of 0 is equivalent to a point source. The position of the Galactic Center Source has been chosen to coincide with Sgr A*

Component	Longitude position (deg)	Latitude position (deg)	Longitude FWHM (deg)	Latitude FWHM (deg)
Narrow bulge	-1.25	-0.25	5.75	5.75
Broad bulge	0.00	0.00	20.55	20.55
Disk	0.00	0.00	141.29	24.73
Galactic Center source	-0.06	-0.05	0.00	0.00

Table 2.2: Spectral components of the 511 keV emission model from Siegert et al. (2016b). One sigma errors are shown in brackets.

Component	Continuum flux density $10^{-5}\,\mathrm{ph\,cm^{-2}\,s^{-1}\,keV^{-1}}$	F_{511} $10^{-4}\,\mathrm{ph\,cm^{-2}\,s^{-1}}$	Γ_{511} keV	ΔE_0 keV	F_{oPs}	f_{oPs}
Bulge	0.27(20)	9.6(7)	2.59(17)	0.09(8)	61.4(7.6)	1.08(3)
Disk (total)	5.58(1.03)	16.6(3.5)	2.47(51)	0.16(18)	52.1(32.5)	0.90(19)
Galactic Center source	0.06(5)	0.8(2)	3.46(64)	-0.27(31)	2.8(1.8)	0.94(19)
Galaxy total	8.79(85)	27.4(3)	2.61(23)	0.15(9)	116.3(29.3)	0.99(7)

Chapter 3

The physics of the Milky Way positron annihilation signal

> If there's any real truth, it's that the entire multidimensional infinity of the Universe is almost certainly being run by a bunch of maniacs.
>
> Douglas Adams

3.1 Positron annihilation

Positrons undergo annihilation when they interact with electrons - in this process, the particles interact via exchange of virtual photons and are converted into energy in the form of gamma rays. The electrons that positrons interact with may be free particles, or they may be bound to atoms or molecules.

3.1.1 Direct annihilation with free electrons

When positrons interact with electrons, they may undergo 'direct annihilation'. In this process, a single, isolated positron interacts with a single, isolated electron. The energy released by this interaction is $2 \times 511\,\mathrm{keV}$ if both particles are at rest (the combined rest mass energy of the positron and electron). The total annihilation cross-section for direct annihilation of relativistic positrons was computed by Dirac before the experimental discovery of the positron, or the observation of positron-electron annihilation,

$$\sigma_d = \pi r_e^2 \frac{1}{\beta^2\gamma(\gamma+1)}\left[\left(\gamma + 4 + \frac{1}{\gamma}\right)\ln(\gamma + \sqrt{\gamma^2-1}) - \beta(\gamma+3)\right], \tag{3.1}$$

where γ is the Lorentz factor for a positron with kinetic energy w, $\beta = v/c$, and r_e is the classical electron radius (Dirac, 1930). In the low-energy, non-relativistic limit where $\beta \ll 1$, it is also important to take into account Coulomb corrections for the electrostatic interaction between the positron and electron (Crannell et al., 1976; Gould, 1989), thus the cross-section

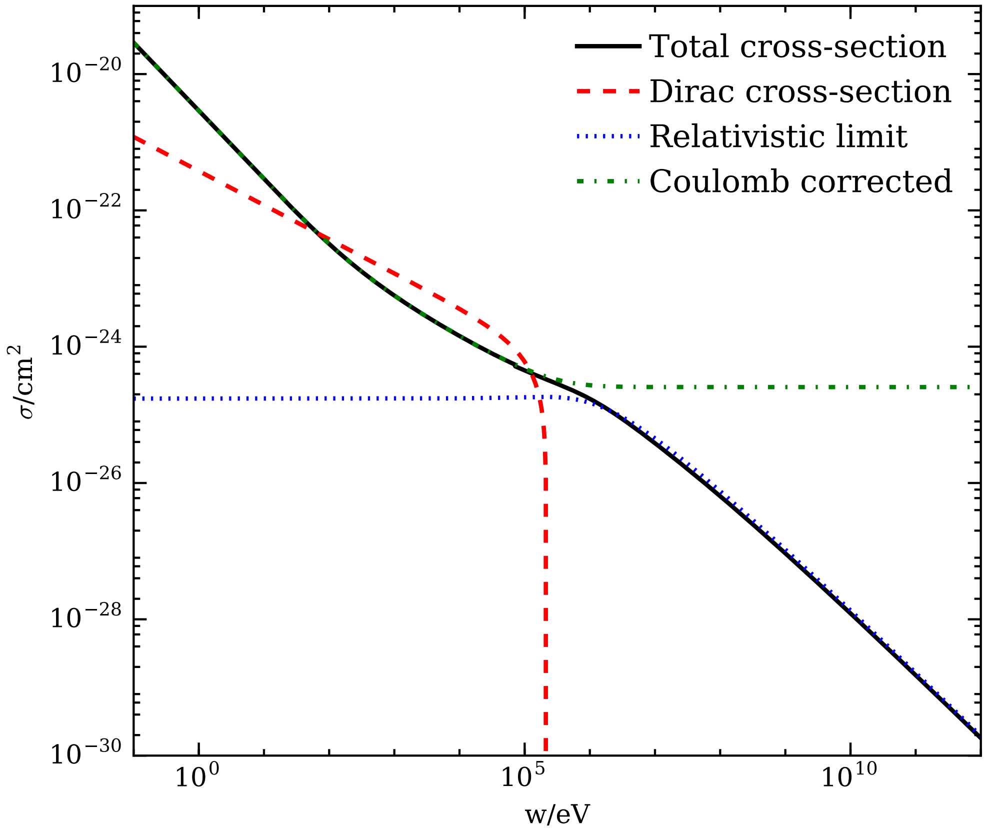

Figure 3.1: Cross-section for positron annihilation via direct annihilation with free electrons as a function of positron kinetic energy.

is given by

$$\sigma_d = \frac{2\pi^2 r_e^2 \alpha}{\beta^2(1-\exp(-2\pi\alpha/\beta))}, \tag{3.2}$$

where α is the fine structure constant. In the ultra-relativistic limit, $\beta \rightarrow 1$, and the cross-section simplifies to

$$\sigma_d = \pi r_e^2 \frac{\ln(2\gamma)}{\gamma}. \tag{3.3}$$

The dependence of the direct annihilation cross-section on positron energy is shown in Figure 3.1.

The gamma ray spectrum resulting from direct annihilation of positrons with electrons can vary depending on the relative velocities of the two species. In the case of positron annihilation in the interstellar medium, it is important to consider the interaction of a high-energy

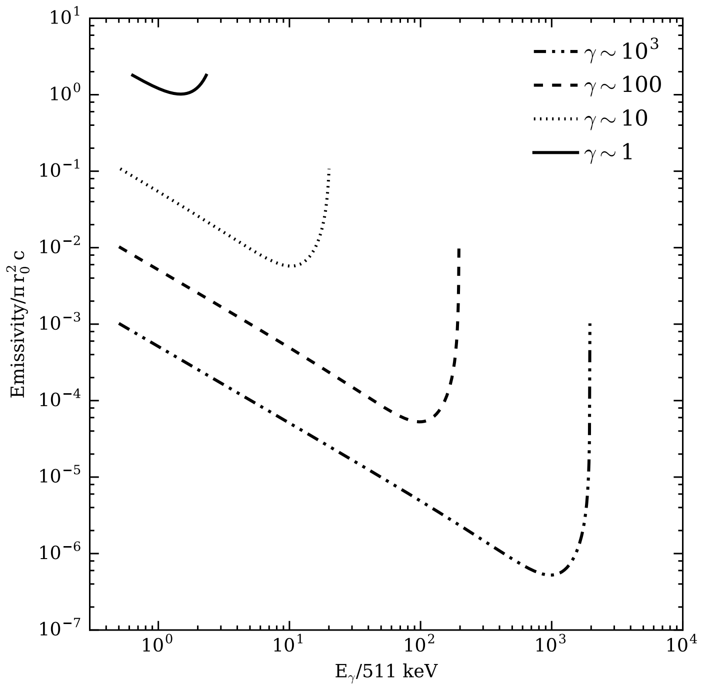

Figure 3.2: Gamma ray emissivity from annihilation of monoenergetic populations of high-energy positrons.

positron with almost stationary electrons.

In this case, the gamma ray emissivity from the annihilation with a high-energy positron with $\gamma_+ = w_e + /m_e c^2$ and dimensionless momentum $p_+ = \sqrt{\gamma_+ - 1}$ with thermal electrons with a density of n_e is given by Aharonian and Atoyan (1981)

$$q_{\text{ann}} = \frac{\pi r_0 c n_e}{\gamma_+ p_+} \left[\left(\frac{\epsilon_\gamma}{\gamma_+ + 1 - \epsilon_\gamma} + \frac{\gamma_+ + 1 - \epsilon_\gamma}{\epsilon_\gamma} \right) + 2\left(\frac{1}{\epsilon_\gamma} + \frac{1}{\gamma_+ + 1 - \epsilon_\gamma} \right) - \left(\frac{1}{\epsilon_\gamma} + \frac{1}{\gamma_+ + 1 - \epsilon_\gamma} \right)^2 \right], \quad \frac{1}{2}(\gamma_+ + 1 - p_+) \leqslant \epsilon_\gamma \leqslant \frac{1}{2}(\gamma_+ + 1 + p_+) \tag{3.4}$$

for photon energies $\epsilon_\gamma = E/m_e c^2$. The emissivity spectrum for different monoenergetic positron populations is shown in figure 3.2.

In the limit that the positron annihilates at rest with a stationary electron, the spectrum is a Dirac delta function. However, thermal broadening due to the motion of the center of mass of the positron-electron pair in astrophysical environments, where neither the positron nor the electron will be 'at rest' leads to a linewidth of $\Gamma_d = 1.1\sqrt{T_4}$ keV, where T_4 is the electron temperature in units of 10^4 K (Crannell et al., 1976).

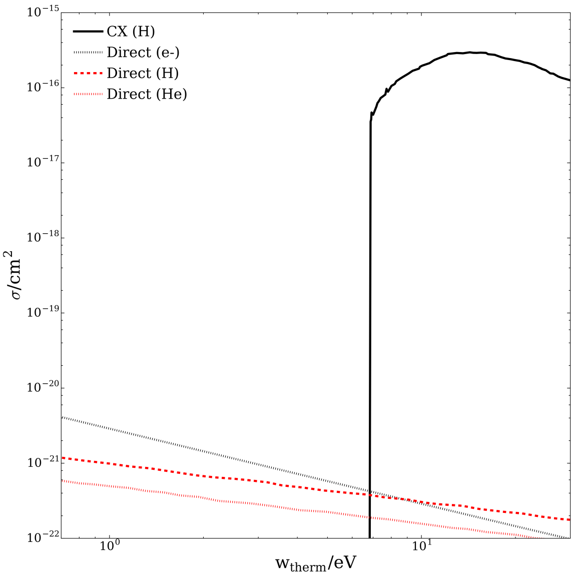

Figure 3.3: Cross-sections for annihilation of positrons with free electrons (black dotted), and electrons bound to hydrogen atoms and helium atoms. Also shown for comparison is the cross-section for charge exchange with hydrogen.

3.1.2 Direct annihilation with bound electrons

Direct annihilation with bound electrons can also occur. In this case, for positrons with very low energy, the bound electron has a larger cross-section than a free electron at energies $> 10\,\mathrm{eV}$ (Figure 3.3). The interaction between the positron and the electron occurs within the atomic potential. Consequently, the charge of the atomic nucleus 'screens' some fraction of the charge of the electron with which the positron is interacting. Thus, the positron interacts with an electron with an effective charge, or Z_{eff}.

The cross-section for direct annihilation with bound electrons of an atom with effective charge Z_{eff} is

$$\sigma_b = Z_{\mathrm{eff}} \alpha^3 \pi r_0^2 \frac{\sqrt{2 m_e w}}{\hbar} \tag{3.5}$$

where α is the fine structure constant, $\hbar = h/2\pi$ is the reduced Planck constant, and r_0 is the classical electron radius and w is the kinetic energy of the positron (Bhatia et al., 1974, 1977).

The cross-section for direct annihilation with bound electrons is thought to be important for interactions of positrons at energies $w < 6.8\,\mathrm{eV}$ (Guessoum et al., 2005). Below this energy threshold, positrons cannot undergo charge exchange with hydrogen and helium. As thermalized positrons in the cold ISM phases will have energies $w < 1\,\mathrm{eV}$, direct annihilation with bound electrons may occur in these conditions as there will be few free electrons as ionization fractions are expected to be low. The linewidth of the line that results from the direct annihilation of positrons with bound electrons can be estimated using the same formula above for direct annihilation.

3.1.3 Charge exchange

The most commonly observed annihilation channel for positrons in nature is charge exchange (Figure 3.4). In this interaction, a positron can interact with bound electrons and form positronium. This interaction differs from direct annihilation as the positron is required to have enough energy to exceed the positronium formation threshold of the atom, $w_{e+} > w_{IP} - w_{Ps}$, where w_{IP} is the ionization potential of the atom, and $w_{Ps} = 6.8\,\text{eV}$, the binding energy of positronium. For hydrogen, the minimium energy a positron must have to form positronium is 6.8 eV. The charge exchange cross-section peaks around 10 eV. The charge exchange cross-sections for hydrogen and helium are shown in Figure 3.3.

The positronium formation threshold differs for different atoms depending on the binding energy of the valence electron, however in most existing simulations of positron microphysics, only interactions with hydrogen, helium and free electrons are considered (e.g. Bussard et al. (1979); Wallyn et al. (1994); Guessoum et al. (2005); Jean et al. (2009)). As a result, a common claim in the literature is that positrons will not undergo charge exchange below 6.8 eV.

Charge exchange cross-sections are computed both theoretically, typically using 'close-coupling' calculations, or by experiment in which the positron scattering cross-section for a given atom is investigated. Cross-sections for charge exchange to form positronium have been computed using various methods for hydrogenic atoms (atoms with a single valence electron), noble gases, and a number of molecules (Campeanu et al., 1987; Bailey et al., 2015; Kauppila et al., 1981; Machacek et al., 2013; Moxom et al., 1996; Weber et al., 1994; Stein et al., 1978; Zhou et al., 1997; Laricchia et al., 2008; Humberston, 1979; Sullivan et al., 2001; Walters, 1988; Kernoghan et al., 1996; Jones et al., 1993; Murtagh et al., 2005; Charlton et al., 1983; Charlton and Humberston, 2000).

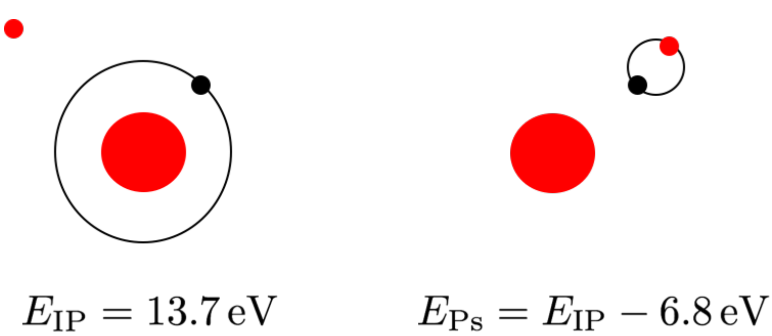

Figure 3.4: Charge exchange with neutral hydrogen. The residual kinetic energy of the positronium bound state is the positron energy less the difference between the binding energy of positronium, and the binding energy of the electron to the hydrogen atom.

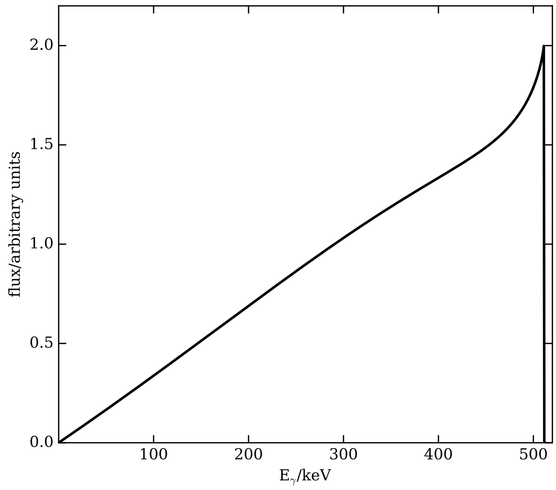

Figure 3.5: Gamma ray spectrum resulting from annihilation of positronium via orthopositronium formation

The gamma ray spectrum resulting from the annihilation of positronium consists of two components. The first is known as the orthopositronium continuum or the 'three-photon continuum'. This component is broad and extends to energies below 511 keV. The spectrum was first described by Ore and Powell (1949). This spectrum, which can be described with the equation

$$\frac{dF_{\rm oPs}}{dE} = 2\left[\frac{E(m-E)}{(2m-E)^2} - \frac{2m(m-E)^2}{(2m-E)^3}\ln\left(\frac{m-E}{m}\right) + \frac{2m-E}{E} + \frac{2m(m-E)}{E^2}\ln\left(\frac{m-E}{m}\right)\right], \tag{3.6}$$

where $m = m_e c^2$, is the result of the annihilation of the orthopositronium configuration of positronium, where an odd number of photons (with the highest probability being the emission of three photons) with a total energy of 1022 keV are released. The orthopositronium continuum is shown in Figure 3.5.

The second component of the positronium spectrum is the 511 keV line resulting from the annihilation of parapositronium. This spectral component is Lorentzian and has a natural linewidth of $\Delta E_{\rm pPs} = 5.3\,\mu$eV, far below the instrumental resolution of even modern gamma ray detectors. In astrophysical environments, where the annihilating positronium has some residual kinetic energy, the linewidth of this component becomes thermally broadened and appears Gaussian, with the linewidth determined by the kinetic energy of the positronium.

3.1.4 Radiative recombination

While positrons cannot undergo charge exchange with hydrogen and helium to form positronium below 6.8 eV, it is still possible for positrons to form positronium. Radiative recombination (sometimes referred to as 'radiative combination', see Guessoum et al. (2005)) of positrons with free electrons can produce positronium. This process is analogous to the formation of hydrogen via radiative recombination of electrons and protons.

The cross-section for radiative recombination was calculated by Crannell et al. (1976) and Gould (1989), however it can be estimated by scaling the radiative recombination rate for hydrogen by the reduced mass of positronium (Sutherland, private comm.). The cross-section for radiative recombination as a function of positron energy is shown in Figure 3.6, with the cross-section for direct annihilation and charge exchange with hydrogen shown for comparison.

The same formula for the thermal broadening of the emission from the direct annihilation of positrons with electrons can be applied to the parapositronium line from radiative recombination. The width of the annihilation line that results from the annihilation of parapositronium was calculated by Crannell et al. (1976). Thermal broadening due to the motion of the center of mass of the positron-electron pair leads to a linewidth of $\Gamma_{rr} = 1.1\sqrt{T_4}\,\mathrm{keV}$, where T_4 is the temperature in units of 10^4 K.

The process of radiative recombination results in the emission of recombination lines in both the infra-red (Ellis and Bland-Hawthorn, 2018) and at radio wavelengths, in analogy with hydrogen. An upper limit on the positronium recombination rate at the Galactic center was made by Anantharamaiah et al. (1989) using the VLA. This upper limit is consistent with

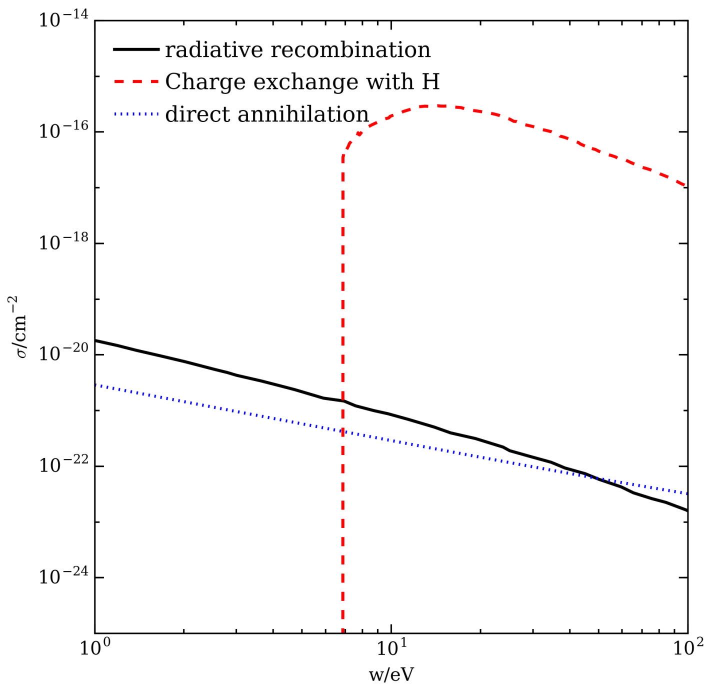

Figure 3.6: Positron annihilation cross-sections, including annihilation via radiative recombination. This cross-section dominates over direct annihilation for annihilation with free electrons for energies $w < 80\,\mathrm{eV}$.

the positron annihilatation rate observed by *INTEGRAL*. An improved upper limit could be arrived at with next-generaton telescopes such as the Square Kilometer Array, providing an opportunity to investigate positron annihilation in the Milky Way using multi-wavelength observations.

3.1.5 Annihilation on organic molecules and dust grains

The Galaxy contains an estimated $3 \times 10^7\,M_\odot$ of dust - $0.5 - 1$ per cent of the total mass of gas (Kruegel, 2003; Guessoum et al., 2005). The abundance and distribution of dust correlates with the abundance and distribution of cold H_2 and CO gas. Dust is produced by massive stars and CCSNe, and is comprised of material which can be broadly classified as follows:

- large particles of amorphous carbon and silicates (Mg_2SiO_4 or Fe_2SiO_4), with radii of $20\,\text{nm} - 0.3\,\mu\text{m}$,
- smaller grains with radii $1\,\text{nm} - 10\,\text{nm}$ composed of graphite, making up around 10 percent of amorphous carbon grains, and
- polycyclic aromatic hydrocarbons (PAHs) - large aromatic molecules which account for $3 - 6$ per cent of large grains in abundance.

Positrons may undergo a number of different interactions with dust grains. Interactions considered in literature on positron astrophysics (e.g. Guessoum et al., 2010, 2005)

- positron re-emission, where the positron is captured by the grain, deposits some kinetic energy, and is subsequently ejected from the grain,
- positron backscattering, in which the positron is scattered by the grain, losing some kinetic energy in the process
- positronium formation in-grain, where positrons undergo charge exchange with particles within the dust grain and annihilation via positronium formation proceeds inside the grain,
- and positronium ejection, where positrons undergo charge exchange to form positronium within the grain, but positronium is ejected from the grain and the positron annihilates in the ISM.

The impact of these processes on the positron annihilation spectrum were considered in detail in Guessoum et al. (2010) and Guessoum et al. (2005), where the characteristic linewidths of positron annihilation on dust were calculated. These linewidths are shown in Table 3.1.

3.2 Positron annihilation in-flight

There is a significant probability that positrons will annihilate before they lose all their energy and thermalize. This process is known as annihilation 'in-flight'. The probability a positron with initial energy w_0 will annihilate before reaching an energy w is (e.g. Prantzos et al. (2011))

$$P(w_0, w) = 1 - \exp\left[\int_w^{w_0} dw' \frac{\sum_T n_T \sigma_T(w')\beta(w')c}{|dw/dt(w')|}\right], \tag{3.7}$$

where n_T is the density of annihilation target T, $\sigma_T(w')$ is the annihilation cross-section of target T at energy w', $\beta(w')c$ is the relativistic velocity of the positron and $|dw/dt(w')|$ is the

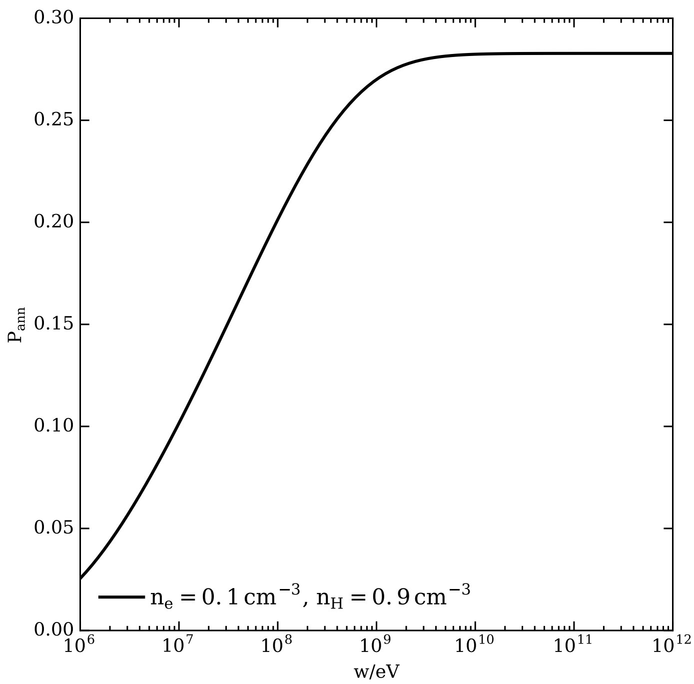

Figure 3.7: Probability a positron annihilates in-flight via direct annihilation as a function of initial positron energy for electron density $n_e = 0.1\,\mathrm{cm}^{-3}$ and neutral hydrogen density $n_H = 0.9\,\mathrm{cm}^{-3}$. Probability of annihilation increases as the initial positron energy increases due to the increased lifetime of the positron in the ISM.

energy loss rate of the positron at energy w', which is typically also a function of n_T.

Two forms of annihilation in flight occur: direct annihilation in flight, which occurs when positrons have kinetic energies $>$ MeV, and positronium formation in-flight, which typically occurs when positrons have kinetic energies between $10\,\mathrm{eV} - 500\,\mathrm{eV}$.

The former process, direct annihilation in flight, enables us to put a strong constraint on the injection energies of positrons (Aharonian and Atoyan, 1981; Beacom and Yüksel, 2006; Sizun et al., 2006). Direct annihilation in flight occurs because positrons with kinetic energies between $1 - 1000\,\mathrm{MeV}$ lose energy relatively slowly, and the probability that they find an electron to interact with increases quickly with the increased time the positron spends in the ISM. Above 1 GeV the fraction of positrons undergoing direct annihilation in flight plateaus because the inverse Compton and synchrotron losses cause positrons with very high energies to lose energy so quickly that the lifetime of a 10 GeV positron is not considerably longer than that of a 1 GeV positron. The probability of a positron annihilating via direct annihilation in flight as a function of its initial kinetic energy is shown in Figure 3.7. As these positrons annihilating in flight are relativistic, the gamma ray spectrum they produce will be that of relativistic positrons annihilating with stationary or thermal electrons, unless the positrons are annihilating in an environment with a large population of relativistic electrons.

Positronium formation in-flight, on the other hand, occurs at low positron energies $< 200\,\text{eV}$ (Bussard et al., 1979; Wallyn et al., 1994; Guessoum et al., 2005). At these energies, the cross-section for charge exchange with neutral atoms becomes rather large and thus the probability that a positron undergoes charge exchange increases very quickly as the energy of the positron decreases. It is thought that a large proportion of Galactic positrons annihilate via positronium formation in flight (Churazov et al., 2005; Jean et al., 2006; Churazov et al., 2011; Siegert et al., 2016b). Calculating the fraction of positrons that form positronium in flight must be calculated via Monte Carlo methods. This is because the processes of atom excitation and ionization compete strongly with the positronium formation process and it becomes highly deterministic. These calculations can also be used to determine the linewidth of the para-positronium line, which is broadened by the kinetic energy of the annihilating positrons.

Positronium formation in flight fractions are typically presented as a function of the ionization fraction of the plasma in which the positron propagates, for fixed proton densities representing either typical ISM densities, or that of Solar flares (Bussard et al., 1979; Wallyn et al., 1994; Guessoum et al., 2005; Murphy et al., 2005). Historically, this is because these are the two environments in which positronium formation in flight typically occurs. However, using these fixed densities is somewhat artificial and there is great scope for the creation of large grids of models that take into account a greater range of plasma densities and conditions.

3.2.1 Annihilation linewidths

The linewidth of the positron annihilation line gives information about the ISM conditions at the annihilation site (A summary of ISM conditions typically found in the Galaxy can be found in Table 3.1). The annihilation line isn't truly Gaussian due to the ortho-positronium continuum contribution, but can be approximated as such. The width of the line is determined by the broadening due to the residual kinetic energy of the annihilating positron. Consequently, annihilation in-flight, when the positron still typically as a significant amount of kinetic energy ($> 50\,\text{eV}$) results in a broader emission line than annihilation after thermalization, which occurs at energies of $< 5\,\text{eV}$ for temperatures of $\sim 10^4\,\text{K}$.

Para-positronium linewidths were calculated most recently by Monte Carlo simulation by Guessoum et al. (2005) (Table 3.1), however the positron annihilation, excitation and ionization cross-sections used in Guessoum et al. (2005) work have recently been superseded by more modern, accurate measurements (e.g. Kadyrov and Bray (2016)). The cross-sections utilized in this thesis are listed in previous sections.

Table 3.1: Effective linewidths (keV) of the para-positronium or direct annihilation line at 511 keV for annihilation in different ISM conditions, adapted from Guessoum et al. (2005). Media described are the Molecular Medium (MM), Warm Neural Medium (WNM), Warm Ionized Medium (WIM) and Hot Ionized Medium (HIM)

Process/medium	MM/keV ($T \sim 10-100\,\mathrm{K}$)	WNM/keV ($T \sim 10^4\,\mathrm{K}$)	WIM/keV ($T \sim 10^4\,\mathrm{K}$)	HIM/keV ($T \sim 10^8\,\mathrm{K}$)
Charge exchange (H in-flight)	5.8	5.8	no neutral H	no neutral H
Charge exchange (He in-flight)	7.4	7.4	8.7	no neutral He
Charge exchange (H thermalized)	below CX theshold	1.16	no neutral H	no neutral H
Charge exchange (He thermalized)	below CX theshold	1.22	no neutral He	no neutral He
Direct annihilation (H)	1.56	1.56	no neutral H	no neutral H
Direct annihilation (He)	2.50	2.50	2.50	no neutral He
Direct annihilation (e-)	no free e-	no free e-	0.98	11
Radiative recombination	no free e-	no free e-	0.98	11
Annihilation on dust	1.4-2.0	1.4-2.0	1.4-2.0	1.4-2.0

3.3 Positron energy losses

Although the positrons annihilating to produce the observed gamma ray line in the Galaxy are constrained to enter the ISM at only mildly relativistic energies ($< 3 - 7\,\mathrm{MeV}$), they must still lose the majority of their energy before they reach energies at which they can annihilate. A fraction of positrons annihilate in-flight, however most positrons forming positronium in-flight in the Galaxy have energies $\sim 100\,\mathrm{eV}$.

Positrons lose energy via interactions with all components of the interstellar medium: neutral atoms, molecules, ions, electrons, photon fields, and the magnetic field. The rate of positron energy losses depends on the density of the component of the ISM the positron is interacting with and the energy of the positron. Different energy loss processes dominate for different positron kinetic energies.

The highest energy positrons ($w > 10\,\mathrm{GeV}$) lose their energy predominantly through Inverse Compton (IC) scattering with cosmic microwave background photons and photons from the interstellar radiation field. In this case, the sum of the photon energy and the positron kinetic energy in the positron rest frame is much greater than the rest mass of the positron, so scattering occurs in the Thomson scattering regime. The energy loss rate of the positron interacting with an isotropic radiation field in this regime can be calculated as

$$\left.\frac{dw}{dt}\right|_{\mathrm{IC}} = -\frac{4}{3}\sigma_T c u_{\mathrm{rad}}\gamma^2\beta^2 \tag{3.8}$$

$$= -2.6 \times 10^{-14} u_{\mathrm{rad}}\gamma^2\beta^2\,\mathrm{eV\,s^{-1}} \tag{3.9}$$

where u_{rad} is the energy density of the radiation field in $\mathrm{eV/cm^3}$, γ is the Lorentz factor for a positron with kinetic energy w, and $\beta = v/c$ is the velocity of the positron as a fraction of the speed of light (Blumenthal and Gould, 1970). The energy density of the radiation field depends on the location of the positron. CMB radiation dominates in the outer regions of the galaxy and in the Galactic halo where the $u_{\mathrm{rad}} \sim 0.23\,\mathrm{eV\,cm^{-3}}$, whereas the radiation field becomes harder toward the Galactic center, where $u_{\mathrm{rad}} \sim 11\,\mathrm{eV\,cm^{-3}}$ (e.g. Prantzos et al. (2011)).

Very high energy positrons also undergo synchrotron losses as they gyrate along magnetic field lines in the Galaxy. The synchrotron losses for a positron of energy w is given by

$$\left.\frac{dw}{dt}\right|_{\mathrm{sy}} = -\frac{e^4\gamma^2\beta^2B^2}{6\pi\epsilon_0 m^2 c}\sin^2(\theta) \tag{3.10}$$

$$= -9.9 \times 10^{-16} B^2\gamma^2\beta^2\sin^2(\theta)\,\mathrm{eV\,s^{-1}} \tag{3.11}$$

where B is the strength of the magnetic field in μG and θ is the angle between the velocity vector of the positron as it gyrates around the magnetic field line, and the magnetic field (the pitch angle) (Blumenthal and Gould, 1970). The small gyroradii of the positrons, especially those with energies $< 1\,\mathrm{GeV}$ means they tend to resonantly interact with the smaller scale turbulence as opposed to the large scale magnetic field structure of the Galaxy (see Chapter 7, and Jean et al. (2009); Martin et al. (2012); Alexis et al. (2014)) and the pitch angle can be averaged to derive the average energy losses of positrons due to synchrotron interactions, i.e. $\langle \sin(\theta) \rangle = 2/3$. In general, IC losses dominate over synchrotron losses, however in highly magnetized environments (such as close to compact objects like neutron stars), and

$B > 6.8\mu G\sqrt{u_{\rm rad}/(1\,{\rm eV\,cm^{-3}})}$ synchrotron losses dominate.

At lower energies ($1 - 10\,$GeV) Bremsstrahlung or 'braking radiation' is the dominant energy loss process for typical ISM conditions. Bremsstrahlung occurs when positrons are accelerated and deflected by the electric field of nuclei or ambient electrons. The rate of the energy loss depends on the properties of the target causing the deflection: its mass, charge and the density. The rate at which positrons lose energy via Bremsstrahlung is equivalent to that for relativistic electrons. A good approximation for Bremsstrahlung losses of positrons in a neutral gas of atom species Y with density n_Y is

$$\left.\frac{dw}{dt}\right|_{\rm br_0} = A_Y n_Y \gamma, \tag{3.12}$$

where $A = -4.1 \times 10^{-10}$ for Y = hydrogen, and $A = -1.1 \times 10^{-9}$ for Y = helium (Ginzburg, 1979). For an ionized gas of atoms with atomic number Z is (Ginzburg, 1979)

$$\left.\frac{dw}{dt}\right|_{\rm br_+} = -3.6 \times 10^{-11} Z(Z+1) n_Y \gamma \left(\ln(2\gamma) - \frac{1}{3} \right), \tag{3.13}$$

where the logarithmic term becomes important because the nucleus is no longer screened from the positrons by the electrons.

Positrons with energies $w < 1\,$GeV lose energy predominantly via the ionization of atoms in the ISM, and Coulomb scatterings with free electrons. While the latter is a continuous process, the former is discrete. It can, however, be formulated continuously, as it is impractical to track particles through the millions of ionization collisions they may undergo in their lifetimes.

In Coulomb interactions where positrons have energies which are much greater than the average thermal energy of the target electrons ($w > 10kT$), the target electrons appear at rest. The rate of e-e Coulomb collisions was calculated by Dermer (1985) and can be approximated as:

$$\left.\frac{dw}{dt}\right|_{\rm Cou} = -7.7 \times 10^{-9} \frac{n_e}{\beta} (\ln(\gamma/n_e) + 73.6)\,{\rm eV\,s^{-1}} \tag{3.14}$$

For positrons approaching thermal energies ($w < 10kT$), target electrons can no longer be considered to be stationary targets. In this case, the full Coulomb energy loss rate which takes into account the energy distribution of the thermal electrons is used:

$$\left.\frac{dw}{dt}\right|_{\rm Cou} = 1.7 \times 10^{-8} \frac{n_e}{\beta} \ln\Lambda \left[\int_0^{w/kT} dx x^{1/2} \exp(-x) - (w/kT)^{1/2} \exp(w/kT) \right] {\rm eV\,s^{-1}} \tag{3.15}$$

where $\ln\Lambda = \ln[(\sqrt{kT/4\pi n_e e^2})/\max(2e^2/m_e u^2, \hbar/m_e u)]$ where n_e is the electron density, T is the ISM temperature, m_e is the electron mass, e is the charge of the electron and $u = \sqrt{2w/m_e} - \sqrt{8kT/\pi m_e}$ is the average thermal velocity of the electrons in the plasma (Huba, 2013).

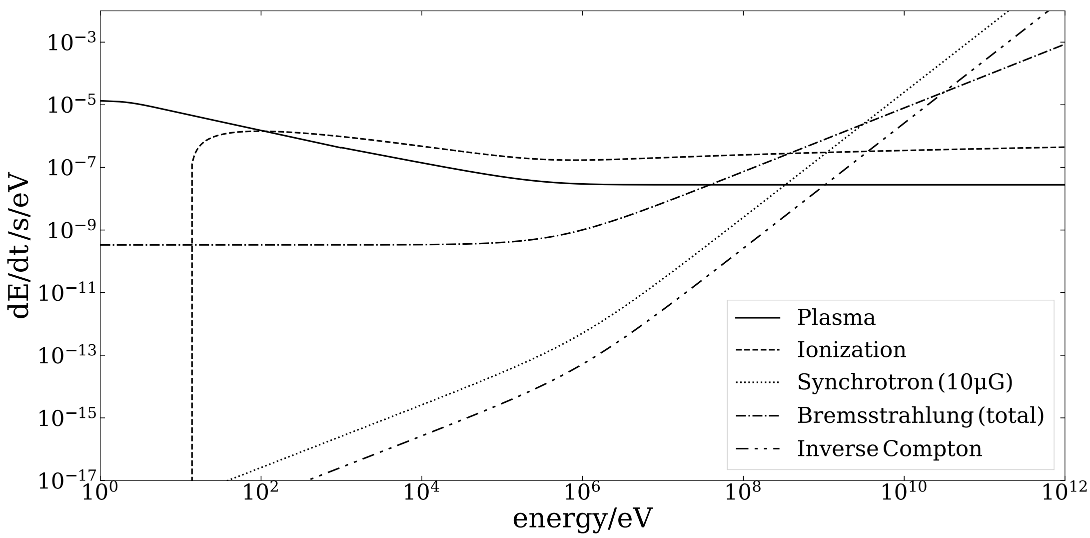

Figure 3.8: Energy loss rates for positrons of varying energy in a medium with $n_H = 1\,\mathrm{cm}^{-3}$, $X_H = 0.1$, $B = 10\,\mu$G, $u_{\rm rad} = 0.26\,\mathrm{eV\,cm}^{-3}$ and $T = 8000\,$K. Synchrotron and IC losses dominate at energies $w > 1\,$GeV whereas ionization and plasma losses dominate at energies $< 1\,$GeV.

For positrons with energies greater than $\sim$ keV, the inelastic collisions of positrons with atoms and molecules can be considered to be a continuous process. The ionization losses dominate over excitation losses and can be evaluated using the Bethe-Bloch formula:

$$\left.\frac{dw}{dt}\right|_{\rm ion} = -7.7\times10^{-9}\frac{n_0 Z}{\beta}\left[\ln\left(\frac{(\gamma-1)(\gamma\beta mc^2)^2}{2I^2}\right)+1/8\right]\mathrm{eV\,s}^{-1} \quad (3.16)$$

where n_0 is the density of neutral atoms, Z the atomic number and I is the ionization potential (Ginzburg, 1979).

For greatest accuracy below $\sim$ 500 eV, Monte Carlo simulations should be used to compute ionization losses as a positron can release a large fraction of its energy in a single interaction (Guessoum et al., 2005; Jean et al., 2009). Above this point, the Bethe-Bloch formula above works appropriately well.

The relative contributions to the positron energy loss rate for a fixed ISM composition are shown in Fig. 3.8. In reality, the ISM composition may change as a positron is transported through the Galaxy so the relative contributions of each energy loss process may depend on the ISM conditions at any point in time. However, for the positrons we observe annihilating in the Milky Way, the energy losses are dominated by the ionization and coulomb scattering losses as the particle propagates.

3.4 Astrophysical positron sources

Positrons are ubiquitous in astrophysical environments. Each class of astrophysical positron source produces positrons with different characteristic energies and in different yields.

3.4.1 Cosmic rays

The earliest established source of astrophysical positrons was arguably in cosmic rays (De Shong et al., 1964). Two different processes occur in cosmic rays to produce positrons. The first is known as p-p collisions. In this process, high energy cosmic ray protons (with energies $> 1\,\mathrm{GeV}$) collide with atomic nuclei in interstellar gas and molecular clouds. These processes are hadronic - i.e. they are associated with protons and heavier nuclei. These collisions initiate a shower of secondary particles composed of π^0, π^+ and π^-, and kaons.

The dominant channel for the production of secondary positrons is then the decay of the charged pions to antimuons and muon neutrinos. The antimuon subsequently decays to produce positrons, i.e.

$$\pi^+ \rightarrow \mu^+ + \nu_\mu \rightarrow e^+ + \nu_e + \bar{\nu}_\mu + \nu_\mu. \tag{3.17}$$

A very small fraction (~ 0.01 per cent) of π^+ may decay directly into positrons,

$$\pi^+ \rightarrow e^+ + \nu_e. \tag{3.18}$$

The positrons produced in these interactions will have high kinetic energies, $w \gg 10\,\mathrm{MeV}$, and a steep energy spectrum that typically peaks $\sim 1\,\mathrm{GeV}$ due to the high energies and rest masses of the parent cosmic ray pions.

There is also a non-negligible contribution to hadronic secondary positrons from the decay of charged kaons (K^+). Kaons may decay into muons, as with the charged pions, and the subsequent muon decay produces the secondary positrons:

$$K^+ \rightarrow \mu^+ + \nu_\mu \rightarrow e^+ + \nu_e + \bar{\nu}_\mu + \nu_\mu. \tag{3.19}$$

They may also decay into charged pions which proceed to decay as shown above,

$$K^+ \rightarrow \pi^+ + \pi^0 \rightarrow \mu^+ + \nu_\mu \rightarrow e^+ + \nu_e + \bar{\nu}_\mu + \nu_\mu + 2\gamma \tag{3.20}$$

where the additional gamma rays originate from the decay of the π^0 particle. A negligible fraction ($\ll 0.01$ per cent) of cosmic ray kaons decay directly into positrons. Cosmic ray positrons produced in the decay of kaons will have energies $w \gg 1\,\mathrm{GeV}$ due to the high mass of the parent kaon.

Seconday cosmic ray positrons may also be produced by pair production. Sufficiently energetic photon pairs can interact and produce electron-positron pairs,

$$\gamma\gamma \rightarrow e^+ + e^-, \tag{3.21}$$

if photon energies exceed $E_{\gamma\gamma} > 2m^2c^4/(1 - \cos\theta)$ where θ is the angle between the incoming photons. It is also possible that in a sufficiently strong magnetic field ($10^{12}\,\mathrm{G}$, such as in magnetars) positrons can be produced from a single photon (effectively via pair production off virtual photons constituing the electromagnetic field). The pair-production mechanism will be discussed in more detail in the section on compact sources, where it is most commonly thought to occur.

Information about the production rates of cosmic rays can be determined from both direct measurements made by space- and balloon-based experiments (e.g. Blasi, 2009; Battiston and AMS Collaboration, 2014), and observations of the gamma ray background as the acceleration and propagation of cosmic rays involve processes that produce high energy radiation (e.g. Strong et al., 2010, 2011). Modern experiments on the International Space Station measure the positron flux at Earth (Blasi, 2009; Battiston and AMS Collaboration, 2014). Depending on the experiment and the energy of the incoming particles, either the flux of positrons, or the positron fraction is measured. The positron fraction is expected to decrease sharply above 10 GeV if the detected cosmic ray positrons originate in secondary cosmic rays (Ibarra et al., 2014).

Observations from experiments such as AMS-02 (Battiston and AMS Collaboration, 2014) and PAMELA (Blasi, 2009), and measurements of the positron cosmic ray flux using the calorimeter experiments on the *FERMI* gamma-ray telescope (Abdollahi and Fermi-LAT Collaboration, 2017), and by Cherenkov telescopes such as HAWC (Hooper et al., 2017), have suggested an excess of cosmic ray positrons at these energies which cannot be explained by the production of secondary positrons (Figure 3.9). The origin of these positrons is currently unknown, however sources such as nearby pulsar wind nebulae such as Geminga and Monogem, or more exotic sources such as Dark Matter annihilation, have been proposed.

These cosmic ray positrons are detected directly at Earth. This is not the case of the annihilating positrons - they are detected only indirectly through their annihilation radiation. The injection energy of secondary CR positrons is very high, $\gg$ 10MeV. Consequently, up to 20% of these positrons are expected to annihilate directly in flight before reaching the thermal energies they would need to reach in order to annihilate and produce the 511 keV line (see figure 3.7).

This direct annihilation of high energy positrons will produce an excess of continuum emission above 511 keV (see figure 3.2). Constraints on this continuum emission from the INTEGRAL and COMPTEL missions indicate that the positrons annihilating to produce the 511 keV line must enter the ISM with kinetic energies no higher than $3 - 7$ MeV (Beacom and Yüksel, 2006). As the annihilation flux resulting from secondary cosmic rays is too low and in light of the constraint of the injection energies of the positrons, secondary cosmic ray positrons cannot make more than a negligible contribution to the population of annihilating positrons in the Galaxy.

3.4.2 Stellar nucleosynthesis

A source of positrons whose injection energies satisfy the constraints on the injection energies is naturally found in positrons which originate from the β^+ decay of radioactive isotopes synthesised by stars. β^+ unstable nuclei have too few neutrons to be stable, and β^+ decay can only occur if the difference between the masses of the parent and daughter nucleus is $\Delta m > m_e c^2$. The decay of a β^+ unstable parent nucleus X with A nucleons, Z protons and N neutrons occurs via the emission of a positron (e^+) and an electron neutrino (ν_e) to conserve

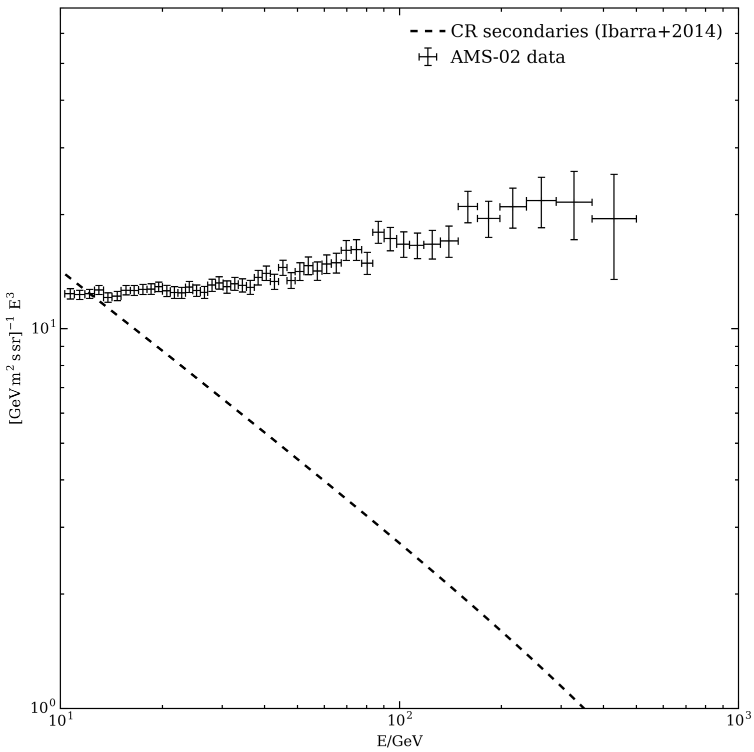

Figure 3.9: Comparison of the expected flux of CR positrons at Earth from Ibarra et al. (2014) with the observed flux of CR positrons from AMS-02 (Maurin et al., 2014). The observed excess of positrons at $> 100\,\mathrm{GeV}$ cannot be explained by CR secondaries

momentum, charge, and lepton number:

$$ {}^{A}_{Z}X_N \rightarrow {}^{A}_{Z-1} Y_{N+1} + e^+ + \nu_e. \quad (3.22)$$

The daughter nucleus Y has one fewer proton and one more neutron. Energy (Q) may also be released in the form of X-rays or gamma-rays as the decay product relaxes to the ground state. This high energy radiation can also be observed with gamma ray and X-ray telescopes.

β^+ unstable radioisotopes can be synthesised both during hydrostatic burning of stars, and explosively at the end of a stars' life. The various astrophysically important β^+ unstable radioisotopes and their expected positron yield and source distribution within the Milky Way are discussed below.

3.4.3 Explosive nucleosynthesis

3.4.3.1 ^{26}Al

^{26}Al is a β^+ unstable radioisotope of Aluminium with a half-life of $\sim 7.3 \times 10^5$ yr. It is synthesised by both massive stars (stars with zero-age main sequence masses $> 2\,M_\odot$) and asymptotic giant branch stars (AGB stars) during hydrostatic burning in the hydrogen burning shell of the star (Prantzos and Diehl, 1996), and also explosively in the C-Ne-O layers of the stellar interior during supernova explosions (Limongi and Chieffi, 2006). Stellar winds and the terminal supernova explosions of these stars eject ^{26}Al into the interstellar medium. ^{26}Al can be traced via the 1.8 MeV gamma ray photons emitted when the nucleus decays via β^+ emission. Thus one can trace the production of positrons from the decay of ^{26}Al via the 1.8 MeV gamma ray line in the Galaxy (Diehl et al., 1995; Diehl, 2006; Kretschmer et al., 2013).

Because massive stars live fast and die young, with lifetimes of only a few Myr, ^{26}Al is known to trace regions of active star formation. In particular, observations by the COMPTEL instrument by Knödlseder et al. (1999) show ^{26}Al gamma ray emission coincident with nearby OB associations (groups of young, hot, massive stars with spectral types O and B) Scorpius-Centaurus, Orion and Cygnus. More recent observations of ^{26}Al gamma rays made by SPI/INTEGRAL reveal the kinematic structure of the emission (Kretschmer et al., 2013). These observations suggest that ^{26}Al collects at the edges of superbubbles - large HII-filled cavities with radii $\sim$ kpc carved out of the ISM by stellar winds and supernova explosions - in the Galactic disk.

The spatial distribution of the 1.8 MeV gamma ray line can be used as a proxy for the spatial distribution of the annihilation of the positrons produced in the same decay (e.g. Churazov et al. (2011)), as positrons are thought to be confined relatively close to their sources (see Chapter 7). Furthermore, the flux of 1.8 MeV gamma rays can also be used to obtain a robust estimate of the positron flux associated with this morphology. Based on observations (Siegert et al., 2016b), the number of positrons produced in the decay of ^{26}Al is $\sim 4 \times 10^{42}\,\mathrm{s}^{-1}$, which can be interpreted as being in a steady state due to the long lifetime of the ^{26}Al nucleus and the short, $<$ Myr duty cycle of the events which produce it in the Milky Way. Thus, the decay of ^{26}Al can explain around 10% of the total positron annihilation rate in the Milky Way. .

In summary, ^{26}Al gamma-rays do not have same morphology as the 511 keV line from the galaxy, and moreover the ^{26}Al positron production rate can only explain ~ 10 per cent of the total Galactic positron luminosity. Thus, we must search for the source of the remaining positrons, particularly in the Galactic bulge.

3.4.3.2 ^{56}Ni

^{56}Ni is synthesised in supernova explosions during explosive carbon burning, and was first suggested as a potential souce of Galactic positrons in Colgate et al. (1980). The daughter nucleus of the ^{56}Ni decay, ^{56}Co, is β^{+} unstable. ^{56}Ni has a half-life of around 6 days, and ^{56}Co has a half-life of around 77 days and produces positrons with a branching ratio of about 20% (Nadyozhin, 1994).

The dominant production site of ^{56}Ni is ordinary themonuclear supernovae, or Type Ia supernovae. While the precise progenitors of these events are unknown, there is a general agreement that SNe Ia originate from the thermonuclear disruption of at least one carbon-oxygen white dwarf star (CO WD). There are a number of different scenarios for the progenitor configurations of these systems, which have historically been divided into single degenerate progenitors (one CO WD with a non-degenerate companion, e.g. Whelan and Iben (1973)) and double degenerate configurations (two WD stars in a close binary system, one of which is a CO WD, e.g. Webbink (1984)). It was thought that the single degenerate channel is dominant until around 2010 (Ruiter et al., 2009; Pakmor et al., 2010). More recently, the different scenarios for the progenitors of SNe Ia have been considered from the perspective of the mass of the WD as opposed to the type of donor responsible for pushing the accreting WD toward explosion. Some SNe Ia are thought to arise from sub-chandrasekar mass WDs, while others are more likely to arise from WDs that have approached the Chandrasekhar mass limit (Hillebrandt et al., 2013; Taubenberger, 2017; Maguire, 2017).

The yield of ^{56}Ni can be calculated using the lightcurves of SNe Ia, as the optical lightcurve is produced by the interaction of gamma ray photons produced by the decay of ^{56}Ni with the ejecta in the first ten days following the peak of the optical lightcurve (maximum, and by gamma ray photons from the decay of ^{56}Co beyond the first ten days (Colgate and McKee, 1969). Typical ^{56}Ni masses produced in SNe Ia explosions range from $0.3 - 0.9\,M_{\odot}$ (Stritzinger et al., 2006), with a mean ^{56}Ni mass of $0.6\,M_{\odot}$. More robust estimates of the ^{56}Ni mass produced in the explosion can be obtained from observations of the nebular spectra of the supernova, in particularly the evolution of the [Co III] emission line complex (Childress et al., 2015). These observations show that the ^{56}Ni masses produced by SNe Ia fall into two regimes: narrow lightcurves with masses clustered near $0.4\,M_{\odot}$ and broader lightcurves with greater total ejecta masses and ^{56}Ni masses of $0.6 - 1.2\,M_{\odot}$ (Childress et al., 2015).

Due to the 77 day half life of the ^{56}Ni decay chain, positrons produced in the decay of daughter nucleus ^{56}Co are produced inside the supernova ejecta. Detailed investigations into the escape fraction of positrons from SNe Ia have been carried out (Chan and Lingenfelter, 1993; Milne et al., 1999). The subject is of particular interest as positrons thermalizing in the SN ejecta and depositing their kinetic energies power the infrared lightcurves of SNe Ia at late times (> 500 days). If a large fraction of positrons escape from the ejecta, the bolometric lightcurve - which includes observing light in the infrared region of the spectrum - will decline at a higher rate than if the positrons are trapped (Kerzendorf et al., 2014).

Simulations investigating positron escape from SNe Ia investigated the impact of the magnetic field configuration on the positron escape fraction. The internal structure of the magnetic field in the ejecta of SNe Ia is not well understood and the positron escape fraction could be a good diagnostic of this in the future. It was found (Chan and Lingenfelter, 1993;

	SN rate/100 yr^{-1}	$N_{e^+}s^{-1}$ (1% esc.)	$N_{e^+}s^{-1}$ (5% esc.)
Bulge	0.062	4.57×10^{41}	2.28×10^{42}
Nuclear Bulge	0.025-0.15	$1.84 \times 10^{41} - 1.10 \times 10^{42}$	$9.21 \times 10^{41} - 5.53 \times 10^{42}$
Thin Disk	0.4	2.95×10^{42}	1.47×10^{43}
Thick Disk	0.022	1.62×10^{41}	8.11×10^{41}
B/D	0.15	-	-
NB/D	0.059-0.35	-	-

Table 3.2: Table showing positron production rates for different regions of the galaxy based on SNe Ia rates from Mannucci et al. (2006), a ^{56}Ni mass of $0.6\,M_\odot$ per supernova and stated escape fractions, and the respective Bulge:Disk and Nuclear Bulge:Disk emissivity ratios (B/D Obs: 0.42 ± 0.09, NB/D Obs: $(8.3 \pm 2.1) \times 10^{-2}$)

Milne et al., 1999) that for SNe with disordered magnetic field configurations, virtually no positrons escape the ejecta, instead annihilating in-situ. On the other hand, up to 10% of positrons could escape from SNe where the magnetic field became radially combed. This is not outside the realm of physical possibility - the moving ejecta, which is radially ejected - may act to comb the magnetic field lines, thus aiding positron escape. Simulations with realistic magnetic field configuration suggest a positron escape fraction of $\ll 5\%$ (Milne et al., 1999).

On January 22 2014, SN2014J, the closest supernova of any type since 2004 and the closest thermonuclear supernova observed in decades was discovered serendipidously by Fossey et al. (2014). Fossey was taking advantage of a brief break in cloud cover over London to demonstrate the use of CCDs to his astronomy class. The explosion date is thought to be 14 January, UT 14.75, with 0.21 d uncertainty (Zheng et al., 2014). It was recognized as a type Ia explosion from early spectra (Cao et al., 2014) and occurred at a distance of only 3.3 Mpc. As it occurred in a region of the host galaxy (M82) which was highly obscured by dust, the observations were subject to significant reddenning (Goobar et al., 2014) with corresponding difficulties to uncover the intrinsic supernova brightness and optical spectra with great precision.

While optical spectra and observations are subject to dust reddening and obscuration, gamma ray observations are not impeded by these effects. As the SN occured so close, it was possible for INTEGRAL/SPI to make a number of observations of the supernova. Detections of the gamma ray lines associated with the decay of ^{56}Co were made by Churazov et al. (2014), Diehl et al. (2014), and Churazov et al. (2015) in the months following the supernova explosion.

The flux of ^{56}Co gamma rays was used to infer the ^{56}Ni mass synthesised in the explosion, determined to be $M_{\rm Ni} = 0.6 \pm 0.1\,M_\odot$ by Churazov et al. (2014), and $M_{\rm Ni} = 0.49 \pm 0.09\,M_\odot$ (Diehl et al., 2014). The differences in the derived Ni masses can be attributed to the differing methods of analysis to determine the Co line fluxes. These observations were the first incontravertible and direct evidence that thermonuclear supernovae are powered by the decay of the ^{56}Ni decay chain (Churazov et al., 2014).
Subsequent observations of SN2014J resulted in an inferred 5% positron escape from the supernova derived (Churazov et al., 2015), however the late time lightcurve suggests a much lower positron escape fraction (Graur, 2019).

The positron yield of SNe Ia in the Milky Way can be estimated based on the rate of SNe Ia, the mean mass of ^{56}Ni produced in each explosion (0.6 $M_\odot$) and assuming the escape fraction of positrons either from simulations (5%, the optimistic case) or from observations of bolometric lightcurves (1% escape, the pessimistic case). The estimated rate of SNe Ia in different regions of the Galaxy (Mannucci et al., 2006; Prantzos et al., 2011) and their calculated positron yields are shown in Table 3.2. Even with the optimistic case of 5% positrons escaping from each SN Ia, the total rate of positron production is inadequate to explain the total number of positrons annihilating in the Milky Way. Moreover, the distribution of SNe Ia as a positron source does not match the observed morphology and cannot reproduce the observed bulge/disk and nuclear bulge/disk ratios (see Table 3.2).

3.4.3.3 ^{44}Ti

Massive stars are usually thought of as the main source of the radioisotope ^{44}Ti. This is the parent nucleus of ^{44}Sc, which is β^+ unstable in $\sim$ 95 per cent of decays with a total half-life to positron production of 59 yr. This isotope is formed during explosive nucleosynthesis during the core collapse supernova that occurs at the end of a $> 8\,M_\odot$ star's life and was first proposed as a Galactic positron source in Clayton (1973). The synthesis of the ^{44}Ti occurs in the alpha-rich freezeout phase of nuclear statistical equilibrium (Thielemann et al., 1996).

There are many uncertainties associated with calculating the yields of core collapse supernovae via simulation. In particular, there are significant uncertainties in the nuclear reaction rates (The et al., 2006), and also in the exact explosion mechanisms which takes place (Timmes et al., 1996; Woosley and Weaver, 1995). It has been found that in asymmetric explosions, larger quantities of ^{44}Ti may be produced (Nagataki et al., 1998; Bruenn et al., 2013). However, these yields are uncertain by up to an order of magnitude.

One method to directly investigate the ^{44}Ti yields of core collapse supernovae is to observe the x-ray and gamma-ray decay lines of the isotope in Milky Way supernova remnants. Observations of the ^{44}Ti decay lines have been made in the CCSN remnant Cassiopoeia A (Cas A, Iyudin et al., 1994). Spatially-resolved spectroscopic x-ray analyses of the ^{44}Ti ejecta have been carried out to determine the total initial mass of ^{44}Ti produced in the explosion, and its velocity structure. In Grefenstette et al. (2016), an initial ^{44}Ti mass of $1.54 \pm 0.21 \times 10^{-4}\,M_\odot$ was found using the x-ray line flux. In comparison, masses of $1.5 \pm 0.4 \times 10^{-4}\,M_\odot$ and $2.4 \pm 0.9 \times 10^{-4}\,M_\odot$ of ^{44}Ti, respectively were found using the 78 keV x-ray line and the 1157 keV gamma ray line in Siegert et al. (2015).

It is possible to also derive the yield of ^{44}Ti in SN1987A, the closest SN for almost 500 years. Late time observations of SN1987A's lightcurve, which declined at a slower rate than predicted by the decay of ^{56}Co alone, generate an estimated yield of ^{44}Ti in the explosion to be $\sim 0.5 \times 10^{-4}\,M_\odot$, lower than the yield estimates from the x-ray and gamma ray flux observed in Cas A (Seitenzahl et al., 2014). Direct measurements of ^{44}Ti emission lines from the remnant of SN1987A suggest a larger ^{44}Ti yield of $3.1 \pm 0.8 \times 10^{-4}\,M_\odot$ (Grebenev et al., 2012; Boggs et al., 2015).

However, there is a dearth of SN remnants which emit the characteristic lines that indicate the presence of ^{44}Ti. As the Milky Way CCSN rate is estimated to be about 1/century, one would expect to see a number of CCSN remnants bright in these decay lines (The et al., 2006). Their absence indicates that the typical yield of ^{44}Ti in CCSNe may be lower than suggested by observations of Cas A and 1987A.

However, there is compelling evidence that there may be an additional Galactic source of ^{44}Ti. The observed abundance of ^{44}Ca (the daughter nucleus of ^{44}Ti) in pre-solar grains, relative to the ^{56}Fe suggests that the CCSN rate, which is predicted to be roughly constant across the lifetime of the Galaxy, indicates that even CCSNe producing ^{44}Ca at $10^{-4}\,M_\odot$ per event cannot supply enough ^{44}Ca (Timmes et al., 1996). This hints that there may be another source of ^{44}Ti in the Galaxy. Such a source would be much rarer, and produce ^{44}Ti in much greater quantities. This is a natural explanation for the absence of observed SNRs with ^{44}Ti decay lines (Crocker et al., 2017).

Thermonuclear supernovae are often thought of as a relative homogeneous class of objects used as standardizable candles to measure cosmological distances. However, these objects exhibit a great deal of variety. Spectroscopically and photometrically peculiar thermonuclear transients suggest that nucleosynthesis beyond the explosive carbon burning these SNe are known for occurs.

Two subtypes of thermonuclear supernovae have been directly implicated in the production of ^{44}Ti. The first is SNe of the subtype SN2005E-like (henceforth 05E-like). A handful of these subluminous and spectroscopically peculiar supernovae have been observed in external galaxies. Their rate is extremely uncertain, with estimates suggesting as low as 2% of the cosmological SNe Ia rate to as high as 90% of the SNe Ia rate (Frohmaier et al., 2018). Their rates are primarily uncertain due to low number statistics. Their faint and fast-declining nature means they may be missed in cosmological SN surveys (Lunnan et al., 2017).

These SNe were suggested as a source of Galactic positrons in Perets et al. (2010). In this paper, the authors suggested that the strong calcium absorption features in the spectra of these SNe suggest that large quantities of ^{44}Ti could be synthesised in the SN explosion, as both ^{44}Ti and Ca are synthesised in similar conditions in thermonuclear supernovae (explosive alpha-process capture). However, the observed distribution of these SNe in galaxies would make them a poor positron source in the Milky Way. 05E-like SNe have been exclusively observed at large offsets from their host galaxies within galactic halos (Lunnan et al., 2017). It was also found in (Frohmaier et al., 2018) that this trend is not due to a selection bias, where the faint SNe are missed against bright Galactic background light. Their large offset makes them an unlikely source of the Galactic positrons, as they would occur predominantly in the halo, and rarely in the Galactic bulge or thick disk.

Another subtype of thermonuclear supernovae is a much more compelling candidate as the origin of Galactic antimatter: SN1991bg-like SNe. 91bg-like SNe events share several key features with their normal SNe Ia cousins, and are clearly thermonuclear supernovae. Specifically, they lack any indication of hydrogen and helium in their spectra while also exhibiting strong Si II in absorption (Filippenko, 1997). Moreover, absorption features in their spectra near maximum light indicate the presence of a number of intermediate mass elements (IME) including silicon, magnesium, calcium, sulphur and oxygen which is consistent with these events belonging to the class of thermonuclear transients (Filippenko, 1997).

However, 91bg-like SNe also exhibit significant photometric and spectroscopic peculiarities compared to normal SNe Ia. This is highly suggestive of a different explosion mechanism and/or progenitor configuration. In particular, the strong Ti II absorption features in their spectra, and the red color of the spectra, indicate that they may synthesise up to a few hundredths of a solar mass of ^{44}Ti. These SNe were suggested as a source of Galactic antimatter in Crocker et al. (2017), particularly in light of their association with old stellar populations, meaning the morphology of positron production sites in these SNRs would correspond well to the observed morphology of the positron annihilation signal in the Galaxy. In this thesis, I will estabilish that these Sne are indeed associated with the old stellar populations suggested in Crocker et al. (2017). Optimistic estimates of the rate of these SNe in the Milky Way and their Ti production rate mean they could produce up to 90% of Galactic positrons.

3.4.3.4 Novae: ^{22}Na and other isotopes

Novae are systems which comprise a close binary system containing a WD, which usually accretes hydrogen from its companion star (although some systems may accrete from a helium donor, e.g. Kato et al. (2008)). The accretion rate is on the order of $\dot{M} \sim 10^{-10} - 10^{-9}\,\mathrm{M_\odot\,yr^{-1}}$, and the accreted hydrogen can build up on the surface of the WD where it is compressed to degenerate conditions. Once sufficient hydrogen has been accreted, the hydrogen layer ignites, leading to a thermonuclear runaway (Hernanz et al., 2005). Depending on the composition of the WD (and hence the mass of the WD), the nuclear products of this thermonuclear runaway may vary. For example, systems containing a CO WD synthesise light nuclei such as Li, C, N, O and F. Systems containing higher mass O Ne synthesise heavier elements such as Ne, Na and Al through the hot NeNa cycle. (José et al., 2006)

The light elements synthesised by CO WD systems which decay via $\beta+$ emission have halflives of only a few minutes to a few hours. Thus, positrons produced by ^{13}N ($\tau_{1/2} = 862\,\mathrm{s}$), ^{15}O ($\tau_{1/2} = 122\,\mathrm{s}$), and ^{18}F ($\tau_{1/2} = 158\,\mathrm{min}$) will be emitted while these nuclei are still in the ejecta of the nova explosion and do not enter the ISM. Thus positron annihilation in CO novae occurs within the ejecta envelope. Gamma ray emission from novae at GeV energies has only been detected recently (Finzell et al., 2018), however positron annihilation gamma rays have not yet been detected. Optical detection of novae occurs a few days after the thermonuclear runaway where gamma ray emitting nuclei are produced, and thus to observe gamma rays from optically detected novae requires the use of archival data. The low yields of the gamma ray emitting material means that archival gamma ray data from INTEGRAL is only just reaching the sensitivities required to detect gamma ray lines from novae.

ONe WD systems produce the $\beta+$ unstable ^{22}Na, which has a half life of 2.6 yr. As this radionuclide is much longer lived than those produced in CO WD systems it may escape from the nova ejecta and thus positrons produced in the decay can be released into the ISM. Based on theoretical estimates and simulations, the yield of ^{22}Na in a single nova event may be up to $\sim 10^{-8}\,\mathrm{M_\odot}$ (José et al., 2003; Hernanz et al., 2005). Based on this upper limit and the rate of ONe novae in the Galaxy ($6 - 20\,\mathrm{yr^{-1}}$, 1/3 of the total Galactic nova rate of $20 - 60, \mathrm{yr^{-1}}$, Shafter et al. (2000); Shafter (2002)), the rate of positron production from ^{22}Na from novae is around $\dot{N}_{e+} \sim 1 \times 10^{-38} - 3 \times 10^{41}\,\mathrm{s^{-1}}$.

ONe novae occur predominantly in the Galactic thin disk, and the short lifetime of ^{22}Na means that the positrons will be injected into the ISM close to their source. As there is currently no observations of^{22}Na decay lines, the exact positron production rate from novae is highly uncertain, as is the morphology of the positron injection/annihilation sites.

3.4.3.5 Rare transients

Hypernovae are hypothetical supernova explosions which are 10-100 times more energetic than normal CCSNe ($10^{52} - 10^{53}$ erg, as opposed to 10^{51} erg) with ^{56}Ni ejecta masses ten times larger than those found in typical CCSNe, around $0.5\,M_\odot$ (Nomoto et al., 2010). Hypernovae are thought to originate from highly asymmetric explosions of rapidly rotating stars with masses $> 30\,M_\odot$ (Woosley, 1993). The implosion of the core of the star drives two jets, which initiate the explosion. Nucleosynthesis occurs in the jets. These explosions are proposed to be the central engine of long duration gamma-ray bursts (lGRBs.)

The high ^{56}Ni yields of hypernovae makes them a potentially compelling positron source, and synthesise as many positrons per event as SNe Ia (Cassé et al., 2004). However, the positron escape fraction from hypernovae is highly uncertain, as is the hypernova rate in the Galaxy. In Cassé et al. (2004), positron escape from hypernovae is calculated assuming homologous expansion of the jet material and calculate that ~ 40 per cent of positrons escape from the jet into the ISM. Thus, a single event synthesising $0.5\,M_\odot$ ^{56}Ni could supply up to 10^{54} positrons to the ISM.

Hypernovae are associated with massive stars, and hence occur in regions of the Galaxy which host ongoing star formation. Thus, we expect that the distribution of positron annihilation associated with these events to be similar to that of the ^{26}Al line in the Galaxy, which traces regions of massive star formation. Thus, it appears hypernovae cannot explain the positron annihilation signal in the Galactic bulge unless positrons can be transported from the disk to the bulge (see Chapter 7).

Hypernovae may also occur in the Galactic center where the Central Molecular Zone (CMZ) forms around $0.1\,M_\odot$ of stars per year (Morris and Serabyn, 1996). Positrons produced in this region may then be transported in the Galactic bulge via the nuclear outflow (see Chapter 9). To explain the Galactic bulge positron annihilation rate, this requires a hypernova rate of $0.02\,100\,\mathrm{yr}^{-1}$ (Cassé et al., 2004).

Further detailed simulations taking into account the magnetic field structure in the jet and the annihilation of positrons in the dense jet material (with a similar experimental configuration to Chan and Lingenfelter (1993); Milne et al. (1999)) would be required to confirm whether the escape fraction is significant. However, it is unlikely that hypernovae make a significant contribution to the Galactic positron annihilation line due to the highly uncertain positron yields and their occurrence in young stellar populations that does not reflect the morphology of the positron annihilation line.

3.4.4 Non-explosive nucleosynthesis: other isotopes

Radioisotopes synthesised during explosive nucleosynthesis account for the largest positron yields from single events. Smaller yields of positrons are synthesised continuously by main sequence stars. A stellar source of positrons may be solar- and sub-solar mass stars which have high levels of flare activity. Particles accelerated in stellar flares interact with the stellar atmosphere, producing radioactive isotopes, and, if enough particles can be accelerated to several hundred MeV, pions. Radioactive isotopes such as ^{11}C and ^{15}O undergo $\beta+$ decay, while pions decay to produce secondary positrons as described in the section on cosmic rays. These positrons subsequently annihilate in the stellar atmosphere (Murphy et al., 1987).

This positron production mechanism, and the subsequent annihilation of positrons, has been observed in the Sun and studied extensively (Ramaty et al., 1975; Kozlovsky et al., 2004). Positron annihilation was first observed in solar flares in 1973 (Chupp et al., 1973). The *Solar Maximum Mission* (*SMM*) satellite, which carried a NaI spectrometer with medium spectral resolution made detailed measurements of positron annihilation (Share et al., 1983, 1996). Subsequent space missions, such as *RHESSI* have made more detailed investigations at much higher spectral resolution (Share et al., 2003). This enables detailed study of the annihilation lineshape in solar flares. The spectral characteristics of positrons annihilating in solar flares is consistent with the spectral characteristics of the annihilation line in the Galaxy (Murphy et al., 2005).

Positrons produced in stellar flares have been proposed as the origin of the Galactic bulge 511 keV line (Bisnovatyi-Kogan and Pozanenko, 2018). The estimated positron production rate from flaring red dwarf stars in the Galactic bulge is $\dot{N_{e^+}} = 5.7\eta \times 10^{40}\,\mathrm{s}^{-1}$ where η is the 'conversion coefficient', the ratio of positron production per bolometric energy of the flare. This has not been well determined: in Solar flares, $\eta \sim 100$. To explain the Galactic bulge 511 keV line requires $\eta \sim 300$, three times larger than in the Sun.

The positron production rate from stellar flares from the Galactic bulge could be more robustly estimated with futher observations of Solar flares, and by searching for the annihilation line in nearby globular clusters containing red-dwarfs. If stellar flares dominate positron production in the Galactic bulge, the 511 keV flux from stellar flares in globular clusters is expected to be within the detection limits of SPI/INTEGRAL.

3.4.5 Compact objects

Compact objects are some of the most extreme objects in the universe. They are stellar remnants - the dead cores of massive stars - that have become compressed to nuclear matter or beyond. Compact objects that have been implicated in positron production include pulsars and millisecond pulsars, magnetars, low-mass x-ray binaries and microquasars.

3.4.5.1 Pulsars, millisecond pulsars and magnetars

When a massive star ends its life, it may end its life as a neutron star. These neutron stars can be rapidly rotating and highly magnetized. Some pulsars are powered by rotation, such as the Crab and Vela pulsars, which are often used as gamma ray standard candles to calibrate instruments. Millisecond pulsars are powered by accretion, and have lower magnetic fields than pulsars and magnetars ($B \sim 10^8\,\mathrm{G}$). Particularly strongly magnetised objects, such as magnetars and soft gamma-ray repeaters may have magnetic fields which are stronger still ($> B \sim 10^9\,\mathrm{G}$) (Prantzos et al., 2011; Caraveo, 2014).

The strong magnetic fields, and intense radiation field associated with all of these classes of objects result in intense production of positron-electron pairs. These pairs are then accelerated in the electric fields at the polar caps of the compact object. The result is a pair cascade: the electron-positron pairs annihilate to produce photon pairs, which then interact to form another electron-positron pair. These particles may eventually escape into the pulsar wind, and eventually into the interstellar medium. The pair cascade is supported by a series of high energy processes (Harding, 1981).

While pair production in these objects is inferred through their gamma ray emission which results from the inverse Compton losses of the electron-positron pairs (e.g. Hooper et al. (2017)), it is not clear how many, if any, positrons escape the object. The multiplicity (the fraction of the spin-down or magnetic energy converted into pairs) of pulsars, millisecond pulsars (MSPs) and magnetars is also not well understood. Moreover, the escaping particles are expected to have high energies, in excess of a few tens of MeV.

There is an interesting coincidence between the gamma-ray excess at 511 keV due to positron annihilation, and the so-called 'GeV excess' or 'Hooper bump' (Goodenough and Hooper, 2009), an excess observed in FERMI telescope data with a bulge-dominated morphology not unlike the bulge component of the 511 keV line.

An unresolved population of millisecond pulsars in the Galactic bulge has been implicated as the source of the GeV excess (Abazajian, 2011; Bartels et al., 2016; Macias et al., 2018). In Bartels et al. (2018), this unresolved population of millisecond pulsars is implicated as not only the source of the GeV excess, but simultaneously as the source of the Galactic bulge positrons. However, as the high energy gamma ray continuum strongly constrains the injection energy of the positrons, it is questionable that these sources could be dominant contributors to Galactic positrons.

In contrast, in Crocker et al. (2017), the connection between the MSPs and the 511 keV line is less direct. In this work, the source of the positrons is described to be the merger of two WD stars, one a pure He WD, and one a CO WD. These systems originate from a stellar population which forms with a range of zero-age main sequence (ZAMS) masses. In Crocker+2017, it is shown that systems with larger ZAMS masses than the systems which produce the thermonuclear explosions in which $\beta+$ unstable radionuclides are synthesised can end their lives as the accretion induced collapse (AIC) of an ONe WD. In Ruiter et al. (2019), binary population synthesis is used to show that these AIC events occur at a rate which would produce a population of MSPs in the Galactic bulge which can explain the GeV excess, while the rate of He WD-CO WD mergers in the same binary population synthesis simulation is sufficient to explain the global rate and morphology of the 511 keV line.

3.4.5.2 X-Ray binaries and microquasars

X-ray binaries consist of an accreting compact object, such as a a neutron star or a black hole, and a companion which donates the accreting material, such as a main sequence or red giant star. The acceleration of stellar material - hydrogen and helium - in the accretion stream results in the emission of x-rays. The mass of a compact object's companion determines whether the system is classified as a high mass x-ray system (HMXRB, if the companion has a mass $> 4\,M_{\odot}$) or a low mass x-ray binary (LMXRB, if the companion is smaller than $4\,M_{\odot}$) (Grimm et al., 2002).

Around 300 x-ray binary systems have been observed in the Milky Way, however population synthesis calculations suggest that there may be more than 10,000 such systems in the Galaxy, many of which may be currently quiescent (Sadowski et al., 2008). They are distributed predonminantly along the plane of the galaxy in the disk, however it is expected that LMXRBs are associated with the older stellar populations due to them containing at least one low-mass star, which will be much older than the stars in HMXRBs (Grimm et al., 2002).

A fraction of XRBs emit in the radio. This is usually associated with synchrotron radiation emitted by electrons which are produced in jets from the central compact object. If the presence of these jets can be confirmed through observation and imaging, the system is referred to as a microquasar, in analogy with radio-loud AGN quasars (Mirabel, 2010). These objects have been proposed as a source of positrons (Guessoum et al., 2006b; Siegert et al., 2016a). Positron yields are highly uncertain, but can be esimated using simple energetic arguments relating the total power of the positrons in the jets to the estimated total x-ray luminosity of the "low luminosity-hard spectrum" galactic LMXRBs (Beloborodov, 1999).

In Guessoum et al. (2006b), the 'canonical average' rate of positron production by a flaring microquasar of $10^{41}\, e^{+}\, \mathrm{s}^{-1}$ is described. In that work, the authors indicate that the total positron emissivity of the collective population of microquasars in the Milky Way is around $6 \times 10^{42}\, \mathrm{s}^{-1}$, however to explain the Galactic bulge annihilation line requires large scale positron transport from disk to bulge (e.g. as described by Higdon et al. (2009)).

Recently, a flare from the microquasar V404-Cygni was observed by SPI/INTEGRAL. The observed spectrum could be interpreted as due to the annihilation of positrons within the jet itself, and the total positron yield determined in the analysis of the spectrum was $\dot{N_{e^+}} \sim 10^{42}\mathrm{s}^{-1}$ (Siegert et al., 2016a).

Thus, to explain the total observed positron annihilation signal, one would require around ten unresolved microquasars to be flaring simultaneousness in the Galaxy. This is consistent with the duty cycle of typical microquasars (Siegert et al., 2016a). However, the distribution of these objects is somewhat uncertain, and while the distribution of the known microquasars, including 1E1740.7-2942 or 'the Great Annihilator' (Bouchet et al., 1991), shows some degree of clustering toward the inner galaxy (Grimm et al., 2002), the data are insufficient for statistically significant conclusions about the contribution of microquasars toward the centrally concentrated nature of the positron annihilation signal.

3.4.5.3 The supermassive black hole

The Galactic center SMBH was first suggested in the 1980s as a positron source as flares from close to the SMBH event horizon and associated positron pair-production could explain the apparent variability observed by HEAO-3 and balloon-borne missions (Riegler et al., 1981; Lingenfelter et al., 1981). Explanations involving the Galactic center black hole fell out of favour when the first maps of positron annihilation emerged during the OSSE mission, which indicated the emission associated with positron annihilation was extended. Interest in the SMBH as a positron source was renewed for a short time as a potential explanation for the PLE (Purcell et al., 1997; Dermer and Skibo, 1997).

More recently, the 'Galactic center source' has been identified in analysis of SPI data (Siegert et al., 2016b). It is not possible to distinguish whether this emission component is associated with a point source or a more distributed region with a size of a few hundred pc due to the poor angular resolution of INTEGRAL. Consequently, it has once again become important to consider the possibility that the SMBH at the Galactic center contributes to the population of Galactic positrons.

The SMBH is observed as a multiwavelength source, Sgr A* (e.g. Eckart et al. (2008)). It has a very low Eddington luminousity, and its bolometric luminosity is far smaller than that of black holes in galaxies of a similar total mass to the Milky Way, and much smaller than that which would be suggested by the Eddington luminosity. Furthermore, the x-ray emissivity of the SMBH is much smaller than the population of Galactic XRBs. Thus, in a steady state scenario, SgrA* is unlikely to be able to supply enough positrons to the Galaxy (Prantzos et al., 2011).

However, if the emission and positron production from the SMBH were highly episiodic, it might turn out to be an important positron source in a time-averaged sense. Proposed models for episodic injection of positrons in the Galactic center include the tidal disruption of stars (Cheng et al., 1997), or the accretion of gas which surrounds the black hole (Totani, 2006).

3.4.5.4 Dark matter

The centrally-concentrated nature of the Galactic positron annihilation signal, in particular the bulge component, has similarities with the predicted distribution of Dark Matter in the Milky Way. A large body of observational evidence for Dark Matter has been assembled including observations temperature anisotropies of theCosmic Microwave Background, baryonic acoustic oscillations, gravitational lensing of galaxy clusters, and rotation curves of galaxies which cannot be explained by the Standard Model of Particle Physics or general relativity alone (Bertone and Tait, 2018).

Understanding the true nature of Dark Matter is a true mystery of modern astrophysics and cosmology. Consequently, indirect detection of Dark Matter via observation of gamma-rays emitted during the rare interactions of Dark Matter with Standard Model particles and forces is an area of great interest (Donato, 2014). In particular, the 511 keV line has been invoked as evidence of Dark Matter decay and annihilation in the Galaxy. There are many potential candidate theories which describe Dark Matter particles which can explain cosmological observations, however here I will focus only on models proposed to explain the Galactic 511 keV line.

The injection energies of the Galactic positrons is constrained by the gamma ray spectrum above 511 keV, and thus the mass of the decaying or annihilating dark matter particles that may produce galactic positrons are similarly constrained. Beacom and Yüksel (2006) and Sizun et al. (2006) obtained a mass upper limit of $m_{\rm dm} \sim 3 - 7\,\rm MeV$. Two main categories of DM candidates which fit this constraint are:

- Light DM particles with $m_{\rm dm} \sim$ MeV mass, either annihilating (Boehm et al., 2004; Gunion et al., 2006), or decaying (Hooper and Wang, 2004; Picciotto and Pospelov, 2005), and
- Heavy DM particles with masses in the GeV – TeV range, deexciting or decaying into another particle, where the mass difference between the initial and final states is a few MeV (Finkbeiner and Weiner, 2007).

One possible example of positron production via the annihilation of light DM particles is in the case where the DM particle is a scalar (spin 0). This DM particle can annihilate into an electron-positron pair via the exchange of a fermionic particle F. In most DM models, the relic density criterion strongly constrains the mass of the DM particle, however in this scenario, as shown by Boehm and Fayet (2004), the characteristics (mass and couplings) of the F particle are constrained instead of the mass of the DM particle. Thus, DM particles which have masses between $\sim$ MeV $-$ GeV can account for the observed dark matter relic density. The fermionic particle may be either a heavy charged particle, or a new neutral gauge boson (Boehm and Fayet, 2004; C Boehm and Silk, 2004).

However the light annihilating DM scenario has since been challenged. Bœhm and Ascasibar (2004) and Bœhm and Silk (2008) showed that if these annihilting light DM particle were the source of the Galactic positrons, their properties should affect the value of the fine structure constant. This argument was thus used to constrain the mass of the light DM particle in this scenario to be $> 7\,\mathrm{MeV}$, at the very upper limit of the allowed DM mass range inferred from the results of Beacom and Yüksel (2006) and Sizun et al. (2006).

Furthermore, the explosion of SN1987A in the LMC was used to further constrain the mass of light DM candidates. Boehm and Fayet (2004) showed that the DM particle must have $m_{\mathrm{dm}} > 10\,\mathrm{MeV}$, close to, but exceeding, the constraints on the upper mass limit for DM particles from the gamma-ray continuum.

The constraint on the injection energy of the positrons seems to rule out annihilating light DM candidates. Another possible scenario where positrons are produced by light DM interactions is the decay of $m_d m < 100 MeV$ DM particles. Decaying DM candidates were proposed by several groups, each proposing a different particle. For example,

- axinos by Hooper and Wang (2004),
- sterile neutrinos by Picciotto and Pospelov (2005),
- moduli by Conlon and Quevedo (2007).

Decay into electron-positron pairs is expected to be among the dominant decay modes of such particles. This is because only electron, neutrino and photon decay channels are kinematically possible due to the low masses of the DM particles.

While sterile neutrino and moduli candidates are ruled out by cosmological constraints on the DM relic density, the plausibility of axinos is challenged by both the high injection energy of the electron-positron pairs produced in the decay, and also the morphology of the positron annihilation line which would result from the annihilation of these positrons. The positron production and annihilation profile is expected to closely follows the DM density profile (if positrons annihilate close to their source, which I will argue to be true in this thesis), which is centrally concentrated. Specifically, the positron production rate from decaying DM is given by

$$\dot{N}_{e+}[r] \propto \Gamma_{\mathrm{X}\rightarrow\mathrm{e}^{+}\mathrm{e}^{-}} n_X[r] \tag{3.23}$$

where $\Gamma_{\mathrm{X}\rightarrow\mathrm{e}^{+}\mathrm{e}^{-}}$ is the interaction rate and $n_X[r]$ is the number density of DM particles as a function of Galactocentric radius. In the case of DM decay, this tends to a maximum at $1/t_H$ where t_H is the Hubble time. While decaying DM may contribute to the bulge component of the positron annihilation signal, positrons from decaying DM cannot explain the observed annihilation line in the Galactic disk.

The second class of candidate DM models invokes particles with masses in the range $m_{\rm dm} \sim 100\,\text{GeV} - 1\,\text{TeV}$, specifically electroweak scale WIMPs **?**. For these particles, the mass difference between the particle excited state and ground state is of the order $\sim$ MeV. The velocity dispersion of DM particles was noted by Finkbeiner and Weiner to be $\sim 100\,\text{km}\,\text{s}^{-1}$, thus a WIMP with $m_{\rm dm} \sim 500\,\text{GeV}$ will posess a kinetic energy $E_k > m_e c^2$. De-excitation of such a particle, excited through inelastic scattering, can proceed via emission of an electron-positron pair, and the emitted positron will have an energy of $\sim 1\,\text{MeV}$.

To explain the positron production rate with de-exciting DM requires the model parameters to be pushed to extreme limits. Moreover, the morphology of positron annihilation if the positrons originate in the de-excitation of WIMPs as described above will differ somewhat from the most recent observations of the annihilation morphology. While positron annihilation from all DM sources will be centrally concentrated due to the nature of DM haloes, in the case of de-exciting (and annihilating) DM, the positron profile is more centrally concentrated (e.g. Prantzos et al. (2011)):

$$\dot{N}_{e+}[r] \propto \Gamma_{\rm X\rightarrow e^+e^-}\, n_X[r] \tag{3.24}$$

In the case of DM de-excitation or annihilation, $\Gamma_{\rm X\rightarrow e^+e^-} = \langle \sigma v \rangle n_X$, and thus

$$\dot{N}_{e+}[r] \propto \langle \sigma v \rangle n_X[r]^2 \tag{3.25}$$

This shape can be also modulated by the possible velocity dependence of the interaction cross section since the typical particle velocities depend on the gravitational potential of the DM halo, however positrons from de-exciting (or annihilating) DM, like those from decaying DM, cannot explain disk component of the morphology.

In summary, regardless of whether or not the above DM candidates can explain the properties of DM in a cosmological context or whether or not they are natural extensions to the standard model of particle physics, based on constraints on the injection energy of the Galactic positrons and also on the morphology of the positron annihilation signal, it seems unlikely that DM decay, annihilation or de-excitation can be a dominant source of positrons in the Milky Way. Whether or not the positron annihilation line is an indirect detection of DM interactions with the Standard Model is a subject still under investigation. The sources of positron annihilation observed in DM dominated systems such as dwarf spheroidal satellite galaxies of the Milky Way may be astrophysical, however a DM source cannot be conclusively ruled out Siegert et al. (2016c).

3.4.5.5 Neutron star and black hole mergers

The first confirmed binary neutron star merger occured in 2017, when the LIGO and VIRGO observatories observed a gravitaitonal wave source (Abbott et al., 2017). Over the next hours, the search began for an electromagnetic counterpart to the gravitational wave source, which was subsequently observed across the electromagnetic spectrum by almost all major observatories both on Earth and in space (Abbott, 2017). This event confirmed that neutron star mergers (as well as black hole mergers) are a source of gravitational waves, and the electromagnetic afterglow of the merger was indicative that a large quantity of r-process material was produced in the neutron rich ejecta.

It was recently proposed by Fuller et al. (2018) that pair production can occur in the hot ejecta in the moments following the neutron star merger. In that work, the authors suggested that the 511 keV line may be used to trace the history of NS-NS and BH-NS mergers in the Galactic center, however the yields of positrons from these events is highly uncertain, as is the proposed production mechanism.

3.5 Evaluating positron sources

A viable galactic positron source must satisfy the following criteria:

- Satisfy the constraints on the morphology of the positron annihilation signal. That is, the flux of the 511 keV line from the bulge relative to the disk, and the GCS relative to the bulge, must replicate observations. Moreover, the positron source should explain the large apparent scale height of the observed 511 keV line in the disk, and
- Satisfy the constraints on the total rate of positron annihilation in the Galaxy without violating constraints on, for example, gamma ray lines from positron producing nuclei.

In Table 3.3, the positron sources discussed in the above text are summarized with information including their theoretical or observed positron yields.

The most viable source of Galactic positrons according to Table 3.3 appears to be SN1991bg-like supernovae. However, this would require positrons to be confined close to their production sites. To evaulate whether SN1991bg-like supernovae are indeed a viable source of Galactic positrons, I will first establish in Chapter 4 the background in scientific literature concerning the transport of positrons. If positrons can be transported from either the disk to the bulge or vice versa, this will reveal the underlying source distribution of positrons. In Chapter 5, I will confirm that the 511 keV line is in steady state and that the positrons we observe annihilating today are not part of a tens of Myr old low energy positron reservoir. In Chapter 6, I will show that the nuclear outflow of the Milky Way cannot disperse positrons into the Galactic bulge and reproduce the observed annihilation spectrum and thus the source of Galactic positrons is likely distributed around the Galaxy. Subsequently, in Chapter 7 I will show that the delay times of SN1991bg-like supernovae, proposed to be the source of Galactic positrons, are consistent with those required for a transient source that produces positrons. Finally, I will summarize the results of previous chapters in Chapter 8, and describe future avenues to investigate further whether SN1991bg-like supernovae can indeed supply the majority of Galactic positrons.

Table 3.3: Summary of Galactic positron sources, from Prantzos et al. (2011), amended with additional information published between 2011-2019, based on references supplied in main text.

Source	Process	$\dot{N}_{e+}/10^{43}\,\mathrm{s}^{-1}$	w_0/MeV	Comments
SNe Ia[1]	^{56}Ni decay	~ 2	~ 1	Cannot reproduce global morphology without large scale transport, assuming $f_{\rm esc} = 5\%$
CCSNe[1]	^{26}Al decay	0.5	~ 1	Yield too low, sources confined to thin disk
	^{44}Ti decay	0.3	~ 1	Yield too low, sources confined to thin disk
SN1991bg-like	^{44}Ti decay	5	~ 1	Reproduces B/D, NB/B & $\dot{N}_{e+}$, exact yield of Ti uncertain
SN2005E-like	^{44}Ti decay	unknown	~ 1	Wrong morphology, yield unknown
Hypernovae/GRB	^{56}Ni decay	2	~ 1	Highly uncertain yields, rates & source distribution. e+ production rate estimate based on fine-tuning HN rate
Novae	^{22}Na decay	0.02	~ 1	Production rate too low, sources confined to thin disk, not observationally constrained
Stellar flares	various	up to 2	~ 1	Positron production rate in flares uncertain, may be observationally constrained in near future.
Pulsars	$\gamma - \gamma$	0.5	> 10	Positron energy too high
MSPs	$\gamma - \gamma$	$0.15 - 2$	$> 1 - 10$	Positron energy too high. Upper limit on positron production rate from Bartels et al.
Magnetars	$\gamma - \gamma$	0.16	> 10	Positron energy too high
LMXRBs	$\gamma - \gamma$	2	> 10	Positron energy too high, cannot replicate morphology, assuming $L_{\rm e+} \sim 0.01 L_{\rm xray}$
Microquasars[1]	$\gamma - \gamma$	$1 - 2$	~ 1	$f_{\rm esc}$ uncertain, total number of objects and duty cycle uncertain
SMBH	$\gamma - \gamma$	unknown	~ 1	Requires large scale transport to explain Bulge, $L_{\rm BH}$ too low to explain GCS
Cosmic rays[1]	$p - p$	0.1	> 30	Positron energy too high
Dark Matter	annihilation	unknown	$> 7 - 10$	Positron energy too high, bulge morphology too centrally peaked, cannot explain disk
	de-excitation	unknown	~ 1	Requires fine-tuning, bulge morphology too centrally peaked, cannot explain disk
	decay	unknown	> 10	Positron energy too high, cannot explain disk
NS-NS mergers	$\gamma - \gamma$	unknown	?	Yield and rate of events highly uncertain

[1] - Rate of positron production is observationally constrained. See text.

Chapter 4

An overview of positron transport in the Milky Way

'Eddies in the space-time continuum.'
'Ah...is he. Is he.'
'What?'
'Er, who is Eddy, then, exactly?'

Douglas Adams

Foreword

To understand the origin of Galactic positrons, we must consider how positrons are transported through the Milky Way between their production and annihilation sites. If positrons can be transported over kpc distance scales, they can be transported far from their sources and thus the observed morphology of the positron annihilation signal does not reflect the morphology of the positron sources in the Galaxy.

The transport of charged particles in interstellar environments is notoriously complex to model and understand, and often requires simplifications and generalizations to be made about the nature of phenomena that are poorly understood: for example, the structure of the magnetic field and the nature of magnetic turbulence.

Charged particles typically travel via two different modes: streaming and diffusion. In the review article I present below, I describe the works which have investigated the transport of positrons in the Milky Way, and the different modes of transport that have been invoked to solve the apparent riddle that while most positron sources are confined to the Galactic disk, a large fraction of the Galactic positrons annihilate in the Galactic bulge. Modern simulations which accurately consider the nature of the turbulent magnetic field in the Galaxy now suggest that positrons are confined close to their production sites.

Understanding positron transport will give us a unique insight into the physics of cosmic rays. If we can understand the origin of the positrons, we will be able to determine with incredible precision how the positrons must be transported to get from their production sites to their annihilation sites. This will allow us to infer information about Galactic magnetic fields, potentially on all size scales, as well as the diffusion coefficient, information which is vital if we are to better model and understand the propagation of cosmic ray particles.

Declaration

This work was published in the journal *MDPI Galaxies* special edition 'Searching for Connections among the Fermi Bubbles, the Galactic Center GeV Excess, and Loop I'. The manuscript is reproduced here with formatting changes to make it consistent with the rest of the work in this thesis. I contributed 100% of the manuscript preparation for this review article.

Positron Transport And Annihilation In The Galactic Bulge

Fiona H. Panther[1]

[1] Research School of Astronomy and Astrophysics, Australian National University, Canberra 2611, Australia

Published in: *Galaxies* 2018, 6(2), 39; https://doi.org/10.3390/galaxies6020039

Abstract

The annihilation of positrons in the Milky Way galaxy has been observed for ~ 50 years however the production sites of these positrons remains hard to identify. The observed morphology of positron annihilation gamma-rays provides information on the annihilation sites of these Galactic positrons. It is understood that the positrons responsible for the annihilation signal originate at MeV energies. The majority of sources of MeV positrons occupy the thin, star forming disk of the Milky Way. If positrons propagate far from their sources, we must develop accurate models of positron propagation through all ISM phases in order to reveal the currently uncertain origin of these Galactic positrons. On the other hand, if positrons annihilate close to their sources, alternative source of MeV positrons with a distribution that matches the annihilation morphology must be identified. In this work, I discuss the various models that have been developed to understand the origin of the 511 keV line from the direction of the Galactic bulge, and the propagation of positrons in the ISM.

4.1 Introduction

The annihilation of positrons (anti-electrons) at rest results in the characteristic emission of a gamma-ray line at ~ 0.5 MeV. This gamma-ray line was the first originating beyond the solar system to be detected from Earth in the early 1970s (Johnson et al., 1972). Since then, the spatial extent and spectral characteristics of gamma-ray emission at ~ 0.5 MeV has been explored by both balloon-borne and space missions. The most recent observations made by *INTEGRAL*/SPI reveal the annihilation of positrons at a rate of $2 \times 10^{43}\,\mathrm{s}^{-1}$ in the central $\sim 20^{\circ}$ of the Galaxy based on the effective distance between Earth and the Galactic bulge being 8.5 kpc (Siegert et al., 2016b) (the Galactic bulge annihilation line). In Siegert et al. (2016b), 11 years of *INTEGRAL*/SPI exposures are combined, and the resulting positron annihilation rate is consistent with earlier analyses (Knödlseder et al., 2005; Weidenspointner et al., 2008a) which also reveal the annihilation of positrons in the bulge region of the Galaxy. The Galactic disk has been detected for some time (e.g. Knödlseder et al. (2005); Weidenspointner et al. (2008a); Churazov et al. (2011) however emission from the Galactic disk was thought to be concentrated in the inner 100 degrees of the Galaxy Skinner et al. (2010); Bouchet et al. (2011). The most recent analysis Siegert et al. (2016b) suggests the emission of positron annihilation gamma-rays across the full extent of the Galactic disk and a higher rate of positron annihilation in the Galactic disk than previous analysis revealed.

Analysis of the gamma-ray spectrum produced by the annihilating positrons indicates they annihilate predominantly in the warm, partially ionized phase of the interstellar medium (ISM) (Churazov et al., 2005; Jean et al., 2006; Churazov et al., 2011; Siegert et al., 2016b) by undergoing interactions with neutral hydrogen after they have slowed to kinetic energies of $\sim 10 - 100$ eV. The reaction rate between positrons and neutral hydrogen dominates in this phase of the ISM due to the large cross-section for interaction between positrons and hydrogen at energies of $\sim$ 10 eV and the low abundances of other neutral species such as helium. Current constraints on the energy at which these positrons are injected into the ISM come from fundamental physics (Aharonian and Atoyan, 1981) and data obtained by the Compton Gamma-Ray Observatory (*CGRO*) and *INTEGRAL* missions, and suggest the initial kinetic energy of the annihilating positrons does not exceed a few MeV. This rules out the origin of the positrons being cosmic ray (CR) secondaries produced in the decay of pions, as well as other sources of relativistic positrons, such as pulsars, millisecond pulsars and magnetars (Prantzos et al., 2011). However, the combination of data from both *INTEGRAL* and *CGRO* may result in systematics which will be present in the data used to derive the constraint, and moreover (Beacom and Yüksel, 2006) assumes that the electrons with which positrons annihilate at high (> MeV) energies are at rest. If positron annihilation is occuring in an environment where relativistic electrons are present (e.g. in a microquasar jet (Guessoum et al., 2006b; Siegert et al., 2016a) or pulsars and millisecond pulsars, (Bartels et al., 2018)) it may be possible to circumvent this constraint. However, the presence of the 511 keV line and ortho-positronium continuum at low gamma-ray energies strongly suggest that the majority of positrons annihilate via interactions with neutral hydrogen at thermal energies.

The origin of these annihilating positrons has puzzled astronomers for half a century. The morphology - gamma-ray emission dominated by a bulge component - does not reflect emission at any other wavelength.
A viable source of MeV positrons of astrophysical origin is the decay of β^+-unstable radionuclides, such as ^{26}Al, ^{44}Ti and ^{56}Ni, produced by massive stars and supernovae. Massive stars and supernovae tend to occur in the star-forming thin disk of the Milky Way (Prantzos et al., 2011) while the highest surface brightness of positron annihilation gamma-rays is observed in the Galactic bulge region. To explain the mismatch between the distribution of prospective positron birth sites, and the observed annihilation sites, we must investigate the propagation of positrons. In this short review, I summarize the various transport mechanisms that have been explored in the literature to date to explain the annihilation of Galactic bulge positrons.

4.2 Positron transport in the ISM

From the annihilation spectrum observed in the inner Galaxy, analysis of the gamma-ray spectrum implies that while positrons are born into the ISM with $\sim$ MeV energies, they must cool to energies < 10 eV before annihilating. Positrons lose energy via ionization and Coulomb interactions, synchrotron losses due to interactions with the magnetic field in the Galaxy, inverse Compton scattering and bremsstrahlung. Positrons may also lose energy through adiabatic energy losses (e.g. (Panther et al., 2017)). Positrons with energies $\leqslant$ GeV lose energy predominantly through ionization and Coulomb interactions with neutral atoms and free electrons in the ISM, whereas positrons with energies > GeV lose their kinetic energy via inverse Compton, synchrotron and bremsstrahlung losses.

As they decelerate, positrons are thought to propagate away from their sources. This propagation may occur through either collisionless or collisional transport. In collisionless transport, positrons scatter off magnetic turbulence in the ISM, wheras in collisional transport scattering occurs between positrons and individual particles in the ISM (e.g. neutral hydrogen atoms and electrons), moderated by Coulomb interactions. Both collisional and collisionless transport have been discussed in the literature, and a summary is provided in the subsequent sections of this work.

4.3 Outside-In Transport

If MeV positrons are produced by processes associated with star formation, the majority of positrons will be born in the star forming thin disk of the Milky Way. One way to then explain the high bulge/disk annihilation ratio is that some disk positrons find their way into the Galactic bulge before they annihilate. Such a mechanism is positron interactions with the large scale magnetic field structure of the Milky Way. In general, such a scenario requires positrons to interact with the poloidal halo component that dominates the inner Galaxy as described in Prantzos (2006). The turbulent magnetic field with which positrons interact in the collisionless transport process has a field strength roughly comparable to that of the large scale magnetic fields ($1-10\,\mu$G) in the disk region where the positrons are produced, and this may tend to confine MeV positrons to the Galactic disk in a similar manner to $\sim$ GeV energy cosmic ray protons that make up the cosmic ray halo Prantzos (2006). However, if positrons can escape the cosmic ray halo, they will begin to interact with the poloidal magnetic field and be transported into the Galactic bulge Prantzos (2006). This idea was explored in detail by Higdon et al. (2009), who include a detailed description of the distribution and filling factors of various ISM phases, as well as accounting for the distribution of positron sources. Specifically, they find that around half of positrons from the sources considered therein are produced in the inner 3 kpc of the Galaxy (the inner disk and Galactic bulge), and that these positrons tend to annihilate in the dense, warm outer shells of molecular clouds that occupy the inner $\sim$ 1.5 kpc of the Galaxy. The remaining half of the total Galactic positron yield calculated in Higdon et al. (2009) is produced in the outer disk of the Galaxy. Around half of these disk positrons annihlate in the disk itself, while the remainder escape into the Galactic halo, lowering the annihilation flux from the disk and consequently the observed $B : D$ annihilation flux ratios. One of the key details of this work is the description of how positrons propagate through the different ISM phases. Positrons in the hot, ionized phases of the ISM tending to diffuse along magnetic flux tubes where the diffusion is controlled by resonant scattering by magnetohydrodynamical (MHD) waves. On the other hand, in the neutral or mostly neutral phases, these waves are damped and positrons tend to stream along the flux tubes with an isotropic pitch angle distribution. The distance positrons can propagate in each phase is controlled by either the diffusion mean free path (which is a function of the magnetic field and incident particle energy) in the ionized phase, or the streaming velocity. The annihilation site of the positrons is determined from comparison of the above propagation distances to the typical scale of the phase in which the positron is born. If the propagation distance exceeds the size scale of the ISM phase in which the positron is born, it escapes. Otherwise, the positron is assumed to annihilate in-situ.

To evaluate whether a given positron production and transport scenario can explain the observed positron annihilation signal from the Galaxy, both the total positron production rate must be replicated, as well as the morphology. As the results based on SPI/*INTEGRAL* data are presented as varying best-fit models, one way of quantifying the morphology is to use the ratio of positron annihilation fluxes in the bulge and disk. This is commonly referred to in the literature as the bulge to disk ratio, or B/D. In the early years of SPI/*INTEGRAL*, B/D was determined to be in excess of 1 ($B/D \sim 1.4$, (Knödlseder et al., 2005; Weidenspointner et al., 2008a)).

The authors of Higdon et al. (2009) find that the scenario they describe, where positrons propagate differently in the ISM of the Galactic bulge compare to the disk, can (within large uncertainties) replicate high B/D values observed by SPI/*INTEGRAL*. However, more recent simulations of positron transport have involved either detailed Monte Carlo simulation of positron trajectories in the ISM Alexis et al. (2014) which take into account , where the probabilities for particle scattering and annihilation take into account both collisional and collisionless scattering, and various annihilation processes (see the Appendix B of Jean et al. (2009) for more details). Alternatively cosmic ray propagation codes such as GALPROP Martin et al. (2012) have been adapted to model positron propagation in the Galaxy. In both cases, it is found that replicating high B/D values is challenging, even for extreme prescriptions that allow transport of positrons several kpc from their birth sites.

4.4 Galactic Center positron sources

Exploration of the idea that positrons annihilating in the Galactic bulge originate in the central regions of the Galaxy predates the *INTEGRAL* mission. In the mid-1990's, the first image reconstructions of the extent of positron annihilation radiation were made with data from the OSSE instrument on *CGRO*, and seemed to reveal an extended emission component stretching up to 8 kpc above the Galactic plane (dubbed the Positive Latitude Enhancement or PLE) Purcell et al. (1997). An explanation for this "annihilation fountain" phenomenon was developed in Dermer and Skibo (1997). This work described a nuclear outflow associated with the Milky Way, capable of sending positrons produced in the Galactic center several kpc above the Galactic plane. Remarkably, this work predates even the first evidence for a nuclear outflow in the Milky Way Bland-Hawthorn and Cohen (2003) and predates the discovery of the Fermi Bubbles Su et al. (2010), another phenomenon associated with the Galactic center region, by almost 15 years. The PLE phenomenon was later shown, however, to be an artefact of the image reconstruction analysis, and not an astrophysical signal Milne et al. (2001a). To date, very little is known about positron annihilation at high Galactic latitudes as the *INTEGRAL* mission has concentrated efforts along the Galactic plane (e.g. see recent exposure maps in (Siegert et al., 2016b)). Future work to extend *INTEGRAL* exposures to high latitudes to search for extended 511 keV emission is now a priority.

While the PLE was shown to be an artefact, a Galactic outflow may still disperse positrons into the Galactic bulge. The enhanced star formation in the central molecular zone (CMZ) of the Galactic center, as well as high energy processes associated with the central SMBH, make the Galactic center a potentially interesting positron source itself. Explaining how positrons produced in the inner few hundred parsecs are transported outward to fill the Galactic bulge where they are observed to annihilate presents a challenge. The possibility that positrons diffuse away from the central regions of the Galaxy into the Galactic bulge was investigated in detail using a Monte Carlo simulation which tracks positron trajectories through the ISM in Jean et al. (2009). While in Higdon et al. (2009), the interaction between positrons and MHD waves was invoked to transport positrons over large distances, Jean et al. (2009) found that the damping of these waves results in positron propagation being controlled by collisions with gas particles. In the collisional transport mode described in the paper, it is found that positrons travel along magnetic field lines and annihilate far from their sources, and the distribution of annihilation positrons depends on the spatial distribution of the Galactic magnetic field. Thus, if the magnetic field is poloidal, positrons tend to stay confined to a cone subtending a small solid angle above and below the Galactic center rather than filling the entire Galactic bulge.

The diffusion lengths initially calculated in (Jean et al., 2009) are far in excess of the typical size scales of the warm ISM, where positrons are thought to annihilate. However, positrons tend to be born in turbulent environments, and the propagation of positrons is likely to be dominated by scattering from MHD waves at higher energies (with propagation lengths of $\sim 20 - 80\,$pc for positrons with energies $\sim$ MeV). As positrons lose energy to the plasma and their kinetic energies drop below a threshold for the Larmor radius to be of a similar scale to the turbulence, positrons then will tend to propagate through collisional transport. The total propoagation distances of MeV positrons, combining the time the positron spends in the collisional and collisionless regime, is evaluated to be $\sim 40 - 160\,$pc. Thus, these authors ultimately conclude that positrons may only travel a few hundred parsecs from their birth sites.

The coupling of positrons to the turbulent plasma in which they were born makes it possible that the propagation of positrons can be dominated by the motion of the plasma itself. While the concept of the "annihilation fountain" (Dermer and Skibo, 1997) was furloughed, powerful evidence for a nuclear outflow associated with the Milky Way has since emerged, first in the mid-infra red (Bland-Hawthorn and Cohen, 2003), and later with the discovery of the gamma-ray emitting "Fermi Bubbles" (Su et al., 2010). The possibility that positrons could be advected into the Galactic bulge by a nuclear outflow was suggested in Jean et al. (2009); Churazov et al. (2011), as this scenario could potentially explain not only the morphology by transporting positrons out to $\sim$kpc scales but also the spectrum of positron annihilation gamma-rays: Positrons born into the hot, $\sim 10^7\,$K plasma at the base of the outflow may not annihilate until the outflowing plasma has cooled to $\sim 10^4\,$K through both adiabatic and radiative cooling processes. An explicit connection between the nuclear outflow, the Fermi Bubbles and Galactic bulge positrons was mentioned in Crocker and Aharonian (2011), and investigated in detail in **?**. The authors perform a parameter study to investigate whether any steady state nuclear outflow with a given input mass and energy flux from star formation can advect positrons to radii consistent with *INTEGRAL* observations. While advection of MeV positrons to size scales of $\sim 2\,$kpc is possible, the development of a strong ionization and temperature gradient in the steady-state outflow ultimately results in the annihilation of the majority of positrons in the hot, ionized phase of the ISM. Constraints from the observed annihilation spectrum indicate no more than a few per cent of positrons annihilate in the hot phase, in the case of annihilation in a multi-phase ISM Churazov et al. (2005).

In (Panther et al., 2017), the study was restricted to a steady-state nuclear outflow and the limits of the work can thus put weak constraints on positron injections in a single burst. Single-burst injection of positrons was investigated in more detail in Cheng et al. (2006); Totani (2006) and was commented on in particular by Alexis et al. Alexis et al. (2014), who find that a burst of either star formation, or activity of the Milky Way's central supermassive black hole (SMBH) producing $10^{57} - 10^{60}$ positrons with energies $< 1\,$MeV could contribute to the Galactic bulge annihilation signal. However, this scenario requires a coincidence with a previous burst of star formation or AGN-like activity from the SMBH, which must have occured $0.3 - 10\,$Myr ago.

4.5 Distributed positron sources

The conclusion that, according to detailed simulations, positrons annihilate close to their sources and that large scale gas motions may be unable to consistently account for all properties of positron annihilation in the Galactic bulge (both the morphology and spectrum of the emission) is not the only motivation to search for a positron source that has a similar distribution to that of the annihilation signal. With 11 years of *INTEGRAL* data, a new best fit model for the morphology of positron annihilation in the Galaxy has emerged Siegert et al. (2016b): observations now favor a model that includes an extended thick disk of emission with a spatial extent similar to that of the Galactic thick disk. Moreover, updated estimates on the flux of not only this thick disk and the Galactic bulge component, but also of a source coincident with the Galactic center reveal flux ratios between bulge and disk, and bulge and "Galactic Center Source" that are consistent with the stellar mass ratios between these regions. In light of the new observations and recent theoretical work on positron propagation, the search has now turned to finding a Galactic positron source associated with the old stellar population. Once again, the usage of B/D to evaluate good morphological fits has been used. In Siegert et al. (2016b), $B/D \sim 0.4$, a large reduction from earlier values (Knödlseder et al., 2005; Weidenspointner et al., 2008a). This is due to the introduction of the extended thick disk model component. It should be emphasised that this value is taken from empirical best-fit models to simplify subsequent analysis and should not be over-interpreted.

The remarkable observation of positron annihilation in the 2015 outburst of microquasar V404 Cygni (Siegert et al., 2016a) lends weight to the conjecture that such a source of positrons is associated with microquasars and low-mass x-ray binaries (LMXRBs) during an outburst, or producing jets Guessoum et al. (2006b). During its 2015 outburst, positron annihilation in the microquasar jet was invoked to explain the broad emission feature at $\sim 0.5\,\mathrm{MeV}$ in the gamma-ray spectrum, which extends above 511 keV, and can naturally be explained by pair production in the jet which then results in pair-plasma annihilation (Aharonian and Atoyan, 1981; Svensson, 1982), annihilation in-flight (Beacom and Yüksel, 2006) or pair cascades (Aharonian and Atoyan, 1981). To explain the positron annihilation rate and morphology, around 10 such sources would be required to be active at any time, with a total of $10^3 - 10^4$ systems being present in the Milky Way (Siegert et al., 2016a). This is consistent with binary population synthesis estimates for the number of these systems Sadowski et al. (2008). However, this is dependent on the total positron yield of each event, a value which is highly uncertain.

An alternative scenario invokes a sub-type of SNe Ia that are observationally connected to old stellar populations. Around 30 per cent of all SNe Ia in early-type host galaxies are observed to be of the sub-type SN1991bg-like (SNe 91bg). These supernovae are both photometrically and spectroscopically peculiar, with their red colors and deep TiII spectral absorption feature. While positrons produced in the decay of the 56-Ni daughter nucleus 56-Co will be predominantly annihilated in the SN ejecta, as with normal SNe Ia (Milne et al., 1999; Taubenberger et al., 2008), positrons from the much longer-lived ^{44}Ti decay chain will escape the SN into the surrounding ISM. In Crocker et al. (2017), binary population synthesis calculations are performed to identify a candidate progenitor channel for these events. Low mass ($\sim 1.4 - 2\,\mathrm{M}_\odot$) binary systems evolve into systems composed of a carbon-oxygen white dwarf ($M \sim 0.9\,\mathrm{M}_\odot$) and a pure helium white dwarf ($M \sim 0.31 - 0.37\,\mathrm{M}_\odot$) which merge at long characteristic delay times (3-6 Gyr). The supernova resulting from this merger would be required to produce $\sim 0.031\,\mathrm{M}_\odot$ 44-Ti per transient event (equivalently $\sim 5.8 \times 10^{-5}\,\mathrm{M}_\odot/\mathrm{yr}$) to explain the origin of the majority of positrons in the Milky Way, and this yield is roughly consistent with existing calculations of Ti-44 yield from sub-Chandrasekhar helium detonations. This long delay time implies a connection between old stars in the Milky Way and these thermonuclear supernovae, and the rate derived for these events from the binary population synthesis calculation is consistent with the expected Galactic rate of SNe 91bg, derived from observations of these supernovae in external Galaxies.

Combining the total positron yield expected from this transient and the expected rate in the disk, bulge and nuclear region of the Galaxy, the authors of Crocker et al. (2017) find that they can account for 90% of the total positron production in the Galaxy (the remaining 10% being accounted for by 26-Al synthesis in massive stars) and replicate B/D and N/B within uncertainties. However, detailed three-dimensional hydrodynamical simulations of the proposed supernova explosion and further post-processing of these simulations with nuclear reaction networks will be required to further evaluate the plausibility of this scenario. Furthermore, these simulations must also be post-processed with radiative transfer networks to investigate whether the proposed scenario provides a match to observed SNe 91bg spectra and light curves.

4.6 Conclusions

Understanding the transport of MeV positrons in the ISM is required to reveal the source of the $\sim 5 \times 10^{43}$ positrons that annihilate each second in the Galaxy. The bulge-dominated morphology of this astrophysical signal is contrasted with the distribution of MeV positron sources, which are usually associated with the star-forming thin disk of the Galaxy, not the more quiescent stellar bulge. The propagation of positrons has been investigated through both theory and simulation, with recent conclusions suggesting that positrons remain confined to within a few hundred parsecs of their birth sites by interstellar turbulence and that the distribution of positron sources is directly reflected by the morphology of annihilation gamma-rays. Such sources are thought to be associated with the old stellar population of the Milky Way. However, uncertainty remains about the dominant modes of positron propagation and the details of collisionless and collisional transport of positrons, which is complicated by the need for more detailed understanding of interstellar magnetic turbulence and the Galactic magnetic field that affects positron propagation. Consequently, there is still much work to be done to understand the birth, life and death of positrons in the interstellar medium.

4.7 Acknowledgements

This research is supported by an Australian Government Research Training Program (RTP) Scholarship. FHP thanks Roland Crocker, Roland Diehl, Eugene Churazov, Thomas Siegert and Torsten Ensslin for useful discussions, and Christoph Weniger and Dmitry Malyshev, organisers of the conference "Three Elephants in the Gamma-Ray Sky".

Chapter 5

Positron annihilation with alkali metal atoms in the Interstellar medium

You just come along with me and have a good time. The Galaxy's a fun place.

Douglas Adams

Foreword

Many laboratories around the world are engaged in the study of the cross-sections of positron interactions with a number of atoms and molecules. These are of great interest in the context of positron annihilation in biological systems, as positron emission tomography is a common and powerful diagnostic tool in the detection of cancers in humans and animals (Gambhir, 2002). It is possible to utilize many of these cross-sections in the context of astrophysics.

Experiments to measure the cross-section of atoms have been performed on atomic species including hydrogen, helium, most alkali metals, and many other light elements. These experiments involve firing a low-energy beam of positrons which are usually produced by a β^+ decaying source such as ^{22}Na into a sample of the material in a high vacuum. Generating this positron beam is a challenging problem itself, as is measuring the number and energy of positrons which survive annihilation with the sample. What is measured are the total scattering cross-section for each atomic species, as well as the ionization and excitation (inelastic process) cross-section. These cross-sections can be combined to compute the positronium formation cross-sections (Guessoum et al., 2006a).

Theoretical calculations of the positronium formation cross-sections can also be made. These involve complex quantum mechanical calculations of scattering cross-sections. The most common modern technique to calculate the scattering cross-section of atomic and molecular species is the closed-coupling calculation (e.g. Kadyrov and Bray, 2016).

In the following paper, I utilize recent closed coupling calculations of the scattering and positronium formation cross-sections of alkali metal atoms to demonstrate that positron interactions with atoms other than hydrogen and helium must be considered in the context of the galactic positron annihilation signal. When only interactions with hydrogen, helium and electrons are considered, we find a low energy reservoir of positrons that may live up to 10 Myr after they lose their energy and thermalize in the interstellar medium.

One of the consequences of the presence of a positron resevoir would be that the positrons we observe annihilating today may not have been produced in a steady state, which is usually assumed in most models to explain the positorn annihilation signal. Instead, the current positron production rate in the galaxy may not be required to be as high as is suggested by the positron annihilation line, and processes which result in the episodic injection of positrons could be responsible for producing the bulk of those we see annihilating today.

Another interesting consequence of such a reservoir is that it implies that these long-lived thermalized positrons could be transported over many kiloparsecs passively in gas motions. This raises the possibility that there may be many more positrons present in the interstellar medium than we observe annihilating which could potentially find their way into the very low density galactic halo before annihilating.

We find that the inclusion of other atoms in the interstellar medium, in particular alkali metal atoms, which have negative positronium formation thresholds and large charge-exchange cross-sections, reduces the lifetime of thermalized positrons to < 1 Myr. This constrains the observed positron annihilation rate to be in steady state with the production rate, and rules out the presence of a reservoir of thermal positrons in the interstellar medium.

Declaration

This work was published in the journal *Physical Review D*. The manuscript is reproduced here with formatting changes to make it consistent with the rest of the work in this thesis. I contributed 95% of the manuscript preparation for this article, and performed 100% of the simulations described in the article myself. Updated information, including model fits to data for positron annihilation cross-sections for positron interactions with hydrogen and helium were supplied by Daniel Murtagh from the sources referenced in the text.

The effect of positron-alkali metal atom interactions in the diffuse ISM

Fiona H. Panther[1], Ivo R. Seitenzahl[2], Roland M. Crocker[1], Joshua R. Machacek[3], Dan J. Murtagh[3,4], Thomas Siegert[5], Roland Diehl[5],

[1] Research School of Astronomy and Astrophysics, Australian National University, Canberra 2611, Australia
[2] School of Physical, Environmental and Mathematical Sciences, University of New South Wales, Australian Defence Force Academy, Canberra 2612, Australia
[3] Plasma Research Laboratory, Research School of Physics and Engineering, Australian National University, Acton, Canberra, 2601
[4] Stefan Meyer Institute for Subatomic Physics, Boltzmanngasse 3,1090 Vienna, Austria
[5] Max-Planck-Institut für extraterrestrische Physik, Giessenbachstr. 1, D-85741 Garching, Germany

Published in: *Physical Review D* 98, 023015, 2018; https://doi.org/10.1103/PhysRevD.98.023015

Abstract

In the Milky Way galaxy, positrons, which are responsible for the diffuse 511 keV gamma ray emission observed by space-based gamma ray observatories, are thought to annihilate predominantly through charge exchange interactions with neutral hydrogen. These charge exchange interactions can only take place if positrons have energies greater than 6.8 eV, the minimum energy required to liberate the electron bound to the hydrogen atom and then form positronium, a short-lived bound state composed of a positron-electron pair. Here we demonstrate the importance of positron interactions with neutral alkali metals in the warm interstellar medium (ISM). Positrons may undergo charge exchange with these atoms at any energy. In particular, we show that including positron interactions with sodium at solar abundance in the warm ISM can significantly reduce the annihilation timescale of positrons with energies below 6.8 eV by at least an order of magnitude. We show that including these interactions in our understanding of positron annihilation in the Milky Way rules out the idea that the number of positrons in the Galactic ISM could be maintained in steady state by injection events occurring at a typical periodicity $>$ Myr.

5.1 Introduction

In 1931, Paul Dirac predicted the existence of a particle with the same mass, but opposite charge, to the electron (Dirac, 1931). The existence of the anti-electron, or positron, was confirmed by Carl Anderson a year later (Anderson, 1932). While the annihilation of positrons through direct interaction with electrons was predicted by Dirac (Dirac, 1931), positrons may also form a short-lived bound state composed of a positron and electron, known as positronium, before subsequently annihilating. The existence of positronium was predicted in 1934 Mohorovičić (1934), but was not confirmed experimentally until the 1950's (Deutsch, 1951). Since the 1930's, positrons have been observed in a variety of astrophysical environments. The presence of positrons is inferred through the detection of characteristic gamma ray emission at $m_e c^2 \sim 0.5\,\mathrm{MeV}$ from the co-annihilation of electrons and positrons. We now see positron annihilation in the diffuse interstellar medium (ISM) Knödlseder et al. (2005); Weidenspointner et al. (2008a); Siegert et al. (2016b), solar flares (Murphy et al., 2005), associated with the synthesis of β^+ unstable radionuclides in supernovae (Churazov et al., 2014), and in microquasar flares Siegert et al. (2016a). Futhermore, the production of positrons in astrophysical environments can also be inferred through the observed presence of the parent nuclei of β^+ unstable radionuclides such as ^{26}Al, ^{22}Na, ^{44}Ti and ^{56}Ni, whose decay lines are observed through both X-ray and gamma ray measurements (see (Diehl et al., 2011) for an overview).

In the early 1970's, emission of gamma rays at $\sim 0.5\,\text{MeV}$ from the central regions of the Milky Way was first detected by balloon-borne spectrometers (Johnson et al., 1972; Leventhal et al., 1978) and subsequently confirmed by a number of space-based missions (Purcell et al., 1997; Knödlseder et al., 2005; Weidenspointner et al., 2008a; Siegert et al., 2016b). Recent observations of diffuse annihilation gamma rays across the Milky Way suggest an annihilation rate of $\sim 5 \times 10^{43}$ positrons per second (Siegert et al., 2016b). These positrons are constrained to be injected into the ISM at mildly relativistic energies ($< 3 - 7\,\text{MeV}$)(Aharonian and Atoyan, 1981; Beacom and Yüksel, 2006) due to the absence of a gamma ray continuum at energies $> 511\,\text{keV}$ produced when relativistic positrons annihilate in flight with free electrons. Positron lifetimes are split into two phases: the "in-flight" phase, when the kinetic energy of the positrons is greater than $w_{\text{therm}} = 3kT_e/2$ (where T_e is the electron temperature) and the "thermalized" phase, when the positron kinetic energy drops below w_{therm} (Guessoum et al., 2005).

In the ISM, positrons can annihilate via a number of channels. For example, they may interact with neutral atoms through charge exchange. In this process, positrons with sufficient energy to overcome the difference between the binding energy of the atom and the binding energy of positronium first strip the valence electrons from atomic nuclei, then form positronium before subsequently annihilating[1]. The total spin angular momentum of the positronium bound state governs the number and energy of emitted gamma rays. Positronium formed with the positron and electron with parallel spins produces the three-photon ortho-positronium continuum (Ore and Powell, 1949). Positronium formed from positron-electron pairs with anti-parallel spins annihilates to produce two gamma rays at 511 keV. In astrophysical environments, the annihilation of singlet positronium or para-positronium results in a Gaussian-shaped emission line centered at 511 keV, whose width is governed either by the temperature of the medium for thermalized positrons, the residual kinetic energy of the positron for positrons annihilating in flight, or by large scale gas dynamics (kinetic broadening).

To form positronium via charge exchange, the positron energy must exceed the difference between the binding energy of positronium (6.8 eV) and the first ionization potential of the atom (e.g. $w_{IP} = 13.6\,\text{eV}$ for hydrogen), that is, $w \geqslant w_{IP} - 6.8\,\text{eV}$, where w is the positron energy. In the case of charge exchange with hydrogen (helium), the mimimum kinetic energy a positron must have to form positronium is 6.8 eV (17.7 eV). If the threshold for positronium formation with an atom is negative, positrons can form positronium at any incident energy in charge exchange interactions with that atom. This is the case for the alkali metal atoms, due to their extremely low ionization potentials.

Positrons may also form positronium via radiative recombination with free electrons in the ISM. Unlike charge exchange, positrons with any energy may undergo radiative recombination. Annihilation via radiative recombination also results in the emission of a superimposed para-positronium Gaussian centered at 511 keV and an additional three-photon ortho-positronium continuum. The temperature of the medium strongly affects the width and shape of the resulting annihilation spectrum (Guessoum et al., 2005), as both the frac-

[1]Annihilation lifetimes of positronium are $1.2 \times 10^{-10}\,\text{s}$ for para-positronium, and $1.4 \times 10^{-7}\,\text{s}$ for ortho-positronium.

tion of positrons forming positronium and the shape of the 511 keV line depend on the ISM temperature. Finally, positrons may undergo direct annihilation either through interactions with free electrons in the ISM, or may directly annihilate with electrons bound to atoms. This process results in emission of a Gaussian spectrum where the characteristic width of the line is determined by the ISM electron temperature.

Analysis of the measured gamma ray spectrum suggests that the majority of positrons annihilate via charge exchange interactions with neutral atoms, assumed to be hydrogen based on ISM composition (Churazov et al., 2005). The characteristic orthopositronium continuum emission and narrow emission line centered at 511 keV observed by *INTEGRAL*/SPI indicates that positrons annihilate in a mostly neutral, $\sim 10^4$ K ISM (Churazov et al., 2005, 2011; Siegert et al., 2016b). Simulations and experiment suggest that $90-98\%$ of positrons will annihilate via charge exchange during the in-flight phase in these ISM conditions (Guessoum et al., 2005; Bussard et al., 1979; Wallyn et al., 1994). The remaining positrons will thermalize with the surrounding ISM (Prantzos et al., 2011) before annihilating. It is usually assumed that these thermalized positrons annihilate instantaneously, or on a timescale shorter than the energy loss timescale if the production of positrons is in steady state with respect to the annihilation rate. However, if the annihilation timescale for the thermalized positrons exceeds the slowing down timescale, it is possible for a 'reservoir' of low energy positrons to form. In this scenario, it is possible for the current annihlation rate to exceed the positron injection rate.ÂăThis opens the door on a scenario where positrons are injected into the Galaxy in some kind of outburst event such as those described in Totani (2006) and Cheng et al. (1997).

In this paper we consider how alkali metals in the ISM substantially reduces the annihilation timescale for thermalized positrons in the ISM, and the potential importance of including alkali metal atoms in simulations of positron transport at low energies in the ISM. We also show how including the alkali metal atoms as annihilation targets closes a door on positron production scenarios which do not occur in a steady state.

5.2 Positron annihilation and alkali metal atoms

In existing simulations and theory of positron annihilation in the ISM e.g. Prantzos (2006); Higdon et al. (2009); Jean et al. (2009); Churazov et al. (2011); Martin et al. (2012); Alexis et al. (2014); Panther et al. (2017), positron interactions with hydrogen (both HI and H_2), helium, and free electrons are considered (henceforth the 'simplified ISM model'). Also of potential importance are dust grains and polycylic aromatic hydrocarbon (PAH) molecules, although the cross-sections and mechanisms associated with annihilation on these species are uncertain (Guessoum et al., 2010), and we do not consider them further in this work.

Hydrogen and helium make up the majority of the diffuse ISM by number density at solar metallicity (Lodders, 2003), while the free electron density is strongly dependent on the temperature of the medium. Herein, we consider the ISM at $T \sim 10^4$ K, the ISM temperature at which most positrons seem to annihilate. In this warm, partially ionized phase (WPIM) where the majority of positrons are thought to annihilate (Churazov et al., 2005; Jean et al., 2009; Churazov et al., 2011; Siegert et al., 2016b), the number density of molecular hydrogen (found in the cold neutral phase) is negligible so we only consider atomic species. The composition and ionization state of the ISM is based on that for the warm ISM described in Guessoum et al. (2005). A summary of the number densities of the considered species in the

Table 5.1: Density of ISM species (per cm^3) in the warm, partially ionized phase of the ISM based on (Guessoum et al., 2005).

Species	Density in WPIM / cm^{-3}
Neutral hydrogen	2.68×10^{-1}
Neutral helium	2.60×10^{-2}
Free electrons	2.71×10^{-3}
Neutral lithium	6.05×10^{-10}
Neutral sodium	6.35×10^{-7}
Neutral potassium	4.26×10^{-8}

warm, partially ionized phase of the ISM is given in Table 5.1.

In this work, we utilize positronium cross-sections with approximate shape and magnitude determined from fits to the available data (Campeanu et al., 1987; Bailey et al., 2015; Kauppila et al., 1981; Machacek et al., 2013; Moxom et al., 1996; Weber et al., 1994; Stein et al., 1978; Zhou et al., 1997; Laricchia et al., 2008; Humberston, 1979; Sullivan et al., 2001; Walters, 1988; Kernoghan et al., 1996; Jones et al., 1993; Murtagh et al., 2005; Charlton et al., 1983; Charlton and Humberston, 2000) for positron interactions with hydrogen and helium. We find the timescale for positron annihilation at low energies is not affected by use of one dataset preferentially over another for two reasons: firstly, at 10^4 K the thermalized positron has too little kinetic energy to form positronium in collisions with hydrogen and helium. Consequently, assuming a simplified ISM at these energies positrons only annihilate by direct annihilation with bound electrons in hydrogen and helium atoms, and these cross-sections are comparable to that for direct annihilation with free electrons (see fig 5.1). Secondly, recent advances in measuring total positron scattering cross-sections have resulted in more precise determination of ionization and excitation cross-sections whereas varying the positronium formation cross-section by $\sim 20\%$ (in accordance with the uncertainties on the combined data set) has a negligible effect on our results[2].

Due to the non-negative positronium formation thresholds of hydrogen and helium atoms, the annihilation cross-section for positrons interacting with hydrogen (helium) drops to zero at 6.8 eV (17.7 eV). In the simplified ISM model, positrons with energies below 6.8 eV can only annihilate via interactions with free electrons. The cross-section for these interactions is several orders of magnitude lower than that for positron interactions with hydrogen and helium (fig 5.1). The impact of this decrease in annihilation cross section is interesting in the context of positron annihilation in the ISM, as positrons thermalizing in the ISM phase where most positrons are expected to annihilate (the warm phase) will have energies < 6.8 eV. The lifetime of a thermalized positron (i.e. the time between the positron reaching an energy of $w = 3kT/2$ and subsequently annihilating) with energy w is (e.g. ref (Jean et al., 2009))

$$\tau_{\text{ann}}(w) = \left(c\beta(w) \sum_{\text{T}} \sigma_{\text{T}}(w) n_{\text{T}} \right)^{-1} \tag{5.1}$$

where c is the speed of light, $c\beta$ is the positron velocity, σ_{T} is the cross section of target species

[2]These advances in measuring total scattering cross-sections will be of importance to positron astrophysics in the context of detailed simulation of collisional transport of positrons in the ISM, where ionization and excitation of atoms in the ISM is responsible for the slowing down of energetic positrons

T and n_T the number density. The impact of the dramatic decrease in the annihilation cross section in the simplified ISM model on the lifetimes of thermalized positrons can be seen as the solid curve in Figure 5.2.

In the simplified ISM model, positrons with energies $< 6.8\,\mathrm{eV}$ are thought to only form positronium via radiative recombination with free electrons. However, if there are atoms present in the ISM which possess positronium formation thresholds below 6.8 eV, positrons may still form positronium via charge exchange at low energies. Moreover, if the cross-sections of these atoms is sufficiently large, it may also substantially decrease the annihilation timescale for thermalized positrons in the warm ISM. The formation of positronium from positron-alkali scattering is known, and the cross sections are known to an order of magnitude. Of particular interest are the alkali metal sodium (Kadyrov and Bray, 2016), which has large cross sections (on the order of $\sim 10^{-15}\,\mathrm{cm}^{-2}$) for charge exchange with positrons at energies $< 6.8\,\mathrm{eV}$. For completeness we consider lithium and potassium - however, their inclusion has a negligible effect as their abundances orders of magnitude lower than that of sodium using the abundance tables of Lodders (2003). In the case of potassium, we find its inclusion does not affect the annihilation timescale significantly as its charge exchange cross-section is around half an order of magnitude lower than that of sodium and lithium at the energies considered (Ratnavelu, K. and Ong, W.E., 2011), and its solar abundance around an order of magnitude lower than that of sodium (Lodders, 2003).

The large cross-section of sodium atoms has a significant impact on the lifetime of positrons with energies $< 6.8\,\mathrm{eV}$ despite the comparably low abundance of sodium compared to that of hydrogen and helium (assuming solar abundance in the diffuse ISM). A summary of the species densities in the ISM phase where most positrons appear to annihilate is given in Table 5.1.

In this ISM phase, positrons will thermalize with an energy of $w_{\mathrm{therm}} = 3kT/2 \sim 1.3\,\mathrm{eV}(T/10^4\,\mathrm{K})$. At $w = 1.3\,\mathrm{eV}$, the lifetime of a thermalized positron can be written in parameterized form as

$$\tau = 1.7 \times 10^5 \, \frac{0.27\,\mathrm{cm}^{-3}}{n_H} \left(\frac{1 - X_H}{0.99} 0.085 + \frac{\zeta_{\mathrm{He}}}{0.096} 0.004 + \frac{\zeta_{Li}}{2.23 \times 10^{-9}} 8.9 \times 10^{-4} + \frac{\zeta_{\mathrm{Na}}}{2.34 \times 10^{-6}} 0.78 + \frac{\zeta_{\mathrm{K}}}{1.57 \times 10^{-7}} 2.4 \times 10^{-4} + \frac{X_{\mathrm{H}}}{3 \times 10^{-3}} 0.0015 \right)^{-1} \mathrm{yr} \quad (5.2)$$

where n_{H} is the total hydrogen density, X_{H} is the ionization fraction for hydrogen, and the factors ζ_{T} are the abundances of target atom T relative to protosolar abundance (Lodders, 2003). At 1.3 eV, the lifetime of positrons in the simplified ISM model is $\tau_{1.3} = 1.67\,\mathrm{Myr}$, figure 5.2. Including sodium at solar abundance, along with all species listed in Table 5.1 ($\zeta_{\mathrm{Na}} = 2.24 \times 10^{-6}$ relative to hydrogen (Lodders, 2003)) reduces the lifetime of such thermalized positrons to $\tau_{1.3} = 0.19\,\mathrm{Myr}$.

In particular, in the simplified ISM model, the annihilation timescale exceeds the energy loss timescale for MeV positrons. This apparently allows for the possibility of a low-energy positron 'reservoir' that could act to maintain the total number of ISM positrons in the Galaxy in a steady state even if the positrons are injected by large-scale events (e.g. outbursts associated with the supermassive black hole (SMBH) at the Galactic Center [24, 25]) with a typical periodicity significantly in excess of 1 Myr. However, accounting for alkali metal atoms as annihilation targets in a realistic ISM model, closes the door on this possibility: the positrons we detect currently annihilating in the ISM must have been created within the last $\sim$ Myr[3].

[3]Even this timescale is probably excluded by combination of the observed distribution of positrons

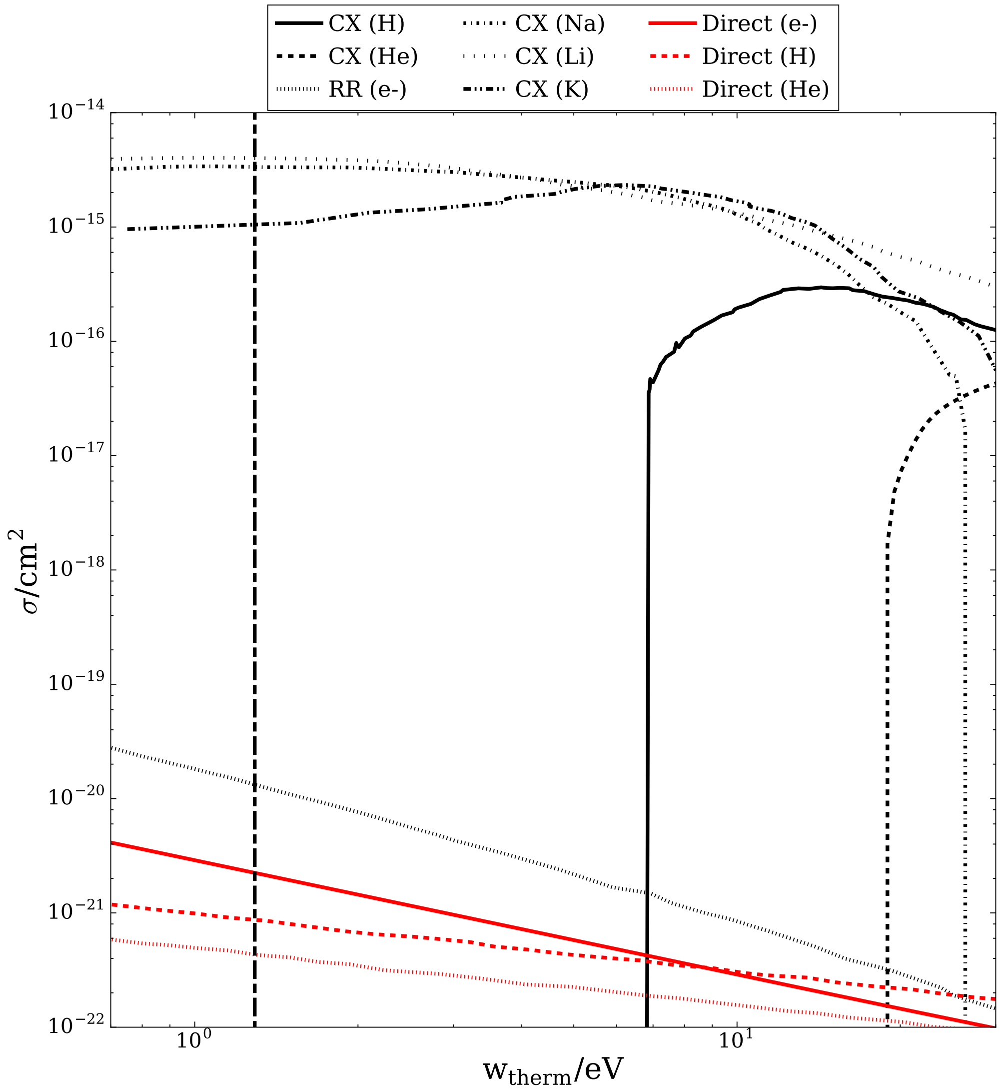

Figure 5.1: Positronium formation and charge-exchange (CX) cross-section for positron annihilation through various channels as a function of incident positron energy. Hydrogen and helium CX cross-sections based on fits to available data, radiative recombination with free electrons from R. Sutherland (priv. comm.) lithium and sodium CX cross-sections from (Kadyrov and Bray, 2016) and potassium CX cross-sections from Ratnavelu, K. and Ong, W.E. (2011). Direct annihilation cross-sections for positron interactions with free and bound electrons are shown in red. The black dashed line shows the average energy of positrons that have thermalized in the WPIM.

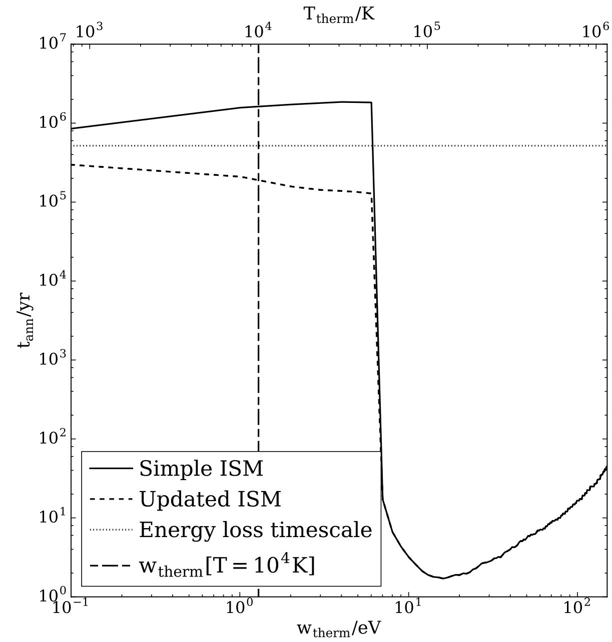

Figure 5.2: Annihilation timescale for thermalized positrons as a function of positron energy. Including the effect of positron interactions with alkali metal atoms, even at solar metallicity, substantially decreases the annihilation timescale for positrons that thermalize with energies < 6.8 eV. The black dashed line shows the average energy of positrons that have thermalized in the WPIM.

5.3 Conclusions

In simple ISM models developed to understand the annihilation of the some 5×10^{43} positrons per second in the diffuse ISM of the Milky Way, it is assumed that positrons with kinetic energies below the charge exchange threshold with neutral hydrogen (< 6.8 eV) can only undergo annihilation through interactions with free electrons, or via direct annihilation with electrons bound to hydrogen and helium atoms (Guessoum et al., 2005; Jean et al., 2009; Churazov et al., 2011; Martin et al., 2012; Alexis et al., 2014; Panther et al., 2017). The consequence of this assumption is that the calculated lifetime for positrons that thermalize in a 10^4 K ISM, thought to be between 2 and 10% of positrons that annihilate in the diffuse ISM, is in excess of 1 Myr. Despite its low abundance at solar metallicity, the inclusion of positron interactions with sodium can reduce the lifetime of thermalized positrons in the ISM to ~ 0.1 Myr, and moreover allows a new channel for positrons to form positronium at energies where positronium formation was only assumed to occur through radiative recombination with free electrons. Finally, we conclude that the number of positrons in the Galactic ISM could be maintained in steady-state by injection events with typical periodicity longer than $>$ Myr.

5.4 Acknowledgements

FHP is supported by an Australian Government Research Training Program (RTP) Scholarship. FHP thanks Ralph Sutherland for the supply of updated annihilation cross-sections for radiative recombination. IRS was supported by the Australian Research Council Grant FT160100028. JRM acknowledges the support of the Australian Research CouncilâĂŹs Discovery Early Career Research Award (DECRA) Fellowship.

5.5 Appendix: Annihilation in the multi-phase ISM

over $\gg$ kpc size scales throughout both the bulge and disk and the fact that large-scale ($>$ kpc) transport of positrons has been ruled out by numerical studies of positron transport Jean et al. (2009); Martin et al. (2012); Alexis et al. (2014); Panther et al. (2017), even where large scale gas dynamics is invoked Panther et al. (2017). In other words, to maintain the inferred smooth and large-scale distribution of positrons across the Galaxy, each $\sim$ kpc-radius patch must have experienced a positron injection event within the last $<$ Myr suggesting that the mean periodicity of positron injection events across the Milky Way is $\gg$ Myr.

Table 5.2: Density of ISM species (per cm^3) in the warm phase of the ISM based on (Guessoum et al., 2005).

Species	Density in HIM / cm^{-3}	Density in WIM / cm^{-3}	Density in WNM / cm^{-3}	w_{IP}/eV
H_0	0	0	0.34	13.6
He_0	0	5.60×10^{-3}	3.20×10^{-2}	24.5
He_+	7.66×10^{-5}	5.60×10^{-3}	0	54.4
e^-	1.75×10^{-3}	0.12	0	0
Li_0	3.56×10^{-12}	2.60×10^{-10}	7.52×10^{-10}	5.39
Na_0	3.73×10^{-9}	2.73×10^{-7}	7.89×10^{-7}	5.13
K_0	2.50×10^{-12}	1.83×10^{-8}	5.30×10^{-8}	4.3407
H_+	1.59×10^{-3}	0.11	0	-
He_2+	7.66×10^{-5}	0	0	-

In Fig 5.3, we show that the inclusion of alkali metal atoms, most notably sodium, reduces the annihilation timescale for thermalized positrons in all phases of the ISM. However, this is most significant in the case of the WNM and WPIM where the majority of positrons are thought to annihilate via interactions with neutral atoms Churazov et al. (2005). In these phases, where $T \sim 10^4$ K, positrons thermalize at ~ 1.3 eV. At this energy, the annihilation timescale for positrons in the simple ISM is significantly longer than the slowing down time for the positrons. Including alkali metal atoms as annihilation targets for thermalized positrons reduces the annihilation timescale, and thus for the updated ISM model we find $\tau_{\text{ann}} < \tau_{\text{loss}}$, with the consequences being the same as those discussed in the main article.

While the observed positron annihilation spectrum suggests that positrons annihilate in a warm, partially ionized ISM, the possibility that positrons annihilate in multiple phases of the ISM is not excluded Churazov et al. (2005). However, the characteristics of the annihilation put strong constraints on the proportion of positrons annihilating in each phase - hot ionised medium (HIM), warm ionized medium (WIM), warm neutral medium (WNM) and cold molecular medium (CMM). In Churazov et al. (2005) it is found that annihilation in a multiphase medium can explain the observed annihilation spectrum only where no more than $\sim 8\%$ of positrons annihilate in the hot ionized phase ($T \geqslant 10^6$ K). Furthermore annihilation in CMM ($T \leqslant 10^3$ K) cannot make a dominant contribution to the annihilation spectrum in the presence of a multiphase medium. Moreover, the presence of the positronium continuum suggests that $> 95\%$ of positrons annihilate via interactions with neutral atoms (usually assumed to be hydrogen and helium). This would suggest that the majority of positrons likely annihilate in the WNM. For completeness, the densities of the species in our updated ISM model are shown in Table 5.2 for each of the HIM, WIM and WNM. We do not consider the CMM based on the constraints on the annihilation spectrum - annihilation on molecular hydrogen in the CMM results in a broad emission line which is inconsistent with the spectrum observed by SPI (Churazov et al., 2005, 2011; Siegert et al., 2016b) - and moreover the spatial morphology of the positron annihilation signal, which is significantly more extended than the distribution of cold molecular gas in the Milky Way.

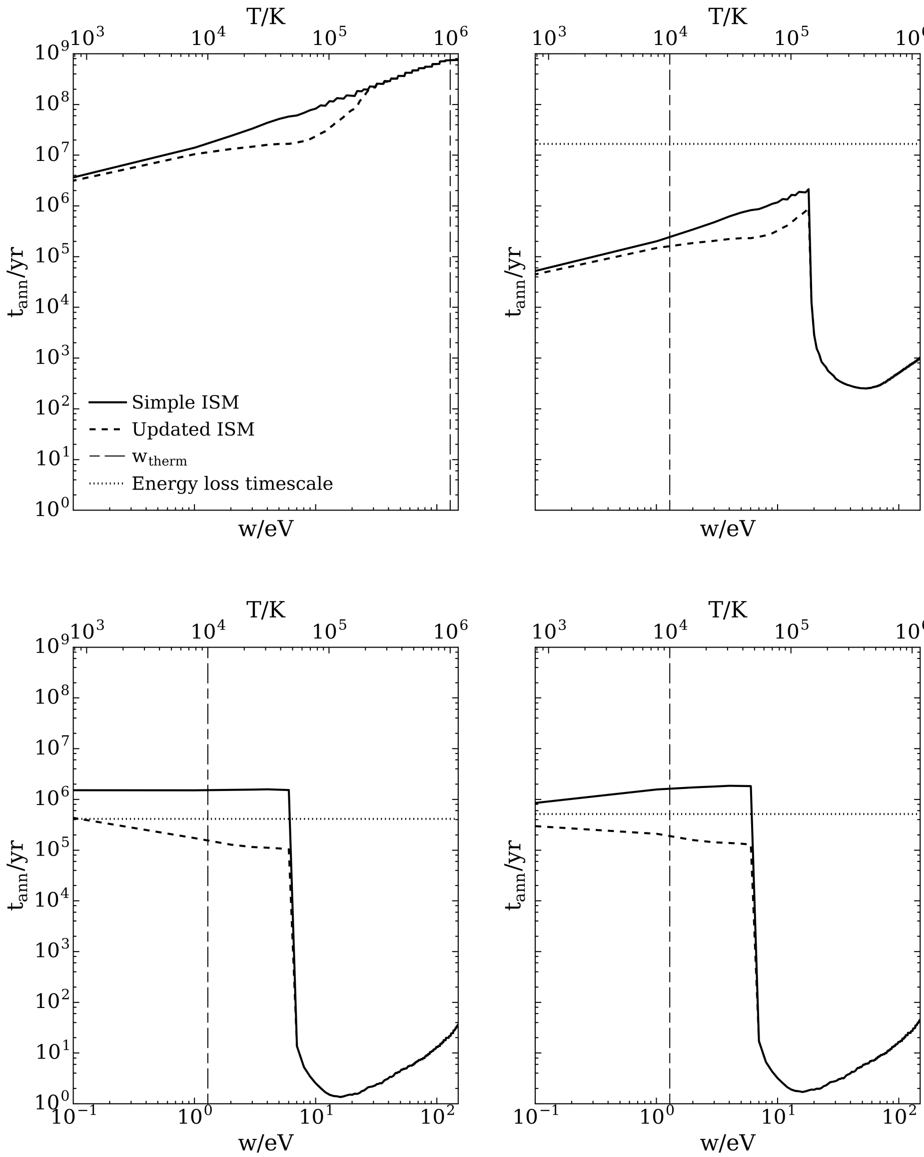

Figure 5.3: Comparison of annihilation timescales for thermalized positrons in the HIM (top left), WIM (top right), WNM (bottom left) and WPIM (bottom right). Vertical dashed lines indicate the average energy of positrons thermalizing in each phase. Horizontal lines show the energy loss timescale for MeV positrons in each phase. In the case of the HIM (top left), the energy loss timescale for MeV positrons is $\sim 10^{11}$ yr

Chapter 6

Positron annihilation in the nuclear outflow of the Milky Way

There is no point in using the word 'impossible' to describe something that has clearly happened.

Douglas Adas

Foreword

My comprehensive review of positron transport shows that in realistic astrophysical scenarios, positrons are confined by small scale turbulent fluctuations in the magnetic field. This means that positrons will tend to be confined close to their sources. Moreover, I have shown that positrons survive only a negligible length of time following thermalization. As a result, thermalized positrons cannot propagate long distances through the interstellar medium. However, large scale transport of positrons has not yet been conclusively ruled out.

In the early 2000s, observations revealed the existence of a nuclear outflow in the Milky Way (Bland-Hawthorn and Cohen, 2003). This observations was confirmed spectacularly in 2010 when the FERMI gamma ray telescope team announced the discovery of the Fermi Bubbles (Su et al., 2010). These gamma ray structures stretch 8 kpc above and below the Galactic plane. The origin of the bubbles is currently unknown, although mechanisms in which past accretion on to the Galactic center SMBH resulting in the launching of relativistic jets have been suggested, as has the ongoing violent star formation activity that occurs in the inner few hundred parsecs of the Milky Way.

The inner 100 pc of the galaxy, or Central Molecular Zone, hosts around 10% of the total star formation activity in the Milky Way (Morris and Serabyn, 1996). This intense star formation activity, and the stellar winds and ejecta from supernova explosions are able to drive a nuclear outflow. This outflow generates a wind-blown bubble that expands adiabatically into the Galactic bulge (Crocker et al., 2015). Material produced by the deaths of stars that drive this bubble may contain large numbers of positrons, such as from the decay of radioactive material. These positrons will be entrained in the gas by magnetic fluctuations in the plasma and can therefore be transported into the Galactic bulge.

It was previously pointed out by Churazov et al. (2011) that the cooling of gas in which positrons may be embedded is an important consideration when evaluating positron production and annihilation scenarios. In particular, Churazov et al. (2011) show that plasma with initial temperatures between a few $\times 10^5 - 10^6$ K can cool to around 10^4 K before positrons annihilate. Thus positrons born in hot gas annihilate to produce a spectrum that is consistent with observations. In the scenario I investigated, it is important to not only consider the radiative cooling of the gas as Churazov et al. (2011) did. An adiabatically expanding bubble of gas will also cool via adiabatic cooling. One of the most interesting aspects of the simulations we performed was the revelation that the adiabatic energy losses of the positrons was the most important energy loss process that positrons undergo.

The idea that positrons could be transported out of the Galactic center became of interest in the 1990s after OSSE/CGRO detected the PLE (Purcell et al., 1997). Works suggested mechanisms by which positrons could be transported up to 8 kpc above the Galactic plane (the latitudinal extent of the PLE). For example, Dermer and Skibo (1997) described a feature called the 'positron annihilation fountain', an outflow of material from the Galactic center which transported positrons into the galactic halo. While INTEGRAL has not shown us any hint of the PLE in recent observations (Siegert et al., 2016b), and the feature was shown to be an artefact of the image reconstruction analysis (Milne et al., 2001b), it is still possible that a nuclear outflow could operate to disperse positrons into the Galaxy on a smaller scale as suggested in Crocker and Aharonian (2011).

In this chapter, I show that advective transport and subsequent annihilation of positrons in the nuclear outflows of the Milky Way cannot simultaneously replicate the observed morphology of positron annihilation in the Galactic bulge and satisfy the requirement that 90 per cent of positrons annihilate once the outflow has cooled to 10^4 K.

Declaration

This work was published in the journal *Monthly Notices of the Royal Astronomical Society: Letters*. The manuscript is reproduced here with formatting changes to make it consistent with the rest of the work in this thesis. I contributed 95% of the manuscript preparation for this article, and performed 90% of the simulations descibed in the article myself. The equation describing the gravitational potential of the Milky Way was obtained from discussion with Geoffrey Bicknell and Roland Crocker at The Australian National University, and the equations describing the effective polytrope γ_{ad} for the adiabatic energy losses of the positrons was obtained via calculation with assistance from Yuval Birnboim.

Positron Annihilation in the Nuclear Outflows of the Milky Way

Fiona H. Panther[1,2], Roland M. Crocker[1], Yuval Birnboim[3], Ivo R. Seitenzahl[1,4], Ashley J. Ruiter[1,2,4]

[1] Research School of Astronomy and Astrophysics, Australian National University, Canberra 2611, Australia
[2] ARC Centre of Excellence for All-Sky Astrophysics (CAASTRO)
[3] Racah Institute of Physics, The Hebrew University, Jerusalem, Israel
[4] School of Physical, Environmental and Mathematical Sciences, UNSW Canberra, Australian Defence Force Academy, Canberra 2612, Australia

Published in: *Monthly Notices of the Royal Astronomical Society: Letters*, Volume 474, Issue 1, 2018; Pages L17-L21, https://doi.org/10.1093/mnrasl/slx183

Abstract

Observations of soft gamma rays emanating from the Milky Way from SPI/*INTEGRAL* reveal the annihilation of $\sim 2 \times 10^{43}$ positrons every second in the Galactic bulge. The origin of these positrons, which annihilate to produce a prominent emission line centered at 511 keV, has remained mysterious since their discovery almost 50 years ago. A plausible origin for the positrons is in association with the intense star formation ongoing in the Galactic center. Moreover, there is strong evidence for a nuclear outflow in the Milky Way. We find that advective transport and subsequent annihilation of positrons in such an outflow cannot simultaneously replicate the observed morphology of positron annihilation in the Galactic bulge and satisfy the requirement that 90 per cent of positrons annihilate once the outflow has cooled to 10^4 K.

6.1 Introduction

The Milky Way hosts the annihilation of $\sim 5 \times 10^{43}$ positrons each second (Siegert et al., 2016b). The annihilation of positrons is detected indirectly through measurements of gamma rays and is characterised by a strong emission line centered at 511 keV, the rest mass energy of the positron (or electron). Positron annihilation in the Milky Way was first detected by balloon-bourne spectrometers in the early 1970s (Johnson et al., 1972): a notable excess of emission at ~ 0.5 MeV was observed to be concentrated toward the center of the Galaxy. However, the spatial resolution of such instruments was poor. The most recent observations with SPI/*INTEGRAL* (Knödlseder et al., 2005; Weidenspointner et al., 2008a; Siegert et al., 2016b) allow detailed morphological models of positron annihilation gamma rays to be constructed.

The most recent morphological models of positron annihilation in the Galactic bulge are described in Siegert et al. (2016b), where the emission is modelled as the superposition of two two-dimensional gaussians. Siegert et al. (2016b) also describe emission from an extended thick disk, an observation highly dependent on the assumed spatial template. The more robust observation of positron annihilation in the Galactic bulge is the focus of this work, and historically the high surface brightness of positron annihilation gamma rays in this region and the high absolute positron annihilation rate - $\sim 2 \times 10^{43}\,e^+\,s^{-1}$ - have been difficult to explain. This is because most putative positrons sources are concentrated in regions of star formation in the Galactic disk (Prantzos et al., 2011; Ramaty et al., 1979), and those associated with the older stellar population of the Galactic bulge have positron yields that are currently not well constrained, such as microquasars (Siegert et al., 2016a). Others employ exotic physics such as the de-excitation or annihilation of dark matter (e.g. Finkbeiner and Weiner, 2007; Bœhm, 2009).

The spectrum of the positron annihilation radiation observed by *INTEGRAL* implies that $\sim$ 100 per cent of positrons annihilate via interactions with neutral hydrogen (charge exchange, see Guessoum et al., 2005, for an overview). Moreover, constraints show positrons are injected into the interstellar medium (ISM) at low energies ($\leqslant\sim 3-7$ MeV, Aharonian and Atoyan, 1981; Beacom and Yüksel, 2006). This likely rules out compact sources such as pulsars and millisecond pulsars as the origin of the annihilating positrons as such sources inject positrons into the ISM at energies greater than a few GeV.

The observed spectrum of positron annihilation in the Galaxy is best explained with annihilation of positrons with intial energies $w_0 \leqslant$ a few MeV in a single phase ISM with a temperature of $\sim 10^4$ K and a degree of ionization of a few $\times 10^{-2}$ (Churazov et al., 2005; Siegert et al., 2016b) or alternatively by annihilation of these 'low energy' positrons in a multiphase medium where no more than $\sim$ 8% of positrons annihilate in the very hot phase ($T \geqslant 10^6$ K). Furthermore annihilation in the hot ($T \geqslant 10^5$ K) or cold ($T \leqslant 10^3$ K) media cannot make a dominant contribution to the annihilation spectrum (Churazov et al., 2005; Siegert et al., 2016b) in the presence of a multiphase medium.

Previous works have attempted to explain the morphology of positron annihilation gamma rays through the diffusive transport of positrons (Martin et al., 2012; Alexis et al., 2014) produced near the Galactic center (refered to herein as 'inside-out' transport, e.g. Jean et al., 2009). However, such works struggle to replicate the observed morphology of the positron annihilation signal and require the presence of a highly ordered magnetic field to aid positron diffusion out into the Galactic bulge (out to radii $\sim$ kpc). In particular, Jean et al. (2009) find that low energy positrons are confined to scales of $\sim$ 200 pc in the presence of magnetic turbulence characterised by a Kolmogorov turbulent spectrum.

Diffusive transport of positrons into the Galactic bulge region was also investigated (Prantzos, 2006; Higdon et al., 2009; Martin et al., 2012; Alexis et al., 2014), however the scenario presented involved positrons produced in the disk. This 'outside-in' transport mechanism invokes diffusion in a similar manner to the 'inside-out' diffusion scenario of Jean et al. (2009). The expected similarity of the diffusion coefficients in the Galactic disk and bulge environments[1] suggests that diffusion in the 'outside-in' transport scenario can be ruled out for the same reasons presented in the 'inside-out' transport case.

Several works have also posited that the origin of positrons is related to our Galaxy's central supermassive black hole (SMBH) (e.g. Totani, 2006; Cheng et al., 2006). In this scenario positrons are produced either in the accretion disk around the SMBH or through pair production in jets. The jet can also be invoked as a transport mechanism to distribute the positrons onto the size scales of the Galactic bulge. However, this scenario implies stringent fine-tuning constraints on the time between the launching of the jet, the total jet power and the subsequent time at which positron annihilation is observed.

Explaining the *morphology* of positron annihilation radiation in the Galaxy represents only part of the solution to the origin of Galactic positrons. In addition, one must explain the *spec-*

[1] $D = 9.8 \times 10^{-4}\,\mathrm{kpc}^2\,\mathrm{Myr}^{-1}$ for $\sim$ MeV positrons in Jean et al. (2009) for the Galactic bulge, as opposed to $4.1 \times 10^{-4}\,\mathrm{kpc}^2\,\mathrm{Myr}^{-1}$ derived in Maurin et al. (2001) for the Galactic disk

trum of positron annihilation gamma rays. In the above works, positrons are transported into neutral material where they subsequently annihilate. An alternative scenario was suggested, and found viable, by Churazov et al. (2011): positrons annihilate in an ISM that radiatively[2] cools from $\sim 10^6$ K to $\sim 10^4$ K on a timescale shorter than the positron lifetime in the ISM. The annihilating positrons retain no 'memory' of the initial thermal conditions of the ISM. Only the ISM conditions at annihilation leave their characteristic imprint on the resulting spectrum of emitted gamma rays. The limitation of the Churazov et al. (2011) model lies in the fact that the transport of positrons is not considered: positrons are assumed to annihilate in locations that replicate the morphology determined from *INTEGRAL*/SPI measurements of the positron annihilation radiation described in the same work.

The influence of large scale motions of gas associated with star formation in the Milky Way's Galactic center have not been considered in detail with respect to resolving the origin of the Galactic bulge positrons, however positron transport in a Galactic nuclear outflow was first posited in Dermer and Skibo (1997) in the context of observations made by OSSE/*CGRO* (Purcell et al., 1997). These observations revealed an extended component of positron annihilation at latitudes of up to $> 15^\circ$, however the observation of this feature in data from OSSE was highly model dependent (Milne et al., 2001a) and the feature did not appear in subsequent analysis. In the context of explaing the highly robust observation of positron annihilation in the Galactic bulge, the plausibility of such a scenario was first raised in Crocker and Aharonian (2011), in the context of the existence of a nuclear outflow in the Milky Way. Evidence for such an outflow emerged in Bland-Hawthorn and Cohen (2003). Gamma ray structures further suggestive of such an outflow (the 'Fermi Bubbles'; Su et al., 2010) were subsequently discovered in data from the *FERMI* satellite. Such an outflow would cool both radiatively and adiabatically as the gas injected at the Galactic center expands (Crocker et al., 2015). Moreover, it is plausible that advection could transport positrons over the $\sim$ kpc distances required to explain the spatial morphology of the positron annihilation signal. Based on the work of Jean et al. (2009), the diffusion timescale for positrons to escape from a region with radius $\sim 200\,\mathrm{pc}$ is $t_{\mathrm{diff}} \sim 40\,\mathrm{Myr}$. This is calculated using the diffusion coefficient for MeV positrons with a Kolgomorov turbulent spectrum, derived in Jean et al. (2009). In comparison, the timescale for positrons comoving with an outflow with wind velocity $v \sim 500\,\mathrm{km\,s^{-1}}$ (Crocker et al., 2015) to advect to 1 kpc is $t_{\mathrm{adv}} \sim 1\,\mathrm{Myr}$, less than the diffusion timescale of the positrons. Thus, positrons can be accurately described as 'frozen-in' to the plasma by magnetic turbulence and we henceforth assume they co-move with any large scale motions of this plasma.

In this work, we consider the transport of positrons in an analytical model of this nuclear wind and investigate whether such a scenario can replicate the two key observations of the Galactic positron annihilation signal: its morphology and the gamma ray energy spectrum.

6.2 Methods

6.2.1 Outflow Model

We model one half of a nuclear outflow. The solid angle subtended by the outflow is fixed at $\Omega = \pi$ Str to replicate the geometry of the Fermi Bubbles (Lacki, 2014), and the geometry

[2] It was noted in this work that adiabatic cooling of the ISM could be important to consider

of the outflow is that of the section of a sphere. The wind launching zone[3] at the base of the outflow has an initial radius of $r_0 = 100\,\mathrm{pc}$ based on the radius of the Central Molecular Zone (CMZ), the region of high star fomation intensity in the Galactic center (Morris and Serabyn, 1996). The evolution of the resulting wind can thus be described by the geometry of the outflow, and the mass flux, $\dot{M}$, and energy flux, $\dot{E}$, into the outflow. The initial temperature of the wind is set self-consistently with the mass and energy flux into the outflow following Strickland and Heckman (2009), as is the initial wind velocity at r_0 i.e. $T_0 = 2\mu m_p \dot{E}(5k\dot{M})^{-1}$ and $v_0 = (2\dot{E}\dot{M}^{-1})^{1/2}$. The mass density of the plasma in the outflow evolves according to mass conservation, with the initial density given by $\rho_0 = \dot{M}(2v_0\Omega r_0^2)^{-1}$. The nuclear wind will decelerate as it does work against the gravitational potential of the Galaxy. To describe the wind deceleration we use a parameterization to approximate the gravitational potential $\Delta\phi$, described by Breitschwerdt et al. (1991):

$$\phi[R,z] \simeq 1.6\times10^5 - \frac{8.82\times10^4}{\sqrt{R^2+z^2+0.245}} - \frac{1.1\times10^6}{\sqrt{R^2+\left(\sqrt{z^2+0.70}+7.26\right)^2}} + \frac{5.81\times10^5}{13+\sqrt{R^2+z^2}}$$
$$+\,4.47\times10^4 \ln\left(13+\sqrt{R^2+z^2}\right)\,(\mathrm{km\,s^{-1}})^2, \quad (6.1)$$

where z is the height above the Galactic plane and R the Galactocentric radius, both in kpc, in cylindrical coordinates. As we assume spherical symmetry, we approximate the value of $\Delta\phi$ by its value on the z-axis (i.e. where $R = 0$ in eqn. 1). In our model, we henceforth refer to the coordinate z as r, the radial distance from the Galactic center. The wind velocity is given as a function of the radial distance from the Galactic center r as (Crocker et al., 2015): $v = v_0(1-\dot{M}\dot{E}^{-1}\Delta\phi[r])^{1/2}$. Here $\Delta\phi[r] = \phi[r] - \phi[r_0]$.

The temperature of the outflow evolves through both radiative and adiabatic cooling. The radiative cooling rate is calculated assuming the plasma is in collisional ionization equilibrium (CIE). We find that in the outflow the electron-ion collision timescale (e.g. Lacki, 2014) is always shorter than the advection timescale for the outflows we describe, hence CIE is an accurate description of the cooling mode of the plasma. In addition to radiative cooling, the gas cools adiabatically as it expands, with an effective polytrope of $\gamma_{\mathrm{ad}} = 5/3$ for the non-relativistic plasma.

The ionization state of the plasma is computed from the CIE tables of Sutherland et al. (2013). We track the evolution of the ionization fraction, and hence calculate the evolution of the neutral hydrogen number density n_H, ionization fraction X_H and electron density n_e, as the energy losses of the positrons depend on the density of all species in the ISM.

6.2.2 Positron Microphysics

We consider the propagation of positrons with initial energies $w_0 < 1.4\,\mathrm{MeV}$ in a nuclear outflow. This upper bound on the initial energy is consistent with a source of positrons produced in β^+ decay of radionuclides synthesised by stars and stellar end products like supernovae, and moreover is consistent with the constraints on the energies of positrons in the Galactic center from Beacom and Yüksel (2006). For positrons emitted from β^+ unstable radionu-

[3] The wind will initially accelerate, however we find that for our chosen parameter space there is no futher acceleration beyond $\sim 100\,\mathrm{pc}$

clides (such as ^{44}Sc and ^{56}Co), positrons are emitted with an energy spectrum with a mean emission energy of $\sim$ 600 keV and a maximum emission energy of $\sim$ 1.5 MeV. We calculate the energy w_{50} such that 50 per cent of positrons are emitted with energies $w_0 \leqslant w_{50}$. We then calculate the mean lower and upper energy at which positrons are emitted based on our calculated w_{50} for positrons emitted in decay of ^{56}Co: $w_{\rm low} \sim 0.4$ MeV and $w_{\rm high} \sim 0.8$ MeV respectively. These values are close to those derived when considering positrons emitted from decay of ^{44}Sc.

Our analysis does not include a detailed treatment of discrete energy loss interactions between positrons and neutral hydrogen atoms, nor do we consider the annihilation of positrons "in-flight" (while their kinetic energies $w_0 \gg 3/2k_bT$). These processes only become important in the last few tens of years of the positrons Myr lifetimes when the positrons reach kinetic energies $w < 100$ eV. The short timescales on which these processes become important, at the end of the positron lifetimes, allows us to consider only the continuous energy loss processes in calculating positron trajectories.

Positrons interact with all components of the ISM: neutral and ionized atoms, free electrons, the magnetic field and the radiation field. However, positrons with energies $w \ll 1$ GeV lose the majority of their energy through ionization and plasma losses. Other radiative energy loss processes (synchrotron losses, bremsstrahlung with neutral and ionized atoms, and inverse Compton losses) are negligible for $\sim$ MeV positrons (Prantzos et al., 2011). The adiabatic expansion of the plasma in which the positrons are embedded mean that the positrons lose energy through adiabatic cooling. We find that the adiabatic energy losses of the positrons tend to dominate over radiative energy loss processes, and as the adiabatic energy losses of the positrons do not depend on the opening angle of the outflow, positron trajectories are not sensitive to the specific choice of opening angle. Unlike the wind fluid, the effective polytrope for the positrons evolves with the positron energy as they transition from a relativistic to non-relativistic fluid during the energy loss process. We assume an ideal equation of state (EoS), and the adiabatic index of the positrons is given by $\gamma_{\rm ad} = 1 + 1/3(\beta^2/(1-(1-\beta^2)^{1/2}))$, where $\beta = (1-(1/(1+\eta)))^{1/2}$, $\eta = w/511$ keV. In reality, the EoS is dependent on the internal energy of the positrons and hence non-ideal, however we find the impact of the non-ideal EoS compared to the ideal EoS is negligible.

6.2.3 Evolution of positron energy in a nuclear outflow

In our model, we assume that positrons co-move with the expanding plasma - low energy positrons are confined by magnetic turbulence in the plasma, and their motion is thus dominated by any large-scale motions the plasma may undergo. In this scenario, positrons are transported radially outward from the wind launching zone at the wind velocity $v[t]$, embedded in an outflow that expands according to mass conservation (adiabatic expansion). Such an outflow cools as it expands.

We calculate the radius at which positrons are expected to annihilate. The thermalization radius, $r_{\rm therm}$ is the maximum radius achieved by a positron co-moving with the outflow as it loses kinetic energy from $w = w_0$ to $w_{\rm therm} = 6.8$ eV, corresponding to thermalization in an ISM with $T \sim 10^4$ K. We choose this characteristic temperature as positrons annihilating in a plasma with this temperature will reproduce the measured linewidth of the positron annihilation line, however the exact choise for $w_{\rm therm}$ does not qualitatively affect our conclusions.

The lifetime of positrons in the outflow depends on the density of the neutral and ionized species in the ISM. As these densities vary not only with the adiabatic expansion of the plasma but also according to the radiative cooling of the plasma, the trajectories of positrons in the outflow are calculated iteratively for a range of different initial conditions. A trajectory is parameterised by the mass and energy flux into the outflow ($\dot{M}$ and $\dot{E}$ respectively) and the intial energy of the positron w_0. We calculate the evolution of positron energies for a grid where $\dot{M} \in \{10^{-3}, 10^{0}\}\,\mathrm{M}_{\odot}\,\mathrm{yr}^{-1}$ and $\dot{E} \in \{10^{38}, 10^{40}\}\,\mathrm{erg\,s}^{-1}$ for positron energies w_{low} and w_{high} calculated above. The range of values chosen for the $\{\dot{E}, \dot{M}\}$ parameter space are conservatively broad estimates for the maximim and miminum values expected from nuclear star formation (Crocker, 2012). The initial temperature, T_0, and wind velocity, v, are defined by $\dot{E}$ and $\dot{M}$ as described above. The ionization fraction of hydrogen in the plasma is given by CIE (Sutherland et al., 2013) which varies as a function of temperature. Typical inital temperatures range from $\sim 10^6 - 10^7\,\mathrm{K}$ with outflow velocities of $\sim 300 - 1500\,\mathrm{km\,s}^{-1}$. The density of the medium evolves due to mass conservation in the outflow, i.e. the density at time t is

$$\rho[t] = \frac{\dot{M}}{2v[t]\Omega(r_0 + r)^2}, \tag{6.2}$$

where $t = 0$ where the flow is launched at r_0 with velocity v_0 and

$$r = \int_0^t v_0 \left(1 - \frac{\dot{M}}{\dot{E}} \Delta\phi[r]\right)^{1/2} dt \tag{6.3}$$

.
The temperature evolves due to adiabatic and radiative losses. The adiabatic cooling rate at time t is

$$\left.\frac{dT}{dt}\right|_{\mathrm{ad}} = -2\frac{(\gamma_{\mathrm{ad}} - 1)v[t]T_0}{(r_0 + r)} \left(\frac{\rho[t]}{\rho_0}\right)^{\gamma_{\mathrm{ad}}-1}, \tag{6.4}$$

where $\gamma_{\mathrm{ad}} = 5/3$ for the non-relativistic gas. The radiative cooling rate is

$$\left.\frac{dT}{dt}\right|_{\mathrm{rad}} = -\frac{\Lambda}{n^2}\frac{2n_{\mathrm{tot}}}{3k_b}, \tag{6.5}$$

where Λ/n^2 is the normalized cooling function from Sutherland et al. (2013) assuming CIE. The ionization state of the medium and the densities of the different species are computed from the same cooling tables.

Positrons with an inital energy of w_0 at r_0 are evolved simultaneously. Positrons lose energy through both adiabatic and radiative loss processes. As the adiabatic losses of the positrons dominate, and continuous radiative losses with species other than hydrogen in the ISM (helium and metals) are subdominant, we assume positrons interact only with hydrogen and free electrons. The adiabatic energy loss rate for positrons at time t is

$$\left.\frac{dw}{dt}\right|_{\mathrm{ad}} = -2\frac{(\gamma_{\mathrm{ad}} - 1)v[t]w_0}{(r_0 + r)} \left(\frac{\rho[t]}{\rho_0}\right)^{\gamma_{\mathrm{ad}}-1}. \tag{6.6}$$

We find that the adiabatic energy losses of the positrons always dominate over the radiative energy losses. Positrons also lose energy through ionization and Coulomb losses. Ionization losses due to interactions with neutral hydrogen are given by (Ginzburg, 1979):

$$\left.\frac{dw}{dt}\right|_{\text{ion}} = -7.7 \times 10^{-9} \frac{n_H}{\beta} \left[\ln \left(\frac{(\gamma - 1)\gamma^2 \beta^2 (511\text{keV})^2}{2I^2} \right) + \frac{1}{8} \right] \text{eV s}^{-1}, \tag{6.7}$$

where n_H is the number density of neutral hydrogen, $I = 13.8\,\text{eV}$ is the ionization energy of hydrogen and γ is the Lorentz factor for a positron with kinetic energy w. The energy loss rate due to coulomb scattering from the ionized ISM component are given by (Huba, 2013),

$$\left.\frac{dw}{dt}\right|_{\text{pla}} = -1.7 \times 10^{-8} \frac{n_e}{\beta} \ln \Lambda_C \int_0^{w/k_b T} dx x^{1/2} e^{-x} - \tag{6.8}$$

$$(w/k_b T)^{1/2} e^{-w/k_b T}) \text{ eV s}^{-1},$$

where $\Lambda_C = (k_b T / 4\pi n_e e^2)^{1/2} (\max(2e^2/mu^2, \hbar/mu))^{-1}$ and $u = (3E/m)^{1/2} - (8k_b T/\pi m)^{1/2}\,\text{cm s}^{-1}$. with n_e the electron density, m is the electron mass and e the electron charge.
Trajectories of positrons are calculated and recorded until they either a) reach a maximum radius of 8 kpc or b) thermalize. In the latter case, we consider positrons thermalized if they reach an energy of 6.8 keV. This positron energy is consistent with an ISM temperature of $\sim 10^4$ K. The ISM conditions (temperature, density and ionization fraction) at thermalization are recorded, as it thermalization radius, r_{therm}. We then consider the regions of our input parameter space occupied by positrons that thermalize

6.3 Results

For our model to replicate observations of positron annihilation in the Galactic bulge, the following must be satisfied: Firstly, the spatial distrubution of annihilating positrons must be consistent with the model described by Siegert et al. (2016b), and secondly, 90 per cent of positrons must annihilate in an ISM that has cooled to $\sim 10^4$ K. To assist in comparing our results to the best fit morphology of the positron annihilation signal described by Siegert et al. (2016b), we transform their two-dimensional intensity map into a one-dimensional radial intensity profile. The best fit Bulge profile from Siegert et al. (2016b) is the superposition of two two-dimensional Gaussian distributions representing a spatially narrow component of emission associated with the Galactic bulge, and a spatially broad component of emission associated with the same region. We calculate a mean inner radius and a mean outer radius to characterise the observed profile, i.e.

$$r_{\text{in}} = \frac{\int_0^{r_{50}} dr I[r] r^2}{\int_0^{r_{50}} dr I[r] r} \sim 360\,\text{pc}, \; r_{\text{out}} = \frac{\int_{r_{50}}^{\infty} dr I[r] r^2}{\int_{r_{50}}^{\infty} dr I[r] r} \sim 1.6\,\text{kpc} \tag{6.9}$$

where r_{50} is the root of the equation $\int_0^{r_{50}} dr I[r] r / \int_0^{\infty} dr I[r] r = 0.5$ - radius inside which 50 per cent of the 511 keV flux $I[r]$ is observed. We choose to proceed with the analysis in this way - as opposed to calculating radial intensity profiles from our model - both to simplify the subsequent analysis and to take into account that the distribution of the positron annihilation radiation described in Siegert et al. (2016b) is a best fit model, and the smooth nature of the profile is a property of the model, not necessarily the positron annihilation signal itself.
The deceleration of the wind due to the gravitational potential of the Galaxy allows us to introduce a further constraint on the scenario we present. If the wind stalls before reaching

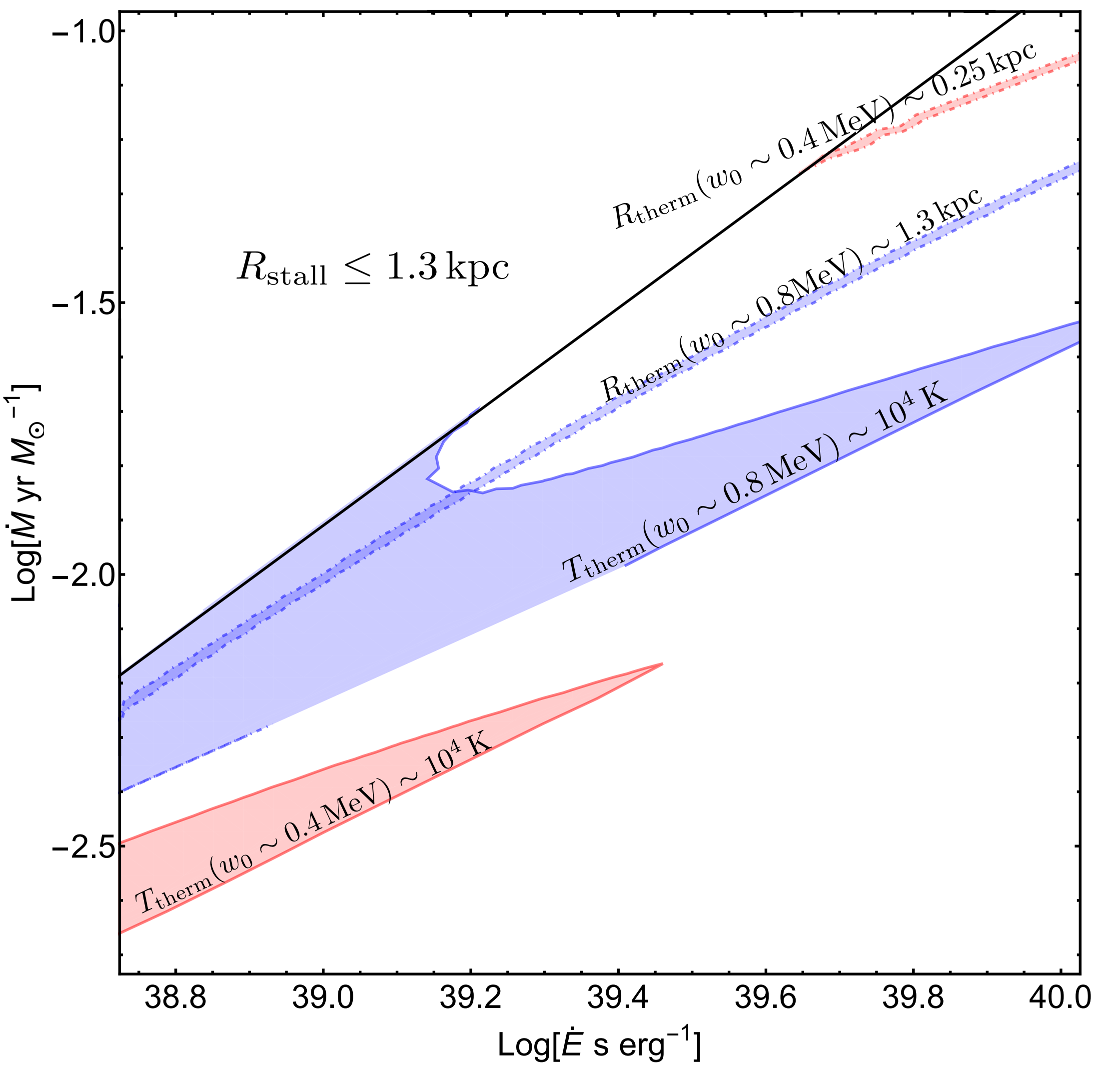

Figure 6.1: Contour showing regions of parameter space where $w_0 \sim 0.8\,\text{MeV}$ positrons thermalize at $r_{\text{therm}}[w_{\text{high}}] \sim r_{\text{out}}$ (blue shaded region, dot-dashed contours) and where the outflow has cooled to $10^4\,\text{K}$ at r_{out} (blue shaded region, solid contours). Similar contours for positrons with $w_0 \sim 0.4\,\text{MeV}$ and $r_{\text{therm}}[w_{\text{high}}] \sim r_{\text{in}}$ are shown in red. The black line delineates the region of the parameter space where the outflow stalls before reaching r_{out}, which are excluded in our model.

r_{out}, it is not possible for positrons to be transported to radii consistent with the observed intensity profile of the radiation. We calculate the regions of parameter space excluded by this constraint, which is plotted as the black solid line in fig. 6.1.

For regions of the parameter space where the wind does not stall, we calculate r_{therm} for positrons with an initial kinetic energy $w_0 = w_{\text{low}}$ in a Galactic outflow as described in Section 6.2, and compare this radius to the inner characteristic radius r_{in}. In Figure 6.1, red contours show regions of the $\{\dot{E}, \dot{M}\}$ parameter space for which positrons with $w_0 = w_{\text{low}}$ thermalize at r_{in} (i.e. where $0.9 < r_{\text{therm}}/r_{\text{in}} < 1.1$). Overplotted, also in red, are the regions of parameter space for which the outflow cools to $8000\,\text{K} \leqslant r_{\text{therm}}[w_0 = w_{\text{low}}] \leqslant 3 \times 10^4\,\text{K}$ at the radius at which positrons thermalize. It is immediately obvious that these two sets of contours are disjoint, and thus there is no region of parameter space where positrons with initial energies $\sim w_{\text{low}}$ can annihilate where the ISM temperature is consistent with the observations.

The solid (dot-dashed) blue contours show where positrons with initial kinetic energies $w_0 = w_{\text{high}}$ thermalize when the ISM has cooled to $8000\,\text{K} \leqslant r_{\text{therm}}[w_0 = w_{\text{low}}] \leqslant 3 \times 10^4\,\text{K}$ (where positrons thermalize at $0.9 < r_{\text{therm}}/r_{\text{in}} < 1.1$). There are regions of the parameter space where positrons with initial energies $\sim w_{\text{high}}$ annihilate in an ISM that has cooled to $\sim 10^4\,\text{K}$. However, for the scenario to be presented to be consistent with observations, less than ten percent of positrons must annihilate in the hot medium. In the scenario described, the low energy positrons (~ 50 percent of positrons in the outflow) annihilate before the ISM has cooled to $10^4\,\text{K}$.

In Figure 6.1, one can see there is no single point in the $\{\dot{E}, \dot{M}\}$ parameter space where positrons at relevant energies annihilate in an ISM with a temperature of $\sim 10^4\,\text{K}$ at radii consistent with the morphology of the observed extent of the 511 keV line. In the scenario we present, there is no region in which positrons with energies $\sim w_{\text{low}}$ annihilate in a medium that has cooled to $10^4\,\text{K}$. Consequently, the spectra of positron annihilation will be considerably broader than the observed spectrum (Guessoum et al., 2005) for all regions of the parameter space, even those in which positrons with energies $w_0 = w_{\text{high}}$ thermalize and annihilate once the ISM has cooled to $\sim 10^4\,\text{K}$, as the broadest component of the spectrum dominates the total observed spectrum.
Based on these results, we rule out a scenario where positrons are advected into the Galactic bulge by a steady state nuclear outflow as the source of Galactic bulge positrons. Our results show no sensitivity to the choice of opening angle of the described outflow. We find that the spectrum of gamma rays resulting from positron annihilation provides a stringent constraint on the annihilation sites of positrons, and our model cannot successfully reproduce the global Galactic bulge positron annihilation spectrum observed by SPI/*INTEGRAL* (Siegert et al., 2016b).

6.4 Conclusion

In this work we find that positron transport in an adiabatically expanding and adiabatically and radiatively cooling steady-state outflow cannot consistently replicate either the observed morphology and spectrum of positron annihilation gamma rays. In particular, constraints on the observed spectrum of the positron annihilation radiation rule out the scenario we propose. In ruling out this scenario, where positrons are transported by large scale motions of gas from the Galactic nucleus to the Galactic bulge, we provide evidence in favour of searching for a source of Galactic positrons that is distributed in the Bulge region of the Galaxy although we do not rule out large scale diffusive transport. A distributed source such as subtypes of thermonuclear supernovae associated with old stellar populations (Crocker et al., 2017) or microquasars (Siegert et al., 2016a) can plausibly explain the observed morphology of the positron annihilation signal without invoking complex, large scale transport of positrons via diffusion.

Acknowledgements

Parts of this research were conducted by the Australian Research Council Centre of Excellence for All-sky Astrophysics (CAASTRO), through project number CE110001020. IRS is supported by the Australian Research Council grant FT160100028. FHP thanks Ralph Sutherland, Geoffrey Bicknell, Dipanjan Mukherjee, Roland Diehl, Thomas Siegert, Felix Aharonian and Eugene Churazov for useful discussions. RMC thanks Geoffrey Bicknell for the calculation of the wind deceleration.

Chapter 7

The host galaxies of SN1991bg-like supernovae

Reality is frequently inaccurate

Douglas Adams

Foreword

Thus far, I have established that positrons we observe annihilating in the Milky Way must have been produced within the last million years, as when we include the physics positrons undergo with atoms other than hydrogen and helium, their thermalized lifetimes decrease dramatically. Furthermore, we have ruled out the possibility that the nuclear outflow disperses positrons into the Galactic bulge as the observed spectra of positrons annihilating in such an outflow cannot be reconciled with observations. Thus, we must search for a positron source that

- has a source morphology that reflects the annihilation morphology. Positrons are not transported from disk to bulge, or vice versa
- can supply a sufficient number of positrons to contribute to the observed positron annihilation flux
- produces positrons at an energy that does not exceed $3-7\,\mathrm{MeV}$.

Such a source should be associated with the $>10\,\mathrm{Gyr}$ old stellar populations of the Milky Way. The flux ratio between the Disk and Bulge, and the disk and nuclear bulge scales consistently with the total stellar mass.

A natural source that is associated with stars would be positrons produced by nucleosynthesis. However, conventional SNe Ia and CCSNe do not produce positrons through the decay chains of radioisotopes such as ^{44}Ti or ^{56}Ni in sufficient quantities nor in the correct spatial distribution to explain the observed positron annihilation morphology and flux.

In Crocker et al. (2017), a transient event with a delay time distribution that peaks toward $3-6\,\mathrm{Gyr}$ could supply positrons to the galaxy with the right morphology and relative fluxes in the different regions of the galaxy is described. Each event would be required to produce around $0.03\,M_{\odot}$ ^{44}Ti to explain the observed positron luminosity. This means the event would have a recurrence time of 1/500 yr. Thus, there is a natural explanation for the lack of Ti-44 decay lines visible in the sky, as the time between events is sufficiently long that we would miss the decays.

Events producing this quantity of ^{44}Ti can only be explained with the detonation of helium. To identify the type of transient event responsible for the production of Galactic positrons we employed binary population synthesis (BPS) using StarTrack (Belczynski et al. (2008)). We find an evolutionary channel that assembles relatively large masses of helium in favorable conditions for detonation at long times ($3 - 6\,$Gyr) subsequent to star formation. This channel involves an interacting binary star system with low zero-age main sequence masses ($1.4 - 2\,M_{\odot}$ per star). These stars evolve to produce a Carbon-Oxygen White Dwarf (COWD) with a pure $0.31 - 0.37\,M_{\odot}$ Helium White Dwarf (HeWD) companion, the latter's progenitor never undergoing core helium burning. A merger event occurs with a characteristic timescale of 3 Gyr. This is in good agreement with the constraints on the delay time of a Galactic positron source derived above.

The proliferation of SN surveys in the past 20 years has lead to the indentification of more and more peculiar thermonuclear transients. The properties of the system described above are thought to result in an explosion consistent with sub-luminous thermonuclear supernovae, specifically the SN1991bg-like subclass (91bg-like SNe). 91bg-like SNe uniquely exhibit a strong Ti II absorption feature at 4200Å in their spectra (Filippenko et al., 1992). The helium detonation proposed results in the synthesis of ^{44}Ti which, together with other isotopes of titanium, give rise to this Ti II absorption feature and the red photemetric colors of the supernova, rendered particularly prominent by the thermodynamic conditions in the ejecta (which has low expansion velocities, $\sim 6000\,\mathrm{kms}^{-1}$).

The SNe 91bg rate is around 15% of the total SNe Ia rate. However this rate rises to around 30% if the analysis is restricted to early type galaxies (Li et al., 2011). In fact, more than any type of SNe, SNe 91bg are associated with early type galaxies (see plot). The cumulative distribution of SNe 91bg across galaxy type is sustantially different from that of CCSNe, which tend to occur in late type galaxies that host active star formation, and measureably different to that of SNe Ia, which occur fairly uniformly across all galaxy types. However, there has been no systematic study to investigate whether there is a causal connection between the properties of early type galaxies and SNe 91bg, nor has a qualitative link been described.

The preponderance of SNe 91bg in early type galaxies is a tantalizing hint that they may have longer delay times than those of SNe Ia, however early type galaxies are also more massive, and tend to be more metal rich, as well as contain less star formation than late type galaxies. Thus, we need to disentangle which of these properties is connected to SNe 91bg. To this end, we use integral field spectroscopy observations of SNe 91bg host galaxies and determine the ages and metallicities of the stellar populations in the $\sim 1\,$kpc vicinity of the SN explosion site. In our sample we include both early type galaxies and a number of late type and irregular galaxies that host SNe 91bg.

Our measurement of the typical stellar population age in the vicinity of the SN enables us to constrain the delay time of the SNe 91bg in our sample. Moreover, by using full spectrum fitting, we can obtain information about the youngest components of the stellar populations. In this work, we are able to perform the first quantitive analysis of the stellar populations that host SNe 91bg. We find that the average ages of the stellar populations are $> 6\,\text{Gyr}$, the oldest stellar populations measured to host any subtype of supernova. Furthermore, we find that the majority of host stellar populations are devoid of recent star formation, and in the galaxies that are found to host recent star formation, there is a significant component of older stars present.

The derived DTD of SN1991bg-like SN progenitors in this work is consistent with the DTD required for a stellar transient that can reproduce the spatial distribution of the positron annihilation line in the Galaxy derived in Crocker et al. (2017).

Declaration

This work was published in the journal *Publications of the Astronomical Society of Australia*. The manuscript is reproduced here with formatting changes to make it consistent with the rest of the work in this thesis. In particular, the color of the plots in figure 7.1 has been altered. The appendix describing the theoretical background to spectral fitting does not appear in the submitted paper and is included in this thesis. I contributed 95% of the manuscript preparation for this article, and performed 95% of the simulations described in the article myself. The text discussing the possible effects of binary stellar evolution on the results presented in this work was contributed by Ashley J. Ruiter. Chris Lidman provided the initial program to perform the analysis of our spectra with `pPXF` which was adapted from a script provided by Michele Capellari as part of the downloadable program files from mxc/software/,. This program was then modified and adapted by myself to obtain the results presented in this work. Several of the spectra of galaxies used in this analysis were obtained by Xi Wang under the supervision of myself.

Age and metallicity of stellar populations hosting SN1991bg-like supernovae

Fiona H. Panther[1,2,3], Ashley J. Ruiter[3,2,1], Ivo R. Seitenzahl[3,1], Roland M. Crocker[1], Chris Lidman[1,2], Xi E. Wang[1], Brad E. Tucker[1,4,5] and Brent Groves[1,4]

[1] The Research School of Astronomy and Astrophysics, Mount Stromlo Observatory, Australian National University, Canberra, ACT 2611, Australia.
[2] ARC Centre of Excellence for All-Sky Astrophysics (CAASTRO)
[3] School of Science, UNSW Canberra, Australian Defence Force Academy, Canberra 2612, Australia
[4] The ARC Centre of Excellence for All-Sky Astrophysics in 3 Dimensions (ASTRO 3D), Australia
[5]National Centre for the Public Awareness of Science, Australian National University, Canberra, ACT 2611, Australia

Published in: *Publications of the Astronomical Society of Australia*, Volume 36, id. e031, 10.1017/pasa.2019.24

Abstract

SN1991bg-like supernovae are a distinct subclass of thermonuclear supernovae (SNe Ia). Their spectral and photometric peculiarities indicate their progenitors and explosion mechanism differ from 'normal' SNe Ia. One method of determining information about supernova progenitors we cannot directly observe is to observe the stellar population adjacent to the apparent supernova explosion site to infer the distribution of stellar population ages and metallicities. We obtain integral field observations and analyse the spectra extracted from regions of projected radius $\sim$ kpc about the apparent SN explosion site for 11 91bg-like SNe in both early- and late-type galaxies. We utilize full-spectrum spectral fitting to determine the ages and metallicities of the stellar population within the aperture. We find that the majority of the stellar populations that hosted 91bg-like supernovae have little recent star formation. The ages of the stellar populations suggest that that 91bg-like SN progenitors explode after delay times of $> 6\,\mathrm{Gyr}$, much longer than the typical delay time of normal SNe Ia, which peaks at $\sim 1\,\mathrm{Gyr}$.

7.1 Introduction

Type Ia supernovae (SNe Ia) are usually described as a photometrically and spectroscopically homogeneous class of astrophysical transients. They are thought to arise from the thermonuclear disruption of a carbon-oxygen (CO) white dwarf star in an interacting binary system (see Hillebrandt et al. (2013); Maguire (2017) for a review). 'Normal' SNe Ia are standardizable candles (Branch and Tammann, 1992): there is a tight relation between their peak luminosity and the width of their light curve (the Phillips (1993) relation), and between their peak luminosity and their optical color at peak luminosity (Tripp, 1998). Thus they make an excellent tool for measuring cosmological distances. As standardizable candles, normal SNe Ia have been employed in cosmology to probe the geometry of the universe (Riess et al., 1998; Perlmutter et al., 1999; Leibundgut, 2001). However, the proliferation of SN surveys over the past 30 years has led to the discovery of several spectroscopically and photometrically peculiar subclasses of these events. The discovery of SN1991bg in particular (Filippenko et al., 1992) - the prototype event for the SN1991bg-like subclass of SNe Ia (hereafter 91bg-like SNe, see Taubenberger (2017) for a review) - challenged the accepted paradigm that SNe Ia are a homogeneous class of events.

91bg-like SNe events share several key features with their normal SNe Ia cousins, and are clearly thermonuclear supernovae. Specifically, they lack any indication of hydrogen and helium in their spectra while also exhibiting strong Si II in absorption (Filippenko, 1997). Moreover, absorption features in their spectra near maximum light indicate the presence of a number of intermediate mass elements (IMEs) including silicon, magnesium, calcium, sulphur and oxygen. The presence of these IMEs is consistent with these events belonging to the class of thermonuclear transients (Filippenko, 1997). However, 91bg-like SNe also exhibit significant photometric and spectroscopic peculiarities compared to normal SNe Ia. This is highly suggestive of a different explosion mechanism and/or progenitor configuration. The subclass differs from 'normal' SNe Ia in the following ways:

- 91bg-like SNe are subluminous compared to SNe Ia by $1.5 - 2.5$ mag at optical maximum, reaching peak absolute magnitudes of only -16.5 to -17.7 in B (Taubenberger, 2017),
- 91bg-like SNe are significanly redder than their normal SNe Ia cousins, with $(B - V)_{\mathrm{max}} = 0.5 - 0.6$ mag,
- 91bg-like SNe light curves decline very quickly, and are characterized by a lightcurve decline parameter $1.8 \leqslant \Delta m_{15}(B) \leqslant 2.1$, compared to $\Delta m_{15}(B) \leqslant 1.7$ for normal SNe Ia. 91bg-like SNe also have a light curve rise time of $\sim 13 - 15$ days (Taubenberger et al., 2008), a few days shorter than normal SNe Ia. Combined with their low peak luminosities, this is consistent with these events synthesising significanlty lower ^{56}Ni masses than their normal SNe Ia counterparts ($\sim 0.05 - 0.1\,M_{\odot}$, Sullivan et al. (2011)).
- 91bg-like SNe lack a secondary maximum in the near infrared (NIR), unlike normal SNe Ia, likely due to the 91bg-like SNe ejecta being cooler and less luminous than that of the normal SNe Ia. Instead, they exhibit a single NIR maximum delayed a few days with respect to the maximum in B (Garnavich et al., 2004), whereas the first NIR peak in a normal SN Ia lightcurve preceeds the B band maximim. The absence of the secondary NIR maximuim makes it impossible to perform a simple time-shift to make the 91bg-like SNe lightcurve map to the standardizable lightcurve of the normal Ia, and the absence of the feature is physically interpreted as a merging of the primary and secondary NIR maxima into a single maximum due to the physical conditions in the SN ejecta (Kasen, 2006; Blondin et al., 2015).
- Spectroscopically, 91bg-like SNe exhibit similar pre-maximum optical spectra to normal SNe Ia - i.e. dominated by IMEs. However a transition to a spectrum dominated by iron group elements happens earlier in 91bg-like SNe than in normal SNe Ia (Taubenberger, 2017).
- Particularly notable is the presence of unusually strong Ti II and O I λ7774 in absorption in the post-maximum spectra. A number of these spectral peculiarities can be attributed to the unusually cool and slow-moving ejecta ($\sim$ 7000 km/s, Taubenberger et al., 2008) when 91bg-like SNe are compared to normal SNe Ia: the lower ionization state favours a higher abundance of neutral and singly ionized species. However, it is considered unlikely that ionization state and temperature explains all these spectral peculiarities.

To explain the spectroscopic and photometric peculiarities of 91bg-like SNe, a variety of progenitors and explosion mechanisms have been suggested. A 'violent merger' of two near-equal mass CO WDs was explored via hydrodynamical simulations in Pakmor et al. (2010). Although the lightcurves of the these explosions were somewhat too broad to reproduce observations of 91bg-like SNe, the synthesised spectra, red colour and low expansion velocities were a fairly good match to observed properties of 91bg-like SNe. To better reproduce the characteristics of 91bg-like SNe light curves, it was suggested by Pakmor et al. (2013) that the faint, fast lightcurves of 91bg-like SNe could result from the merger of a CO WD and a helium WD (e.g. see their figure 4). The smaller ejecta mass that is expected in such an explosion can naturally explain the observed narrower lightcurves of 91bg-like SNe compared to their 'normal', brighter counterparts. A specific formation channel of the same progenitor scenario (CO WD + He WD merger) was found by Crocker et al. (2017) to plausibly supply the high ^{44}Ti yield that is necessary for these merging events to also explain the positron annihilation signal in the Milky Way.

While a number of progenitor configurations and explosion mechanisms have been suggested to explain the properties of 91bg-like SNe, no direct observations of the progenitor systems have been made, and so the exact progenitors of these SNe remain unknown. One method of inferring information about the progenitors of SNe independent of the observed properties of the explosion is to consider the galaxies in which they occur. A qualitative connection between host galaxy properties and the occurrence of 91bg-like SNe has already been well established. In LOSS (the Lick Observatory Supernova Search, Li et al. (2011)), around 15 per cent of all SNe Ia were of the 91bg-like SNe subclass. However, considering only early type galaxies, the fraction of SNe Ia that are of the 91bg-like SNe subtype rises to 30 per cent. Furthermore, in Perets et al. (2010) the cumulative distribution of 91bg-like SNe occuring in galaxies of various Hubble types was found to be different to that of SNe Ia. More recently, the LOSS sample was used to quantify the SNe luminosity-stellar age connection in Shen et al. (2017) together with binary population synthesis models. In that work, it was shown that double WD systems with less massive primaries result in fainter SNe Ia at long (> 1 Gyr delay times, in agreement with the simulations of Pakmor et al. (2010) and the theoretical arguments of Crocker et al. (2017).

SNe Ia are observed to occur in all galaxy types, from passive to star forming, and there is some evidence that they are found in regions of galaxies occupied by older, several Gyr-old stars (e.g. the vertical distribution of SNe Ia is greater than the vertical distribution of CCSNe in edge-on spiral galaxies Hakobyan et al. (2017)). On the other hand, 91bg-like SNe occur predominantly in early type galaxies (Perets et al., 2010). While this is clear, a specific connection between the properties of early type galaxies (which tend to be more massive, more metal-rich, host significantly less star formation, and contain older stellar populations) and 91bg-like SNe is yet to be firmly established.

A number of works (Gallagher et al., 2008; Stanishev et al., 2012; Rigault et al., 2013; Galbany et al., 2014; Rigault et al., 2018) have now investigated the connection between the global properties of galaxies and the observed stretch and colour of SNe Ia, as this may be a source of bias in cosmology. While the focus has been on 'normal' SNe Ia, Gallagher et al. (2008) noted a correlation between older stellar populations and lower luminosity SNe Ia. Several of their low luminosity supernovae were classified spectroscopically as SNe 91bg in the Berkeley Supernova Project (Silverman et al., 2012), and their host galaxies were found to contain stars with an average age of ~ 10 Gyr.

The observations of Gallagher et al. (2008) were restricted to early-type galaxies and utilized slit spectroscopy. Consequently, the ages and metallicties of the stellar populations derived represent a single global average for these SNe host galaxies. Since these host galaxies are early-type galaxies where the stellar populations will be well-mixed, the global galaxy properties are a good approximation for the stellar population that gives rise to the supernova progenitor (Galbany et al., 2014). However, the method employed by Gallagher et al. (2008) makes it hard to exclude the presence of recent local star formation within a few kpc of the supernova progenitor. Furthermore, the Gallagher et al. (2008) work makes use of the Lick/IDS Index system (Worthey, 1994; Worthey and Ottaviani, 1997) to derive the average age and metallicity of the stellar populations of the observed galaxies, and does not take into account that stellar population will be composed of stars that formed at different times and thus cannot be characterized by a single stellar age.

Global galaxy properties may help with the standardization of supernova lightcurves, however to determine whether a supernova subtype is associated with an old ($> 2-3\,$Gyr old) stellar population requires one to rule out the presence of recent star formation within a few kpc of the apparent supernova explosion site.

To do this, it is necessary to consider a spectrum of the stellar population adjaced to the apparent supernova explosion site. Integral Field Unit (IFU) observations can be utilized to investigate this. For nearby supernova hosts (up to $z \sim 0.03$), an aperture with a radius of $\sim 1.5''$ can resolve a region around 1 kpc in projected radius on the galaxy. Furthermore, a local measurement can also be used to determine the distribution of stellar population ages using a method such as penalized pixel fitting of the stellar spectrum extracted from the same apeture used in step one (Cappellari and Emsellem, 2004; Cappellari, 2017).

In this work, we will utilize penalized pixel fitting to investigate the age distribution of the stellar populations that hosted 91bg-like supernovae in a range of galaxies of all morphophological types. We choose to use the local stellar spectra at the supernova explosion site as opposed to integrated galaxy spectra. For example, in the case of a late-type host galaxy, star formation may be localized to the disk of a galaxy. In an integrated spectrum of the galaxy, this star formation can dominate the observed light due to the luminosity of O-A stars. Thus, if a supernova occurs in the bulge of a spiral galaxy, one is likely to underestimate the age of the population that gave rise to the SN progenitor of only global host galaxy properties are considered. On the other hand, if a SN occurs in an early-type galaxy where significant stellar migration may have occured, one can still use the IFU technique to constrain the age of the supernova progenitor: if a SN progenitor is formed within the last Gyr, evidence of this star formation will still be apparent in the stellar spectra as stars will not migrate far from their birthplaces in this timeframe (Fujii and Baba, 2012). Furthermore, the local stellar population will have a distribution of ages representative of that of the whole galaxy (Galbany et al., 2014).

Several works have utilized a similar method, employing IFU spectroscopy to investigate the region in the immediate projected vicinity of SNe Ia to determine the relationship between the scatter in SNe Ia properties after standardization, and star formation rate (Stanishev et al., 2012; Rigault et al., 2013, 2018). Those works are particularly important in the context of cosmology, as the dispersion in Hubble residuals can affect the precision and accuracy of measurement of the cosmological parameters, such as the Hubble constant and the dark energy equation of state parameter. However, the properties of stellar populations at the explosion sites of different subtypes of SNe Ia have not yet been studied in detail. 91bg-like SNe are a distinct subclass which are empirically shown to occur predominantly in old stellar populations. Thus, they provide a perfect opportunity to use IFU spectroscopy to quantify the age of stellar populations close to the SN explosion site and constrain the presence of recent star formation.

In this paper, we present the results of our observations of 91bg-like SNe host galaxies using IFU spectroscopy based on data obtained at Siding Spring Observatory. We derive the distribution of stellar population ages and metallicities of the stars in a region of radius $\sim 1\,\text{kpc}$ around the apparent SN explosion site using full-spectrum fitting. Our observations and data reduction are described in section 7.2, and the results of the full-spectrum fitting procedure is described in section 7.3. Finally, we present a discussion of our results in section 7.4 and our conclusions in section 7.5.

7.2 Observations and Data Reduction

7.2.1 Sample selection

Our sample of 91bg-like SNe host galaxies is composed of 15 hosts of SNe spectroscopically identified as 91bg-like SNe by Silverman et al. (2012) visible from Siding Spring Observatory, as well as the host of SN2012fx (Pastorello et al., 2012) and the host of lsq15bb (Fremling et al., 2015). We do not make any selection cuts based on galaxy morphology, luminosity or mass. Nor do we make a selection cut against supernovae that have large offsets from their host as there may be a diffuse stellar population present at the explosion site not obvious in the Digitized Sky Survey 2 (DSS-2[1]) images which were used to create finder charts for each observation.

7.2.2 Observations

We obtained integral field observations of 17 spectroscopically identified 91bg-like SNe host stellar populations using the WiFeS instrument (Dopita et al., 2007) on the Australian National University 2.3m Advanced Technology Telescope at Siding Spring Observatory (SSO).

Observations were obtained over a total of 14 nights between July 2016 and February 2017. WiFeS is a wide-field Integral Field Unit with a total field of view of $25'' \times 38''$. The instrument configuration is shown in Table 7.2. The aperture of WiFeS is centered on the apparent location of each SN, with the position angle of the aperture chosen to minimize contamination from nearby stars but, as we only extract spectra from pixels close to the apparent SN location, the position angle has little practical importance.

Exposure times reflect changes in our observation strategy to account for inclement weather conditions. A summary of our science observations is given in Table 7.1. Bias frames, Cu-Ar arcs and dome flats were obtained at the beginning and end of the night. Wire frames[2] were obtained at the end of each night, and sky flats were obtained at the beginning of each night.

[1]http://archive.eso.org/dss/dss
[2]A wire frame ensures the spectrograph slits are appropriately aligned on the CCD

Table 7.1: Summary of observations

SN Name	Host Galaxy	SN RA	SN DEC	t_{exp} (s)	Morph[1]	A_{ap} (kpc^2)	z
SN1993aa	Anon J230322-0620	23 03 22.02	-06 20 56.1	2×1800	10	1.23	0.018
SN2000ej	IC1371	21 20 15.66	-04 52 40.5	2×1800	-5	3.6	0.0308
SN2002ey[4]	Anon J23101188+0732541	23 10 12.33	+07 32 59.9	2×1800	-1	5.7	0.0388
SN2007ba	UGC9798	15 16 41.83	+07 23 48.1	2×1800	0	5.5	0.03825
SN2007cf	MCG+02-39-021	15 23 07.66	+08 31 45.5	2×1800	-2	4.1	0.03293
SN2007fq	MCG-04-48-19	20 34 55.92	-23 06 15.84	2×1800	-2	6.8	0.04245
SN2006gt[4]	Anon J005618-0137	00 56 17.30	-01 37 46.0	3×1800	-5	7.5	0.0447
SN2012fx[2]	ESO417-03	02 55 41.20	-27 25 27.59	4×1800	5	1.2	0.0176
SN2005er[4]	NGC7385	22 50 00.84	+11 37 05.7	3×1800	-2	2.6	0.02616
SN2005ke[4]	NGC1317	03 35 04.35	-24 56 38.8	3×1200	0	0.2	0.00643
SN2002cf	NGC4786	12 54 31.30	-06 51 24.8	3×1200	-5	0.9	0.015
SN2002jm	IC603	10 19 25.20	-05 39 14.5	2×1200	1	1.3	0.0182
SN2007al	Anon J095919-1928	09 59 18.48	-19 28 25.8	3×1200	-5	0.6	0.0121
SN2007N[4]	MCG-01-33-12	12 49 01.25	-09 27 10.2	3×1200	1	0.6	0.0126
SN2008ca	SDSS J122901.28-263305.6	12 29 01.20	+12 22 18.84	3×1200	10	55	0.123
SN2008bt	NGC3404	10 50 16.99	-12 06 31.5	3×1200s	1	0.91	0.0154
lsq15bb[3,4]	2dFGRS TGN352Z120	09 58 51.95	+01 01 04.12	3×1200	0	23	0.08

[1] - Morphology based on DSS R-band images classified by the authors using numerical Hubble types where negative numbers represent early-type galaxies, and positive numbers late-type (de Vaucouleurs, 1959).
[2] - SN classification from Pastorello et al. (2012)
[3] - SN classification from Fremling et al. (2015)
[4] - Removed from sample due to low SNR in extracted spectrum

Table 7.2: WiFeS instrument Configuration

Component	Configuration
Red Grating	R3000
Blue Grating	B3000
Dichroic	RT560
Wavelength range	$\sim$ 3300 Å- $\sim$ 9200 Å

For each individual galaxy observation, Cu-Ar arcs (required for accurate wavelength solution, which may drift a few Angstrom over the course of a night) and bias frames are obtained within 30 minutes of the observation, and each galaxy observation is accompanied by at least one sky frame, which is used to remove skyline contamination. Finally, a spectrophotometric standard star is observed on each night of observation. Where weather conditions did not permit time for these observations, spectrophotometric calibration was carried out using a spectrophotometric standard taken in earlier runs, with the standard frames being taken in similar photometric weather conditions and at similar airmass to the galaxy being observed.

7.2.3 Data Reduction

Data reduction was facilitated by the `PyWiFeS` data reduction package (Childress et al. (2014a)). The pipeline produces a spectrophotometrically calibrated and fully coadded datacube, and a corresponding parallel-processed error cube.

Spectra of the stellar populations local to each SN were then extracted from the calibrated datacube. We use a seeing-limited aperture of $3'' \times 3''$ centered on the apparent location of the SN in each host galaxy (the physical size of these apertures varies with redshift and is shown in Table 7.1). These spectra are processed to remove residual sky lines using a nearby area free from galaxy light, offset from the host galaxy from the same final datacube, and the mean resulting spectrum is extracted from the $3'' \times 3''$ region of interest.

Each spectrum is then shifted to rest-frame wavelength according to the host redshift listed on NED[3], which is checked against the redshift we derive from either the narrow Hα line if present, or the H and K lines for the remaining galaxies. The spectra are then corrected for Milky Way dust reddening using `brutus 0.3.1`[4]. Galactic extinction is derived using NASA Extragalactic Database (NED) from the Schlafly and Finkbeiner (2011) recalibration of Schlegel et al. (1998) infrared based dust map. The map is based on dust emission from COBE/DIRBE and IRAS/ISSA; the recalibration assumes a Fitzpatrick (1999) reddening law with $Rv = 3.1$ and different source spectrum than Schlegel et al. (1998). The resulting spectra are subsequently ready for analysis.

[3]https://ned.ipac.caltech.edu/ The NASA/IPAC Extragalactic Database (NED) is operated by the Jet Propulsion Laboratory, California Institute of Technology, under contract with the National Aeronautics and Space Administration.

[4]http://fpavogt.github.io/brutus/index.html

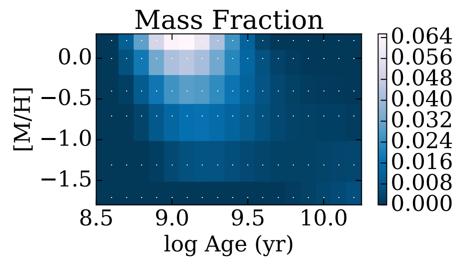

(a) Stellar pop. within 0.57 kpc of SN1993aa

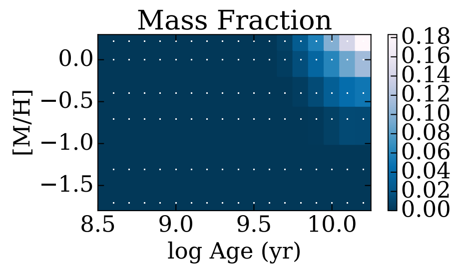

(b) Stellar pop. within 0.96 kpc of SN2000ej

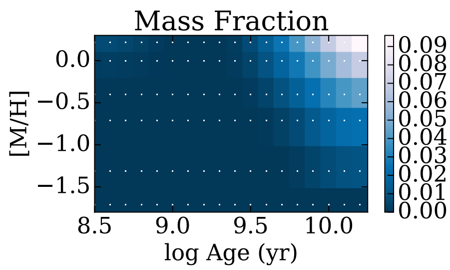

(c) Stellar pop. within 0.49 kpc of SN2008bt

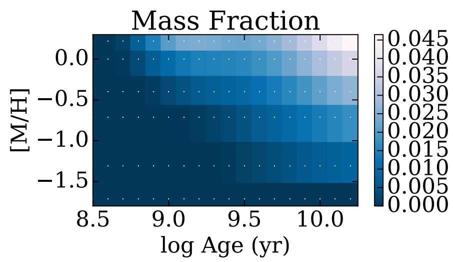

(d) Stellar pop. within 3.44 kpc of SN2008ca

Figure 7.1: Mass fraction of stars in different age and metallicity bins based on spectra extracted from 3"x3" regions centered on the SN explosion site in each Galaxy. The radius of the aperture in physical units is shown in each subcaption. The population shown in (b) is representative of the remaining seven galaxies for which the stellar populations are fitted with pPXF

7.3 Results

7.3.1 Full Spectrum Fitting

Deriving stellar population ages requires simultaneous determination of both the age of stars and their metallicity as there is a significant degeneracy between the effect of metallicity and age on galaxy spectra.

We use the publicly available penalized pixel fitting code (pPXF, Cappellari and Emsellem (2004); Cappellari (2017)) to fit linear combinations of simple stellar populations (SSPs) from the MILES stellar library (Sánchez-Blázquez et al., 2006; Vazdekis et al., 2010), which provides 985 stellar spectra across a wavelength range of $3525 - 7500$ Å at 2.5 Å spectral resolution, for stellar metallicities ranging from $[M/H] = 0.22$ to $[M/H] = -2.3$. The 'solution' of the problem - to fit multiple SSPs to an observed spectrum - is defined by different weights applied to each SSP in a regular grid in log-age and metallicity space. The program outputs a weighted average age of the stellar population and a weighted average metallicity according to these weights, along with information about the weights applied to each age-metallicity bin. This allows us to determine both the weighted average age of the stellar population, as well as whether any substantially younger or older stellar population than the average is present.

For several of our observed galaxies, we cannot perform a robust spectral fit as there is no flux in the aperture used to extract the spectra. We remove six of galaxies from our sample

(Table 7.1) noting that the region of interest is situated at a large offset from the galaxy itself or the observed galaxy has a low surface brightness. For the remaining 11 galaxies, we obtain a fit to the total spectrum (with flux normalized by the flux at 5500 Å). pPXF decomposes the spectra into nebular and stellar components, and determines the mass fraction of stars into age and metallicity bins determined by the available grid of SSP models.

In Fig. 7.1 we show outputs from pPXF which display the mass fraction of stars in age and metallicity bins. The majority of stellar populations we observe exhibit similar characteristics to Fig. 7.1(b), including the local stellar population of SN2012fx, which occured in the bulge of a late-type galaxy. These stellar populations have a large mass fraction of stars at ages $\sim 10\,\mathrm{Gyr}$ at super-solar metallicities ($[M/H] > 0$). The weighted average stellar population properties of seven of our observed SN explosion sites suggest that 91bg-like SNe occur preferentially in stellar populations with ages $\sim 10\,\mathrm{Gyr}$ with solar, or slightly sub-solar metallicities (Fig 7.3).

Three of the observed stellar populations, however, contain a younger stellar component: the host of SN1993aa (Fig 7.1(a)), the host of SN2008bt (Fig 7.1(c)) and the host of SN2008ca (Fig 7.1(d)). The spectra of these galaxies are also unusual in comparison to the majority of the galaxies observed. An example of a typical spectrum we analyse with pPXF is shown in Fig. 7.2(a). This spectrum corresponds to the population shown in Fig 7.1(b), and is composed predominantly of old, metal rich stars. In comparison, the spectrum of the host population of SN1993aa (Fig 7.2(b)) is significantly bluer and exhibits strong emission lines of Hα, [N II], [S II], [O III] and Hβ. The strong emission lines indicate there may be ongoing star formation in this stellar population, in good agreement with the high mass fraction of stars with ages $\sim 1\,\mathrm{Gyr}$ seen in Fig 7.1(a). Similarly, the host population of SN2008ca also exhibits strong emission lines (Fig 7.2(d)), however the spectrum is (within the noise) somewhat less blue than that of SN1993aa, suggesting an older stellar component may also be present (Fig 7.1(d)). While the physical area of the aperture within the host of SN1993aa encompasses $\sim 1\,\mathrm{kpc}$, it should be noted that the host of SN2008ca is significantly more distant than that of SN1993aa and therefore the entire galaxy, with an area of $\sim 50\,\mathrm{kpc}$ is sampled in the aperture. This may be the reason we observe apparent multiple stellar populations in this SN host galaxy. An example of a more resolved galaxy that also exhibits multiple stellar populations is the host of SN2008bt. This galaxy has strong Hα, [N II] and [S II] emission (fig 7.2(c)), and while it has a predominantly old stellar population, there is a small mass fraction of stars which have an age of $\sim 0.5\,\mathrm{Gyr}$ (fig 7.1(c)). When we consider the position of the aperture on the host galaxy, we see that while the SN has occured in a position that may be coincident with the bulge of the galaxy, because the galaxy is viewed almost edge on, there may be some contamination of starlight and nebular emission from a younger, star-forming disk. While we cannot rule out that the supernova occured in this region, we do find that the majority of the stellar mass within the aperture is concentrated in the old, metal rich stellar population.

7.3.2 Comparison sample of SNe Ia

While we wish to quantify the ages and metallicities of the stellar populations that host 91bg-like SNe, we also wish to compare the distribution of stellar population ages and metallicities to a sample of SNe Ia host galaxies to investigate whether 91bg-like SNe differ in some way. Unfortunately, a representative sample of SNe Ia host galaxies with spectra of the stellar population in the immediate vicinity of the apparent SN location is not publicly available. However, in Maoz et al. (2012) a sample of SDSS galaxies that hosted SNe Ia is compiled. As a

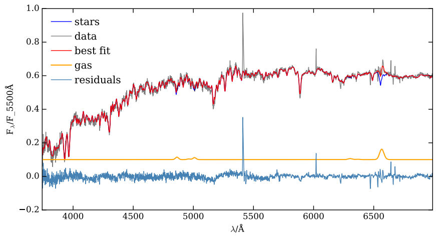

(a) Fitted spectrum of SN2000ej host

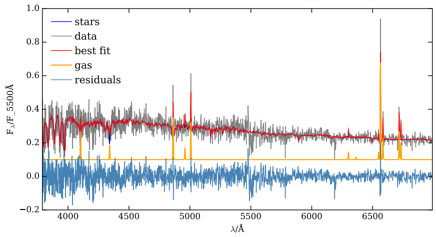

(b) Fitted spectrum of SN1993aa host

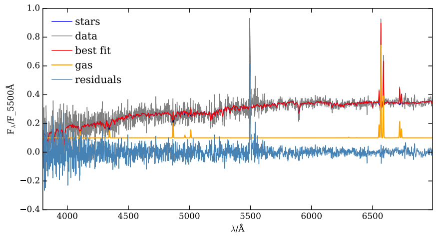

(c) Fitted spectrum of SN2008bt host

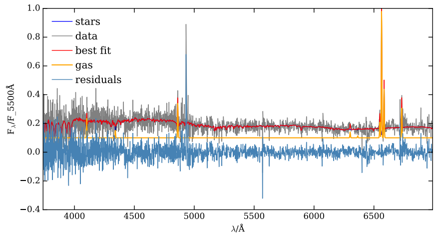

(d) Fitted spectrum of SN2008ca host

Figure 7.2: Spectra fitted using pPXF. Data is shown in grey, and the best fit to the total spectrum (nebular plus stars) is shown in red. The spectrum is also decomposed into stellar(dark blue) and nebular spectra (orange). Residuals for the best fit are shown in light blue. For several of the spectra, there are substantially larger residuals toward bluer wavelengths due to the lower SNR at blue wavelengths.

comparison sample, we compute the weighted average stellar population age and metallicity for these galaxies using pPXF. We note that this average is for the integrated light of the host galaxy where the SDSS fiber is centered on the core of the galaxy, and not solely the stellar population $\sim$ 1 kpc from the apparent supernova location, however it has been previously noted that the global properties of SNe Ia host galaxies correlate well with the properties local to the SN explosion site (Galbany et al., 2014).

We find that the weighted average ages of stellar populations have a wide, almost uniform distribution, with ages between $\sim$ 30 Myr and $>$ 10 Gyr. The metallicity distribution is peaked toward super-solar metallicities ($[M/H] > 0$). We also find that the older the stellar population of the galaxy, the more metal-poor the weighted average metallicity becomes.

7.3.3 Stellar populations hosting SNe 91bg

As a further comparison, we overplot the stellar population ages and metallicities determined using slit spectroscopy for early type galaxies hosting SNe 91bg from Gallagher et al. (2008). The black markers in Figure 7.3 show the ages and metallicities of these galaxies. These ages and metallicities are determined using Lick indicies (Worthey, 1994; Worthey and Ottaviani, 1997) which relies on comparing the measured equivalent width of different absorption lines found in galaxy spectra to an irregular diagnostic grid computed from simple stellar populations. As these galaxies were observed using slit spectroscopy, the stellar populations are representative of the average age of the stars contained in the whole galaxy. Compared to the SNe Ia comparison sample taken from Maoz et al. (2012), the galaxies that host SNe 91bg in Gallagher et al. (2008) appear to contain older stellar populations. Furthermore, the ages

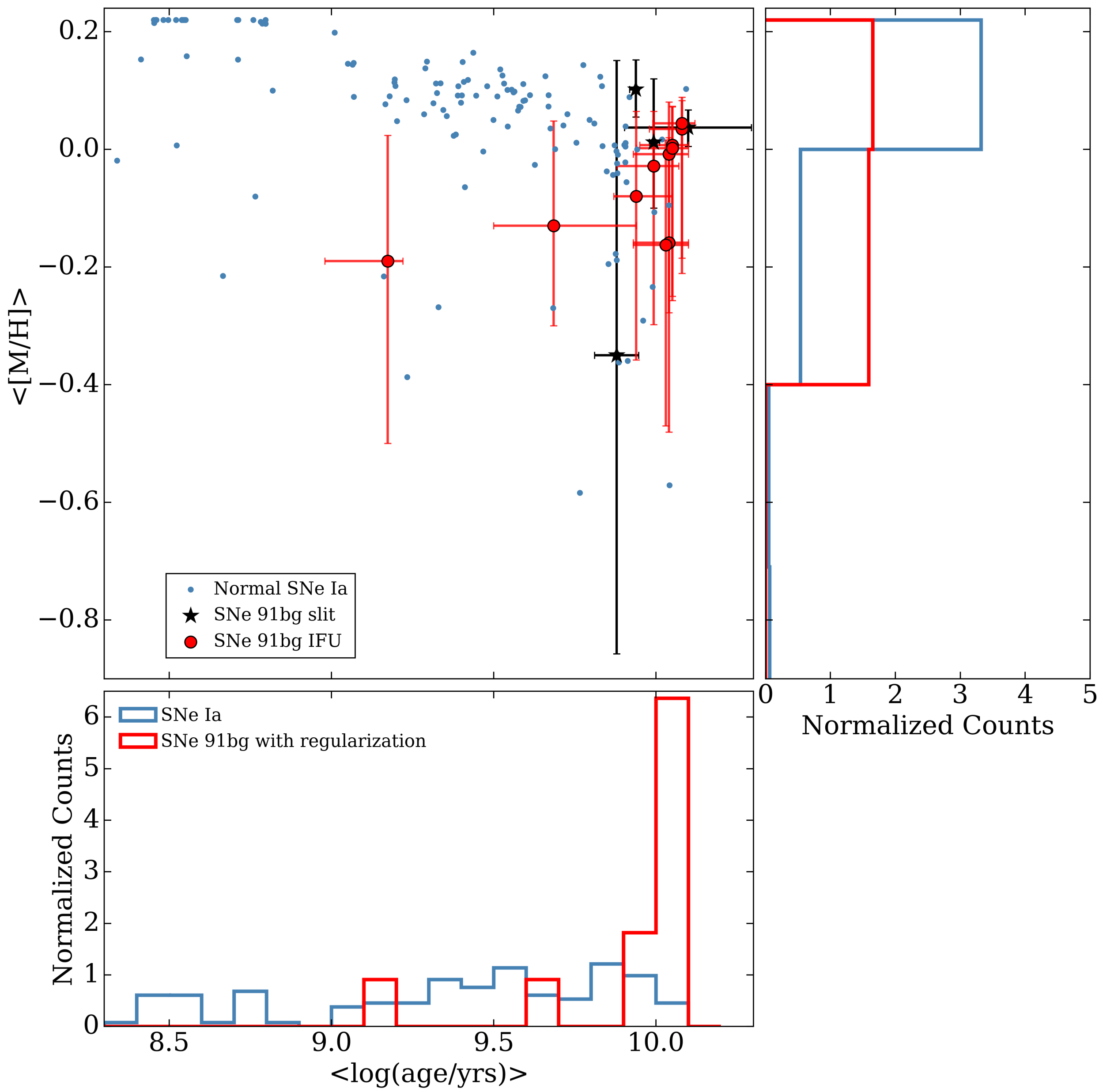

Figure 7.3: Weighted average stellar population ages for SDSS spectra of galaxies that hosted SNe Ia, based on the sample presented in Maoz et al. 2012 (blue) and for the local stellar populations of SNe 91bg galaxies (red). Error bars show the 16th and 84th percentile of the distrubution of stellar population ages and metallicities based on the CDF of stellar population properties. Black points show the ages and metallicities of SNe 91bg host galaxies observed in Gallagher et al. 2008, derived using Lick/IDS indicies and their respective errors. The histograms show the distribution of weighted average stellar population ages (bottom) and metallicities (right). The binning reflects the available metallicities and ages of the stellar population templates in the MILES library used to fit the spectra.

Table 7.3: Summary of results

SN Name	Host Galaxy	$< \log(\mathrm{age/yrs}) >$	$< [M/H] >$
SN1993aa	Anon J230322-0620	$9.173^{+0.047}_{-0.193}$	$-0.19^{+0.21}_{-0.31}$
SN2000ej	IC1371	$10.08^{+0.05}_{-0.19}$	$0.03^{+0.05}_{-0.25}$
SN2007ba	UGC9798	$10.04^{+0.06}_{-0.11}$	$-0.01^{+0.09}_{-0.27}$
SN2007cf	MCG+02-39-021	$10.05^{+0.05}_{-0.11}$	$0.00^{+0.07}_{-0.26}$
SN2007fq	MCG-04-48-19	$10.08^{+0.04}_{-0.09}$	$0.04^{+0.04}_{-0.23}$
SN2012fx[2]	ESO417-03	$9.993^{+0.08}_{-0.11}$	$-0.03^{+0.09}_{-0.27}$
SN2002cf	NGC4786	$10.04^{+0.06}_{-0.11}$	$-0.16^{+0.19}_{-0.32}$
SN2002jm	IC603	$10.05^{+0.05}_{-0.10}$	$0.01^{+0.07}_{-0.26}$
SN2007al	Anon J095919-1928	$10.03^{+0.07}_{-0.10}$	$-0.16^{+0.18}_{-0.31}$
SN2008ca	SDSS J122901.28-263305.6	$9.685^{+0.255}_{-0.185}$	$-0.13^{+0.18}_{-0.17}$
SN2008bt	NGC3404	$9.939^{+0.11}_{-0.07}$	$-0.08^{+0.14}_{-0.28}$

and metallicities derived for these galaxies are consistent with the ages and metalliticies of the local stellar populations of SNe 91bg we derive from our observations.

7.4 Discussion

In this work we analyzed the spectra of galaxies observed with the WiFeS IFU. This allowed us to isolate the stellar population within a few kiloparsecs of the apparent SN explosion site, and determine the age and metallicity of the stellar population in the vicinity of the SN. The age of the stellar population surrounding the SN explosion site in particular may constrain the delay time distribution of 91bg-like SNe (the distribution of times between the SN progenitor formation and the subsequent SN explosion).

In particular, we find that the stellar populations that host SNe 91bg have greater weighted average stellar population ages than those of SNe Ia and many lack evidence of recent star formation. This is strong evidence that 91bg-like SNe are not associated with recent star formation (within the last $\sim$ 1 Gyr, as the stellar spectra lack evidence of a significant number of O-A stars being present. Furthermore, these results suggest that the delay time distribution of 91bg-like SNe is peaked toward very long delay times (10 Gyr), in contrast with SNe Ia, whose delay times peak at $\sim$ 1 Gyr (Childress et al., 2014b). We compared our derived average stellar population ages and metallicities for the local stellar populations of SNe 91bg with the stellar population ages and metallicities of SNe 91bg host galaxies found by Gallagher et al. (2008) and find a good agreement within the error bars between the two results.

We note, however, the large errors on the metallicity of the stellar populations in both our own measurements and those from Gallagher et al. (2008). While two different methods are used to determine the stellar population parameters - full spectrum fitting with pPXF in this work and the Lick/IDS index system in Gallagher et al. (2008) - the stellar model library used to compute stellar population ages and metallicities is identical (the MILES library Vazdekis et al., 2010). While these stellar templates are well sampled in the age parameter space, there are only seven available metallicities between $[M/H] = -2.3$ and $[M/H] = 0.2$. Although the metallicity computed by full spectrum fitting is accurate, it lacks the precision that would be possible with a finer grid of models in metallicity space. This is reflected by the error bars shown in Fig 7.3.

The SNe 91bg host galaxies from Gallagher et al. (2008) are part of a larger sample of massive elliptical galaxies that hosted thermonuclear supernovae. As massive elliptical galaxies typically contain older stellar populations, there is likely a bias toward sampling host stellar populations where we expect the relative rate of SNe 91bg to normal SNe Ia to be somewhat higher than average. In our sample, we make no selection cuts and select galaxies of any morphological classification that hosted SNe 91bg. The majority of the host galaxies we observe are selected from the BSNIP sample (Silverman et al., 2012). These supernovae were observed as part of a targeted, local survey. Consequently, the galaxies in which SNe in a targeted survey occur tend to be more massive, and SNe that occur in less massive galaxies may be missed. As a result, there may be some bias toward sampling older stellar populations, since more massive galaxies tend to contain older, more metal-rich stars. However, we have also observed SNe 91bg hosts that were not targeted by BSNIP and in which 91bg-like SN occured more recently, in particular the host of SN2012fx, a nearby spiral galaxy for which the apparent SN explosion site is in the galactic bulge. The stellar population local to the SN explosion site is found to be relatively typical of those found in the BSNIP sample and has a weighted average stellar population age of $\sim 10\,\mathrm{Gyr}$.

We also compare our stellar population average ages and metallicities with those derived for the host galaxies of SNe Ia as observed by SDSS, based on a sample from Maoz et al. (2012). There may be some bias associated with our measurement of stellar population ages for these SNe Ia host galaxies as the SDSS fiber is placed over the center of the galaxies they observe. This means that one is likely to observe most of the integrated light from the central, bulge regions of these galaxies, biasing our results to older ages as the star-forming, younger outer regions of some galaxies observed by SDSS are missed by the fiber. Consequently the weighted average plotted in figure 7.3 may not represent the exact properties of the stellar population close to the explosion site and therefore may represent an upper limit on the stellar population age.

We find that SNe Ia are hosted by galaxies that exhibit a broad range of weighted average stellar population ages, from the very young at $30\,\mathrm{Myr}$ to the very old ($\sim 10\,\mathrm{Gyr}$). This is in contrast to the stellar populations that host SNe 91bg, which cluster at the substantially older end of this distribution. This demonstrates that SNe 91bg may be associated with progenitors that tend to occur at longer delay times than SNe Ia (e.g. as suggested in Crocker et al. (2017)). We find that while around half of our observed galaxies have Hα emission and nebular emission indicating recent star-formation activity, the majority of galaxies are dominated by absorption lines and have no strong emission lines. Moreover, with the exception of the host of SN1993aa, the regions of the galaxies that hosted 91bg-like SNe that exhibit emission lines are also found to contain older, $\sim 10\,\mathrm{Gyr}$ stellar populations.

Note that while we find that 91bg-like SNe are associated with older populations than SNe Ia, this result does not preclude that the same galaxy could host both types of supernovae. Indeed, two examples of galaxies hosting both supernovae are SN1991bg and SN1957B (a SN Ia), which both occurred in M84, and of the 91bg-like supernova SN2006mr in Fornax A ((Maoz and Mannucci, 2008), which also hosted five SNe Ia. The point here is that while the delay time distribution of SNe Ia may peak at 1 Gyr (Childress et al., 2014b), SNe Ia can still occur in stellar populations with much greater ages (see Fig 3). Moreover, both M84 and Fornax A are early-type galaxies, and will likely be dominated (in terms of number) by an old stellar population from which the 91bg-like supernova progenitors may arise but they may also contain younger populations that could host SNIa progenitors. It is important to note that while we find that 91bg-like SNe are associated with older populations than SNe Ia, our results are not contradicted by these observations. Our comparison sample of SNe Ia from Maoz et al. (2012) shows evidence that while the delay time distribution of SNe Ia may peak at 1 Gyr (Childress et al., 2014b), SNe Ia can still occur in stellar populations with much greater ages (see Fig 7.3). Moreover, M84 and Fornax A are early-type galaxies, and will likely be dominated by an old stellar population from which the 91bg-like supernova progenitors may arise. Thus it is possible for SNe Ia and 91bg-like supernovae to occur in the same host galaxy even if the delay time distribution of the progenitors is quite different.

We note that the MILES stellar population models we used with `pPXF` assumes the evolution of single stellar populations only. While tracking the stellar evolution and corresponding spectral morphology of single stars is relatively straightforward, it is fairly complicated in the case of interacting stars. Though the majority of stars in the Universe are likely part of a binary (or higher order) star system (Moe and Di Stefano, 2017), most spectral synthesis codes ignore the effects that binary (and multiple) stellar evolution have on the integrated light from galaxies due to the added layer of complexity (e.g. mass transfer and variation from single star evolutionary pathways) that must be taken into account. However, recent work has shown that incorporating binary star evolution models into spectral synthesis analysis codes does indeed result in different derived physical properties (Stanway et al., 2016). On the other hand, the difference between single star spectral synthesis codes, such as GALEXEV, and binary spectral synthesis programs, like BPASS, is more prominent at early times, in particular for stellar ages $\lesssim 1$ Gyr (see Stanway and Eldridge, 2018, fig. 2, right column). Since the explosion sites that we are probing mostly consist of relatively old stellar populations, we are thus not overly concerned that our derived stellar properties are very different from the properties we would expect those stellar populations to have. A comparison of derived stellar properties with a spectral synthesis program that incorporates binaries (such as BPASS) is beyond the scope of this work, though based on the work of Stanway and Eldridge (2018), we would plausibly expect our derived stellar ages to decrease slightly, while the derived metallicities may slightly increase.

7.5 Summary and Conclusions

We obtained integral field observations of the apparent explosion sites of 17 91bg-like SNe. 11 of these observations yielded spectra of sufficiently high signal-to-noise to derive information about the stellar population within ~ 1 kpc projected radius of the explosion site. Using full-spectrum fitting, we found that the majority of the stellar populations that host 91bg-like SNe we observe are dominated by old, metal-rich stars. The majority lack evidence of recent star formation. We conclude that the SNe 91bg progenitors are unlikely to be associated with recent star formation, and likely have delay times > 6 Gyr. This favors a progenitor model such as that proposed in Pakmor et al. (2013) or Crocker et al. (2017), which is composed of a He WD and CO WD.

Acknowledgements

FHP is supported by an Australian Government Research Training Program (RTP) Scholarship. Parts of this research were conducted by the Australian Research Council Centre of Excellence for All-sky Astrophysics (CAASTRO), through project number CE110001020. IRS is supported by the Australian Research Council grant FT160100028. AJR is supported by the Australian Research Council grant FT170100243. BG is supported by the Australian Research Council grant FT140101202. The authors thank Rob Sharp, Fang Yuan, Stuart Sim, Rüdiger Pakmor, Friedrich Röpke, Anais Moller and Brian Schmidt for useful discussions. FHP thanks Peter Verwayen, Ian Adams and Henry Zovaro for their assistance with an occasionally temperamental telescope. This research has made use of the NASA/IPAC Extragalactic Database (NED), which is operated by the Jet Propulsion Laboratory, California Institute of Technology, under contract with the National Aeronautics and Space Administration. This research has made use of the Digitized Sky Survey (DSS-2) based on photographic data obtained using The UK Schmidt Telescope. The UK Schmidt Telescope was operated by the Royal Observatory Edinburgh, with funding from the UK Science and Engineering Research Council, until 1988 June, and thereafter by the Anglo-Australian Observatory. The Digitized Sky Survey was produced at the Space Telescope Science Institute under US Government grant NAG W-2166. We acknowledge the traditional owners of the land on which the ANU 2.3m telescope stands, the Gamilaraay people, and pay our respects to elders past and present.

Appendix: Spectral Fitting

One of the greatest challenge in determining information about a stellar population is in disentangling the effects of age and metallicity on the integrated star light observed in a galaxy spectrum. The spectra of young stars are dominated by near UV and blue emission, and often exhibit strong hydrogen Balmer absorption in the optical. This Balmer absorption may be superimposed with Balmer emission lines which result from the excitation of nebular gas from which the stars form.

As stars increase in age, more and more absorption lines, due to heavier elements such as calcium and iron, appear in the spectra (see figure 7.4). However, for a stellar population of a given age, there is a strong degeneracy between absorption features which appear due to increased stellar age, and absorption features which appear due to high metallicity (figure 7.5). This degeneracy is greatest at ages $> 5 - 10\,$Gyr (figs 7.4 and 7.5) and at these ages precisely determining the metallicity of a stellar population becomes difficult. Disentangling these two effects is the key in determining the age and metallicity of the stellar population in a galaxy spectrum.

Many works have used both observations and theoretical models to develop diagnostics, features in the stellar spectra of galaxies that can be used to provide robust diagnostics of both stellar age and metallicity. For example, a robust, coarse estimate of stellar age is the amplitude of the 4000Å break. This spectral discontinuity comes from the accumulation of many overlapping spectral lines within a narrow wavelength region, and the opacity edge is exhibited as a sharp break in the spectrum (Bruzual A., 1983). The elements that contribute to the opacity edge are ionized metals, particularly calcium, and thus the discontinuity follows a strong trend with stellar temperature.

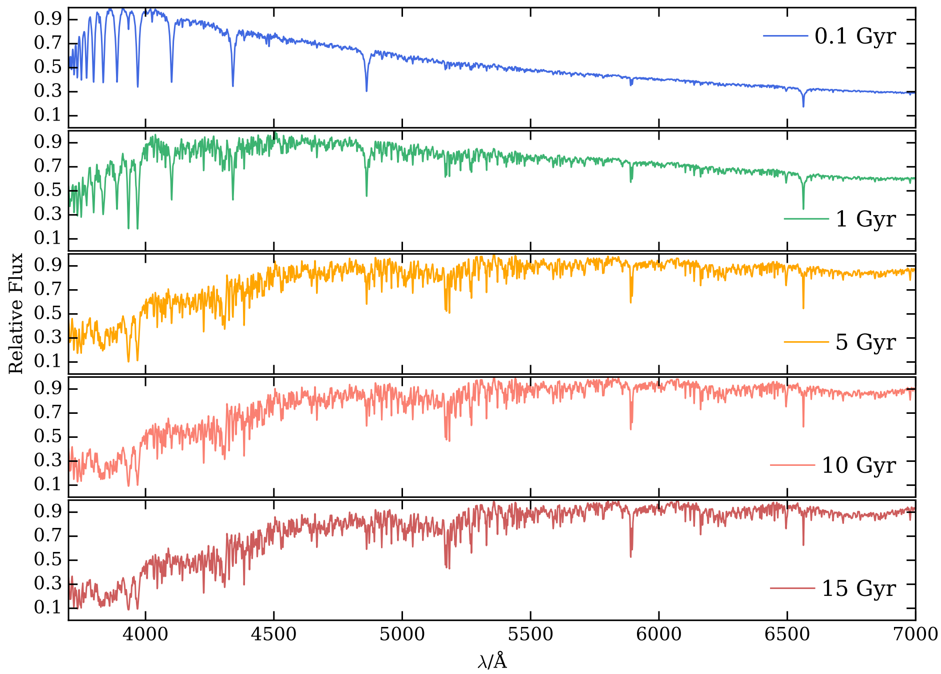

Figure 7.4: MILES library simple stellar populations with ages 0.1, 1, 5, 10, and 15 Gyr at a fixed metallicity of $Z = 0$ (solar metallicity) showing the evolution of spectral features with stellar age, in particular the increasing amplitude of the 4000Å break, and the Hδ equivalent width, both of which increase with stellar age.

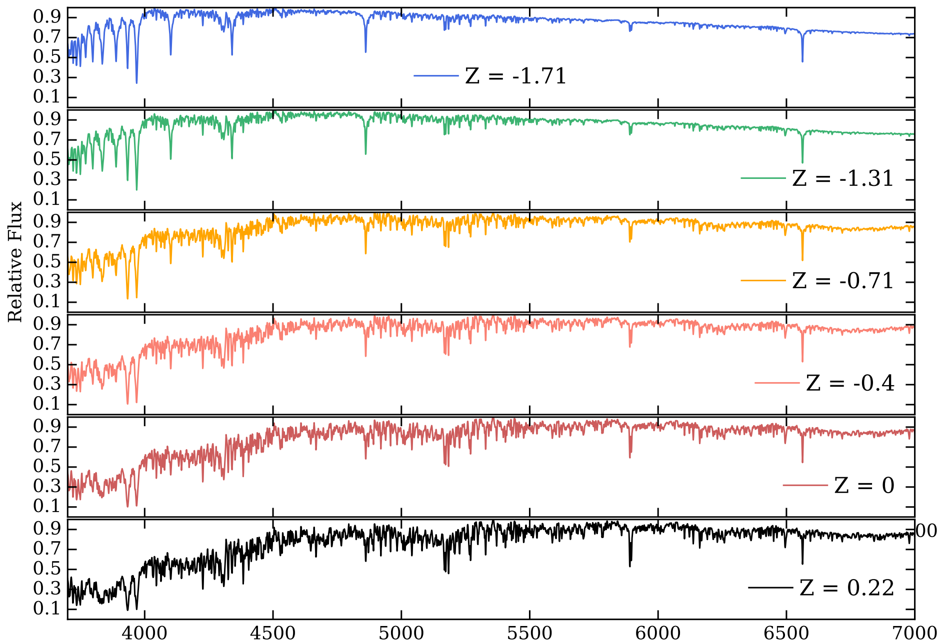

Figure 7.5: MILES library simple stellar populations with metallicities $Z = -1.71$ with a fixed age of 5 Gyr showing the evolution of spectral features with increasing metallicity. By comparing this figure to Fig 7.4 it is apparent that there is a degeneracy between high metallicity and increasing age of a stellar population.

In populations containing young, hot stars, these metals in the stellar atmospheres are typically multiply ionized, and the opacity decreases. The decrease in opacity is observed as a smaller spectral discontinuity at 4000Å. As stars age and cool, metals in the stellar atmospheres are significantly less ionized, or are neutral, and the opacity increases, increasing the amplitude of the 4000Å break. Thus, the amplitude of the 4000Åbreak increases with stellar age. A measure of how the amplitude correlates with stellar age is provided by Kauffmann et al. (2003), specifically adopting the narrow passbands introduced by Balogh et al. (1999). This definition was utilized in Kauffmann et al. (2003) to compute the ages of 10^4 SDSS galaxies.

The presence of the H and K absorption lines are also a good indicator of advanced stellar age. These absorption features are prominent in the spectra of early type galaxies and are composed of a forest of calcium lines which appear in the stellar atmospheres of cool, A-F type stars.

Another spectral feature highly sensitive to stellar ages up to $\sim 1\,\mathrm{Gyr}$ is Hβ absorption (Kauffmann et al., 2003). For galaxies where the stellar population is dominated by O and B stars there is little Hβ absorption as these stars have intrinsically weak balmer absorption lines (Figure 7.4, top). The absorption equivalent width of Hβ is a sensitive diagnostic for bursts of star formation in the preceeding $<= 1Gyr$ (Kauffmann et al., 2003).

Unlike the 4000Å break, one complication in using the strength of the Hβ absorption to measure stellar ages is the presence of nebular emission lines in gas rich galaxies. If nebular gas is present in a galaxy, it is possible for the nebular emission line to superimpose with the Hβ from the stellar continuum, resulting in a measurement of a smaller absoprtion equivalent width (e.g. this effect impacted the results of Gallagher et al., 2008).

It is possible to perform emission line corrections to remove the Hβ emission. This involves fitting the Hα line flux. As the Hβ flux is proportional to the Hα flux (the Balmer decrement, e.g. Table 4.4 of Dopita and Sutherland, 2003), the measured equivalent width can be corrected. An alternative solution, if for example the Hα line is poorly or not resolved, is to measure the absorption equivalent width of the Hδ line. If the Hα flux in the galaxy is small, this solution will suffice, as the Balmer decrement means there will be very little emission left over. The latter solution is often effective in works which focus on early-type galaxies, which are gas poor and lack strong Hα emission.

These diagnostics provide only a coarse estimate of the age of the stellar population, and can be somewhat sensitive to metallicity. However, when they are combined with measurements of absorption equivalent widths that are sensitive primarily to metallicity, it is possible to disentangle the two effects. The Lick/IDS index system provides a number of absorption lines present in stellar spectra that are highly sensitive to metallicity (Worthey, 1994; Worthey and Ottaviani, 1997). These include iron lines Fe λ5270 and Fe λ4383, and molecular indicies such as Mg b. The Lick/IDS system was originally developed based on observations of several hundered stars at the Lick observatory where the $\log g$ and temperature of the stars (and thus their ages) is well understood. Now it is common to compare the measured Lick indicies of galaxy spectra to those determined from simple stellar population (SSP) models (Sánchez-Blázquez et al., 2006; Vazdekis et al., 2010).

An SSP is a theoretical population of stars created during a single starburst event. Realistically, even early-type galaxies have stellar populations that form in not one, but continuous bursts of star formation. Thus when a stellar populationâĂŹs age is determined through comparison to SSPs, the age estimate is sensitive to the youngest stellar component. A variety of different SSPs exist, using different programs which employ different stellar evolution tracks and alpha enhancements (Sánchez-Blázquez et al., 2006; Vazdekis et al., 2010; Eldridge et al., 2017).

An alternative method for determining the properties of the stellar populations of galaxies has emerged in the past few years and has now grown in popularity. Full-spectrum fitting uses more information than the more traditional Lick indicies, and is thus more robust. Moreover, the use of regularization algorithms to optimize the fitting of the spectra without overfitting allow the determination of whether a stellar population has multiple age or metallicity components. In contrast, Lick indicies will provide information only about the youngest stellar population that is present in a galaxy.

Moreover, full-spectrum fitting codes such as the penalized pixel fitting algorithm of (Cappellari and Emsellem, 2004; Cappellari, 2017) allow for the use of improved stellar population models or empirical libraries. With the increased availability of more realistic stellar population synthesis libraries which incoroporate a greater range of physics, it is now possible for the individual to determine which stellar library best fits their needs, as well as for the libraries to be independently compared for their performance.

In this work, we choose to utilize the full-spectrum fitting algorithm `pPXF` to fit linear combinations of simple stellar populations (SSPs) from the MILES stellar library (Sánchez-Blázquez et al., 2006; Vazdekis et al., 2010), which provides 985 stellar spectra across a wavelength range of $3525 - 7500$ Å at 2.5 Å spectral resolution, for stellar metallicities ranging from $[M/H] = 0.22$ to $[M/H] = -2.3$.

Chapter 8

Summary, future work and conclusions

> There was a point to this story, but it has temporarily escaped the chronicler's mind.
>
> Douglas Adams

8.1 Summary

In this thesis, I explored the potential origins of this antimatter in the Milky Way. I have shown that the positrons we observe annihilating today must have been produced close to their sources within the Milky Way, in the past one million years. I have also demonstrated that peculiar type of sub-luminous thermonuclear supernovae could be responsible for the origin of a large fraction of the Milky Way's positrons, and can be a natural explanation for the observed distribution of the annihilation radiation.

In Chapter Two, I discussed the history of the observation of positron annihilation in the Milky Way, from the theoretical and experimental discovery of the positron to the most recent observations of the Galactic 511 keV line with gamma ray satellites.

In Chapter Three, I described the physics that underlies the formation of the positron annihilation line in the Milky Way, and the various astrophysical positron sources that must be evaluated as potential sources of Galactic antimatter.

In Chapter Four, I presented a review of positron transport in the interstellar medium. I show how the propagation of positrons has been investigated through both theory and simulation. Recent conclusions suggest that positrons remain confined to within a few hundred parsecs of their birth sites by interstellar turbulence. Consequently, the distribution of positron sources is directly reflected by the morphology of annihilation gamma-rays. Such sources are then thought to be associated with the old stellar population of the Milky Way.

In Chapter Five, I utilized recent closed coupling calculations of the scattering and positronium formation cross-sections of alkali metal atoms to demonstrate that positron interactions with atoms other than hydrogen and helium must be considered in the context of the galactic positron annihilation signal. Inclusion of these positronium cross-sections in particular enables me to rule out the presence of a low energy resevoir of positrons that may live up to 10 Myr after they lose their energy and thermalize in the interstellar medium. I determined that the positrons we observe annihilating today must have been produced within the last < 1 Myr. I also demonstrated the existence of a new channel for positrons to form positronium at energies where positronium formation was only assumed to occur through radiative recombination with free electrons. This rules out many transient sources which have duty cycles > 1 Myr, such as the central SMBH, however this result is consistent with distributed positron sources such as supernovae.

In Chapter Six, I showed that advective transport and subsequent annihilation of positrons in the nuclear outflows of the Milky Way cannot simultaneously replicate the observed morphology of positron annihilation in the Galactic bulge and satisfy the requirement that 90 per cent of positrons annihilate once the outflow has cooled to 10^4 K. Having ruled out the large scale transport of positrons within the Galaxy and constrained the lifetimes of Galactic positrons to be < 1 Myr, indicating they are produced in a steady state, I have shown that positrons likely originate from a source distributed throughout the Galaxy with a source morphology that reflects the distribution of the observed 511 keV line.

In Chapter Seven, I performed the first quantitative analysis of the stellar populations that host SN1991bg-like supernovae, proposed as a distributed positron source. I found that the average ages of the stellar populations are > 6 Gyr, the oldest stellar populations measured to host any subtype of supernova. Furthermore, I found that the majority of host stellar populations are devoid of recent star formation, and in the galaxies that are found to host recent star formation, there is a significant component of older stars present.

8.2 Future work

8.2.1 Constraining the distribution of the Galactic 511 keV line

8.2.1.1 The *INTEGRAL* medium-latitude sky survey

INTEGRAL's spectrometers provide observations of the Galaxy over an energy range from 3 keV to several MeV with no gaps in energy coverage. Uniform coverage in terms of exposure time has not yet been achieved. Over 16 years of exposure time with SPI has been accumulated in some regions of the galactic plane and center. The exposure map for galactic latitudes of $|b| < 10^\circ$ remains uneven and the exposures shallow even after 15 years of the *INTEGRAL* mission. Consequently, parameters such as the scale height of the 511 keV line are poorly constrained, and little is known about positron escape from the Galaxy, and annihilation in the Galactic halo.

The *INTEGRAL* medium-latitude sky survey (TIMELESS) is an observational program designed to increase the depth of *INTEGRAL*'s exposures in the region $7^\circ < |b| < 33^\circ$. The science objectives of TIMELESS include resolving the vertical extent of 511 keV emission to study the processes that generate and move positrons away from the Galactic Center, and as an indirect test for dark matter.

TIMELESS was awarded 1 Ms of of observing time in June 2018, and all data from the program will be made publicly available. Results from the TIMELESS dataset, including

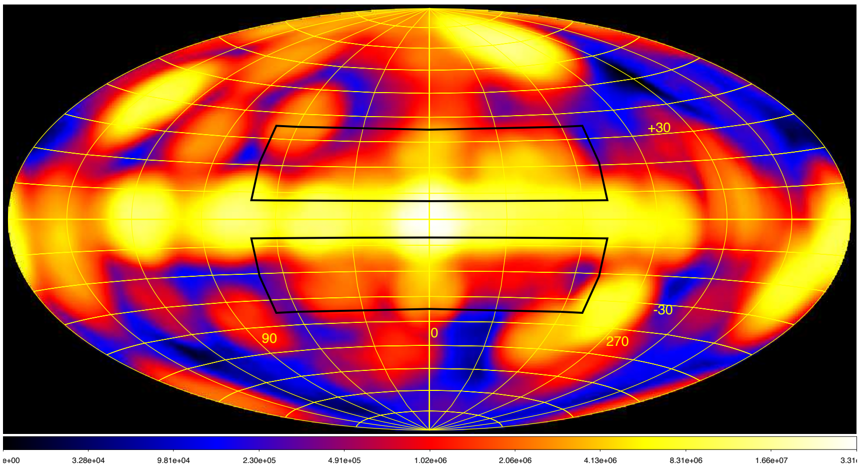

Figure 8.1: All-sky exposure map, from SPI data accumulated through *INTEGRAL* Cycle 15, in Galactic coordinates. Each grid line corresponds to a sky distance of 30° longitude and 10° latitude. The logarithmic colour scale represents the exposure time (in units of seconds) at each sky location. TIMELESS will cover the regions to the north and south of the Galactic Plane (thick black lines) to obtain an additional 1 Ms of coverage.

strong constraints of the scale height of the 511 keV line in the Milky Way, are expected to be published over the next two years. TIMELESS is expected to pave the way for future all-sky MeV gamma-ray surveys like the All-sky Medium Gamma-Ray Observatory (AMEGO; Rando, 2017).

8.2.2 Positron transport and annihilation

8.2.2.1 Understanding positron transport and annihilation

I developed a state-of-the-art Monte Carlo particle transport program to simulate the propagation and annihilation of positrons. The program is able to simulate the microphysics of positron interactions for energies 0.1 eV − 1 TeV in a range of environments where positrons are found, from the ISM to solar flares to supernova ejecta. The microphysics included in the program were employed in my work investigating positron advection in the Milky Way's nuclear outflow (Panther et al., 2017), and my work on positron annihilation on material other than hydrogen and helium (Panther et al., 2018) inspired me to include a wider range of annihilation and interaction cross-sections in the program, enabling the program to be employed in a wider range of applications.

A perfect opportunity to study in detail the production, transport and annihilation of positrons is presented by the case of the dwarf spheroidal (dSph) galaxy Reticulum II (Ret II). A $\sim 2\sigma$ detection of the 511 keV line emitted by Ret II was made by (Siegert et al., 2016c). This suggests that positrons are produced, and annihilate, within the system. It is now possible to model in detail the production of positrons, their transport and annihilation within this dSph galaxy. A detailed estimate of the number of positrons produced by astrophysical sources within Ret II can be made based on the characteristics of its stellar population. As Ret II is a DM dominated system, positron production via DM decay and annihilation must also be considered. Thus, dSph galaxies are an ideal laboratory in which positron production, transport and annihilation can be studied.

8.2.2.2 Constraining positron injection energies

A robust, single-instrument measurement of the gamma-ray spectrum in the inner galaxy at energies $0.2 - 8\,\mathrm{MeV}$ has not yet been made. This energy range is important to probe the injection energies of the positrons we observe annihilating. An earlier constraint used data from multiple instruments and suggests positrons are injected at energies $3 - 7\,\mathrm{MeV}$ (Beacom and Yüksel, 2006). However, there are a number of systematic uncertainties associated with this constraint. This leaves many questions regarding the origin of Galactic positrons uncertain, as a precise measurement of their injection energies would be a particularly important constraint in the context of Dark Matter indirect searches (Bœhm, 2009).

Data from more than 16 years of SPI observations of the inner 20° of the Galaxy can now be used to obtain a spectrum of gamma-ray emission from the inner Galaxy. By fitting all components of emission which contribute to this spectrum (Figure 8.2), including continuum emission and gamma ray lines from positron annihilation and nuclear decays one can obtain a constraint on the contribution of direct positron annihilation in-flight to the gamma ray continuum at energies $> 511\,\mathrm{keV}$. This analysis is the subject of a paper currently in preparation.

8.2.3 Constraining the delay time distribution of SN1991bg-like supernovae

If 91bg-like supernovae are indeed associated with old stellar populations, we expect to see a reduced rate of these objects at higher redshift, where stars are systematically younger. There are suggestions that this is indeed the case - the Supernova Legacy Survey (SNLS) observed a reduced rate of extreme low-stretch SNe (SNe 91bg) at higher redshift (up to $z \sim 0.6$) compared to a local volumetric sample (González-Gaitán et al., 2011) of 91bg-like SNe. Such a reduction in rate is not seen in standard SNe Ia at higher redshift (see Figure 8.3).

However, the SNLS analysis had a very small sample (18 sub-luminous SNe and 1 91bg-like SN) and large systematic uncertainties (González-Gaitán et al., 2011). Ultimately, it is desirable to determine the rate evolution of SNe 91bg with redshift with a larger sample. Using the SNLS rate estimates, we expect ~ 100 91bg-like SNe to be discovered at $Z < 0.2$ in the Dark Energy Survey (Dark Energy Survey Collaboration et al., 2016). After quality and selection cuts, this will still yield a far larger sample size than that of González-Gaitán et al. (2011).

This work involves first determining which transients observed in the DES are 91bg-like SNe. As the majority of photometric transients do not receive spectroscopic followup (the typical way in which 91bg-like SNe are identified), a robust method to identify 91bg-like SNe from photometric data alone must be developed.

Machine learning algorithms that employ supervised learning are an ideal technique to apply to classification of photometric data, however a training set is required (an unsupervised learning algorithm may also be trialled, which does not require a training set). SNANA is a program designed for supernova analysis (Kessler et al., 2009), and contains contains a simulation, a light-curve fitter, and a cosmology fitter. Simulations of SN photometry for

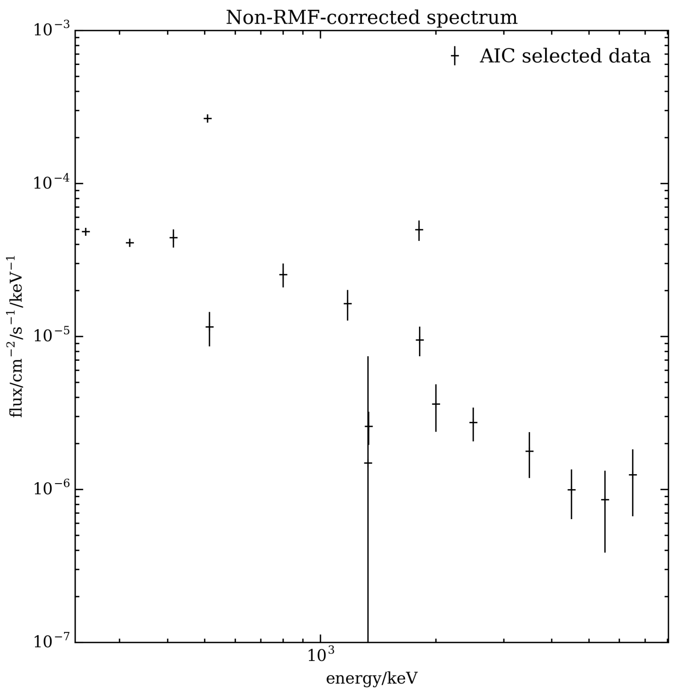

Figure 8.2: Spectrum of gamma-ray emission for the inner 20° of the Galaxy based on $\sim$ 16 yr of SPI/*INTEGRAL*. The 511 keV line from positron annihilation, and the 1.8, MeV line from the decay of ^{26}Al are visible. This is a preliminary analysis of data to constrain the injection energies of positrons.

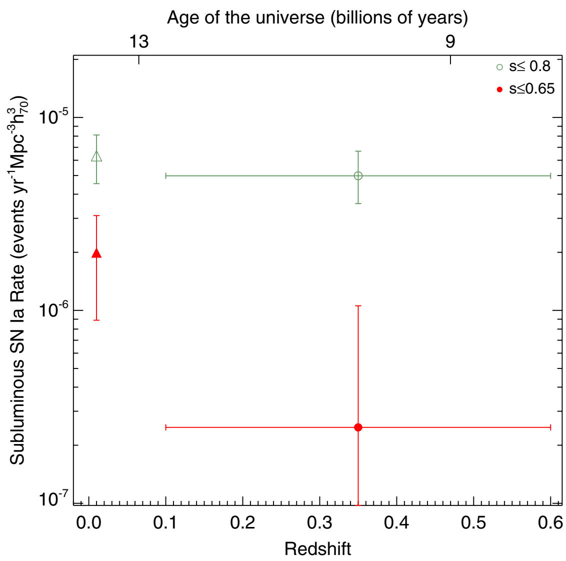

Figure 8.3: Volumetric rate as a function of redshift for normal SNe Ia (red) and low-stretch SNe, analogous to 91bg-like SNe, from González-Gaitán et al. (2011). The rate of 91bg-like supernovae appears to decrease at higher redshifts (green), suggesting the events have a delay time distribution that peaks to higher stellar ages than SNe Ia (red)

ordinary SNe Ia, 91bg-like SNe (based on lightcurve templates from Jones) and CCSN can be utilized to create a training set (e.g. Kessler et al. (2018)). This training set can be utilized to create a classification algorithm which can distinguish 91bg-like supernovae in DES. The classifier must also be verified on simulated data, before it is applied to real data obtained by the DES to identify 91bg-like supernova candidates from the catalog of transient events. These candidates can then be used to compute the rate evolution of 91bg-like SNe across cosmic time (González-Gaitán et al., 2011).

8.3 Conclusions

Explaining the origin of the $\sim 5 \times 10^{43}$ positrons that annihilate each second in the Milky Way is an enduring problem in high energy astrophysics. In this thesis, I have attempted to tackle this challenging problem in three ways.

Firstly, by constraining the lifetimes of positrons in the interstellar medium. I found that including cross-sections of atoms such as alkali metals constrains the lifetimes of the positrons in the ISM from production to annihilation to be $\sim 1\,$Myr (Chapter Five). This is a significant advance as it rules out several positron production scenarios which involve highly episodic bursts of positron production, such as from the Galactic center SMBH. My result implies that positrons are produced and annihilate in what is approximately a steady state.

Secondly, I investigated whether positrons can be transported over Galactic scale distances by large-scale motions of gas in the Milky Way. While literature results suggest that positrons are confined close (within a few hundred parsecs) if their sources by turbulent magnetic fields, this does not rule out the large scale transport of positrons entrained in gas which expands into the Milky Way's nuclear outflow. In Chapter Six, I show that the nuclear outflow cannot simultaneously inflate the Fermi Bubbles and distribute positrons into the Galactic bulge. The strong temperature gradient which develops in the outflow results in the majority of positrons annihilating in the hot phase of the ISM, producing an annihilation spectrum with a characteristic linewidth too broad to explain observations.

Finally, I utilized spectra of the stellar populations surrounding the explosion sites of SN1991bg-like supernovae to quantitatively constrain the delay time distribution of this peculiar thermonuclear supernova subtype. I find that the stellar population ages derived from these spectra ($> 6\,$Gyr are consistent with those required for these supernovae to be antimatter factors in the Milky Way as described in Crocker et al. (2017). Moreover, I also find that the local stellar populations of these SNe are predominantly devoid of star formation, indicating that the SNe are associated with old stars.

In conclusion, I find that the most plausible explanation for the origin of the Milky Way's positrons is a source that is distributed amongst the old stellar population. Such a source is 91bg-like SNe, a peculiar, subluminous thermonuclear transient. These 'antimatter factory' supernova can synthesise sufficient ^{44}Ti to explain up to 90 per cent of the Milky Way's antimatter.

Bibliography

Abazajian, K. N., 2011. The consistency of Fermi-LAT observations of the galactic center with a millisecond pulsar population in the central stellar cluster. , 3 (Mar. 2011), 010. doi:10.1088/1475-7516/2011/03/010. (cited on page 50)

Abbott, B. P.; Collaboration, L. S.; and Collaboration, V., 2017. Gw170817: Observation of gravitational waves from a binary neutron star inspiral. *Phys. Rev. Lett.*, 119 (Oct 2017), 161101. doi:10.1103/PhysRevLett.119.161101. https://link.aps.org/doi/10.1103/PhysRevLett.119.161101. (cited on page 54)

Abbott, B. P. e. a., 2017. Multi-messenger Observations of a Binary Neutron Star Merger. *ApJ*, 848 (Oct. 2017), L12. doi:10.3847/2041-8213/aa91c9. (cited on page 54)

Abdollahi, S. and Fermi-LAT Collaboration, 2017. Cosmic-ray electron-positron spectrum from 7 GeV to 2 TeV with the Fermi Large Area Telescope. *Phys. Rev. D*, 95 (Apr. 2017), 082007. doi:10.1103/PhysRevD.95.082007. (cited on page 40)

Aharonian, F. A. and Atoyan, A. M., 1981. On the origin of the galactic annihilation radiation. *Pisma v Astronomicheskii Zhurnal*, 7 (Dec. 1981), 714–719. (cited on pages 27, 33, 60, 64, 70, and 84)

Ahmadi, M.; Alves, B. X. R.; Baker, C. J.; Bertsche, W.; Butler, E.; Capra, A.; Carruth, C.; Cesar, C. L.; Charlton, M.; Cohen, S.; Collister, R.; Eriksson, S.; Evans, A.; Evetts, N.; Fajans, J.; Friesen, T.; Fujiwara, M. C.; Gill, D. R.; Gutierrez, A.; Hangst, J. S.; Hardy, W. N.; Hayden, M. E.; Isaac, C. A.; Ishida, A.; Johnson, M. A.; Jones, S. A.; Jonsell, S.; Kurchaninov, L.; Madsen, N.; Mathers, M.; Maxwell, D.; McKenna, J. T. K.; Menary, S.; Michan, J. M.; Momose, T.; Munich, J. J.; Nolan, P.; Olchanski, K.; Olin, A.; Pusa, P.; Rasmussen, C. Ø.; Robicheaux, F.; Sacramento, R. L.; Sameed, M.; Sarid, E.; Silveira, D. M.; Stracka, S.; Stutter, G.; So, C.; Tharp, T. D.; Thompson, J. E.; Thompson, R. I.; van der Werf, D. P.; and Wurtele, J. S., 2017. Observation of the hyperfine spectrum of antihydrogen. *Nature*, 548 (08 2017), 66 EP –. https://doi.org/10.1038/nature23446. (cited on page 1)

Albernhe, F.; Le Borgne, J. F.; Vedrenne, G.; Boclet, D.; Durouchoux, P.; and da Costa, J. M., 1981. Detection of the positron annihilation gamma ray line from the Galactic Center region. *A&A*, 94 (Feb. 1981), 214–218. (cited on page 12)

Alexis, A.; Jean, P.; Martin, P.; and Ferrière, K., 2014. Monte Carlo modelling of the propagation and annihilation of nucleosynthesis positrons in the Galaxy. *A&A*, 564 (Apr. 2014), A108. doi:10.1051/0004-6361/201322393. (cited on pages 36, 62, 63, 71, 76, and 84)

Anantharamaiah, K. R.; Radhakrishnan, V.; Morris, D.; Vivekanand, M.; Downes, D.; and Shukre, C. S., 1989. A Search for Radio Recombination Lines of Positronium Near the Galactic Center. In *The Center of the Galaxy*, vol. 136 of *IAU Symposium*, 607–616. (cited on page 31)

Anderson, C. D., 1932. The apparent existence of easily deflectable positives. *Science*, 76, 1967 (1932), 238–239. http://www.jstor.org/stable/1658257. (cited on pages xv, 1, 6, 7, 9, and 69)

Bailey, J. J.; Kadyrov, A. S.; and Bray, I., 2015. Internal consistency in positron-hydrogen-scattering calculations. *Physical Review A*, 91, 1 (Jan. 2015), 012712. doi:10.1103/PhysRevA.91.012712. https://link.aps.org/doi/10.1103/PhysRevA.91.012712. (cited on pages 29 and 72)

Balogh, M. L.; Morris, S. L.; Yee, H. K. C.; Carlberg, R. G.; and Ellingson, E., 1999. Differential Galaxy Evolution in Cluster and Field Galaxies at z˜0.3. *ApJ*, 527 (Dec. 1999), 54–79. doi:10.1086/308056. (cited on page 113)

Bartels, R.; Calore, F.; Storm, E.; and Weniger, C., 2018. Galactic Binaries Can Explain the Fermi Galactic Center Excess and 511 keV Emission. *ArXiv e-prints*, (Mar. 2018). (cited on pages 50 and 60)

Bartels, R.; Krishnamurthy, S.; and Weniger, C., 2016. Strong Support for the Millisecond Pulsar Origin of the Galactic Center GeV Excess. *Physical Review Letters*, 116, 5 (Feb. 2016), 051102. doi:10.1103/PhysRevLett.116.051102. (cited on page 50)

Battiston, R. and AMS Collaboration, 2014. Precision measurements of e^+e^- in Cosmic Ray with the Alpha Magnetic Spectrometer on the ISS. *Physics of the Dark Universe*, 4 (Sep. 2014), 6–9. doi:10.1016/j.dark.2014.05.002. (cited on page 40)

Beacom, J. F. and Yüksel, H., 2006. Stringent Constraint on Galactic Positron Production. *Physical Review Letters*, 97, 7 (Aug. 2006), 071102. doi:10.1103/PhysRevLett.97.071102. (cited on pages 33, 40, 52, 53, 60, 64, 70, 84, 86, and 118)

Beloborodov, A. M., 1999. Electron-positron outflows from gamma-ray emitting accretion discs. *MNRAS*, 305 (May 1999), 181–189. doi:10.1046/j.1365-8711.1999.02384.x. (cited on page 51)

Bertone, G. and Tait, T. M. P., 2018. A new era in the search for dark matter. *Nature*, 562 (Oct. 2018), 51–56. doi:10.1038/s41586-018-0542-z. (cited on page 52)

Bhatia, A. K.; Drachman, R. J.; and Temkin, A., 1974. Annihilation during positron-hydrogen collisions. *Phys. Rev. A*, 9 (Jan 1974), 223–225. doi:10.1103/PhysRevA.9.223. https://link.aps.org/doi/10.1103/PhysRevA.9.223. (cited on page 28)

Bhatia, A. K.; Drachman, R. J.; and Temkin, A., 1977. Annihilation during positron-hydrogen collisions: Addendum and erratum. *Phys. Rev. A*, 16 (Oct 1977), 1719–1722. doi:10.1103/PhysRevA.16.1719. https://link.aps.org/doi/10.1103/PhysRevA.16.1719. (cited on page 28)

Bisnovatyi-Kogan, G. and Pozanenko, A., 2018. Annihilation line from the galactic bulge due to action of low-mass flare stars. *International Journal of Modern Physics D*, 27 (2018), 1844003. doi:10.1142/S0218271818440030. (cited on page 49)

Blackett, P. M. S. and Occhialini, G. P. S., 1933. Some photographs of the tracks of penetrating radiation. *Proceedings of the Royal Society of London. Series A, Containing Papers of a Mathematical and Physical Character*, 139, 839 (1933), 699–726. http://www.jstor.org/stable/96057. (cited on pages 7 and 9)

Bland-Hawthorn, J. and Cohen, M., 2003. The Large-Scale Bipolar Wind in the Galactic Center. *ApJ*, 582 (Jan. 2003), 246–256. doi:10.1086/344573. (cited on pages 62, 63, 81, and 85)

Blasi, P., 2009. Origin of the Positron Excess in Cosmic Rays. *Phys. Rev. Lett.*, 103 (Jul. 2009), 051104. doi:10.1103/PhysRevLett.103.051104. (cited on page 40)

Blondin, S.; Dessart, L.; and Hillier, D. J., 2015. A one-dimensional Chandrasekhar-mass delayed-detonation model for the broad-lined Type Ia supernova 2002bo. *MNRAS*, 448 (Apr. 2015), 2766–2797. doi:10.1093/mnras/stv188. (cited on page 97)

Blumenthal, G. R. and Gould, R. J., 1970. Bremsstrahlung, Synchrotron Radiation, and Compton Scattering of High-Energy Electrons Traversing Dilute Gases. *Reviews of Modern Physics*, 42 (1970), 237–271. doi:10.1103/RevModPhys.42.237. (cited on page 36)

Bœhm, C., 2009. The dark matter interpretation of the 511 keV line. *New Journal of Physics*, 11, 10 (Oct. 2009), 105009. doi:10.1088/1367-2630/11/10/105009. (cited on pages 84 and 118)

Bœhm, C. and Ascasibar, Y., 2004. More evidence in favor of light dark matter particles? *Phys. Rev. D*, 70 (Dec 2004), 115013. doi:10.1103/PhysRevD.70.115013. https://link.aps.org/doi/10.1103/PhysRevD.70.115013. (cited on page 53)

Boehm, C. and Fayet, P., 2004. Scalar dark matter candidates. *Nuclear Physics B*, 683, 1 (2004), 219 – 263. doi:https://doi.org/10.1016/j.nuclphysb.2004.01.015. http://www.sciencedirect.com/science/article/pii/S0550321304000306. (cited on page 53)

Boehm, C.; Hooper, D.; Silk, J.; Casse, M.; and Paul, J., 2004. Mev dark matter: Has it been detected? *Phys. Rev. Lett.*, 92 (Mar 2004), 101301. doi:10.1103/PhysRevLett.92.101301. https://link.aps.org/doi/10.1103/PhysRevLett.92.101301. (cited on page 52)

Bœhm, C. and Silk, J., 2008. A new test for dark matter particles of low mass. *Physics Letters B*, 661 (Mar. 2008), 287–289. doi:10.1016/j.physletb.2008.02.019. (cited on page 53)

Boggs, S. E.; Harrison, F. A.; Miyasaka, H.; Grefenstette, B. W.; Zoglauer, A.; Fryer, C. L.; Reynolds, S. P.; Alexander, D. M.; An, H.; Barret, D.; Christensen, F. E.; Craig, W. W.; Forster, K.; Giommi, P.; Hailey, C. J.; Hornstrup, A.; Kitaguchi, T.; Koglin, J. E.; Madsen, K. K.; Mao, P. H.; Mori, K.; Perri, M.; Pivovaroff, M. J.; Puccetti, S.; Rana, V.; Stern, D.; Westergaard, N. J.; and Zhang, W. W., 2015. ^{44}Ti gamma-ray emission lines from SN1987A reveal an asymmetric explosion. *Science*, 348 (May 2015), 670–671. doi:10.1126/science.aaa2259. (cited on pages 9 and 45)

Bouchet, L.; Jourdain, E.; Roques, J.-P.; Strong, A.; Diehl, R.; Lebrun, F.; and Terrier, R., 2008. INTEGRAL SPI All-Sky View in Soft Gamma Rays: A Study of Point-Source and Galactic Diffuse Emission. *ApJ*, 679 (Jun. 2008), 1315–1326. doi:10.1086/529489. (cited on page 20)

Bouchet, L.; Mandrou, P.; Roques, J. P.; Vedrenne, G.; Cordier, B.; Goldwurm, A.; Lebrun, F.; Paul, J.; Sunyaev, R.; Churazov, E.; Gilfanov, M.; Pavlinsky, M.; Grebenev, S.; Babalyan, G.; Dekhanov, I.; and Khavenson, N., 1991. Sigma discovery of variable e(+)-e(-) annihilation radiation from the near Galactic center variable compact source 1E 1740.7 - 2942. *ApJ*, 383 (Dec. 1991), L45–L48. doi:10.1086/186237. (cited on pages 13 and 51)

Bouchet, L.; Roques, J. P.; Ballet, J.; Goldwurm, A.; and Paul, J., 2001. The SIGMA/Granat Telescope: Calibration and Data Reduction. *ApJ*, 548 (Feb. 2001), 990–1009. doi:10.1086/318997. (cited on page 13)

Bouchet, L.; Roques, J. P.; and Jourdain, E., 2010. On the Morphology of the Electron-Positron Annihilation Emission as Seen by Spi/integral. *ApJ*, 720 (Sep. 2010), 1772–1780. doi:10.1088/0004-637X/720/2/1772. (cited on page 20)

Bouchet, L.; Strong, A. W.; Porter, T. A.; Moskalenko, I. V.; Jourdain, E.; and Roques, J.-P., 2011. Diffuse Emission Measurement with the SPectrometer on INTEGRAL as an Indirect Probe of Cosmic-Ray Electrons and Positrons. *ApJ*, 739 (Sep. 2011), 29. doi:10.1088/0004-637X/739/1/29. (cited on pages 20 and 59)

Branch, D. and Tammann, G. A., 1992. Type IA supernovae as standard candles. *ARA&A*, 30 (1992), 359–389. doi:10.1146/annurev.aa.30.090192.002043. (cited on page 96)

Breitschwerdt, D.; McKenzie, J. F.; and Voelk, H. J., 1991. Galactic winds. I - Cosmic ray and wave-driven winds from the Galaxy. *A&A*, 245 (May 1991), 79–98. (cited on page 86)

Bruenn, S. W.; Mezzacappa, A.; Hix, W. R.; Lentz, E. J.; Messer, O. E. B.; Lingerfelt, E. J.; Blondin, J. M.; Endeve, E.; Marronetti, P.; and Yakunin, K. N., 2013. Axisymmetric Ab Initio Core-collapse Supernova Simulations of 12-25 M Stars. *ApJ*, 767, 1 (Apr 2013), L6. doi:10.1088/2041-8205/767/1/L6. (cited on page 45)

Bruzual A., G., 1983. Spectral evolution of galaxies. I - Early-type systems. *ApJ*, 273 (Oct. 1983), 105–127. doi:10.1086/161352. (cited on page 110)

Bussard, R. W.; Ramaty, R.; and Drachman, R. J., 1979. The annihilation of galactic positrons. *ApJ*, 228 (Mar. 1979), 928–934. doi:10.1086/156920. (cited on pages 29, 34, and 71)

C Boehm, T. A. E. and Silk, J., 2004. Can annihilating dark matter be lighter than a few gevs? *Journal of Physics G: Nuclear and Particle Physics*, 30, 3 (2004), 279. http://stacks.iop.org/0954-3899/30/i=3/a=004. (cited on page 53)

Campeanu, R. I.; Fromme, D.; Kruse, G.; McEachran, R. P.; Parcell, L. A.; Raith, W.; Sinapius, G.; and Stauffer, A. D., 1987. Partitioning of the positron-helium total scattering cross section. *Journal of Physics B: Atomic and Molecular Physics*, 20, 14 (1987), 3557. doi:10.1088/0022-3700/20/14/027. http://stacks.iop.org/0022-3700/20/i=14/a=027. (cited on pages 29 and 72)

Canetti, L.; Drewes, M.; and Shaposhnikov, M., 2012. Matter and antimatter in the universe. *New Journal of Physics*, 14 (Sep. 2012), 095012. doi:10.1088/1367-2630/14/9/095012. (cited on page 1)

Cao, Y.; Kasliwal, M. M.; McKay, A.; and Bradley, A., 2014. Classification of Supernova in M82 as a young, reddened Type Ia Supernova. *The Astronomer's Telegram*, 5786 (Jan. 2014). (cited on page 44)

Cappellari, M., 2017. Improving the full spectrum fitting method: accurate convolution with Gauss-Hermite functions. *MNRAS*, 466 (Apr. 2017), 798–811. doi:10.1093/mnras/stw3020. (cited on pages 99, 103, and 114)

Cappellari, M. and Emsellem, E., 2004. Parametric Recovery of Line-of-Sight Velocity Distributions from Absorption-Line Spectra of Galaxies via Penalized Likelihood. *PASP*, 116 (Feb. 2004), 138–147. doi:10.1086/381875. (cited on pages 99, 103, and 114)

Caraveo, P. A., 2014. Gamma-ray pulsar revolution. *Annual Review of Astronomy and Astrophysics*, 52, 1 (2014), 211–250. doi:10.1146/annurev-astro-081913-035948. https://doi.org/10.1146/annurev-astro-081913-035948. (cited on page 49)

Cassé, M.; Cordier, B.; Paul, J.; and Schanne, S., 2004. Hypernovae/Gamma-Ray Bursts in the Galactic Center as Possible Sources of Galactic Positrons. *ApJ*, 602 (Feb. 2004), L17–L20. doi:10.1086/381884. (cited on page 48)

Chan, K.-W. and Lingenfelter, R. E., 1993. Positrons from supernovae. *ApJ*, 405 (Mar. 1993), 614–636. doi:10.1086/172393. (cited on pages 43 and 48)

Chardin, G. and Manfredi, G., 2018. Gravity, antimatter and the dirac-milne universe. *Hyperfine Interactions*, 239, 1 (Oct 2018), 45. doi:10.1007/s10751-018-1521-3. https://doi.org/10.1007/s10751-018-1521-3. (cited on page 1)

Charlton, M.; Griffith, T. C.; Heyland, G. R.; and Wright, G. L., 1983. Total scattering cross sections for low-energy positrons in the molecular gases H2, N2, CO2, O2 and CH4. *Journal of Physics B: Atomic and Molecular Physics*, 16 (1983), 323. http://iopscience.iop.org/0022-3700/16/2/019. (cited on pages 29 and 72)

Charlton, M. and Humberston, J. W., 2000. *Positron Physics*. Cambridge University Press. ISBN 978-0-521-41550-7. (cited on pages 29 and 72)

Cheng, K. S.; Chernyshov, D. O.; and Dogiel, V. A., 2006. Annihilation Emission from the Galactic Black Hole. *ApJ*, 645 (Jul. 2006), 1138–1151. doi:10.1086/504583. (cited on pages 63 and 84)

Cheng, L. X.; Leventhal, M.; Smith, D. M.; Purcell, W. R.; Tueller, J.; Connors, A.; Dixon, D.; Kinzer, R. L.; and Skibo, J. G., 1997. A Maximum Entropy Map of the 511 keV Positron Annihilation Line Emission Distribution Near the Galactic Center. *ApJ*, 481 (May 1997), L43–L46. doi:10.1086/310638. (cited on pages 52 and 71)

Childress, M. J.; Hillier, D. J.; Seitenzahl, I.; Sullivan, M.; Maguire, K.; Taubenberger, S.; Scalzo, R.; Ruiter, A.; Blagorodnova, N.; Camacho, Y.; Castillo, J.; Elias- Rosa, N.; Fraser, M.; Gal-Yam, A.; Graham, M.; Howell, D. A.; Inserra, C.; Jha, S. W.; Kumar, S.; Mazzali, P. A.; McCully, C.; Morales-Garoffolo, A.; Pandya, V.; Polshaw, J.; Schmidt, B.; Smartt, S.; Smith, K. W.; Sollerman, J.; Spyromilio, J.; Tucker, B.; Valenti, S.; Walton, N.; Wolf, C.; Yaron, O.; Young, D. R.; Yuan, F.; and Zhang, B., 2015. Measuring nickel masses in Type Ia supernovae using cobalt emission in nebular phase spectra. *MNRAS*, 454 (Dec. 2015), 3816–3842. doi:10.1093/mnras/stv2173. (cited on page 43)

Childress, M. J.; Vogt, F. P. A.; Nielsen, J.; and Sharp, R. G., 2014a. PyWiFeS: a rapid data reduction pipeline for the Wide Field Spectrograph (WiFeS). *Ap&SS*, 349 (Feb. 2014), 617–636. doi:10.1007/s10509-013-1682-0. (cited on page 102)

Childress, M. J.; Wolf, C.; and Zahid, H. J., 2014b. Ages of Type Ia supernovae over cosmic time. *MNRAS*, 445 (Dec. 2014), 1898–1911. doi:10.1093/mnras/stu1892. (cited on pages 107, 108, and 109)

Chupp, E. L.; Forrest, D. J.; Higbie, P. R.; Suri, A. N.; Tsai, C.; and Dunphy, P. P., 1973. Solar Gamma Ray Lines observed during the Solar Activity of August 2 to August 11, 1972. *Nature*, 241 (Feb. 1973), 333–335. doi:10.1038/241333a0. (cited on page 49)

Chupp, E. L.; Forrest, D. J.; and Suri, A. N., 1975. High energy gamma-ray radiation above 300 keV associated with solar activity. In *Solar Gamma-, X-, and EUV Radiation*, vol. 68 of *IAU Symposium*, 341–359. (cited on page 12)

Chupp, E. L.; Sarkady, A. A.; and Gilman, H. P., 1967. The 0.5 MeV gamma ray flux and the energy loss spectrum in CsI(Tl) at 4 g/cm ^{2}. *Planet. Space Sci.*, 15 (May 1967), 881–892. doi:10.1016/0032-0633(67)90122-5. (cited on page 10)

Churazov, E.; Sazonov, S.; Tsygankov, S.; Sunyaev, R.; and Varshalovich, D., 2011. Positron annihilation spectrum from the Galactic Centre region observed by SPI/INTEGRAL revisited: annihilation in a cooling ISM? *MNRAS*, 411 (Mar. 2011), 1727–1743. doi:10.1111/j.1365-2966.2010.17804.x. (cited on pages 22, 23, 34, 42, 59, 63, 71, 76, 78, 82, and 85)

Churazov, E.; Sunyaev, R.; Isern, J.; Bikmaev, I.; Bravo, E.; Chugai, N.; Grebenev, S.; Jean, P.; Knödlseder, J.; Lebrun, F.; and Kuulkers, E., 2015. Gamma-rays from Type Ia Supernova SN2014J. *ApJ*, 812 (Oct. 2015), 62. doi:10.1088/0004-637X/812/1/62. (cited on pages 9 and 44)

Churazov, E.; Sunyaev, R.; Isern, J.; Knödlseder, J.; Jean, P.; Lebrun, F.; Chugai, N.; Grebenev, S.; Bravo, E.; Sazonov, S.; and Renaud, M., 2014. Cobalt-56 γ-ray emission lines from the type Ia supernova 2014J. *Nature*, 512 (Aug. 2014), 406–408. doi:10.1038/nature13672. (cited on pages 9, 44, and 69)

Churazov, E.; Sunyaev, R.; Sazonov, S.; Revnivtsev, M.; and Varshalovich, D., 2005. Positron annihilation spectrum from the Galactic Centre region observed by SPI/INTEGRAL. *MNRAS*, 357 (Mar. 2005), 1377–1386. doi:10.1111/j.1365-2966.2005.08757.x. (cited on pages 22, 34, 59, 63, 71, 78, and 84)

Clayton, D. D., 1973. Positronium Origin of 476 keV Galactic Feature. *Nature Physical Science*, 244 (Aug. 1973), 137–138. doi:10.1038/physci244137b0. (cited on page 45)

Colgate, S. A. and McKee, C., 1969. Early Supernova Luminosity. *ApJ*, 157 (Aug. 1969), 623. doi:10.1086/150102. (cited on page 43)

Colgate, S. A.; Petschek, A. G.; and Kriese, J. T., 1980. The luminosity of type I supernovae. *ApJ*, 237 (May 1980), L81–L85. doi:10.1086/183239. (cited on page 43)

Conlon, J. P. and Quevedo, F., 2007. Astrophysical and cosmological implications of large volume string compactifications. , 8 (Aug. 2007), 019. doi:10.1088/1475-7516/2007/08/019. (cited on page 53)

Crannell, C. J.; Joyce, G.; Ramaty, R.; and Werntz, C., 1976. Formation of the 0.511 MeV line in solar flares. *ApJ*, 210 (Dec. 1976), 582–592. doi:10.1086/154863. (cited on pages 25, 27, and 31)

Crocker, R. M., 2012. Non-thermal insights on mass and energy flows through the Galactic Centre and into the Fermi bubbles. *MNRAS*, 423 (Jul. 2012), 3512–3539. doi:10.1111/j.1365-2966.2012.21149.x. (cited on page 88)

Crocker, R. M. and Aharonian, F., 2011. Fermi Bubbles: Giant, Multibillion-Year-Old Reservoirs of Galactic Center Cosmic Rays. *Physical Review Letters*, 106, 10 (Mar. 2011), 101102. doi:10.1103/PhysRevLett.106.101102. (cited on pages 63, 82, and 85)

Crocker, R. M.; Bicknell, G. V.; Taylor, A. M.; and Carretti, E., 2015. A Unified Model of the Fermi Bubbles, Microwave Haze, and Polarized Radio Lobes: Reverse Shocks in the Galactic Center Giant Outflows. *ApJ*, 808 (Aug. 2015), 107. doi:10.1088/0004-637X/808/2/107. (cited on pages 81, 85, and 86)

Crocker, R. M.; Ruiter, A. J.; Seitenzahl, I. R.; Panther, F. H.; Sim, S.; Baumgardt, H.; MÃűller, A.; Nataf, D. M.; Ferrario, L.; Eldridge, J. J.; White, M.; Tucker, B. E.; and Aharonian, F., 2017. Diffuse galactic antimatter from faint thermonuclear supernovae in old stellar populations. 1 (2017), 0135. http://dx.doi.org/10.1038/s41550-017-0135. (cited on pages 46, 47, 50, 64, 92, 93, 95, 98, 108, 109, and 121)

Dark Energy Survey Collaboration; Abbott, T.; Abdalla, F. B.; Aleksić, J.; Allam, S.; Amara, A.; Bacon, D.; Balbinot, E.; Banerji, M.; Bechtol, K.; Benoit-Lévy, A.; Bernstein, G. M.; Bertin, E.; Blazek, J.; Bonnett, C.; Bridle, S.; Brooks, D.; Brunner, R. J.; Buckley-Geer, E.; Burke, D. L.; Caminha, G. B.; Capozzi, D.; Carlsen, J.; Carnero-Rosell, A.; Carollo, M.; Carrasco-Kind, M.; Carretero, J.; Castander, F. J.; Clerkin, L.; Collett, T.; Conselice, C.; Crocce, M.; Cunha, C. E.; D'Andrea, C. B.; da Costa, L. N.; Davis, T. M.; Desai, S.; Diehl, H. T.; Dietrich, J. P.; Dodelson, S.; Doel, P.; Drlica-Wagner, A.; Estrada, J.; Etherington, J.; Evrard, A. E.; Fabbri, J.; Finley, D. A.; Flaugher, B.; Foley, R. J.; Fosalba, P.; Frieman, J.; García-Bellido, J.; Gaztanaga, E.; Gerdes, D. W.; Giannantonio, T.; Goldstein, D. A.; Gruen, D.; Gruendl, R. A.; Guarnieri, P.; Gutierrez, G.; Hartley, W.; Honscheid, K.; Jain, B.; James, D. J.; Jeltema, T.; Jouvel, S.; Kessler, R.; King, A.; Kirk, D.; Kron, R.; Kuehn, K.; Kuropatkin, N.; Lahav, O.; Li, T. S.; Lima, M.; Lin, H.; Maia, M. A. G.; Makler, M.; Manera, M.; Maraston, C.; Marshall, J. L.; Martini, P.; McMahon, R. G.; Melchior, P.; Merson, A.; Miller, C. J.; Miquel, R.; Mohr, J. J.; Morice-Atkinson, X.; Naidoo, K.; Neilsen, E.; Nichol, R. C.; Nord, B.; Ogando, R.; Ostrovski, F.; Palmese, A.; Papadopoulos, A.; Peiris, H. V.; Peoples, J.; Percival, W. J.; Plazas, A. A.; Reed, S. L.; Refregier, A.; Romer, A. K.; Roodman, A.; Ross, A.; Rozo, E.; Rykoff, E. S.; Sadeh, I.; Sako, M.; Sánchez, C.; Sanchez, E.; Santiago, B.; Scarpine, V.; Schubnell, M.; Sevilla-Noarbe, I.; Sheldon, E.; Smith, M.; Smith, R. C.; Soares- Santos, M.; Sobreira, F.; Soumagnac, M.; Suchyta, E.; Sullivan, M.; Swanson, M.; Tarle, G.; Thaler, J.; Thomas, D.; Thomas, R. C.; Tucker, D.; Vieira, J. D.; Vikram, V.; Walker, A. R.; Wechsler, R. H.; Weller, J.; Wester, W.; Whiteway, L.; Wilcox, H.; Yanny, B.; Zhang, Y.; and Zuntz, J., 2016. The Dark Energy Survey: more than dark energy - an overview. *MNRAS*, 460 (Aug. 2016), 1270–1299. doi:10.1093/mnras/stw641. (cited on page 118)

De Angelis, A. and Mallamaci, M., 2018. Gamma-ray astrophysics. *European Physical Journal Plus*, 133 (Aug. 2018), 324. doi:10.1140/epjp/i2018-12181-0. (cited on page 8)

De Shong, J. A.; Hildebrand, R. H.; and Meyer, P., 1964. Ratio of electrons to positrons in the primary cosmic radiation. *Phys. Rev. Lett.*, 12 (Jan 1964), 3–6. doi:10.1103/PhysRevLett.12.3. https://link.aps.org/doi/10.1103/PhysRevLett.12.3. (cited on pages 10 and 39)

de Vaucouleurs, G., 1959. Classification and Morphology of External Galaxies. *Handbuch der Physik*, 53 (1959), 275. (cited on page 101)

Dermer, C. D., 1985. Binary collision rates of relativistic thermal plasmas. I Theoretical framework. *ApJ*, 295 (Aug. 1985), 28–37. doi:10.1086/163345. (cited on page 37)

Dermer, C. D. and Skibo, J. G., 1997. Annihilation Fountain in the Galactic Center Region. *ApJ*, 487 (Sep. 1997), L57–L60. doi:10.1086/310870. (cited on pages 14, 51, 62, 63, 82, and 85)

Deutsch, M., 1951. Evidence for the formation of positronium in gases. *Phys. Rev.*, 82 (May 1951), 455–456. doi:10.1103/PhysRev.82.455. https://link.aps.org/doi/10.1103/PhysRev.82.455. (cited on pages 7 and 69)

Diehl, R., 2006. Measuring ^{26}Al and ^{60}Fe in the Galaxy. *New Astronomy Reviews*, 50 (Oct. 2006), 534–539. doi:10.1016/j.newar.2006.06.082. (cited on page 42)

Diehl, R.; Dupraz, C.; Bennett, K.; Bloemen, H.; Hermsen, W.; Knoedlseder, J.; Lichti, G.; Morris, D.; Ryan, J.; Schoenfelder, V.; Steinle, H.; Strong, A.; Swanenburg, B.; Varendorff, M.; and Winkler, C., 1995. COMPTEL observations of Galactic ˆ26ˆAl emission. *A&A*, 298 (Jun. 1995), 445. (cited on page 42)

Diehl, R.; Hartmann, D. H.; and Prantzos, N., 2011. Distributed Radioactivities. In *Lecture Notes in Physics, Berlin Springer Verlag*, vol. 812 of *Lecture Notes in Physics, Berlin Springer Verlag*, 345–438. (cited on page 70)

Diehl, R.; Siegert, T.; Greiner, J.; Krause, M.; Kretschmer, K.; Lang, M.; Pleintinger, M.; Strong, A. W.; Weinberger, C.; and Zhang, X., 2017. INTEGRAL/SPI γ-ray line spectroscopy. *ArXiv e-prints*, (Oct. 2017). (cited on pages 9, 13, and 18)

Diehl, R.; Siegert, T.; Hillebrandt, W.; Grebenev, S. A.; Greiner, J.; Krause, M.; Kromer, M.; Maeda, K.; Röpke, F.; and Taubenberger, S., 2014. Early 56ni decay gamma rays from sn2014j suggest an unusual explosion. *Science*, 345, 6201 (2014), 1162–1165. doi:10.1126/science.1254738. http://science.sciencemag.org/content/345/6201/1162. (cited on pages 9 and 44)

Dirac, P. A. M., 1930. On the annihilation of electrons and protons. *Mathematical Proceedings of the Cambridge Philosophical Society*, 26, 3 (1930), 361âĂŞ375. doi:10.1017/S0305004100016091. (cited on page 25)

Dirac, P. A. M., 1931. Quantised singularities in the electromagnetic field,. *Proceedings of the Royal Society of London A: Mathematical, Physical and Engineering Sciences*, 133, 821 (1931), 60–72. doi:10.1098/rspa.1931.0130. (cited on pages 1, 3, 5, and 69)

Donato, F., 2014. Indirect searches for dark matter. *Physics of the Dark Universe*, 4 (2014), 41 – 43. doi:https://doi.org/10.1016/j.dark.2014.06.001. http://www.sciencedirect.com/science/article/pii/S221268641400020X. DARK TAUP2013. (cited on page 52)

Dopita, M.; Hart, J.; McGregor, P.; Oates, P.; Bloxham, G.; and Jones, D., 2007. The Wide Field Spectrograph (WiFeS). *Ap&SS*, 310 (Aug. 2007), 255–268. doi:10.1007/s10509-007-9510-z. (cited on page 100)

Dopita, M. A. and Sutherland, R. S., 2003. *Astrophysics of the diffuse universe*. (cited on page 113)

Eckart, A.; Schödel, R.; Baganoff, F. K.; Morris, M.; Bertram, T.; Dovciak, M.; Dowries, D.; Duschl, W. J.; Karas, V.; König, S.; Krichbaum, T.; Krips, M.; Kunneriath, D.; Lu, R.-S.; Markoff, S.; Mauerhan, J.; Meyer, L.; Moultaka, J.; Muzic, K.; Najarro, F.; Schuster, K.; Sjouwerman, L.; Straubmeier, C.; Thum, C.; Vogel, S.; Wiesemeyer, H.; Witzel, G.; Zamaninasab, M.; and Zensus, A., 2008. Coordinated multi-wavelength observations of Sgr A*. In *Journal of Physics Conference Series*, vol. 131 of *Journal of Physics Conference Series*, 012002. doi:10.1088/1742-6596/131/1/012002. (cited on page 52)

Eldridge, J. J.; Stanway, E. R.; Xiao, L.; McClelland, L. A. S.; Taylor, G.; Ng, M.; Greis, S. M. L.; and Bray, J. C., 2017. Binary Population and Spectral Synthesis Version 2.1: Construction, Observational Verification, and New Results. , 34 (Nov. 2017), e058. doi:10.1017/pasa.2017.51. (cited on page 114)

Ellis, S. C.; Bauer, S.; Bacigalupo, C.; Bland-Hawthorn, J.; Bryant, J. J.; Case, S.; Content, R.; Fechner, T.; Giannone, D.; Haynes, R.; Hernandez, E.; Horton, A. J.; Klauser, U.; Lawrence, J. S.; Leon-Saval, S. G.; Lindley, E.; Löhmannsröben, H.-G.; Min, S.-S.; Pai, N.; Roth, M.; Shortridge, K.; Waller, L.; Xavier, P.; and Zhelem, R., 2018. PRAXIS: an OH suppression optimised near infrared spectrograph. In *Ground-based and Airborne Instrumentation for Astronomy VII*, vol. 10702 of *Society of Photo-Optical Instrumentation Engineers (SPIE) Conference Series*, 107020P. doi:10.1117/12.2311898. (cited on page 7)

Ellis, S. C. and Bland-Hawthorn, J., 2018. Astrophysical signatures of leptonium. *European Physical Journal D*, 72 (Jan. 2018), 18. doi:10.1140/epjd/e2017-80488-7. (cited on pages 7 and 31)

Filippenko, A. V., 1997. Optical Spectra of Supernovae. *ARA&A*, 35 (1997), 309–355. doi:10.1146/annurev.astro.35.1.309. (cited on pages 46 and 97)

Filippenko, A. V.; Richmond, M. W.; Branch, D.; Gaskell, M.; Herbst, W.; Ford, C. H.; Treffers, R. R.; Matheson, T.; Ho, L. C.; Dey, A.; Sargent, W. L. W.; Small, T. A.; and van Breugel, W. J. M., 1992. The subluminous, spectroscopically peculiar type IA supernova 1991bg in the elliptical galaxy NGC 4374. *AJ*, 104 (Oct. 1992), 1543–1556. doi:10.1086/116339. (cited on pages 94 and 96)

Finkbeiner, D. P. and Weiner, N., 2007. Exciting dark matter and the INTEGRAL/SPI 511keV signal. *Phys. Rev. D*, 76, 8 (Oct. 2007), 083519. doi:10.1103/PhysRevD.76.083519. (cited on pages 52 and 84)

Finzell, T.; Chomiuk, L.; Metzger, B. D.; Walter, F. M.; Linford, J. D.; Mukai, K.; Nelson, T.; Weston, J. H. S.; Zheng, Y.; Sokoloski, J. L.; Mioduszewski, A.; Rupen, M. P.; Dong, S.; Starrfield, S.; Cheung, C. C.; Woodward, C. E.; Taylor, G. B.; Bohlsen, T.; Buil, C.; Prieto, J.; Wagner, R. M.; Bensby, T.; Bond, I. A.; Sumi, T.; Bennett, D. P.; Abe, F.; Koshimoto, N.; Suzuki, D.; Tristram, P. J.; Christie, G. W.; Natusch, T.; McCormick, J.; Yee, J.; and Gould, A., 2018. A Detailed Observational Analysis of V1324 Sco, the Most Gamma-Ray-luminous Classical Nova to Date. *ApJ*, 852 (Jan. 2018), 108. doi:10.3847/1538-4357/aaa12a. (cited on page 47)

Fitzpatrick, E. L., 1999. Correcting for the Effects of Interstellar Extinction. *PASP*, 111 (Jan. 1999), 63–75. doi:10.1086/316293. (cited on page 102)

Fossey, S. J.; Cooke, B.; Pollack, G.; Wilde, M.; and Wright, T., 2014. Supernova 2014J in M82 = Psn J09554214+6940260. *Central Bureau Electronic Telegrams*, 3792 (Jan. 2014). (cited on page 44)

Fremling, C.; Nyholm, A.; Taddia, F.; Migotto, K.; Karamehmetoglu, E.; Sollerman, J.; Ergon, M.; De Cia, A.; Fraser, M.; Inserra, C.; Maguire, K.; Smartt, S. J.; Smith, K. W.; Sullivan, M.; Valenti, S.; Yaron, O.; Young, D.; Manulis, I.; Baltay, C.; Ellman, N.;

Hadjiyska, E.; McKinnon, R.; Rabinowitz, D.; Rostami, S.; Feindt, U.; Kowalski, M.; Nugent, P.; and Wyrzykowski, L., 2015. PESSTO spectroscopic classification of optical transients. *The Astronomer's Telegram*, 6909 (Jan. 2015). (cited on pages 100 and 101)

Frohmaier, C.; Sullivan, M.; Maguire, K.; and Nugent, P., 2018. The Volumetric Rate of Calcium-rich Transients in the Local Universe. *ApJ*, 858 (May 2018), 50. doi:10.3847/1538-4357/aabc0b. (cited on page 46)

Fujii, M. S. and Baba, J., 2012. Destruction of star clusters due to the radial migration in spiral galaxies. *Monthly Notices of the Royal Astronomical Society: Letters*, 427, 1 (11 2012), L16–L20. doi:10.1111/j.1745-3933.2012.01336.x. https://doi.org/10.1111/j.1745-3933.2012.01336.x. (cited on page 99)

Fuller, G. M.; Kusenko, A.; Radice, D.; and Takhistov, V., 2018. Positrons and 511 keV radiation as tracers of recent binary neutron star mergers. *arXiv e-prints*, (Oct. 2018). (cited on page 55)

Galbany, L.; Stanishev, V.; Mourão, A. M.; Rodrigues, M.; Flores, H.; García-Benito, R.; Mast, D.; Mendoza, M. A.; Sánchez, S. F.; Badenes, C.; Barrera-Ballesteros, J.; Bland-Hawthorn, J.; Falcón-Barroso, J.; García-Lorenzo, B.; Gomes, J. M.; González Delgado, R. M.; Kehrig, C.; Lyubenova, M.; López-Sánchez, A. R.; de Lorenzo-Cáceres, A.; Marino, R. A.; Meidt, S.; Mollá, M.; Papaderos, P.; Pérez-Torres, M. A.; Rosales-Ortega, F. F.; and van de Ven, G., 2014. Nearby supernova host galaxies from the CALIFA Survey. I. Sample, data analysis, and correlation to star-forming regions. *A&A*, 572 (Dec. 2014), A38. doi:10.1051/0004-6361/201424717. (cited on pages 98, 99, and 105)

Gallagher, J. S.; Garnavich, P. M.; Caldwell, N.; Kirshner, R. P.; Jha, S. W.; Li, W.; Ganeshalingam, M.; and Filippenko, A. V., 2008. Supernovae in Early-Type Galaxies: Directly Connecting Age and Metallicity with Type Ia Luminosity. *ApJ*, 685 (Oct. 2008), 752-766. doi:10.1086/590659. (cited on pages 98, 99, 105, 107, 108, and 113)

Gambhir, S. S., 2002. Molecular imaging of cancer with positron emission tomography. *Nature Reviews Cancer*, 2 (09 2002), 683 EP –. https://doi.org/10.1038/nrc882. (cited on page 67)

Gardner, B. M.; Forrest, D. J.; Dunphy, P. P.; and Chupp, E. L., 1982. Emission in the 0.3 to 1.0 mev range from the galactic center region. *AIP Conference Proceedings*, 83, 1 (1982), 144–147. doi:10.1063/1.33503. https://aip.scitation.org/doi/abs/10.1063/1.33503. (cited on page 12)

Garnavich, P. M.; Bonanos, A. Z.; Krisciunas, K.; Jha, S.; Kirshner, R. P.; Schlegel, E. M.; Challis, P.; Macri, L. M.; Hatano, K.; Branch, D.; Bothun, G. D.; and Freedman, W. L., 2004. The Luminosity of SN 1999by in NGC 2841 and the Nature of "Peculiar" Type Ia Supernovae. *ApJ*, 613 (Oct. 2004), 1120–1132. doi:10.1086/422986. (cited on page 97)

Gilfanov, M.; Churazov, E.; Sunyaev, R.; Khavenson, N.; Novikov, B.; Dyachkov, A.; Tserenin, I.; Sukhanov, K.; Bouchet, L.; Denis, M.; Schmitz-Frraysse, M. C.; Mandrou, P.; Paul, J.; Cordier, B.; Goldwurm, A.; and Lebrun, F., 1994. Observation of transient high-energy emission features in the spectra of black hole candidates and the Crab Nebula by Granat/SIGMA. *ApJS*, 92 (Jun. 1994), 411–418. doi:10.1086/191987. (cited on page 13)

Ginzburg, V. L., 1956. The nature of cosmic radio emission and the origin of cosmic rays. *Il Nuovo Cimento (1955-1965)*, 3, 1 (Jan 1956), 38–48. doi:10.1007/BF02745509. https://doi.org/10.1007/BF02745509. (cited on page 10)

Ginzburg, V. L., 1979. *Theoretical physics and astrophysics*. (cited on pages 37, 38, and 89)

Goldwurm, A.; Ballet, J.; Cordier, B.; Paul, J.; Bouchet, L.; Roques, J. P.; Barret, D.; Mandrou, P.; Sunyaev, R.; Churazov, E.; Gilfanov, M.; Dyachkov, A.; Khavenson, N.; Kovtunenko, V.; Kremnev, R.; and Sukhanov, K., 1992. Sigma/GRANAT soft gamma-ray observations of the X-ray nova in Musca - Discovery of positron annihilation emission line. *ApJ*, 389 (Apr. 1992), L79–L82. doi:10.1086/186353. (cited on page 13)

González-Gaitán, S.; Perrett, K.; Sullivan, M.; Conley, A.; A. Howell, D.; G. Carlberg, R.; Astier, P.; Balam, D.; Balland, C.; Basa, S.; Dominique, F.; Guy, J.; Hardin, D.; Hook, I.; Pain, R.; Pritchet, C.; Regnault, N.; Rich, J.; and C. Lidman, a., 2011. Subluminous type ia supernovae at high redshift from the supernova legacy survey. *The Astrophysical Journal*, 727 (01 2011), 107. doi:10.1088/0004-637X/727/2/107. (cited on pages 118 and 120)

Goobar, A.; Johansson, J.; Amanullah, R.; Cao, Y.; Perley, D. A.; Kasliwal, M. M.; Ferretti, R.; Nugent, P. E.; Harris, C.; Gal-Yam, A.; Ofek, E. O.; Tendulkar, S. P.; Dennefeld, M.; Valenti, S.; Arcavi, I.; Banerjee, D. P. K.; Venkataraman, V.; Joshi, V.; Ashok, N. M.; Cenko, S. B.; Diaz, R. F.; Fremling, C.; Horesh, A.; Howell, D. A.; Kulkarni, S. R.; Papadogiannakis, S.; Petrushevska, T.; Sand, D.; Sollerman, J.; Stanishev, V.; Bloom, J. S.; Surace, J.; Dupuy, T. J.; and Liu, M. C., 2014. The Rise of SN 2014J in the Nearby Galaxy M82. *ApJ*, 784 (Mar. 2014), L12. doi:10.1088/2041-8205/784/1/L12. (cited on page 44)

Goodenough, L. and Hooper, D., 2009. Possible Evidence For Dark Matter Annihilation In The Inner Milky Way From The Fermi Gamma Ray Space Telescope. *arXiv e-prints*, (Oct. 2009). (cited on page 50)

Gould, R. J., 1989. Direct positron annihilation and positronium formation in thermal plasmas. *ApJ*, 344 (Sep. 1989), 232–238. doi:10.1086/167792. (cited on pages 25 and 31)

Graur, O., 2019. Late-time Observations of the Type Ia Supernova SN 2014J with the Hubble Space Telescope Wide Field Camera 3. *ApJ*, 870 (Jan. 2019), 14. doi:10.3847/1538-4357/aaf1c3. (cited on page 44)

Grebenev, S. A.; Lutovinov, A. A.; Tsygankov, S. S.; and Winkler, C., 2012. Hard-X-ray emission lines from the decay of ^{44}Ti in the remnant of supernova 1987A. *Nature*, 490 (Oct. 2012), 373–375. doi:10.1038/nature11473. (cited on page 45)

Grefenstette, B.; Boggs, S. E.; Fryer, C.; Harrison, F.; Madsen, K.; Miyasaka, H.; Reynolds, S. P.; and Zoglauer, A., 2016. The 3D Distribution of 44-Ti in Cassiopeia A. In *AAS/High Energy Astrophysics Division #15*, vol. 15 of *AAS/High Energy Astrophysics Division*, 306.01. (cited on pages 9 and 45)

Grimm, H.-J.; Gilfanov, M.; and Sunyaev, R., 2002. The Milky Way in X-rays for an outside observer. Log(N)-Log(S) and luminosity function of X-ray binaries from RXTE/ASM data. *A&A*, 391 (Sep. 2002), 923–944. doi:10.1051/0004-6361:20020826. (cited on pages 50 and 51)

Guessoum, N.; Jean, P.; and Gillard, W., 2005. The lives and deaths of positrons in the interstellar medium. *A&A*, 436 (Jun. 2005), 171–185. doi:10.1051/0004-6361:20042454. (cited on pages 22, 28, 29, 30, 32, 34, 35, 38, 70, 71, 72, 76, 77, 84, and 91)

Guessoum, N.; Jean, P.; and Gillard, W., 2006a. Relevance of slow positron beam research to astrophysical studies of positron interactions and annihilation in the interstellar medium. *Applied Surface Science*, 252 (Feb. 2006), 3352–3361. doi:10.1016/j.apsusc.2005.08.056. (cited on page 67)

Guessoum, N.; Jean, P.; and Gillard, W., 2010. Positron annihilation on polycyclic aromatic hydrocarbon molecules in the interstellar medium. *MNRAS*, 402 (Feb. 2010), 1171–1178. doi:10.1111/j.1365-2966.2009.15954.x. (cited on pages 32 and 71)

Guessoum, N.; Jean, P.; and Prantzos, N., 2006b. Microquasars as sources of positron annihilation radiation. *A&A*, 457 (Oct. 2006), 753–762. doi:10.1051/0004-6361:20065240. (cited on pages 51, 60, and 64)

Gunion, J. F.; Hooper, D.; and McElrath, B., 2006. Light neutralino dark matter in the next-to-minimal supersymmetric standard model. *Phys. Rev. D*, 73 (Jan 2006), 015011. doi:10.1103/PhysRevD.73.015011. https://link.aps.org/doi/10.1103/PhysRevD.73.015011. (cited on page 52)

Hakobyan, A. A.; Barkhudaryan, L. V.; Karapetyan, A. G.; Mamon, G. A.; Kunth, D.; Adibekyan, V.; Aramyan, L. S.; Petrosian, A. R.; and Turatto, M., 2017. Supernovae and their host galaxies - V. The vertical distribution of supernovae in disc galaxies. *MNRAS*, 471, 2 (Oct 2017), 1390–1400. doi:10.1093/mnras/stx1608. (cited on page 98)

Harding, A. K., 1981. Pulsar gamma-rays - Spectra, luminosities, and efficiencies. *ApJ*, 245 (Apr. 1981), 267–273. doi:10.1086/158807. (cited on page 50)

Harris, M. J.; Share, G. H.; and Leising, M. D., 1994. SMM observations of gamma-ray transients. 3: A search for a broadened, redshifted positron annihilation line from the direction of the Galactic center. *ApJ*, 433 (Sep. 1994), 87–95. doi:10.1086/174627. (cited on page 13)

Haymes, R.; Glenn, S.; Fishman, G.; and Harnden, J., F.R., 1969. *J. Geophys. Research, Space Physics*, 74 (1969), 5792. Cited By 1. (cited on pages 10 and 11)

Haymes, R. C.; Walraven, G. D.; Meegan, C. A.; Hall, R. D.; Djuth, F. T.; and Shelton, D. H., 1975. Detection of nuclear gamma rays from the galactic center region. *ApJ*, 201 (Nov. 1975), 593–602. doi:10.1086/153925. (cited on page 12)

Hernanz, M.; Isern, J.; Hirschmann, A.; Bravo, E.; and José, J., 2005. Models and observation of high energy emission from stellar explosions: novae and type Ia supernovae. In *39TH ESLAB Symposium on Trends in Space Science and Cosmic Vision 2020*, vol. 588 of *ESA Special Publication*, 351. (cited on page 47)

Higdon, J. C.; Lingenfelter, R. E.; and Rothschild, R. E., 2009. The Galactic Positron Annihilation Radiation and the Propagation of Positrons in the Interstellar Medium. *ApJ*, 698 (Jun. 2009), 350–379. doi:10.1088/0004-637X/698/1/350. (cited on pages 51, 61, 62, 71, and 84)

Hillebrandt, W.; Kromer, M.; Röpke, F. K.; and Ruiter, A. J., 2013. Towards an understanding of Type Ia supernovae from a synthesis of theory and observations. *Frontiers of Physics*, 8 (Apr. 2013), 116–143. doi:10.1007/s11467-013-0303-2. (cited on pages 43 and 96)

Hooper, D.; Cholis, I.; Linden, T.; and Fang, K., 2017. HAWC observations strongly favor pulsar interpretations of the cosmic-ray positron excess. *Phys. Rev. D*, 96 (Nov. 2017), 103013. doi:10.1103/PhysRevD.96.103013. (cited on pages 40 and 50)

Hooper, D. and Wang, L.-T., 2004. Possible evidence for axino dark matter in the galactic bulge. *Phys. Rev. D*, 70 (Sep 2004), 063506. doi:10.1103/PhysRevD.70.063506. https://link.aps.org/doi/10.1103/PhysRevD.70.063506. (cited on pages 52 and 53)

Huba, J. D., 2013. *NRL PLASMA FORMULARY Supported by The Office of Naval Research*. Naval Research Laboratory, Washington, DC. ISBN 9781234126070. http://wwwppd.nrl.navy.mil/nrlformulary/. (cited on pages 37 and 89)

Humberston, J. W., 1979. Theoretical Aspects of Positron Collisions in Gases. *Advances in Atomic and Molecular Physics*, 15 (Jan. 1979), 101–133. doi:10.1016/S0065-2199(08)60296-1. http://www.sciencedirect.com/science/article/pii/S0065219908602961. (cited on pages 29 and 72)

Ibarra, A.; Lamperstorfer, A. S.; and Silk, J., 2014. Dark matter annihilations and decays after the AMS-02 positron measurements. *Phys. Rev. D*, 89, 6 (Mar. 2014), 063539. doi:10.1103/PhysRevD.89.063539. (cited on pages 40 and 41)

Iyudin, A. F.; Diehl, R.; Bloemen, H.; Hermsen, W.; Lichti, G. G.; Morris, D.; Ryan, J.; Schoenfelder, V.; Steinle, H.; Varendorff, M.; de Vries, C.; and Winkler, C., 1994. COMPTEL observations of Ti-44 gamma-ray line emission from CAS A. *A&A*, 284 (Apr. 1994), L1–L4. (cited on pages 9 and 45)

Jean, P.; Gillard, W.; Marcowith, A.; and Ferrière, K., 2009. Positron transport in the interstellar medium. *A&A*, 508 (Dec. 2009), 1099–1116. doi:10.1051/0004-6361/200809830. (cited on pages 29, 36, 38, 62, 63, 71, 72, 76, 84, and 85)

Jean, P.; Knödlseder, J.; Gillard, W.; Guessoum, N.; Ferrière, K.; Marcowith, A.; Lonjou, V.; and Roques, J. P., 2006. Spectral analysis of the Galactic e^+e^- annihilation emission. *A&A*, 445 (Jan. 2006), 579–589. doi:10.1051/0004-6361:20053765. (cited on pages 22, 23, 34, and 59)

Johnson, W. N., III; Harnden, F. R., Jr.; and Haymes, R. C., 1972. The Spectrum of Low-Energy Gamma Radiation from the Galactic-Center Region. *ApJ*, 172 (Feb. 1972), L1. doi:10.1086/180878. (cited on pages 9, 10, 11, 12, 59, 70, and 83)

Joliot, F. and Curie, I., 1934. Artificial production of a new kind of radio-element. *Nature*, 133 (02 1934), 201 EP –. https://doi.org/10.1038/133201a0. (cited on page 10)

Jones, G. O.; Charlton, M.; Slevin, J.; Laricchia, G.; Kover, A.; Poulsen, M. R.; and Chormaic, S. N., 1993. Positron impact ionization of atomic hydrogen. *Journal of Physics B: Atomic, Molecular and Optical Physics*, 26, 15 (1993), L483. doi:10.1088/0953-4075/26/15/009. http://stacks.iop.org/0953-4075/26/i=15/a=009. (cited on pages 29 and 72)

José, J.; Hernanz, M.; García-Berro, E.; and Gil-Pons, P., 2003. The Impact of the Chemical Stratification of White Dwarfs on the Classification of Classical Novae. *ApJ*, 597 (Nov. 2003), L41–L44. doi:10.1086/379782. (cited on page 47)

José, J.; Hernanz, M.; and Iliadis, C., 2006. Nucleosynthesis in classical novae. *Nuclear Physics A*, 777 (Oct. 2006), 550–578. doi:10.1016/j.nuclphysa.2005.02.121. (cited on page 47)

Jung, G. V.; Kurfess, D. J.; Johnson, W. N.; Kinzer, R. L.; Grove, J. E.; Strickman, M. S.; Purcell, W. R.; Grabelsky, D. A.; and Ulmer, M. P., 1995. OSSE observations of 1E 1740.7-2942 in 1992 September. *A&A*, 295 (Mar. 1995), L23–L26. (cited on page 13)

Kadyrov, A. S. and Bray, I., 2016. Recent progress in the description of positron scattering from atoms using the convergent close-coupling theory. 49, 22 (2016), 222002. (cited on pages 34, 67, 73, and 74)

Kasen, D., 2006. Secondary Maximum in the Near-Infrared Light Curves of Type Ia Supernovae. *ApJ*, 649 (Oct. 2006), 939–953. doi:10.1086/506588. (cited on page 97)

Kato, M.; Hachisu, I.; Kiyota, S.; and Saio, H., 2008. Helium Nova on a Very Massive White Dwarf: A Revised Light-Curve Model of V445 Puppis (2000). *ApJ*, 684 (Sep. 2008), 1366–1373. doi:10.1086/590329. (cited on page 47)

Kauffmann, G.; Heckman, T. M.; White, S. D. M.; Charlot, S.; Tremonti, C.; Brinchmann, J.; Bruzual, G.; Peng, E. W.; Seibert, M.; Bernardi, M.; Blanton, M.; Brinkmann, J.; Castander, F.; Csábai, I.; Fukugita, M.; Ivezic, Z.; Munn, J. A.; Nichol, R. C.; Padmanabhan, N.; Thakar, A. R.; Weinberg, D. H.; and York, D., 2003. Stellar masses and star formation histories for 10^5 galaxies from the Sloan Digital Sky Survey. *MNRAS*, 341 (May 2003), 33–53. doi:10.1046/j.1365-8711.2003.06291.x. (cited on page 113)

Kauppila, W. E.; Stein, T. S.; Smart, J. H.; Dababneh, M. S.; Ho, Y. K.; Downing, J. P.; and Pol, V., 1981. Measurements of total scattering cross sections for intermediate-energy positrons and electrons colliding with helium, neon, and argon. *Physical Review A*, 24, 2 (Aug. 1981), 725–742. doi:10.1103/PhysRevA.24.725. https://link.aps.org/doi/10.1103/PhysRevA.24.725. (cited on pages 29 and 72)

Kernoghan, A. A.; Robinson, D. J. R.; McAlinden, M. T.; and Walters, H. R. J., 1996. Positron scattering by atomic hydrogen. *Journal of Physics B: Atomic, Molecular and Optical Physics*, 29, 10 (1996), 2089. doi:10.1088/0953-4075/29/10/017. http://stacks.iop.org/0953-4075/29/i=10/a=017. (cited on pages 29 and 72)

Kerzendorf, W. E.; Taubenberger, S.; Seitenzahl, I. R.; and Ruiter, A. J., 2014. Very Late Photometry of SN 2011fe. *ApJ*, 796 (Dec. 2014), L26. doi:10.1088/2041-8205/796/2/L26. (cited on page 43)

Kessler, R.; Bernstein, J. P.; Cinabro, D.; Dilday, B.; Frieman, J. A.; Jha, S.; Kuhlmann, S.; Miknaitis, G.; Sako, M.; Taylor, M.; and Vanderplas, J., 2009. SNANA: A Public Software Package for Supernova Analysis. *PASP*, 121 (Sep. 2009), 1028. doi:10.1086/605984. (cited on page 118)

Kessler, R.; Brout, D.; D'Andrea, C. B.; Davis, T. M.; Hinton, S. R.; Kim, A. G.; Lasker, J.; Lidman, C.; Macaulay, E.; Möller, A.; Sako, M.; Scolnic, D.; Smith, M.; Sullivan, M.; Zhang, B.; Andersen, P.; Asorey, J.; Avelino, A.; Calcino, J.; Carollo, D.; Challis, P.; Childress, M.; Clocchiatti, A.; Crawford, S.; Filippenko, A. V.; Foley, R. J.; Glazebrook, K.; Hoormann, J. K.; Kasai, E.; Kirshner, R. P.; Lewis, G. F.; Mandel, K. S.; March, M.; Morganson, E.; Muthukrishna, D.; Nugent, P.; Pan, Y.-C.; Sommer, N. E.; Swann, E.; Thomas, R. C.; Tucker, B. E.; Uddin, S. A.; Abbott, T. M. C.; Allam, S.; Annis, J.; Avila, S.; Banerji, M.; Bechtol, K.; Bertin, E.; Brooks, D.; Buckley-Geer, E.; Burke, D. L.; Carnero Rosell, A.; Carrasco Kind, M.; Carretero, J.; Castander, F. J.; Crocce, M.; da Costa, L. N.; Davis, C.; De Vicente, J.; Desai, S.; Diehl, H. T.; Doel, P.; Eifler, T. F.; Flaugher, B.; Fosalba, P.; Frieman, J.; Garcia-Bellido, J.; Gaztanaga, E.; Gerdes, D. W.; Gruen, D.; Gruendl, R. A.; Gutierrez, G.; Hartley, W. G.; Hollowood, D. L.; Honscheid, K.; James, D. J.; Johnson, M. W. G.; Johnson, M. D.; Krause, E.; Kuehn, K.; Kuropatkin, N.; Lahav, O.; Li, T. S.; Lima, M.; Marshall, J. L.; Martini, P.; Menanteau, F.; Miller, C. J.; Miquel, R.; Nord, B.; Plazas, A. A.; Roodman, A.; Sanchez, E.; Scarpine, V.; Schindler, R.; Schubnell, M.; Serrano, S.; Sevilla-Noarbe, I.; Soares-Santos, M.; Sobreira, F.; Suchyta, E.; Tarle, G.; Thomas, D.; Walker, A. R.; and Zhang, Y., 2018. First Cosmology Results using Type Ia Supernova from the Dark Energy Survey: Simulations to Correct Supernova Distance Biases. *arXiv e-prints*, (Nov. 2018). (cited on page 120)

Kierans, C. A.; Boggs, S. E.; Chiu, J.-L.; Lowell, A.; Sleator, C.; Tomsick, J. A.; Zoglauer, A.; Amman, M.; Chang, H.-K.; Tseng, C.-H.; Yang, C.-Y.; Lin, C.-H.; Jean, P.; and von Ballmoos, P., 2017. The 2016 Super Pressure Balloon flight of the Compton Spectrometer and Imager. *arXiv e-prints*, (Jan. 2017), arXiv:1701.05558. (cited on page 12)

Knödlseder, J.; Dixon, D.; Bennett, K.; Bloemen, H.; Diehl, R.; Hermsen, W.; Oberlack, U.; Ryan, J.; Schönfelder, V.; and von Ballmoos, P., 1999. Image reconstruction of COMPTEL 1.8 MeV (26) AL line data. *A&A*, 345 (May 1999), 813–825. (cited on page 42)

Knödlseder, J.; Jean, P.; Lonjou, V.; Weidenspointner, G.; Guessoum, N.; Gillard, W.; Skinner, G.; von Ballmoos, P.; Vedrenne, G.; Roques, J.-P.; Schanne, S.; Teegarden, B.; Schönfelder, V.; and Winkler, C., 2005. The all-sky distribution of 511 keV electron-positron annihilation emission. *A&A*, 441 (Oct. 2005), 513–532. doi:10.1051/0004-6361:20042063. (cited on pages 18, 19, 20, 59, 61, 64, 69, 70, and 83)

Knödlseder, J.; Lonjou, V.; Jean, P.; Allain, M.; Mandrou, P.; Roques, J. P.; Skinner, G. K.; Vedrenne, G.; von Ballmoos, P.; Weidenspointner, G.; Caraveo, P.; Cordier, B.; Schönfelder, V.; and Teegarden, B. J., 2003. Early SPI/INTEGRAL constraints on the morphology of the 511 keV line emission in the 4th galactic quadrant. *A&A*, 411 (Nov. 2003), L457–L460. doi:10.1051/0004-6361:20031437. (cited on page 20)

Kozlovsky, B.; Murphy, R. J.; and Share, G. H., 2004. Positron-Emitter Production in Solar Flares from ^{3}He Reactions. *ApJ*, 604 (Apr. 2004), 892–899. doi:10.1086/381969. (cited on page 49)

Kretschmer, K.; Diehl, R.; Krause, M.; Burkert, A.; Fierlinger, K.; Gerhard, O.; Greiner, J.; and Wang, W., 2013. Kinematics of massive star ejecta in the Milky Way as traced by ^{26}Al. *A&A*, 559 (Nov. 2013), A99. doi:10.1051/0004-6361/201322563. (cited on page 42)

Kruegel, E., 2003. *The physics of interstellar dust*. (cited on page 32)

Kurfess, J. D.; Johnson, W. N.; Kinzer, R. L.; Kroeger, R. A.; Strickman, M. S.; Grove, J. E.; Leising, M. D.; Clayton, D. D.; Grabelsky, D. A.; Purcell, W. R.; Ulmer, M. P.; Cameron, R. A.; and Jung, G. V., 1992. Oriented Scintillation Spectrometer Experiment observations of Co-57 in SN 1987A. *ApJ*, 399 (Nov. 1992), L137–L140. doi:10.1086/186626. (cited on page 9)

Lacki, B. C., 2014. The Fermi bubbles as starburst wind termination shocks. *MNRAS*, 444 (Oct. 2014), L39–L43. doi:10.1093/mnrasl/slu107. (cited on pages 85 and 86)

Laricchia, G.; Armitage, S.; Kövér, A.; and Murtagh, D. J., 2008. Ionizing Collisions by Positrons and Positronium Impact on the Inert Atoms. *Advances In Atomic, Molecular, and Optical Physics*, 56 (Jan. 2008), 1–47. doi:10.1016/S1049-250X(08)00010-4. http://www.sciencedirect.com/science/article/pii/S1049250X08000104. (cited on pages 29 and 72)

LEIBUNDGUT, B., 2001. Cosmological Implications from Observations of Type Ia Supernovae. *ARA&A*, 39 (2001), 67–98. doi:10.1146/annurev.astro.39.1.67. (cited on page 96)

LEVENTHAL, M., 1973. Positronium-Formation Redshift of the 511-ke V Annihilation Line. *ApJ*, 183 (Aug. 1973), L147. doi:10.1086/181274. (cited on page 10)

LEVENTHAL, M.; MACCALLUM, C. J.; BARTHELMY, S. D.; GEHRELS, N.; TEEGARDEN, B. J.; AND TUELLER, J., 1989. Reappearance of the annihilation line source at the Galactic Centre. *Nature*, 339 (May 1989), 36–38. doi:10.1038/339036a0. (cited on page 13)

LEVENTHAL, M.; MACCALLUM, C. J.; HUTERS, A. F.; AND STANG, P. D., 1980. Gamma-ray lines and continuum radiation from the galactic center direction. *ApJ*, 240 (Aug. 1980), 338–343. doi:10.1086/158237. (cited on page 12)

LEVENTHAL, M.; MACCALLUM, C. J.; AND STANG, P. D., 1978. Detection of 511 keV positron annihilation radiation from the galactic center direction. *ApJ*, 225 (Oct. 1978), L11–L14. doi:10.1086/182782. (cited on pages 12 and 70)

LI, W.; LEAMAN, J.; CHORNOCK, R.; FILIPPENKO, A. V.; POZNANSKI, D.; GANESHALINGAM, M.; WANG, X.; MODJAZ, M.; JHA, S.; FOLEY, R. J.; AND SMITH, N., 2011. Nearby supernova rates from the Lick Observatory Supernova Search - II. The observed luminosity functions and fractions of supernovae in a complete sample. *MNRAS*, 412 (Apr. 2011), 1441–1472. doi:10.1111/j.1365-2966.2011.18160.x. (cited on pages 94 and 98)

LIMONGI, M. AND CHIEFFI, A., 2006. The Nucleosynthesis of ^{26}Al and ^{60}Fe in Solar Metallicity Stars Extending in Mass from 11 to 120 M_{solar}: The Hydrostatic and Explosive Contributions. *ApJ*, 647 (Aug. 2006), 483–500. doi:10.1086/505164. (cited on page 42)

LINGENFELTER, R. E. AND RAMATY, R., 1989. The nature of the annihilation radiation and gamma-ray continuum from the Galactic center region. *ApJ*, 343 (Aug. 1989), 686–695. doi:10.1086/167740. (cited on page 13)

LINGENFELTER, R. E.; RAMATY, R.; AND LEITER, D., 1981. Origin of 0.511 MeV emission from the Galactic center. *International Cosmic Ray Conference*, 1 (1981), 112–115. (cited on pages 12 and 51)

LODDERS, K., 2003. Solar System Abundances and Condensation Temperatures of the Elements. *ApJ*, 591 (Jul. 2003), 1220–1247. doi:10.1086/375492. (cited on pages 71 and 73)

LUND, N.; BUDTZ-JØRGENSEN, C.; WESTERGAARD, N. J.; BRANDT, S.; RASMUSSEN, I. L.; HORNSTRUP, A.; OXBORROW, C. A.; CHENEVEZ, J.; JENSEN, P. A.; LAURSEN, S.; ANDERSEN, K. H.; MOGENSEN, P. B.; RASMUSSEN, I.; OMØ, K.; PEDERSEN, S. M.; POLNY, J.; ANDERSSON, H.; ANDERSSON, T.; KÄMÄRÄINEN, V.; VILHU, O.; HUOVELIN, J.; MAISALA, S.; MORAWSKI, M.; JUCHNIKOWSKI, G.; COSTA, E.; FEROCI, M.; RUBINI, A.; RAPISARDA, M.; MORELLI, E.; CARASSITI, V.; FRONTERA, F.; PELLICIARI, C.; LOFFREDO, G.; MARTÍNEZ NÚÑEZ, S.; REGLERO, V.; VELASCO, T.; LARSSON, S.; SVENSSON, R.; ZDZIARSKI, A. A.; CASTRO-TIRADO, A.; ATTINA, P.; GORIA, M.; GIULIANELLI, G.; CORDERO, F.; REZAZAD, M.; SCHMIDT, M.; CARLI, R.; GOMEZ, C.; JENSEN, P. L.; SARRI, G.; TIEMON, A.; ORR, A.; MUCH, R.; KRETSCHMAR, P.; AND SCHNOPPER, H. W., 2003. JEM-X: The X-ray monitor aboard INTEGRAL. *A&A*, 411 (Nov. 2003), L231–L238. doi:10.1051/0004-6361:20031358. (cited on page 15)

LUNNAN, R.; KASLIWAL, M. M.; CAO, Y.; HANGARD, L.; YARON, O.; PARRENT, J. T.; MCCULLY, C.; GAL-YAM, A.; MULCHAEY, J. S.; BEN-AMI, S.; FILIPPENKO, A. V.; FREMLING, C.; Fruchter, A. S.; Howell, D. A.; Koda, J.; Kupfer, T.; Kulkarni, S. R.; Laher, R.; Masci, F.; Nugent, P. E.; Ofek, E. O.; Yagi, M.; and Yan, L., 2017. Two New Calcium-rich Gap Transients in Group and Cluster Environments. *ApJ*, 836 (Feb. 2017), 60. doi:10.3847/1538-4357/836/1/60. (cited on page 46)

Machacek, J. R.; Anderson, E. K.; Makochekanwa, C.; Buckman, S. J.; and Sullivan, J. P., 2013. Positron scattering from molecular hydrogen. *Physical Review A*, 88, 4 (Oct. 2013), 042715. doi:10.1103/PhysRevA.88.042715. https://link.aps.org/doi/10.1103/PhysRevA.88.042715. (cited on pages 29 and 72)

Macias, O.; Gordon, C.; Crocker, R. M.; Coleman, B.; Paterson, D.; Horiuchi, S.; and Pohl, M., 2018. Galactic bulge preferred over dark matter for the Galactic centre gamma-ray excess. *Nature Astronomy*, 2 (Mar. 2018), 387–392. doi:10.1038/s41550-018-0414-3. (cited on page 50)

Maguire, K., 2017. *Type Ia Supernovae*, 293. doi:10.1007/978-3-319-21846-5_36. (cited on pages 43 and 96)

Mahoney, W. A.; Ling, J. C.; and Wheaton, W. A., 1994. HEAO 3 observations of the Galactic center 511 keV line. *ApJS*, 92 (Jun. 1994), 387–391. doi:10.1086/191983. (cited on page 13)

Mannucci, F.; Della Valle, M.; and Panagia, N., 2006. Two populations of progenitors for Type Ia supernovae? *MNRAS*, 370 (Aug. 2006), 773–783. doi:10.1111/j.1365-2966.2006.10501.x. (cited on pages 44 and 45)

Maoz, D. and Mannucci, F., 2008. A search for the progenitors of two TypeIa Supernovae in NGC 1316. *MNRAS*, 388 (Jul 2008), 421–428. doi:10.1111/j.1365-2966.2008.13403.x. (cited on page 108)

Maoz, D.; Mannucci, F.; and Brandt, T. D., 2012. The delay-time distribution of Type Ia supernovae from Sloan II. *MNRAS*, 426 (Nov. 2012), 3282–3294. doi:10.1111/j.1365-2966.2012.21871.x. (cited on pages 104, 105, 108, and 109)

Martin, P.; Strong, A. W.; Jean, P.; Alexis, A.; and Diehl, R., 2012. Galactic annihilation emission from nucleosynthesis positrons. *A&A*, 543 (Jul. 2012), A3. doi:10.1051/0004-6361/201118721. (cited on pages 36, 62, 71, 76, and 84)

Mas-Hesse, J. M.; Giménez, A.; Jamar, C.; McBreen, B.; Culhane, J. L.; Fabregat, J.; Swings, J. P.; Meurs, E.; Torra, J.; Hudec, R.; and OMC Technical Team, 1998. OMC: An optical monitoring camera for INTEGRAL. *Physica Scripta Volume T*, 77 (1998), 44. (cited on page 15)

Maurin, D.; Donato, F.; Taillet, R.; and Salati, P., 2001. Cosmic Rays below Z=30 in a Diffusion Model: New Constraints on Propagation Parameters. *ApJ*, 555 (Jul. 2001), 585–596. doi:10.1086/321496. (cited on page 84)

Maurin, D.; Melot, F.; and Taillet, R., 2014. A database of charged cosmic rays. *A&A*, 569 (Sep. 2014), A32. doi:10.1051/0004-6361/201321344. (cited on page 41)

Milne, P. A.; Kurfess, J. D.; Kinzer, R. L.; and Leising, M. D., 2001a. Comparative studies of line and continuum positron annihilation radiation. In *Gamma 2001: Gamma-Ray Astrophysics*, vol. 587 of *American Institute of Physics Conference Series*, 11–15. doi:10.1063/1.1419363. (cited on pages 13, 14, 62, and 85)

Milne, P. A.; Kurfess, J. D.; Kinzer, R. L.; Leising, M. D.; and Dixon, D. D., 2001b. OSSE/SMM/TGRS observations of positron annihilation radiation. In *Exploring the Gamma-Ray Universe*, vol. 459 of *ESA Special Publication*, 145–148. (cited on pages 14 and 82)

Milne, P. A.; The, L.-S.; and Leising, M. D., 1999. Positron Escape from Type IA Supernovae. *ApJS*, 124 (Oct. 1999), 503–526. doi:10.1086/313262. (cited on pages 43, 44, 48, and 64)

Mirabel, I. F., 2010. *Microquasars: Summary and Outlook*, 1. doi:10.1007/978-3-540-76937-8_1. (cited on page 51)

Mirabel, I. F.; Morris, M.; Wink, J.; Paul, J.; and Cordier, B., 1991. 1E 1740.7 - 2942 - A black hole in a molecular cloud? *A&A*, 251 (Nov. 1991), L43–L46. (cited on page 13)

Moe, M. and Di Stefano, R., 2017. Mind Your Ps and Qs: The Interrelation between Period (P) and Mass-ratio (Q) Distributions of Binary Stars. *ApJS*, 230 (Jun. 2017), 15. doi:10.3847/1538-4365/aa6fb6. (cited on page 109)

Mohorovičić, S., 1934. Möglichkeit neuer Elemente und ihre Bedeutung für die Astrophysik. *Astronomische Nachrichten*, 253 (Nov. 1934), 93. doi:10.1002/asna.19342530402. (cited on pages 7 and 69)

Morris, M. and Serabyn, E., 1996. The Galactic Center Environment. *ARA&A*, 34 (1996), 645–702. doi:10.1146/annurev.astro.34.1.645. (cited on pages 48, 81, and 86)

Moxom, J.; Ashley, P.; and Laricchia, G., 1996. Single ionization by positron impact. *Canadian Journal of Physics*, 74, 7-8 (Jul. 1996), 367–372. doi:10.1139/p96-053. http://www.nrcresearchpress.com/doi/abs/10.1139/p96-053. (cited on pages 29 and 72)

Murphy, R. J.; Dermer, C. D.; and Ramaty, R., 1987. High-energy processes in solar flares. *ApJS*, 63 (Mar. 1987), 721–748. doi:10.1086/191180. (cited on page 48)

Murphy, R. J.; Share, G. H.; Skibo, J. G.; and Kozlovsky, B., 2005. The physics of positron annihilation in the solar atmosphere. *The Astrophysical Journal Supplement Series*, 161, 2 (2005), 495. http://stacks.iop.org/0067-0049/161/i=2/a=495. (cited on pages 7, 8, 34, 49, and 69)

Murtagh, D. J.; SzÅĆuiÅĎska, M.; Moxom, J.; Reeth, P. V.; and Laricchia, G., 2005. Positron-impact ionization and positronium formation from helium. *Journal of Physics B: Atomic, Molecular and Optical Physics*, 38, 21 (2005), 3857. doi:10.1088/0953-4075/38/21/008. http://stacks.iop.org/0953-4075/38/i=21/a=008. (cited on pages 29 and 72)

Nadyozhin, D. K., 1994. The properties of NI to CO to Fe decay. *ApJS*, 92 (Jun. 1994), 527–531. doi:10.1086/192008. (cited on page 43)

Nagataki, S.; Hashimoto, M.-a.; Sato, K.; Yamada, S.; and Mochizuki, Y. S., 1998. The High Ratio of ^{44}Ti/^{56}Ni in Cassiopeia A and the Axisymmetric Collapse-driven Supernova Explosion. *ApJ*, 492 (Jan. 1998), L45–L48. doi:10.1086/311089. (cited on page 45)

Nomoto, K.; Tanaka, M.; Tominaga, N.; and Maeda, K., 2010. Hypernovae, gamma-ray bursts, and first stars. , 54 (Mar. 2010), 191–200. doi:10.1016/j.newar.2010.09.022. (cited on page 48)

Ore, A. and Powell, J. L., 1949. Three-photon annihilation of an electron-positron pair. *Phys. Rev.*, 75 (Jun 1949), 1696–1699. doi:10.1103/PhysRev.75.1696. https://link.aps.org/doi/10.1103/PhysRev.75.1696. (cited on pages 7, 30, and 70)

Pakmor, R.; Kromer, M.; Röpke, F. K.; Sim, S. A.; Ruiter, A. J.; and Hillebrandt, W., 2010. Sub-luminous type Ia supernovae from the mergers of equal-mass white dwarfs with mass ~0.9M$_{solar}$. *Nature*, 463 (Jan. 2010), 61–64. doi:10.1038/nature08642. (cited on pages 43, 97, and 98)

Pakmor, R.; Kromer, M.; Taubenberger, S.; and Springel, V., 2013. Helium-ignited Violent Mergers as a Unified Model for Normal and Rapidly Declining Type Ia Supernovae. *ApJ*, 770 (Jun. 2013), L8. doi:10.1088/2041-8205/770/1/L8. (cited on pages 98 and 109)

Panther, F. H.; Crocker, R. M.; Birnboim, Y.; Seitenzahl, I. R.; and Ruiter, A. J., 2017. Positron annihilation in the nuclear outflows of the milky way. *Monthly Notices of the Royal Astronomical Society: Letters*, (2017), slx183. doi:10.1093/mnrasl/slx183. (cited on pages 60, 63, 71, 76, and 117)

Panther, F. H.; Seitenzahl, I. R.; Crocker, R. M.; Machacek, J. R.; Murtagh, D. J.; Siegert, T.; and Diehl, R., 2018. Effect of positron-alkali metal atom interactions in the diffuse interstellar medium. *Phys. Rev. D*, 98 (Jul 2018), 023015. doi:10.1103/PhysRevD.98.023015. https://link.aps.org/doi/10.1103/PhysRevD.98.023015. (cited on page 117)

Pastorello, A.; Inserra, C.; Cellier-Holzem, F.; Fraser, M.; Smartt, S. J.; Wright, D.; Young, D. R.; Smith, K. W.; Valenti, S.; Benetti, S.; Taubenberger, S.; Sullivan, M.; Gal-Yam, A.; Yaron, O.; Monard, B.; Baltay, C.; Ellman, N.; Hadjiyska, E.; McKinnon, R.; Rabinowitz, D.; Feindt, U.; Kowalski, M.; and Nugent, P., 2012. PESSTO spectroscopic classification of optical transients. *The Astronomer's Telegram*, 4339 (Aug. 2012). (cited on pages 100 and 101)

Perets, H. B.; Gal-Yam, A.; Mazzali, P. A.; Arnett, D.; Kagan, D.; Filippenko, A. V.; Li, W.; Arcavi, I.; Cenko, S. B.; Fox, D. B.; Leonard, D. C.; Moon, D.-S.; Sand, D. J.; Soderberg, A. M.; Anderson, J. P.; James, P. A.; Foley, R. J.; Ganeshalingam, M.; Ofek, E. O.; Bildsten, L.; Nelemans, G.; Shen, K. J.; Weinberg, N. N.; Metzger, B. D.; Piro, A. L.; Quataert, E.; Kiewe, M.; and Poznanski, D., 2010. A faint type of supernova from a white dwarf with a helium-rich companion. *Nature*, 465 (May 2010), 322–325. doi:10.1038/nature09056. (cited on pages 46 and 98)

Perlmutter, S.; Aldering, G.; Goldhaber, G.; Knop, R. A.; Nugent, P.; Castro, P. G.; Deustua, S.; Fabbro, S.; Goobar, A.; Groom, D. E.; Hook, I. M.; Kim, A. G.; Kim, M. Y.; Lee, J. C.; Nunes, N. J.; Pain, R.; Pennypacker, C. R.; Quimby, R.; Lidman, C.; Ellis, R. S.; Irwin, M.; McMahon, R. G.; Ruiz-Lapuente, P.; Walton, N.; Schaefer, B.; Boyle, B. J.; Filippenko, A. V.; Matheson, T.; Fruchter, A. S.; Panagia, N.; Newberg, H. J. M.; Couch, W. J.; and Project, T. S. C., 1999. Measurements of Ω and Λ from 42 High-Redshift Supernovae. *ApJ*, 517 (Jun. 1999), 565–586. doi:10.1086/307221. (cited on page 96)

Peterson, L. E., 1963. The 0.5-Mev Gamma-Ray and the Low-Energy Gamma-Ray Spectrum to 6 Grams per Square Centimeter over Minneapolis. *J. Geophys. Res.*, 68 (Feb. 1963), 979–987. doi:10.1029/JZ068i004p00979. (cited on page 10)

Phillips, M. M., 1993. The absolute magnitudes of Type IA supernovae. *ApJ*, 413 (Aug. 1993), L105–L108. doi:10.1086/186970. (cited on page 96)

Picciotto, C. and Pospelov, M., 2005. Unstable relics as a source of galactic positrons. *Physics Letters B*, 605, 1 (2005), 15 – 25. doi:https://doi.org/10.1016/j.physletb.2004.11.025.

http://www.sciencedirect.com/science/article/pii/S0370269304015813. (cited on pages 52 and 53)

Prantzos, N., 2006. On the intensity and spatial morphology of the 511 keV emission in the Milky Way. *A&A*, 449 (Apr. 2006), 869–878. doi:10.1051/0004-6361:20052811. (cited on pages 18, 61, 71, and 84)

Prantzos, N.; Boehm, C.; Bykov, A. M.; Diehl, R.; Ferrière, K.; Guessoum, N.; Jean, P.; Knoedlseder, J.; Marcowith, A.; Moskalenko, I. V.; Strong, A.; and Weidenspointner, G., 2011. The 511 keV emission from positron annihilation in the Galaxy. *Reviews of Modern Physics*, 83 (Jul. 2011), 1001–1056. doi:10.1103/RevModPhys.83.1001. (cited on pages 32, 36, 45, 49, 52, 54, 56, 60, 71, 83, and 87)

Prantzos, N. and Diehl, R., 1996. Radioactive 26Al in the galaxy: observations versus theory. *Phys. Rep.*, 267 (Mar. 1996), 1–69. doi:10.1016/0370-1573(95)00055-0. (cited on page 42)

Purcell, W. R.; Cheng, L.-X.; Dixon, D. D.; Kinzer, R. L.; Kurfess, J. D.; Leventhal, M.; Saunders, M. A.; Skibo, J. G.; Smith, D. M.; and Tueller, J., 1997. OSSE Mapping of Galactic 511 keV Positron Annihilation Line Emission. *ApJ*, 491 (Dec. 1997), 725–748. doi:10.1086/304994. (cited on pages 14, 51, 62, 70, 82, and 85)

Purcell, W. R.; Grabelsky, D. A.; Ulmer, M. P.; Johnson, W. N.; Kinzer, R. L.; Kurfess, J. D.; Strickman, M. S.; and Jung, G. V., 1994. The distribution of galactic 511 keV positron annihilation radiation. In *American Institute of Physics Conference Series*, vol. 304 of *American Institute of Physics Conference Series*, 403–412. doi:10.1063/1.45596. (cited on page 14)

Ramaty, R.; Kozlovsky, B.; and Lingenfelter, R. E., 1975. Solar gamma rays. *Space Sci. Rev.*, 18 (Dec. 1975), 341–388. doi:10.1007/BF00212911. (cited on page 49)

Ramaty, R.; Kozlovsky, B.; and Lingenfelter, R. E., 1979. Nuclear gamma-rays from energetic particle interactions. *ApJS*, 40 (Jul. 1979), 487–526. doi:10.1086/190596. (cited on page 83)

Rando, R., 2017. The all-sky medium energy gamma-ray observatory. *Journal of Instrumentation*, 12, 11 (2017), C11024. http://stacks.iop.org/1748-0221/12/i=11/a=C11024. (cited on page 117)

Ratnavelu, K. and Ong, W.E., 2011. Electron and positron scattering from atomic potassium. *Eur. Phys. J. D*, 64, 2 (2011). doi:10.1140/epjd/e2011-20099-x. https://doi.org/10.1140/epjd/e2011-20099-x. (cited on pages 73 and 74)

Riegler, G. R.; Ling, J. C.; Mahoney, W. A.; Wheaton, W. A.; Willett, J. B.; Jacobson, A. S.; and Prince, T. A., 1981. Variable positron annihilation radiation from the galactic center region. *ApJ*, 248 (Aug. 1981), L13–L16. doi:10.1086/183613. (cited on pages 12, 13, and 51)

Riess, A. G.; Filippenko, A. V.; Challis, P.; Clocchiatti, A.; Diercks, A.; Garnavich, P. M.; Gilliland, R. L.; Hogan, C. J.; Jha, S.; Kirshner, R. P.; Leibundgut, B.; Phillips, M. M.; Reiss, D.; Schmidt, B. P.; Schommer, R. A.; Smith, R. C.; Spyromilio, J.; Stubbs, C.; Suntzeff, N. B.; and Tonry, J., 1998. Observational Evidence from Supernovae for an Accelerating Universe and a Cosmological Constant. *AJ*, 116 (Sep. 1998), 1009–1038. doi:10.1086/300499. (cited on page 96)

Rigault, M.; Brinnel, V.; Aldering, G.; Antilogus, P.; Aragon, C.; Bailey, S.; Baltay, C.; Barbary, K.; Bongard, S.; Boone, K.; Buton, C.; Childress, M.; Chotard, N.; Copin, Y.; Dixon, S.; Fagrelius, P.; Feindt, U.; Fouchez, D.; Gangler, E.; Hayden, B.; Hillebrandt, W.; Howell, D. A.; Kim, A.; Kowalski, M.; Kuesters, D.; Leget, P.-F.; Lombardo, S.; Lin, Q.; Nordin, J.; Pain, R.; Pecontal, E.; Pereira, R.; Perlmutter, S.; Rabinowitz, D.; Runge, K.; Rubin, D.; Saunders, C.; Smadja, G.; Sofiatti, C.; Suzuki, N.; Taubenberger, S.; Tao, C.; and Thomas, R. C., 2018. Strong Dependence of Type Ia Supernova Standardization on the Local Specific Star Formation Rate. *ArXiv e-prints*, (Jun. 2018). (cited on pages 98 and 99)

Rigault, M.; Copin, Y.; Aldering, G.; Antilogus, P.; Aragon, C.; Bailey, S.; Baltay, C.; Bongard, S.; Buton, C.; Canto, A.; Cellier-Holzem, F.; Childress, M.; Chotard, N.; Fakhouri, H. K.; Feindt, U.; Fleury, M.; Gangler, E.; Greskovic, P.; Guy, J.; Kim, A. G.; Kowalski, M.; Lombardo, S.; Nordin, J.; Nugent, P.; Pain, R.; Pécontal, E.; Pereira, R.; Perlmutter, S.; Rabinowitz, D.; Runge, K.; Saunders, C.; Scalzo, R.; Smadja, G.; Tao, C.; Thomas, R. C.; and Weaver, B. A., 2013. Evidence of environmental dependencies of Type Ia supernovae from the Nearby Supernova Factory indicated by local Hα. *A&A*, 560 (Dec. 2013), A66. doi:10.1051/0004-6361/201322104. (cited on pages 98 and 99)

Ruiter, A. J.; Belczynski, K.; and Fryer, C., 2009. Rates and Delay Times of Type Ia Supernovae. *ApJ*, 699 (Jul. 2009), 2026–2036. doi:10.1088/0004-637X/699/2/2026. (cited on page 43)

Ruiter, A. J.; Ferrario, L.; Belczynski, K.; Seitenzahl, I. R.; Crocker, R. M.; and Karakas, A. I., 2019. On the formation of neutron stars via accretion-induced collapse in binaries. *MNRAS*, (Jan. 2019). doi:10.1093/mnras/stz001. (cited on page 50)

Rutherford, E., 1911. Lxxix. the scattering of Îś and Îš particles by matter and the structure of the atom. *The London, Edinburgh, and Dublin Philosophical Magazine and Journal of Science*, 21, 125 (1911), 669–688. doi:10.1080/14786440508637080. https://doi.org/10.1080/14786440508637080. (cited on page 3)

Sadowski, A.; Ziółkowski, J.; Belczyński, K.; and Bulik, T., 2008. Calculations of the Galactic Population of Black Hole X-Ray Binaries. In *A Population Explosion: The Nature & Evolution of X-ray Binaries in Diverse Environments*, vol. 1010 of *American Institute of Physics Conference Series*, 404–406. doi:10.1063/1.2945086. (cited on pages 50 and 64)

Sakharov, A. D., 1991. Violation of cp invariance, c asymmetry, and baryon asymmetry of the universe. *Soviet Physics Uspekhi*, 34, 5 (1991), 392. http://stacks.iop.org/0038-5670/34/i=5/a=A08. (cited on page 1)

Sánchez-Blázquez, P.; Peletier, R. F.; Jiménez-Vicente, J.; Cardiel, N.; Cenarro, A. J.; Falcón-Barroso, J.; Gorgas, J.; Selam, S.; and Vazdekis, A., 2006. Medium-resolution Isaac Newton Telescope library of empirical spectra. *MNRAS*, 371 (Sep. 2006), 703–718. doi:10.1111/j.1365-2966.2006.10699.x. (cited on pages 103, 113, and 114)

Schlafly, E. F. and Finkbeiner, D. P., 2011. Measuring Reddening with Sloan Digital Sky Survey Stellar Spectra and Recalibrating SFD. *ApJ*, 737 (Aug. 2011), 103. doi:10.1088/0004-637X/737/2/103. (cited on page 102)

Schlegel, D. J.; Finkbeiner, D. P.; and Davis, M., 1998. Maps of Dust Infrared Emission for Use in Estimation of Reddening and Cosmic Microwave Background Radiation Foregrounds. *ApJ*, 500 (Jun. 1998), 525–553. doi:10.1086/305772. (cited on page 102)

SEITENZAHL, I. R.; TIMMES, F. X.; AND MAGKOTSIOS, G., 2014. The Light Curve of SN 1987A Revisited: Constraining Production Masses of Radioactive Nuclides. *ApJ*, 792 (Sep. 2014), 10. doi:10.1088/0004-637X/792/1/10. (cited on page 45)

SHAFTER, A. W., 2002. The Galactic Nova Rate. In *Classical Nova Explosions*, vol. 637 of *American Institute of Physics Conference Series*, 462–471. doi:10.1063/1.1518246. (cited on page 47)

SHAFTER, A. W.; CIARDULLO, R.; AND PRITCHET, C. J., 2000. Novae in External Galaxies: M51, M87, and M101. *ApJ*, 530 (Feb. 2000), 193–206. doi:10.1086/308349. (cited on page 47)

SHARE, G. H.; CHUPP, E. L.; FORREST, D. J.; AND RIEGER, E., 1983. Positron annihilation radiation from solar flares. In *Positron-Electron Pairs in Astrophysics*, vol. 101 of *American Institute of Physics Conference Series*, 15–20. doi:10.1063/1.34086. (cited on page 49)

SHARE, G. H.; KINZER, R. L.; KURFESS, J. D.; MESSINA, D. C.; PURCELL, W. R.; CHUPP, E. L.; FORREST, D. J.; AND REPPIN, C., 1988. SMM detection of diffuse Galactic 511 keV annihilation radiation. *ApJ*, 326 (Mar. 1988), 717–732. doi:10.1086/166130. (cited on page 12)

SHARE, G. H.; LEISING, M. D.; MESSINA, D. C.; AND PURCELL, W. R., 1990. Limits on a variable source of 511 keV annihilation radiation near the Galactic center. *ApJ*, 358 (Aug. 1990), L45–L48. doi:10.1086/185776. (cited on page 12)

SHARE, G. H.; MURPHY, R. J.; AND SKIBO, J. G., 1996. Positron Annihilation Radiation in Solar Flares. In *American Astronomical Society Meeting Abstracts*, vol. 28 of *Bulletin of the American Astronomical Society*, 1346. (cited on page 49)

SHARE, G. H.; MURPHY, R. J.; SKIBO, J. G.; SMITH, D. M.; HUDSON, H. S.; LIN, R. P.; SHIH, A. Y.; DENNIS, B. R.; SCHWARTZ, R. A.; AND KOZLOVSKY, B., 2003. High-resolution observation of the solar positron-electron annihilation line. *The Astrophysical Journal Letters*, 595, 2 (2003), L85. http://stacks.iop.org/1538-4357/595/i=2/a=L85. (cited on page 49)

SHEN, K. J.; TOONEN, S.; AND GRAUR, O., 2017. The Evolution of the Type Ia Supernova Luminosity Function. *ApJ*, 851, 2 (Dec 2017), L50. doi:10.3847/2041-8213/aaa015. (cited on page 98)

SIEGERT, T.; DIEHL, R.; GREINER, J.; KRAUSE, M. G. H.; BELOBORODOV, A. M.; BEL, M. C.; GUGLIELMETTI, F.; RODRIGUEZ, J.; STRONG, A. W.; AND ZHANG, X., 2016a. Positron annihilation signatures associated with the outburst of the microquasar V404 Cygni. *Nature*, 531 (Mar. 2016), 341–343. doi:10.1038/nature16978. (cited on pages 51, 60, 64, 69, 83, and 92)

SIEGERT, T.; DIEHL, R.; KHACHATRYAN, G.; KRAUSE, M. G. H.; GUGLIELMETTI, F.; GREINER, J.; STRONG, A. W.; AND ZHANG, X., 2016b. Gamma-ray spectroscopy of positron annihilation in the Milky Way. *A&A*, 586 (Feb. 2016), A84. doi:10.1051/0004-6361/201527510. (cited on pages 18, 20, 21, 23, 24, 34, 42, 51, 59, 62, 63, 64, 69, 70, 71, 78, 82, 83, 84, 89, and 91)

SIEGERT, T.; DIEHL, R.; KRAUSE, M. G. H.; AND GREINER, J., 2015. Revisiting INTEGRAL/SPI observations of ^{44}Ti from Cassiopeia A. *A&A*, 579 (Jul. 2015), A124. doi:10.1051/0004-6361/201525877. (cited on pages 9 and 45)

SIEGERT, T.; DIEHL, R.; VINCENT, A. C.; GUGLIELMETTI, F.; KRAUSE, M. G. H.; AND BOEHM, C., 2016c. Search for 511 keV emission in satellite galaxies of the Milky Way with INTEGRAL/SPI. *A&A*, 595 (Oct. 2016), A25. doi:10.1051/0004-6361/201629136. (cited on pages 54 and 117)

Silverman, J. M.; Foley, R. J.; Filippenko, A. V.; Ganeshalingam, M.; Barth, A. J.; Chornock, R.; Griffith, C. V.; Kong, J. J.; Lee, N.; Leonard, D. C.; Matheson, T.; Miller, E. G.; Steele, T. N.; Barris, B. J.; Bloom, J. S.; Cobb, B. E.; Coil, A. L.; Desroches, L.-B.; Gates, E. L.; Ho, L. C.; Jha, S. W.; Kandrashoff, M. T.; Li, W.; Mandel, K. S.; Modjaz, M.; Moore, M. R.; Mostardi, R. E.; Papenkova, M. S.; Park, S.; Perley, D. A.; Poznanski, D.; Reuter, C. A.; Scala, J.; Serduke, F. J. D.; Shields, J. C.; Swift, B. J.; Tonry, J. L.; Van Dyk, S. D.; Wang, X.; and Wong, D. S., 2012. Berkeley Supernova Ia Program - I. Observations, data reduction and spectroscopic sample of 582 low-redshift Type Ia supernovae. *MNRAS*, 425 (Sep. 2012), 1789–1818. doi:10.1111/j.1365-2966.2012.21270.x. (cited on pages 98, 100, and 108)

Sizun, P.; Cassé, M.; and Schanne, S., 2006. Continuum γ-ray emission from light dark matter positrons and electrons. *Phys. Rev. D*, 74 (Sep 2006), 063514. doi:10.1103/PhysRevD.74.063514. https://link.aps.org/doi/10.1103/PhysRevD.74.063514. (cited on pages 33, 52, and 53)

Skinner, G.; Diehl, R.; Zhang, X.-L.; Bouchet, L.; and Jean, P., 2015. The galactic distribution of the 511 kev e+/e- annihilation radiation. 054. doi:10.22323/1.228.0054. (cited on pages 20 and 21)

Skinner, G.; Jean, P.; Knödlseder, J.; Martin, P.; von Ballmoos, P.; and Weidenspointer, G., 2010. The Galactic positron annihilation radiation: an update based on recent SPI observations. In *Eighth Integral Workshop. The Restless Gamma-ray Universe (INTEGRAL 2010)*, 20. (cited on page 59)

Smith, D. M.; Leventhal, M.; Cavallo, R.; Gehrels, N.; Tueller, J.; and Fishman, G., 1996. BATSE observations of galactic positron-annihilation radiation. *A&AS*, 120 (Dec. 1996), 361–364. (cited on page 13)

Stanishev, V.; Rodrigues, M.; Mourão, A.; and Flores, H., 2012. Type Ia supernova host galaxies as seen with IFU spectroscopy. *A&A*, 545 (Sep. 2012), A58. doi:10.1051/0004-6361/201219188. (cited on pages 98 and 99)

Stanway, E. R. and Eldridge, J. J., 2018. Re-evaluating old stellar populations. *MNRAS*, 479 (Sep. 2018), 75–93. doi:10.1093/mnras/sty1353. (cited on page 109)

Stanway, E. R.; Eldridge, J. J.; and Becker, G. D., 2016. Stellar population effects on the inferred photon density at reionization. *MNRAS*, 456 (Feb. 2016), 485–499. doi:10.1093/mnras/stv2661. (cited on page 109)

Stein, T. S.; Kauppila, W. E.; Pol, V.; Smart, J. H.; and Jesion, G., 1978. Measurements of total scattering cross sections for low-energy positrons and electrons colliding with helium and neon atoms. *Physical Review A*, 17, 5 (May 1978), 1600–1608. doi:10.1103/PhysRevA.17.1600. https://link.aps.org/doi/10.1103/PhysRevA.17.1600. (cited on pages 29 and 72)

Strickland, D. K. and Heckman, T. M., 2009. Supernova Feedback Efficiency and Mass Loading in the Starburst and Galactic Superwind Exemplar M82. *ApJ*, 697 (Jun. 2009), 2030–2056. doi:10.1088/0004-637X/697/2/2030. (cited on page 86)

Stritzinger, M.; Leibundgut, B.; Walch, S.; and Contardo, G., 2006. Constraints on the progenitor systems of type Ia supernovae. *A&A*, 450 (Apr. 2006), 241–251. doi:10.1051/0004-6361:20053652. (cited on page 43)

Strong, A. W.; Orlando, E.; and Jaffe, T. R., 2011. The interstellar cosmic-ray electron spectrum from synchrotron radiation and direct measurements. *A&A*, 534 (Oct. 2011), A54. doi:10.1051/0004-6361/201116828. (cited on page 40)

Strong, A. W.; Porter, T. A.; Digel, S. W.; Jóhannesson, G.; Martin, P.; Moskalenko, I. V.; Murphy, E. J.; and Orlando, E., 2010. Global Cosmic-ray-related Luminosity and Energy Budget of the Milky Way. *ApJ*, 722 (Oct. 2010), L58–L63. doi:10.1088/2041-8205/722/1/L58. (cited on page 40)

Su, M.; Slatyer, T. R.; and Finkbeiner, D. P., 2010. Giant Gamma-ray Bubbles from Fermi-LAT: Active Galactic Nucleus Activity or Bipolar Galactic Wind? *ApJ*, 724 (Dec. 2010), 1044–1082. doi:10.1088/0004-637X/724/2/1044. (cited on pages 62, 63, 81, and 85)

Sullivan, J. P.; Marler, J. P.; Gilbert, S. J.; Buckman, S. J.; and Surko, C. M., 2001. Excitation of Electronic States of Ar, ${H}_{2}$, and ${N}_{2}$ by Positron Impact. *Physical Review Letters*, 87, 7 (Jul. 2001), 073201. doi:10.1103/PhysRevLett.87.073201. https://link.aps.org/doi/10.1103/PhysRevLett.87.073201. (cited on pages 29 and 72)

Sullivan, M.; Kasliwal, M. M.; Nugent, P. E.; Howell, D. A.; Thomas, R. C.; Ofek, E. O.; Arcavi, I.; Blake, S.; Cooke, J.; Gal-Yam, A.; Hook, I. M.; Mazzali, P.; Podsiadlowski, P.; Quimby, R.; Bildsten, L.; Bloom, J. S.; Cenko, S. B.; Kulkarni, S. R.; Law, N.; and Poznanski, D., 2011. The Subluminous and Peculiar Type Ia Supernova PTF 09dav. *ApJ*, 732 (May 2011), 118. doi:10.1088/0004-637X/732/2/118. (cited on page 97)

Sunyaev, R.; Churazov, E.; Gilfanov, M.; Dyachkov, A.; Khavenson, N.; Grebenev, S.; Kremnev, R.; Sukhanov, K.; Goldwurm, A.; Ballet, J.; Cordier, B.; Paul, J.; Denis, M.; Vedrenne, G.; Niel, M.; and Jourdain, E., 1992. X-ray nova in Musca (GRS 1124 - 68) - Hard X-ray source with narrow annihilation line. *ApJ*, 389 (Apr. 1992), L75–L78. doi:10.1086/186352. (cited on page 13)

Sunyaev, R.; Churazov, E.; Gilfanov, M.; Pavlinsky, M.; Grebenev, S.; Babalyan, G.; Dekhanov, I.; Khavenson, N.; Bouchet, L.; Mandrou, P.; Roques, J. P.; Vedrenne, G.; Cordier, B.; Goldwurm, A.; Lebrun, F.; and Paul, J., 1991. Three spectral states of 1E 1740.7 - 2942 - From standard Cygnus X-1 type spectrum to the evidence of electron-positron annihilation feature. *ApJ*, 383 (Dec. 1991), L49–L52. doi:10.1086/186238. (cited on page 13)

Sutherland, R.; Dopita, M.; Binette, L.; and Groves, B., 2013. MAPPINGS III: Modelling And Prediction in PhotoIonized Nebulae and Gasdynamical Shocks. Astrophysics Source Code Library. (cited on pages 86 and 88)

Svensson, R., 1982. The pair annihilation process in relativistic plasmas. *ApJ*, 258 (Jul. 1982), 321–334. doi:10.1086/160081. (cited on page 64)

Taubenberger, S., 2017. The Extremes of Thermonuclear Supernovae. *ArXiv e-prints*, (Mar. 2017). (cited on pages 43, 96, and 97)

Taubenberger, S.; Hachinger, S.; Pignata, G.; Mazzali, P. A.; Contreras, C.; Valenti, S.; Pastorello, A.; Elias-Rosa, N.; Bärnbantner, O.; Barwig, H.; Benetti, S.; Dolci, M.; Fliri, J.; Folatelli, G.; Freedman, W. L.; Gonzalez, S.; Hamuy, M.; Krzeminski, W.; Morrell, N.; Navasardyan, H.; Persson, S. E.; Phillips, M. M.; Ries, C.; Roth, M.; Suntzeff, N. B.; Turatto, M.; and Hillebrandt, W., 2008. The underluminous Type Ia supernova 2005bl and the class of objects similar to SN 1991bg. *MNRAS*, 385 (Mar. 2008), 75–96. doi:10.1111/j.1365-2966.2008.12843.x. (cited on pages 64 and 97)

The, L.-S.; Clayton, D. D.; Diehl, R.; Hartmann, D. H.; Iyudin, A. F.; Leising, M. D.; Meyer, B. S.; Motizuki, Y.; and Schönfelder, V., 2006. Are ^{44}Ti-producing supernovae exceptional? *A&A*, 450 (May 2006), 1037–1050. doi:10.1051/0004-6361:20054626. (cited on page 45)

Thielemann, F.-K.; Nomoto, K.; and Hashimoto, M.-A., 1996. Core-Collapse Supernovae and Their Ejecta. *ApJ*, 460 (Mar. 1996), 408. doi:10.1086/176980. (cited on page 45)

Thomson, J. J., 1897. Xl. cathode rays. *The London, Edinburgh, and Dublin Philosophical Magazine and Journal of Science*, 44, 269 (1897), 293–316. doi:10.1080/14786449708621070. https://doi.org/10.1080/14786449708621070. (cited on page 3)

Timmes, F. X.; Woosley, S. E.; Hartmann, D. H.; and Hoffman, R. D., 1996. The Production of 44Ti and 60Co in Supernovae. *ApJ*, 464 (Jun. 1996), 332. doi:10.1086/177323. (cited on pages 45 and 46)

Totani, T., 2006. A RIAF Interpretation for the Past Higher Activity of the Galactic Center Black Hole and the 511 keV Annihilation Emission. *PASJ*, 58 (Dec. 2006), 965–977. doi:10.1093/pasj/58.6.965. (cited on pages 52, 63, 71, and 84)

Tripp, R., 1998. A two-parameter luminosity correction for Type IA supernovae. *A&A*, 331 (Mar. 1998), 815–820. (cited on page 96)

Ubertini, P.; Lebrun, F.; Di Cocco, G.; Bazzano, A.; Bird, A. J.; Broenstad, K.; Goldwurm, A.; La Rosa, G.; Labanti, C.; Laurent, P.; Mirabel, I. F.; Quadrini, E. M.; Ramsey, B.; Reglero, V.; Sabau, L.; Sacco, B.; Staubert, R.; Vigroux, L.; Weisskopf, M. C.; and Zdziarski, A. A., 2003. IBIS: The Imager on-board INTEGRAL. *A&A*, 411 (Nov. 2003), L131–L139. doi:10.1051/0004-6361:20031224. (cited on page 15)

Vazdekis, A.; Sánchez-Blázquez, P.; Falcón-Barroso, J.; Cenarro, A. J.; Beasley, M. A.; Cardiel, N.; Gorgas, J.; and Peletier, R. F., 2010. Evolutionary stellar population synthesis with MILES - I. The base models and a new line index system. *MNRAS*, 404 (Jun. 2010), 1639–1671. doi:10.1111/j.1365-2966.2010.16407.x. (cited on pages 103, 107, 113, and 114)

Vedrenne, G.; Roques, J.-P.; Schönfelder, V.; Mandrou, P.; Lichti, G. G.; von Kienlin, A.; Cordier, B.; Schanne, S.; Knödlseder, J.; Skinner, G.; Jean, P.; Sanchez, F.; Caraveo, P.; Teegarden, B.; von Ballmoos, P.; Bouchet, L.; Paul, P.; Matteson, J.; Boggs, S.; Wunderer, C.; Leleux, P.; Weidenspointner, G.; Durouchoux, P.; Diehl, R.; Strong, A.; Cassé, M.; Clair, M. A.; and André, Y., 2003. SPI: The spectrometer aboard INTEGRAL. *A&A*, 411 (Nov. 2003), L63–L70. doi:10.1051/0004-6361:20031482. (cited on pages 15 and 16)

Wallyn, P.; Chapuis, C.; and Durouchoux, P., 1994. Charge exchange reaction rates of thermal positrons in H, H2, and He. *ApJS*, 92 (Jun. 1994), 551–553. doi:10.1086/192014. (cited on pages 29, 34, and 71)

Walters, H. R. J., 1988. Positron scattering by atomic hydrogen at intermediate energies: 1s to 1s, 1s to 2s and 1s to 2p transitions. *Journal of Physics B: Atomic, Molecular and Optical Physics*, 21, 10 (1988), 1893. doi:10.1088/0953-4075/21/10/021. http://stacks.iop.org/0953-4075/21/i=10/a=021. (cited on pages 29 and 72)

Webbink, R. F., 1984. Double white dwarfs as progenitors of R Coronae Borealis stars and Type I supernovae. *ApJ*, 277 (Feb. 1984), 355–360. doi:10.1086/161701. (cited on page 43)

Weber, M.; Hofmann, A.; Raith, W.; Sperber, W.; Jacobsen, F.; and Lynn, K. G., 1994. Results of the Bielefeld-Brookhaven e<Superscript>+</Superscript>-H experiment. *Hyperfine Interactions*, 89, 1 (Dec. 1994), 221–242. doi:10.1007/BF02064508. https://link-springer-com.ezproxy.cern.ch/article/10.1007/BF02064508. (cited on pages 29 and 72)

Weidenspointner, G.; Shrader, C. R.; Knödlseder, J.; Jean, P.; Lonjou, V.; Guessoum, N.; Diehl, R.; Gillard, W.; Harris, M. J.; Skinner, G. K.; von Ballmoos, P.; Vedrenne, G.; Roques, J.-P.; Schanne, S.; Sizun, P.; Teegarden, B. J.; Schönfelder, V.; and Winkler, C., 2006. The sky distribution of positronium annihilation continuum emission measured with SPI/INTEGRAL. *A&A*, 450 (May 2006), 1013–1021. doi:10.1051/0004-6361:20054046. (cited on pages 18 and 19)

Weidenspointner, G.; Skinner, G.; Jean, P.; Knödlseder, J.; von Ballmoos, P.; Bignami, G.; Diehl, R.; Strong, A. W.; Cordier, B.; Schanne, S.; and Winkler, C., 2008a. An asymmetric distribution of positrons in the Galactic disk revealed by γ-rays. *Nature*, 451 (Jan. 2008), 159–162. doi:10.1038/nature06490. (cited on pages 18, 20, 59, 61, 64, 69, 70, and 83)

Weidenspointner, G.; Skinner, G. K.; Jean, P.; Knödlseder, J.; von Ballmoos, P.; Diehl, R.; Strong, A.; Cordier, B.; Schanne, S.; and Winkler, C., 2008b. Positron astronomy with SPI/INTEGRAL. , 52 (Oct. 2008), 454–456. doi:10.1016/j.newar.2008.06.019. (cited on page 20)

Whelan, J. and Iben, I., Jr., 1973. Binaries and Supernovae of Type I. *ApJ*, 186 (Dec. 1973), 1007–1014. doi:10.1086/152565. (cited on page 43)

Winkler, C.; Courvoisier, T. J.-L.; Di Cocco, G.; Gehrels, N.; Giménez, A.; Grebenev, S.; Hermsen, W.; Mas-Hesse, J. M.; Lebrun, F.; Lund, N.; Palumbo, G. G. C.; Paul, J.; Roques, J.-P.; Schnopper, H.; Schönfelder, V.; Sunyaev, R.; Teegarden, B.; Ubertini, P.; Vedrenne, G.; and Dean, A. J., 2003. The INTEGRAL mission. *A&A*, 411 (Nov. 2003), L1–L6. doi:10.1051/0004-6361:20031288. (cited on page 15)

Woosley, S. E., 1993. Gamma-ray bursts from stellar mass accretion disks around black holes. *ApJ*, 405 (Mar. 1993), 273–277. doi:10.1086/172359. (cited on page 48)

Woosley, S. E. and Weaver, T. A., 1995. The Evolution and Explosion of Massive Stars. II. Explosive Hydrodynamics and Nucleosynthesis. *ApJS*, 101 (Nov. 1995), 181. doi:10.1086/192237. (cited on page 45)

Worthey, G., 1994. Comprehensive stellar population models and the disentanglement of age and metallicity effects. *ApJS*, 95 (Nov. 1994), 107–149. doi:10.1086/192096. (cited on pages 99, 105, and 113)

Worthey, G. and Ottaviani, D. L., 1997. Hγ and Hδ Absorption Features in Stars and Stellar Populations. *ApJS*, 111 (Aug. 1997), 377–386. doi:10.1086/313021. (cited on pages 99, 105, and 113)

Zheng, W.; Shivvers, I.; Filippenko, A. V.; Itagaki, K.; Clubb, K. I.; Fox, O. D.; Graham, M. L.; Kelly, P. L.; and Mauerhan, J. C., 2014. Estimating the First-light Time of the Type Ia Supernova 2014J in M82. *ApJ*, 783 (Mar. 2014), L24. doi:10.1088/2041-8205/783/1/L24. (cited on page 44)

Zhou, S.; Li, H.; Kauppila, W. E.; Kwan, C. K.; and Stein, T. S., 1997. Measurements of total and positronium formation cross sections for positrons and electrons scattered by hydrogen atoms and molecules. *Physical Review A*, 55, 1 (Jan. 1997), 361–368. doi: 10.1103/PhysRevA.55.361. https://link.aps.org/doi/10.1103/PhysRevA.55.361. (cited on pages 29 and 72)